Title
Superpave Implementation Phase II: Comparison of Performance-Related Test Results

Authors
Harvey, J.
Liu, A.
Zhou, J.
et al.

Publication Date
2014-07-01

July 2014
UCPRC-RR-2015-01

Superpave Implementation Phase II: Comparison of Performance-Related Test Results

Authors:
J. Harvey, A. Liu, J. Zhou, J. M. Signore, E. Coleri, and Y. He

Part of Partnered Pavement Research Program (PPRC) Strategic Plan Element 3.18.3: Implementation of the "Superpave" Asphalt Mix Design Procedure in California

PREPARED FOR:

California Department of Transportation
Division of Research, Innovation, and System Information
Office of Roadway Material Testing, Materials and Engineering Services

PREPARED BY:

University of California
Pavement Research Center
UC Davis, UC Berkeley

(page blank)

DOCUMENT RETRIEVAL PAGE	**UCPRC Research Report No.:** UCPRC-RR-2015-01

Title: Superpave Implementation Phase II: Comparison of Performance-Related Test Results

Authors: J. Harvey, A. Liu, J. Zhou, J. M. Signore, E. Coleri, and Y. He

Caltrans Technical Reviewers: J. Peterson, S. Balasubramanian

Prepared for:	**FHWA No.:**	**Date Work Submitted:**	**Date:**
California Department of Transportation Division of Research, Innovation, and System Information Office of Roadway Material Testing, Materials and Engineering Services	CA162356A	February 4, 2015	July 2014

Strategic Plan No:	**Status:**	**Version No:**
3.18.3	Stage 6 final version	1

Abstract:

Although Caltrans has utilized the Hveem mix design process for hot mix asphalt for decades, it is currently implementing the Superpave mix design procedure, and is interested in including performance-related tests for mix design and quality assurance. Performance-related tests are also used for Caltrans mechanistic-empirical (ME) pavement design.

This report includes descriptions of current performance-related tests and alternatives, including tests using the Asphalt Mixture Performance Tester (AMPT) device for permanent deformation, stiffness and fatigue, and other alternatives to the flexural beam and repeated shear tests currently used for ME characterization by Caltrans. The tests are compared for mixture design and quality assurance, and for characterization for ME design in terms of the usefulness of the results, and the difficulty and time required to obtain results. The report also presents an evaluation of the effects on mix properties for Hveem versus Superpave mix designs and the results of ME simulation of the effects on pavement performance for rutting and cracking.

The results indicate that there is potential to use the unconfined Repeated Load Triaxial (RLT) test as a substitute for the repeated shear at constant height (RSCH) test for mix design and quality assurance, and to use the confined or unconfined RLT for ME characterization. However, the preliminary results regarding use of shift factors to convert results from RLT to RSCH to enable application to previously calibrated models needs more comprehensive evaluation. The results indicate that the direct tension (DT) test offers no advantages over flexural beam testing for ME fatigue characterization, and that the fracture energy index and fracture toughness parameters from the Semicircular Beam (SCB) Test may be useful for quality assurance and mix design. Results indicated that the Indirect Tension Test (IDT) did not correlate with flexural fatigue life. Results for the Hamburg Wheel-Track Testing (HWTT) indicated poor correlation with the RSCH for rutting potential.

Keywords: Superpave, Mix Design, Hveem, Fatigue, Shear, AMPT, IDT, SCB, Repeated Load Triaxial, Stiffness, Direct Tension

Proposals for implementation:

Improve shift factors by additional comparison testing of RSCH and confined and unconfined RLT on the same materials using field RSCH specimens and gyratory-compacted RLT specimens. Once more mixes have been tested, perform sensitivity analysis for *CalME* results for differences between mix-by-mix versus average shift factors; if results are acceptable, consider use of RLT for development of rutting parameters for ME design along with other factors that will influence risks to successful deployment. Continue with use of flexural fatigue and stiffness for mechanistic-empirical design. Improve correlation between SCB fracture energy index and flexural fatigue to further develop use of SCB fracture energy index as a less expensive and faster mix design and quality assurance test where flexural fatigue is not warranted.

Related documents:

- Zhou, J., J. M. Signore, and J. T. Harvey. 2013. Superpave Implementation Phase I: Determining Optimum Binder Content (UCPRC-TM-2012-03)

Signatures

J. Harvey **First Author**	D. Jones **Technical Review**	D. Spinner **Editor**	J. Harvey **Principal Investigator**	J. Peterson S. Balasubramanian **Caltrans Technical Leads**	T. J. Holland **Caltrans Contract Manager**

DISCLAIMER

This document is disseminated in the interest of information exchange. The contents of this report reflect the views of the authors who are responsible for the facts and accuracy of the data presented herein. The contents do not necessarily reflect the official views or policies of the State of California or the Federal Highway Administration. This publication does not constitute a standard, specification or regulation. This report does not constitute an endorsement by the Department of any product described herein.

For individuals with sensory disabilities, this document is available in alternate formats. For information, call (916) 654-8899, TTY 711, or write to California Department of Transportation, Division of Research, Innovation and System Information, MS-83, P.O. Box 942873, Sacramento, CA 94273-0001.

PROJECT OBJECTIVES

The goal of this project is to support development and implementation of a new mix design procedure for hot/warm mix asphalt for California using AASHTO "Superpave" mix design principles. This will be achieved through completion of the following objectives:

1. Completion of a literature review on recent national Superpave mix design and mix design test equipment-related research, including rutting and cracking performance, and moisture sensitivity
2. Creation of a laboratory testing matrix that considers key variables identified in the literature review
3. Collection of aggregates, binders, and current Hveem or rubberized mix designs for them
4. Development of Superpave volumetric mix designs and comparison with current mix designs
5. Preparation and completion of laboratory testing of Repeated Shear Constant Height (RSCH) and Repeated Load Triaxial (RLT) specimens and analysis of the results
    a. To compare expected rutting resistance of Superpave and Hveem mix designs
    b. To compare results of RSCH and RLT testing
6. Delivery of recommendations for changes in preliminary new mix design procedure
7. Evaluation of comparison of RSCH and RLT results and required changes in *CalME* to use RLT testing to produce design inputs
8. Preparation and laboratory testing for different performance-related tests for rutting, fatigue cracking, and moisture sensitivity for possible use in new mix design method
9. Delivery of recommendations for performance-related tests for use in new mix design procedure
10. Preparation of reports documenting the study and study results

The results of objectives 1 through 4 were reported in a previous technical memorandum. The results of objectives 5 through 10 are completed with delivery of this report.

EXECUTIVE SUMMARY

In the 1940s Caltrans started using a standard Hveem mix design process for HMA to determine binder contents for conventional dense-graded mixes and later for polymer-modified asphalt mixes. In the 1990s they began to use a modified version of the Hveem method for gap-graded rubberized mixes. Caltrans is now implementing a California version of the Superpave mix design procedure for HMA. The Superpave (SUperior PERforming Asphalt PAVEments) system was developed as part of the first Strategic Highway Research Program (SHRP) and completed in 1992. Most state highway agencies in the U.S. have adopted all or part of Superpave, nearly always with refinements to suit local conditions, practice, and requirements.

Caltrans has also made the decision to change from empirical pavement design methods to the *CalME* mechanistic-empirical (ME) pavement design method, in which asphalt rutting (permanent deformation) models are based on the characterization of rutting behavior under different stresses and temperatures using repeated load testing, which has been calibrated against measured rutting performance in Heavy Vehicle Simulator (HVS) tests, the FHWA WesTrack full-scale test track experiment, and several sections at the National Center for Asphalt Technology (NCAT) and MnROAD test tracks. The repeated load test for rutting used for that calibration was the Repeated Shear Test at Constant Height (RSCH, AASHTO T 320), and the testing was done at the time of the HVS or test track experiment.

Although there are approximately ten laboratories in the U.S. that own RSCH equipment, as of 2014 only two laboratories, at the University of California Pavement Research Center (UCPRC) and at Road Science in Oklahoma, were known to be routinely using the equipment. Instead, many laboratories are using a new type of equipment called the Asphalt Mixture Performance Tester (AMPT) that can also perform a repeated load test for rutting: the Repeated Load Triaxial (RLT) test. As of 2014, approximately twenty states and several consultants in the U.S. had purchased an AMPT and began working with it, although it appears that none have implemented it yet as part of standard mix design and/or quality assurance.

As of 2015, no approach has been implemented for using AMPT/RLT results in mechanistic-empirical (ME) design for rutting, although the NCHRP 9-30A project has provided recommendations for using the AMPT/RLT (confined) or the RSCH to produce inputs to the MEPDG software, provided that there is calibration for either approach.

The Superpave system primarily addresses two pavement distresses: permanent deformation (rutting), which results from inadequate shear strength in the asphalt mix, and low-temperature cracking, which occurs when an

asphalt layer shrinks and the tensile stress exceeds the tensile strength. The system consists of three interrelated elements:

- An asphalt binder specification (implemented by Caltrans in 2005)
- A volumetric mix design and analysis system based on gyratory compaction (implementation process began in 2011 with full implementation in 2014)
- Performance-related mix analysis tests and a performance prediction system that includes environmental and performance models. There has been no consistency in national implementation of this last element, as different states use a variety of tests and performance prediction methods, and a number of states do not use this element at all except for a moisture sensitivity test (AASHTO T 283).

There is increasing use of Hamburg Wheel-Track Testing (HWTT) for both rutting and moisture damage. Although fatigue/reflective cracking performance are not assessed in the Superpave mix design process, longer-term evaluations of roads in a number of states where the Superpave mix design procedure is used have indicated that early cracking may be a problem on roads where rutting resistance was the primary focus of the mix design and was addressed through volumetric specifications that are conservative for rutting or included a performance-related test for rutting but not for cracking.

An optimal mix design will balance rutting and fatigue-cracking performance by reducing the risk of rutting to an acceptable level, while at the same time maximizing fatigue-cracking performance and achieving at least a minimum required cracking performance.

The work completed in this project is intended to assess Superpave and other nationally available tests and testing equipment for possible adoption in California. The study considered the following:

- Conventional, rubberized, and polymer-modified binders
- Dense and gap gradations
- Rutting and fatigue/reflective cracking performance, and moisture sensitivity
- Compatibility of test results with ME design and long-life asphalt specifications

The objectives for the project were completed in two phases, with Phase I Part A comparing Hveem and Superpave mix designs, Phase I Part B assessing the relative rutting performance of the two mix designs and comparing RSCH and AMPT/RLT results, and Phase II comparing other performance-related tests. A breakdown of the tasks taken to complete these objectives is shown below.

Phase I

Part A

1. Completion of a literature review on recent national Superpave mix design and mix design test equipment-related research, including rutting and cracking performance, and moisture sensitivity
2. Creation of a laboratory testing matrix that considers key variables identified in the literature review
3. Collection of aggregates, binders, and current Hveem or rubberized mix designs for them
4. Development of Superpave volumetric mix designs and comparison with current mix designs

Part B

5. Preparation and laboratory testing of RSCH and RLT specimens and analysis of the results
    a. To compare expected rutting resistance of Superpave and Hveem mix designs
    b. To compare results of RSCH and RLT testing
6. Delivery of recommendations for changes in preliminary new mix design procedure
7. Evaluation of comparison of RSCH and RLT results and required changes in *CalME* to use RLT testing to produce design inputs

Phase II

8. Preparation and laboratory testing for different performance-related tests for rutting, fatigue cracking, and moisture sensitivity for possible use in new mix design method
9. Delivery of recommendations for performance-related tests for use in new mix design procedure
10. Preparation of reports documenting the study and study results

The results of Phase I Part A (Tasks 1 through 4) were reported in a previous technical memorandum. The results of the remainder of the tasks (5 through 10) are discussed in this report.

This report presents answers for six specific questions sought in the results from Phase I Part B and Phase II of this project:

1. How is HMA shear test performance, which is related to rutting, affected by changing from the Hveem mix design to the Superpave mix design for the mixes tested?
2. How are the HMA flexural fatigue test and flexural stiffness performance, which are related to cracking, affected by changing from the Hveem mix design to the Superpave mix design for the mixes tested?
3. How do any changes in shear, flexural fatigue, and flexural stiffness test performance affect expected pavement rutting and cracking performance, as evaluated using the *CalME* mechanistic-empirical analysis procedures?
4. Can faster and less expensive tests than shear and flexural fatigue tests be successfully used as surrogates for currently used mechanistic performance-related tests for mix design and quality assurance?

5. Can the Asphalt Mixture Performance Tester's (AMPT) tests for rutting, fatigue, and stiffness be used for ME pavement designs in place of shear, flexural fatigue, and flexural stiffness tests, and can results from one test be converted into results from another?
6. What are the practical issues, such as test duration, specimen preparation, test variability, and test difficulty, for the AMPT?

Chapter 2 describes the individual laboratory tests conducted to evaluate mix performance for the five Superpave-designed mixes selected from the nineteen mixes in Phase I Part A of the study. Brief descriptions of the HMA specimen preparation process are also given. Specific performance measures assessed with each of these performance tests were:

- Rutting: Repeated Shear Test at Constant Height (RSCH, AASHTO T 320), AMPT Repeated Load Triaxial (RLT), both confined and unconfined (AASHTO TP 79, same test setup and operation as the flow number although using a different parameter than flow number), Hamburg Wheel-Track Testing (HWTT, AASHTO T 324)
- Cracking: AMPT tension/compression fatigue (AASHTO TP 79), flexural fatigue (AASHTO T 321), semicircular beam (parameter to be determined), indirect tensile strength (dry)
- Stiffness in terms of dynamic modulus: AMPT dynamic modulus (stiffness, AASHTO TP 79), flexural frequency sweep (AASHTO T 321)
- Moisture sensitivity: Hamburg Wheel-Track Testing and CT 371 (Caltrans version of AASHTO T 283)

Chapter 3 presents the results for all five Superpave mixes with laboratory-produced material for each performance-related test conducted, and descriptive analysis of the results.

Chapter 4 compares the performance-related testing results from three of the five Superpave mix designs and results from using the same tests on Hveem mix designs for the same mix materials for stiffness using the flexural frequency sweep test, for fatigue performance using the flexural fatigue test, and for permanent deformation performance using the RSCH. It was expected that the higher binder contents and consideration of the dust-to-asphalt ratio of the Superpave mix designs would result in slightly reduced stiffness, improved fatigue performance, and some reduction in permanent deformation resistance. This change was desired since the Hveem mix design method has traditionally been considered overly risk averse with regard to permanent deformation and not risk averse enough for fatigue cracking for the designs for most segments on the state highway network—with potential exceptions where there is heavy slow traffic in very hot environments.

The results for the three Hveem mix designs confirmed the expectation that the higher binder contents and consideration of the dust-to-asphalt ratio of the Superpave mix designs would result in slight reductions in stiffness and improved fatigue resistance. And, the extent of the reduction in permanent deformation resistance was greater than expected. However, looking at test results alone without considering the context of traffic loading and climate does not answer the question as to how the change in mix design affects the expected performance of the pavement under different conditions and whether the reduction in rutting resistance puts the pavement at significant risk of rutting. Mechanistic-empirical simulations were performed in order to provide a more complete analysis of the impacts of the differences between the Superpave and Hveem mix designs.

Chapter 5 presents the results of simulated rutting and fatigue-cracking performance of the Hveem and Superpave mix designs based on *CalME* analysis to evaluate the expected effects on field performance of the change in the mix design procedure. The mix test data were used to analyze the performance of three structures:

- A flexible pavement analyzed for rutting and cracking,
- A flexible structure with a thin rubberized overlay, analyzed for cracking when built as a new pavement and when the overlay is placed after the underlying asphalt has already cracked, and
- A composite structure of asphalt on concrete, analyzed for cracking when built as a new pavement and when the overlay is placed after the concrete has already cracked.

The purpose of the simulations was to evaluate the expected effect on pavement performance of the change from Hveem mix designs to Superpave mix designs for the same three materials (Mixes A, B, and I). Simulated performance for rutting, bottom-up fatigue, and reflective cracking performance produced the following findings:

- For rutting, it was observed that mix design method was an important factor affecting the simulated rutting in the asphalt layers. Statistical analysis indicated that the mean predicted asphalt layer rutting for Hveem mixes is significantly less than that of Superpave mixes. However, the Superpave mix designs still met Caltrans design criteria for rutting performance in 34 of 36 scenarios analyzed at the 50 percent reliability level, indicating that the Hveem mix designs may have been overly conservative for rutting.
- For fatigue and reflective cracking, some improvement in simulated cracking performance was shown when using the Superpave mix design as compared to the Hveem mix design, with one of three mixes showing a large improvement and the other two showing lesser improvement.

These results indicate that for the cases simulated, the hypothesis that Superpave mix designs would show poorer, but likely still sufficient, rutting performance, while improving cracking performance is reasonable. Additionally, based on these findings, it is recommended that construction projects with Superpave and Hveem

mix designs be evaluated annually using Automated Pavement Condition Survey data over the next five years to compare actual field performance of the two mix design approaches.

Chapter 6 presents a summary of testing that looked at the sensitivity of shear and AMPT repeated load triaxial test results to compaction method, air-void content, and temperature. This chapter also compares the confined and unconfined approaches for the RLT, and presents the results of initial shift factors for translating RLT results to shear test results for use in existing *CalME* mechanistic-empirical design and analysis models. This testing was performed using a field sample mix with 25 percent reclaimed asphalt pavement (RAP).

This chapter answers the following key questions:

1. How does compaction method affect test results?
2. How does air-void content affect test results?
3. How does temperature affect test results?
4. Do on-specimen linear variable differential transducer (LVDT) results match repeated load triaxial (RLT) actuator LVDT results?
5. Is it possible to relate typical RLT and RSCH test results? And if yes, then how?

The following findings are based on the results from the testing using one mix:

- Based on results from testing up to 3 percent permanent axial strain or 20,000 axial load repetitions for the confined RLT test and 5 percent permanent shear strain or 30,000 shear load repetitions for the RSCH test, a preliminary indication is that a shift factor of approximately 2 provides the best fit to convert the relationship between load repetitions versus permanent axial strain from the confined RLT test (7 percent air-void content, Superpave gyratory compaction [SGC]) to a relationship between load repetitions and permanent shear strain from the RSCH test (3 percent air-void content, field compaction).
- Through visual observation and statistical analysis, compaction type, compaction level, and temperature all appear to be significant variables in the confined RLT test. Compaction type affects permanent axial deformations the most, temperature has less effect, and air-void content has the least effect. The low sensitivity to temperature was surprising.
- The permanent axial deformation of Superpave gyratory-compacted specimens is less than that of rolling-wheel–compacted specimens and field-compacted specimens. These differences in compaction method need to be accounted for in evaluating confined RLT/SGC test results for construction compliance, mix design, and pavement design. However, if SGC specimens are used in the RLT rutting test, the predicted repetitions to failure would be larger than those expected for the

same mix compacted in the field. This conclusion is somewhat biased by differences in heating time for the SGC and field specimens used in this experiment. This finding regarding compaction method effects is similar to that from previous observations on RSCH tests.

- In general, as the test temperature increased, the permanent strain also increased for both the confined RLT and RSCH tests, as expected. However, the temperature effect was observed more on RSCH test results than on confined RLT test results.
- The confined RLT test results are also statistically sensitive to compaction level, although to a much lesser degree than compaction method and test temperature. The results did not show consistent trends for permanent deformation resistance relative to air-void content. For rolling-wheel (RW) compacted and Superpave gyratory-compacted cores, the lower the air-void content, the greater the permanent deformation resistance; for field-compacted cores, the opposite relation was found, which was unexpected. It is not certain why this occurred, although greater variability would be expected from the field cores, which were sampled at various locations across a large project, and the laboratory-compacted specimens, which were made with material sampled in a few locations.
- Use of the LVDT in the actuator for permanent axial strain measurement in the RLT provides very good data quality. Use of the actuator LVDT is recommended because it provides measurements similar to an on-specimen LVDT and is much easier to use.
- A preliminary indication was that the unconfined RLT test has much greater sensitivity to temperature than the confined RLT test. Because rutting in the field is known to be extremely sensitive to temperature, the indication is that the unconfined test configuration may produce better results than the confined configuration.
- Comparison of dynamic modulus master curves from the AMPT device for field and SGC specimens compacted to the same air-void contents indicates that both specimens have similar results at higher frequencies and lower temperatures. SGC specimens can have on the order of 30 percent greater stiffness at low frequencies and high temperatures, which can have a large influence on pavement structural design.

Chapter 7 gives a comparative analysis of the use of alternative tests as surrogates for currently used mechanistic performance-related (shear and flexure) tests for mix design and quality assurance. This chapter also presents the results of the development of shift factors for translating RLT results to shear test results for the five mixes, and the preliminary recommended shift factors. The current tests—the flexural fatigue, flexural frequency sweep, repeated shear at constant height (RSCH), and Hamburg Wheel-Track Testing (HWTT)—were compared with the following alternative tests for mix design and quality assurance: semicircular beam (SCB), indirect tensile strength (IDT), and the tests that can be performed using the AMPT, that is, the repeated

load triaxial (RLT), dynamic modulus (DM), and direct tension (DT) tests. Comparisons are made with regard to fatigue, shear, stiffness, and moisture sensitivity. Shift factors are also developed to convert the RLT results for both the confined and unconfined tests to RSCH results at different stress levels, improving the shift factors from the preliminary study presented in Chapter 6. These tests were evaluated and compared using results from the five mixes discussed in Chapter 2 with a few additional tests on three other mixes.

It is difficult to draw strong conclusions regarding the correlation of different tests with only five mixes (with results from three additional mixes for some tests), however the following preliminary findings are based on the results presented in this chapter:

- There is a general but weak trend of increased fatigue life with lower secant stiffness measured using the semicircular beam test, which is typical for most stiffness parameters and controlled-deformation fatigue life. Similarly there are weak trends between flexural fatigue life and fracture toughness and fracture energy index from the SCB test. However, the fracture toughness has a trend that is the opposite of what is expected, with higher fracture toughness corresponding to lower fatigue life. Based on these results, the fracture energy index appears to be the best of the SCB test parameters for relatively fast and low-cost comparison with flexural fatigue life.
- There is almost no correlation between flexural fatigue life and dry indirect tensile strength, except that the mix with the highest fatigue life has the lowest strength.
- Flexural fatigue and direct tension damage relations (loss of stiffness versus repetitions at 200 microstrain) show similar trends.
- None of the mixes tested demonstrated “tertiary flow” in the confined condition in the RLT, and it was difficult to clearly identify tertiary flow in many of the unconfined RLT tests, making use of the flow number difficult.
- Shift factors were developed for translating repeated load triaxial confined and unconfined test results to repeated shear test at constant height (RSCH) results by considering the entire permanent deformation damage curve in each test.
    - The shift factors for 45°C and 55°C are about 30 percent different for both the confined and unconfined results, with the absolute values of the shift factors for different temperatures being much larger for the confined RLT results. The lack of consistency between temperatures may require different shift factors for different temperatures.
    - The results are promising for use of the shifted RLT and RSCH results for quality assurance. Additional data collection is recommended to further identify the errors caused by using shifted RLT results in ME design models calibrated with the RSCH. The allowable difference for

shifting RLT results to RSCH equivalents for use in ME design that would be considered acceptable has not been determined.

- The mixes tested did not show a "creep slope" in the Hamburg Wheel-Track Test. The HWTT and the RSCH present opposite trends for rutting for the mixes tested. This may indicate that the HWTT is more of a moisture sensitivity test than a rutting test, despite the lack of a creep slope.
- Stiffness master curves from dynamic modulus frequency sweeps run on the AMPT are generally stiffer than master curves from flexural frequency sweeps. This is to be expected since the dynamic modulus test primarily measures the compressive modulus with some shearing, while the flexural test measures a mix of tensile and compressive moduli in the beam, and asphalt should be stiffer in compression than tension.
- If dynamic modulus master curves are used in *CalME* instead of flexural curves for ME design calculations, models will need to be recalibrated or shift factors will need to be developed.
- No clear trend was observed between HWTT rut depth and the wet indirect tensile strength, and the HWTT showed an opposite trend compared with the tensile strength ratio.

Chapter 8 presents a summary and comparison of productivity and practical aspects for current tests and AMPT testing and simple tests. Tables in this chapter compare the practical issues between the AMPT and the flexural beam and RSCH tests in terms of test preparation, test duration, variability, and other practical considerations identified by direct comparison by UCPRC during this study. Other practical differences between the AMPT and current flexural beam and RSCH are also discussed.

It was found that the unconfined RLT test is much faster and easier to perform than the RSCH test or the confined RLT test. The confined RLT ranking for permanent axial strain for the five mixes tested in this study at 45°C and 55°C was the same. The unconfined RLT test had somewhat similar rankings as the RSCH at 45°C, but the ranking results were dissimilar at 55°C. This indicates that the unconfined RLT test may be a viable construction quality assurance test when used at lower temperatures.

Chapter 9 summarizes the conclusions and recommendations regarding the questions to be answered from this study based on the findings presented in each chapter, as follows:

1. *Question:* How is HMA shear test performance, which is related to rutting, affected by changing from Hveem mix design to Superpave mix design for the mixes tested?
   Conclusion: Overall, the Hveem mixes had higher rutting resistance based on their shear test performance. The RSCH results for the four mixes tested with both the Superpave and Hveem designs

(A, B, J, and N) showed that the Hveem designs had significantly higher performance in terms of repetitions to 5 percent permanent shear strain for three of the mixes (greater than a factor of 1,000 at 45°C and a factor of 10 at 55°C) and a factor of 2 to 5 for the fourth mix at these same temperatures.

2. *Question:* How are the HMA flexural fatigue test and flexural stiffness performance, which are related to cracking, affected by changing from Hveem mix design to Superpave mix design for the mixes tested?
   Conclusion: In flexural fatigue, the Superpave mixes outperformed the Hveem mixes for the three mixes compared (A, B, and I), typically by a factor of 3 to 5 for Mixes A and B in terms of repetitions to 50 percent loss of stiffness. The, Superpave mixes had higher binder contents than the Hveem mixes for Mixes A and B. For Mix I, performance of the Hveem and Superpave mixes varied, depending on the testing strain level. Flexural frequency sweep results indicated that the stiffness master curves were similar for the three mixes tested.

3. *Question:* How do any changes in shear, flexural fatigue, and flexural stiffness test performance in changing from Hveem to Superpave mix designs for the same mixes affect expected pavement rutting and cracking performance as evaluated using the *CalME* mechanistic-empirical analysis procedures?
   Conclusion: The hypothesis that Superpave mix designs would generally have better fatigue performance and worse rutting performance than the Hveem mix designs because of their often higher binder contents was generally proved true by the results of mechanistic simulation of performance for a range of structures, climate regions, and traffic. However, simulations also showed that most of the Superpave mixes were predicted to have satisfactory rutting performance even with the higher binder contents. Preliminary analysis performed to estimate the net effects on total asphalt binder used in an asphalt design indicated that the total binder content required to obtain the same performance could be less for the Superpave mixes than for the Hveem mixes. Net change in binder content was evaluated since the total binder used in a treatment design is a major driver of both cost and environmental emissions. The net reduction in asphalt binder found for the mix evaluated (Mix A) was the result of increased binder content in the mix for the Superpave mix, offset by the decreased asphalt thickness required to obtain the required cracking performance. In addition, trucking and aggregate costs would be less because of the reduced thickness required to obtain the same cracking performance. These results indicate that the Superpave mixes could provide reduced costs for the same performance, provided that the rutting performance is satisfactory.

Recommendation: Continue with implementation of the Superpave mix design process, with further calibration and potential use of performance-related quality assurance testing with the unconfined RLT test for rutting.

4. *Question:* Can faster and less expensive tests than the shear and flexural fatigue tests be successfully used as surrogates for currently used mechanistic performance-related tests for mix design and quality assurance?

   Conclusions: With regard to rutting performance:

   - Strong trends were found between the RSCH and both the confined and unconfined RLT tests for the development of permanent deformation versus repetitions. In terms of ranking the mixes, the confined RLT testing ranked the mixes the same as the RSCH at both 45°C and 55°C, while the unconfined RLT testing also had similar rankings as the RSCH at the lower temperature and but dissimilar rankings at the higher temperature.
   - The unconfined RLT test has speed and difficulty advantages over the RSCH and the confined RLT for mix design and quality assurance, which indicates that it is a candidate as a rutting test for mix design and quality assurance, particularly when performed at 45°C as opposed to 55°C.
   - An opposite correlation was observed between the RSCH test and the HWTT for rutting performance, which indicates that the HWTT is not an appropriate alternative for mix design and quality assurance as a rutting test.

   Regarding fatigue performance evaluation for mix design and quality assurance:

   - No trend was found between the dry IDT results and flexural fatigue life.
   - Opposing trends were found between fatigue life and many of the SCB tests; however, the SCB test with fracture energy index as the parameter showed some correlation with flexural fatigue life and may prove useful as a quality assurance test.
   - There is a strong correlation between fatigue performance in the flexural and direct tension tests, with the primary difference being faster damage during the first 100 repetitions of the direct tension tests.

   Regarding moisture sensitivity, none of the HWTT tests on the five mixes showed evidence of a "creep slope," which is taken from a change in the slope of rutting versus load repetitions and is generally interpreted as indicating where extensive moisture damage is occurring in the mix. No clear trend was observed between HWTT rut depth and wet indirect tensile strength, and HWTT rut depth development showed an opposite trend compared with the tensile strength ratio. This indicates that additional calibration of moisture damage tests against field performance is needed. A previous initial calibration

of the HWTT against field performance, on field samples as opposed to the laboratory specimens used in this study, indicated that "the [HWTT] procedure can correctly identify the effect of antistripping additives, but may underestimate the performance of mixes containing soft binders at the fixed test temperature 50°C. The correlation between test results and field performance seems acceptable except that the test procedure may fail mixes that perform well in the field and, in a very few cases, give false positive results" (Lu and Harvey, 2005).

Recommendations:

- Consider use of the unconfined RLT test for mix design and quality assurance for rutting; collect additional comparison data between this test and the RSCH. If consistent shift factors can be found to convert from the RLT to the RSCH then no recalibration of the *CalME* models will be needed if a switch is made to using the RLT for mix characterization.
- Perform additional testing and comparison of the SCB fracture energy index with flexural fatigue life for use as a mix design and quality assurance test.
- Continue with current use of the HWTT as a moisture damage test; consider additional calibration against field performance.

5. *Question:* Can the Asphalt Mixture Performance Tester's (AMPT) tests for rutting, fatigue, and stiffness be used for ME pavement designs in place of shear, flexural fatigue, and flexural stiffness tests, including transformation of data from one test to another?

   Conclusions: For the characterization of rutting performance for ME design, the RLT test performed using the AMPT equipment has potential as a substitute for the RSCH test. Results from this study indicate that shift factors may be developed for use in ME design to convert both confined and unconfined RLT results to similar RSCH results for use in existing models calibrated against RSCH results. However, it appears that different shift factors may be needed for specific test temperatures for both the confined and unconfined tests, with shift factors for the unconfined test being somewhat less sensitive to temperature than those for the confined test. There is on the order of 30 percent variability in the shift factors at a given temperature across the five mixes tested. The RSCH and RLT results are both sensitive to compaction method (gyratory, field, or rolling-wheel compaction). The models in *CalME* were calibrated with RSCH results primarily using field cores. The initial shift factors in this report are based on correlating RSCH results for rolling-wheel cores with RLT results for gyratory cores. The sensitivity of designs to errors in the shifting requires additional test results and further analysis to determine whether it is acceptable for the use of shifted RLT results with existing models calibrated with RSCH results.

For the characterization of fatigue and stiffness performance for ME design, the respective AMPT tests (direct tension and dynamic modulus) can provide similar data, but do not appear to offer any advantages in terms of productivity or difficulty. The only advantage is that the AMPT specimens can be produced from gyratory specimens. Shift factors would need to be developed for changing the stiffness test from flexural frequency sweep to dynamic modulus frequency sweep because the master curves from dynamic modulus frequency sweeps are consistently stiffer than master curves from flexural frequency sweeps across all five mixes tested in this study.

Recommendations: See summary recommendation after Question 6.

6. *Question:* What are the practical issues such as test duration, specimen preparation, test variability, and test difficulty for the AMPT?

   Conclusions: The results from the LVDT in the actuator of the AMPT produce similar average results compared with the LVDTs mounted on the middle half of the specimen itself, and use of the actuator LVDT speeds up and simplifies the testing. For rutting, the unconfined RLT test is faster and easier to perform than the RSCH or the confined RLT test. The confined RLT and RSCH tests have similar productivity and difficulty. Variability for the unconfined RLT is less than that of the confined RLT and RSCH because the unconfined RLT results in fewer repetitions to failure at a given temperature than the other two tests, and the variability of repeated load tests typically increases as the number of repetitions to failure increases.

   For fatigue, the DT test is likely to be more expensive and more difficult, and to take the same amount of time as the flexural fatigue test.

   For stiffness master curves, the cost of the dynamic modulus frequency sweep test is likely to be similar to that of the flexural frequency sweep test, the difficulty is likely to be similar, and the time required to complete a frequency sweep is also likely to be similar. Using the dynamic modulus results will require expensive recalibration of current *CalME* mechanistic-empirical models.

   Recommendations:

   - Improve shift factors by additional comparison testing of RSCH and confined and unconfined RLT on same materials and, if results remain promising, then move to the next recommendation; continue comparisons using field (preferable) or rolling wheel-compacted (if field cores are unavailable) RSCH specimens and gyratory-compacted RLT specimens.
   - Once more mixes have been tested, perform sensitivity analysis for *CalME* results for differences between mix by mix versus average shift factors; if results are acceptable, consider use of RLT for development of rutting parameters for ME design along with other factors that will influence risks to successful deployment.

(page blank)

TABLE OF CONTENTS

LIST OF TABLES

LIST OF FIGURES

LIST OF TEST METHODS AND SPECIFICATIONS

AASHTO T 2	Standard Method of Test for Sampling of Aggregates
AASHTO T 11A (wet sieve)	Standard Method of Test for Materials Finer Than 75-µm (No. 200) Sieve in Mineral Aggregates by Washing
AASHTO T 27 (dry sieve)	Standard Method of Test for Sieve Analysis of Fine and Coarse Aggregates
AASHTO Proposed Test Method to be reviewed	Standard Method of Test for Determining the Fracture Energy of Asphalt Mixtures Using the Semi Circular Bend Geometry (SCB)
AASHTO PP3-94	AASHTO PP3-1994 (R 1996) Standard Practice for Preparing Hot Mix (HMA) Specimens by Means of the Rolling Wheel Compactor
AASHTO PP 60	Standard Practice for Preparation of Cylindrical Performance Test Specimens Using the Superpave Gyratory Compactor (SGC)
AASHTO TP 79	Standard Method of Test for Determining the Dynamic Modulus and Flow Number for Hot Mix Asphalt (HMA) Using the Asphalt Mixture Performance Tester (AMPT)
AASHTO TP 107-14	Method Of Test For Determining The Damage Characteristic Curve Of Asphalt Mixtures From Direct Tension Cyclic Fatigue Tests
AASHTO T 166A	Bulk Specific Gravity of Compacted Hot Mix Asphalt Using Saturated Surface‑Dry Specimens
AASHTO T 248	Reducing Samples of Aggregate to Testing Size
AASHTO T 269	Standard Method of Test for Percent Air Voids in Compacted Dense and Open Asphalt Mixtures
AASHTO T 283	Standard Method of Test for Resistance of Compacted Hot Mix Asphalt (HMA) to Moisture-Induced Damage
AASHTO T 312	Standard Method of Test for Preparing and Determining the Density of Hot Mix Asphalt (HMA) Specimens by Means of the Superpave Gyratory Compactor
AASHTO T 320	Standard Method of Test for Determining the Permanent Shear Strain and Stiffness of Asphalt Mixtures Using the Superpave Shear Tester (SST)
AASHTO T 321	Standard Method of Test for Determining the Fatigue Life of Compacted Hot-Mix Asphalt (HMA) Subjected to Repeated Flexural Bending
AASHTO T 324 (Modified)	Standard Method of Test for Hamburg Wheel-Track Testing of Compacted Hot Mix Asphalt (HMA)
CT 371	Method of Test for Resistance of Compacted Bituminous Mixture to Moisture Induced Damage
LLP-AC2	Caltrans – Sample Preparation and Testing for Long-Life Hot Mix Asphalt Pavements

LIST OF ABBREVIATIONS

AASHTO	American Association of State Highway and Transportation Officials
AC%	Asphalt Binder Content Percent
AMPT	Asphalt Mixture Performance Tester
ANOVA	Analysis Of Variance
DM	Dynamic Modulus test
DT	Direct Tension test
ESAL	Equivalent Single Axle Loads
FEI	Fracture Energy Index
FHWA	Federal Highway Administration
FN	Flow Number test
%Gmm	Percent Mixture Density
HMA	Hot mix asphalt
HWTT	Hamburg Wheel-Track Tester
IDT	Indirect Tension test
IQR	Interquartile Range
LLAP	Long-Life Asphalt Pavement
LVDT	Linear Variable Displacement Transducer
ME	Mechanistic-Empirical
MEPDG	Mechanistic-Empirical Pavement Design Guide (now called AASHTOWare Pavement ME Design)
NCAT	National Center for Asphalt Technology
NCHRP	National Cooperative Highway Research Program
NMAS	Nominal Maximum Aggregate Size
OBC	Optimal Binder Content
PAS	Permanent Axial Strain
PM	Polymer-modified (asphalt binder type)
PPRC SPE	Partnered Pavement Research Center Strategic Plan Element
PSS	Permanent Shear Strain
RAP	Reclaimed Asphalt Pavement
RB	Rubberized (asphalt binder type)
RHMA	Rubberized hot mix asphalt
RLT	Repeated Load Triaxial test
RSCH	Repeated Shear Constant Height test, also referred to as RSST (see below)
RSST	Repeated Simple Shear Test
RW	Rolling Wheel Compactor
SCB	Semicircular Bending Test
SGC	Superpave Gyratory Compactor
SHRP	Strategic Highway Research Program
SP	Superpave Design Method
SSP	Specification for Superpave
Superpave	SUperior PERforming asphalt PAVEment
TSR	Tensile Strength Ratio, also referred to as Tensile Strength Retained
UCPRC	University of California Pavement Research Center
VTS	Viscosity Temperature Susceptibility

1 INTRODUCTION

1.1 Background

In 2011, the California Department of Transportation (Caltrans) began implementation of the Superpave mix design procedure for hot mix asphalt (HMA). The Superpave (SUperior PERforming Asphalt PAVEments) system was developed as part of the first Strategic Highway Research Program (SHRP) and was completed in 1992 to "give highway engineers and contractors the tools they need to design asphalt pavements that will perform better under extremes of temperature and heavy traffic loads" *(1).* Most state highway agencies in the U.S. have adopted all or part of Superpave, nearly always with refinements to suit local conditions, practice, and requirements.

In the 1940s Caltrans started using a standard Hveem mix design process for HMA to determine binder contents for conventional dense-graded mixes and later for polymer-modified asphalt mixes. In the 1990s they began to use a modified version of the Hveem method for gap-graded rubberized mixes. However, as of 2013 very few other states were using the Hveem procedure and consequently the equipment used in the tests, specifically the kneading compactor and the Stabilometer, have become increasingly difficult to acquire and maintain. The Hveem method includes the use of successful aggregate gradations developed in the state since the 1930s, which research showed had equal or better performance for both rutting *(2)* and fatigue *(3)* compared with the gradations and the concept of the "restricted zone" originally proposed for use in the Superpave method *(4, 5).* As a result, Caltrans has retained the use of the Hveem gradations, along with some adjustments and considerations regarding the dust proportion in the mix design criteria. Caltrans has also retained a Tensile Strength Ratio test (TSR, California Test 371, similar to AASHTO T 283) to assess moisture sensitivity.

Caltrans is also currently implementing the *CalME* mechanistic-empirical (ME) pavement design method in which asphalt rutting (permanent deformation) models are based on the characterization of rutting behavior under different stresses and temperatures using repeated load tests that were calibrated against the measured rutting performance from thirty-three Heavy Vehicle Simulator (HVS) tests conducted between 1995 and 2007 *(6),* twenty-six sections of the FHWA WesTrack full-scale test track experiment conducted from 1995 to 1997 *(7),* and several sections at the NCAT *(8)* and MnROAD *(9)* test tracks. The repeated load test for rutting used for that calibration was the Repeated Shear Test at Constant Height (RSCH, AASHTO T 320), with the testing done at the time of the HVS or test track experiment. All of the specimens for the RSCH calibration testing were prepared using rolling-wheel compaction, which produced specimens that best matched those made by field compaction in tests carried out using the RSCH during the 1990s *(10).*

Although there were approximately ten laboratories in the U.S. that own RSCH equipment in 2014, there were only two laboratories, at the UCPRC and at Road Science in Oklahoma, known to be routinely using the equipment. Instead, many laboratories are using a new type of equipment called the Asphalt Mixture Performance Tester (AMPT) *(11)* that can also perform an alternate repeated load test for rutting: the Repeated Load Triaxial (RLT) test. By 2014, approximately twenty states and several consultants in the U.S. had purchased an AMPT and were working with it—although it appears that none of them have implemented it yet as part of standard mix design and/or quality assurance. Another difference between the RSCH and the AMPT/RLT is that the RLT uses specimens prepared using the Superpave Gyratory Compactor (SGC) rather than the Hveem compactor. As of 2015 there are provisional AASHTO standards for coring and cutting the SGC specimens for the AMPT/RLT (AASHTO PP 60-11) and for performing dynamic modulus and flow number tests (AASHTO TP 79-11).

The results from the AMPT/RLT were originally proposed for use in finding the flow number (FN), which is defined as the load repetition at which the rate of permanent deformation accumulation accelerates, and is intended to capture the point at which rutting changes from a slowly decreasing rate to rapid acceleration of rutting. But, as was noted in a 2003 report *(12),* the National Cooperative Highway Research Program (NCHRP) Project 9-43 found the repeatability and reproducibility of determination of the flow number from the AMPT/RLT to be problematic. NCHRP Project 9-30A *(13)* also questioned the validity of the flow number in a 2012 report, and provided recommendations for use of the permanent strain versus repetitions relation from the test to assess rutting performance. NCHRP 9-30A also tried to compare RSCH results from rolling wheel-compacted specimens and AMPT/RLT results from SGC-prepared specimens, and did not find a good correlation. Insufficient funding prevented the study from further considering whether the lack of correlation was due to the compaction method or the stress states in the test.

As of 2015, no implemented approach has been adopted for using AMPT/RLT results in mechanistic-empirical (ME) design for rutting, although the NCHRP 9-30A provided recommendations for how to use the AMPT/RLT or the RSCH to produce inputs to the MEPDG software, provided that there is calibration for either approach.

1.2 Overview of Current Superpave Mix Design Procedure and Tests

The Superpave system primarily addresses two pavement distresses: permanent deformation (rutting), which results from inadequate shear strength in the asphalt mix, and low-temperature cracking, which occurs when an asphalt layer shrinks and the tensile stress exceeds the tensile strength. The system consists of three interrelated elements:

- An asphalt binder specification (implemented by Caltrans in 2005)
- A volumetric mix design and analysis system based on gyratory compaction (implementation process began in 2011 with full implementation in 2014)
- Performance-related mix analysis tests and a performance prediction system that includes environmental and performance models. There has been no consistency in national of implementation of this last element, as different states use a variety of tests and performance prediction methods, and a number of states do not using this element at all except for a moisture sensitivity test (AASHTO T 283).

Most states that have adopted Superpave continue to use the TSR test (AASHTO T 283) to assess moisture sensitivity, although there is growing interest in switching to Hamburg Wheel-Track Testing (AASHTO T 324) as it is quicker, reportedly provides more consistent results, and provides visible evidence of the rutting and stripping behavior of the mix.

Fatigue/reflective cracking performance are not assessed in the Superpave mix design. However, longer-term evaluations of roads in a number of states where the Superpave mix design procedure was used indicate that early cracking may be a problem on roads where rutting resistance was the primary focus of the mix design and was addressed through volumetric specifications that are conservative for rutting or included a performance-related test for rutting but not for cracking, approaches that typically lead to relatively low binder contents. Another consequence of lower binder contents is raveling, which leads to poorer riding quality.

An optimal mix design will balance rutting and fatigue-cracking performance by reducing the risk of rutting to an acceptable level, while at the same time maximizing fatigue-cracking performance in order to achieve at least a minimum required cracking performance.

1.3 Problem Statement

The equipment used for Hveem mix designs is becoming obsolete and consequently new test procedures will need to be adopted for asphalt mix designs in California. The new procedures will need to produce mix designs that result in performance (short- [rutting], medium- [moisture sensitivity], and long-term [cracking]) equal to or better than that of mixes designed with the current Hveen mix design procedure. They will also need to be sufficiently versatile (and/or modular) to address initial mix design (empirical and mechanistic-empirical) requirements, job mix formula verification, and quality assurance testing. To help Caltrans develop the new asphalt mix design procedures, Partnered Pavement Research Center Strategic Plan Element 3.18.3 was developed: “Implementation of the Superpave Asphalt Mix Design Procedure in California.”

1.4 Study Objectives and Tasks

The work completed in this project is intended to assess Superpave and other nationally available tests and testing equipment for possible adoption in California. The study considered the following:

- Conventional, rubberized, and polymer-modified binders
- Dense and gap gradations
- Rutting and fatigue/reflective cracking performance, and moisture sensitivity
- Compatibility of test results with ME design and mechanistic specifications such as those used on the four projects of this type completed to date *(14, 15)* or put out to bid in 2011 and 2012 *(16, 17, 18)*

The objectives for the project were completed in two phases, with Phase I Part A comparing Hveem and Superpave mix designs, Phase I Part B assessing the relative rutting performance of the two mix designs and comparing RSCH and AMPT/RLT results, and Phase II comparing other performance-related tests. A breakdown of the tasks taken to complete these objectives is shown below:

Phase I

Part A

1. Completion of a literature review on recent national Superpave mix design and mix design test equipment-related research, including rutting and cracking performance, and moisture sensitivity
2. Creation of a laboratory testing matrix that considers key variables identified in the literature review
3. Collection of aggregates, binders, and current Hveem or rubberized mix designs for them
4. Development of Superpave volumetric mix designs and comparison with current mix designs

Part B

5. Preparation and laboratory testing of RSCH and RLT specimens and analysis of the results
    a. To compare expected rutting resistance of Superpave and Hveem mix designs
    b. To compare results of RSCH and RLT testing
6. Delivery of recommendations for changes in preliminary new mix design procedure
7. Evaluation of comparison of RSCH and RLT results and required changes in *CalME* to use RLT testing to produce design inputs

Phase II

8. Preparation and laboratory testing for different performance-related tests for rutting, fatigue cracking, and moisture sensitivity for possible use in new mix design method
9. Delivery of recommendations for performance-related tests for use in new mix design procedure
10. Preparation of reports documenting the study and study results

The results of Phase I Part A (Tasks 1 through 4) were reported in a previous technical memorandum *(19)*. The results of the remainder of the tasks (5 through 10) are discussed in this report. These results come from the performance-based testing of five Superpave mix designs selected from fifteen Superpave mix designs evaluated in Phase I Part A, and additional testing using a mix sampled in the field.

1.5 Key Questions to Answer in Phase I Part B and Phase II

There are six specific questions for which answers were sought in this research:

1. How is HMA shear test performance, which is related to rutting, affected by changing from the Hveem mix design to the Superpave mix design for the mixes tested?
2. How are the HMA flexural fatigue test and flexural stiffness performance, which are related to cracking, affected by changing from the Hveem mix design to the Superpave mix design for the mixes tested?
3. How do any changes in shear, flexural fatigue, and flexural stiffness test performance affect expected pavement rutting and cracking performance, as evaluated using the *CalME* mechanistic-empirical analysis procedures?
4. Can faster and less expensive tests than shear and flexural fatigue tests be successfully used as surrogates for currently used mechanistic performance-related tests for mix design and quality assurance?
5. Can the Asphalt Mixture Performance Tester's (AMPT) tests for rutting, fatigue, and stiffness be used for ME pavement designs in place of shear, flexural fatigue, and flexural stiffness tests, and can results from one test be converted into results from another?
6. What are the practical issues, such as test duration, specimen preparation, test variability, and test difficulty, for the AMPT?

1.6 Structure and Content of this Report

The report is structured as follows:

- Chapter 2 describes the individual laboratory tests conducted to evaluate mix performance. Brief descriptions of the HMA specimen preparation process are also given.
- Chapter 3 presents the results for all five Superpave mixes with laboratory-produced material for each performance-related test conducted and descriptive analysis of the results.
- Chapter 4 compares the performance-related testing results from the Superpave mix designs and the results from using the same tests on Hveem mix designs for the same mix materials.
- Chapter 5 presents the results of simulated rutting and fatigue-cracking performance of the Hveem and Superpave mix designs based on *CalME* analysis to evaluate the expected effects on field performance of the change in the mix design procedure.
- Chapter 6 presents a summary of testing that looked at the sensitivity of shear and AMPT repeated load triaxial (RLT) test results to compaction method, air-void content, and temperature. This chapter also compares the confined and unconfined approaches for the RLT, and presents the results of initial shift factors for translating RLT results to shear test results for use in existing *CalME* mechanistic-empirical

design and analysis models. This testing was performed using a field sample mix with 25 percent reclaimed asphalt pavement (RAP).

- Chapter 7 gives a comparative analysis of the use of alternative tests as surrogates for currently used mechanistic performance-related (shear and flexure) tests for mix design and quality assurance. This chapter also presents the results of the development of shift factors for translating RLT results to shear test results for the five mixes, and the preliminary recommended shift factors.
- Chapter 8 presents a summary of productivity and practical aspects for AMPT testing and simple tests.
- Chapter 9 summarizes findings, draws conclusions, and makes recommendations based on the results of the Phase II testing.

2 SUMMARY OF PERFORMANCE TESTS

This chapter discusses the performance tests conducted on the five mixes selected for Phase II. The following are the specific performance measures assessed with each of these performance tests:

- Cracking: AMPT tension/compression fatigue (AASHTO TP 79), flexural fatigue (AASHTO T 321), semicircular beam (parameter to be determined), and indirect tensile strength (dry)
- Rutting: Repeated Shear Test at Constant Height (RSCH, AASHTO T 320), AMPT Repeated Load Triaxial (RLT) (AASHTO TP 79, same test setup and operation as the Flow Number although using a different parameter than Flow Number), and Hamburg Wheel-Track Testing (HWTT, AASHTO T 324)
- Stiffness in terms of dynamic modulus: AMPT dynamic modulus (stiffness, AASHTO TP 79) and flexural frequency sweep (AASHTO T 321)
- Moisture sensitivity: Hamburg Wheel-Track Testing (AASHTO T 324) and CT 371 (a version of AASHTO T 283)

Specimens for these tests were prepared using either the rolling-wheel (RW) compactor following the procedures in Caltrans Laboratory Procedure LLP-AC2 *(Sample Preparation and Testing for Long-Life Hot Mix Asphalt Pavements*) *(20)* or the Superpave Gyratory Compactor (SGC). The results from some specimens presented in Chapter 6 were prepared from field-mixed, field-compacted material, in addition to results from specimens prepared using the RW and SGC. Each of these tests and preparation methods is described with more detail below.

2.1 Flexural Beam Testing

Testing conducted on HMA beams consisted of two types of tests, flexural fatigue and flexural frequency sweep, which are both included in the AASHTO T 321 specification. Beam specimens had dimensions of 15 inches length, 2.0 inches height, and 2.5 inches width (381 mm length, 50.8 mm height, 63.5 mm width). Specimens tested for this study were compacted using the RW.

2.1.1 Flexural Fatigue

The principle behind flexural fatigue testing of HMA beams is to apply cyclic loading to maintain the same peak strain in each cycle to beams under third-point loading, to determine the rate at which these beams lose stiffness, and ultimately to find the number of cycles required to reach a prescribed "failure" stiffness. Alternatively, for *CalME* characterization, the full curve of stiffness reduction versus repetitions, referred to as the *fatigue damage* relationship, was used rather than the single parameter for repetitions to a failure stiffness ratio. Both the repetitions to 50 percent loss of stiffness and the damage relationship were considered in this study.

Figure 2.1 shows an example of the fatigue test apparatus, which is housed in an environmental testing chamber to maintain constant temperature during the test. Tests in this project were performed at a constant temperature (20°C) and two levels of strain; 200 με and 400 με for up to 5,000,000 cycles. The loading waveform shape was haversine (Figure 2.2) and the rate was 10 cycles per second (Hz). Specifications are often stated in terms of repetitions to 50 percent loss of stiffness. If beams did not reach 50 percent loss of stiffness by 5,000,000 cycles, which often occurred at the low strain, then an extrapolation process using Three-Stage Weibull analysis developed by Tsai *(21)* was performed to determine the failure cycle. This procedure is included in Reference *(20)*.

Figure 2.1: Flexural beam test apparatus.

2.1.2 Flexural Frequency Sweep

Flexural frequency sweep tests were conducted to measure the stiffness (flexural dynamic modulus) of HMA beams under different loading rates or frequencies. The testing waveform was a sine wave and the loads were applied at frequencies of 15, 10, 5, 2, 1, 0.5, 0.2, 0.1, 0.05, 0.02, and 0.01 Hz and temperatures of 50, 68, and 86ºF (10, 20, 30ºC). In the test, the sine wave was controlled to maintain the same deformation in each cycle. For the testing in this study the sine wave was set to produce a tensile strain at the extreme fiber of the beam of 100 με at 10ºC and 20ºC and 200 με at 30ºC.

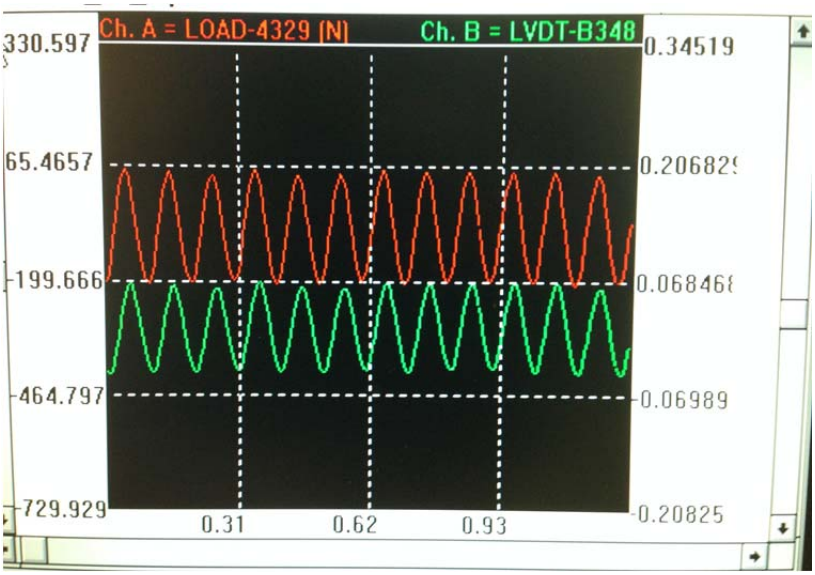

Figure 2.2: Flexural beam test 10 Hz waveform showing load (load) and deformation (LVDT).

Stiffness *master curves* for each mix showing mix stiffness versus *reduced time*, meaning the equivalent frequency at the standard temperature after accounting for the test temperature, were developed from these tests; a master curve for an example mix appears in Figure 2.3. Master curves are used for pavement design to adjust mix stiffness for different pavement temperatures and traffic speeds.

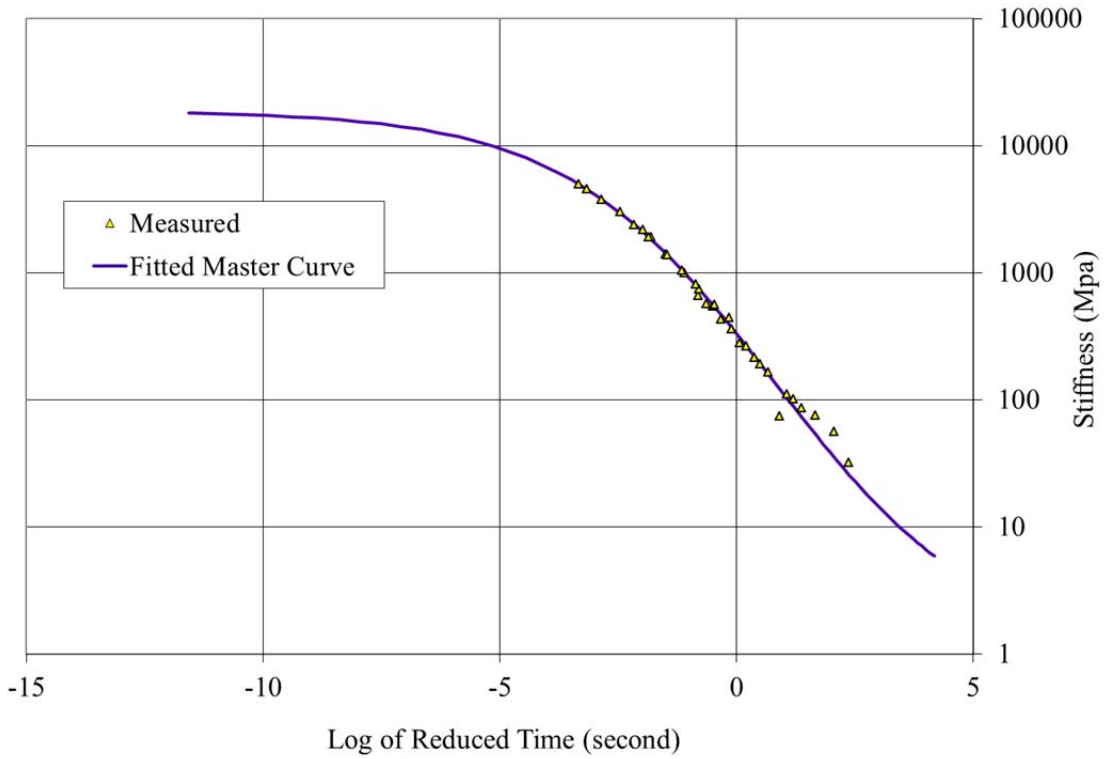

Figure 2.3: Example HMA master curve from frequency sweep testing.

2.2 Repeated Shear Testing at Constant Height (RSCH)

Repeated Shear Testing at Constant Height (RSCH) was conducted on HMA cores following AASHTO T 320 to assess mix shear performance for rutting potential. For this study the RSCH specimens had dimensions of 6 inches diameter and 2.0 inches height (152 mm diameter and 50.8 mm height), although other dimensions can be used. In this testing, the compacted shear cores are subjected to a repeated shear stress while their height is maintained at a constant value. The loading shape was haversine with a loading cycle of 0.7 seconds, which consisted of 0.1 second loading/unloading and a 0.6 second rest. Shear stress peak values of 10.0, 14.3, and 18.6 psi (70 kPa, 100 kPa, and 130 kPa) were used in this study, and the number of cycles to 5 percent permanent shear strain (PSS) and the permanent shear strain at 5,000 cycles were determined. Alternatively, for *CalME* characterization, the full curve of permanent shear strain versus repetitions, referred to as the *permanent deformation damage* relationship, was used rather than the parameter repetitions to 5 percent PSS. Both the individual parameters and the damage relationship were considered in this study.

The simple shear tester is shown in Figure 2.4 and the testing concept is shown in Figure 2.5. A specimen after testing is shown in Figure 2.6; note the permanent strain as evidenced by the "slanted" specimen. Specimens were compacted for this study using the rolling-wheel, except for the results shown in Chapter 6 where results were compared for specimens compacted in the field and using the Superpave gyratory compactor and the rolling-wheel.

Figure 2.4: Simple shear testing machine.

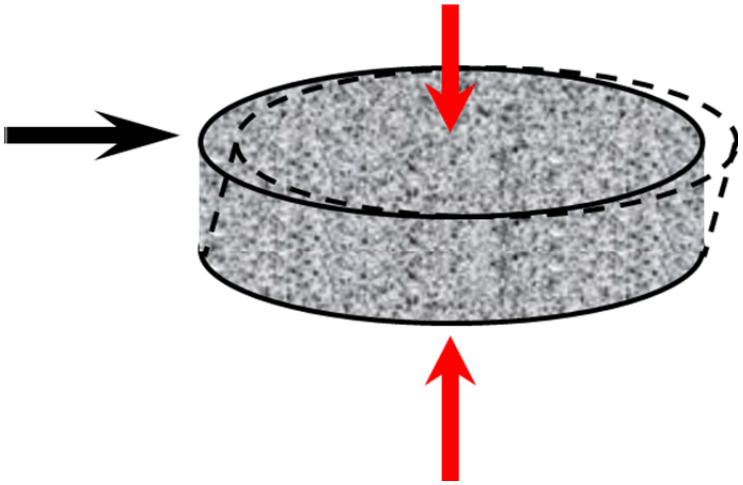

Figure 2.5: Simple shear testing concept.

Figure 2.6: Core following testing.

2.3 Testing with the Asphalt Mixture Performance Tester (AMPT)

The Asphalt Mixture Performance Tester (AMPT) is a repeated load testing machine that can test cylindrical HMA specimens for a variety of properties, including stiffness (dynamic modulus [DM]), permanent deformation using a repeated load triaxial (RLT) configuration, and cyclic compression/tension loading for fatigue (often referred to as *direct tension fatigue testing).* Figure 2.7 shows the AMPT equipment used in this study. Specific details for testing for dynamic modulus and permanent deformation using the RLT configuration are described in the AASHTO TP 79 specification, and compression/tension (referred to as *direct tension* [DT]) procedures are described in a provisional AASHTO TP 107 specification. Further details for each of the test modes are described in the following sections.

For RLT and DM testing, a pair of latex membranes with grease between them is placed at both ends of the specimen to provide slip, which is intended to minimize the lateral confining stresses that would occur if the specimen was bonded to the end caps. For the DT fatigue testing the specimens are glued to the end caps so tension can be transmitted. Specimens for AMPT testing were compacted using the SGC, except for the results shown in Chapter 6, where results are presented for specimens compacted in the field and using the SGC and RW.

Figure 2.7: AMPT machine.

2.3.1 Repeated Load Triaxial (RLT)

In a Repeated Load Triaxial (RLT) test a repeated axial cyclic stress of fixed magnitude, load duration, and cyclic duration is applied to a cylindrical test specimen. Cumulative axial permanent deformation as a function of the number of load cycles is recorded and can be correlated to rutting potential. Tests can be run at different temperatures and varying loads to characterize permanent deformation behavior for different field conditions. The load is applied as a 0.1 second haversine pulse followed by a 0.9 second rest period. While the specimen is subjected to this dynamic cyclic stress, it can also subjected to a static confining stress provided by a pneumatic pressure chamber—this is referred to as the *confined* condition—or the test can be run with no confining stress—this is referred to as the *unconfined* condition. Figure 2.8 shows the stresses when confining pressure is applied.

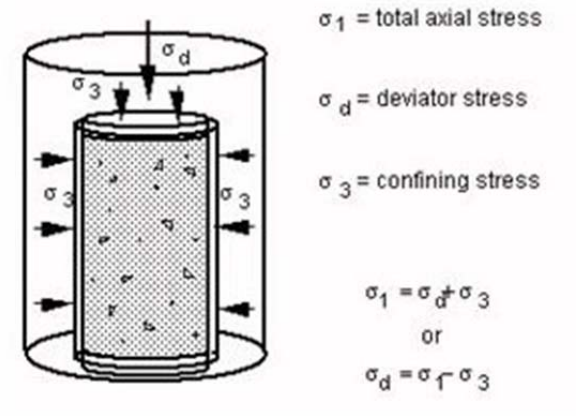

Figure 2.8: Stresses acting on triaxial specimen.
(Note: adapted from Pavement Interactive)

In this project, a 10 psi (69 kPa) confining pressure was used for the confined condition, and specimens were also tested in the unconfined condition. A 70 psi (483 kPa) deviator stress and 4.3 psi (30 kPa) contact stress between the loading head and the specimens were used for all the tests in this study, as recommended in NCHRP Report 719 *(13)*. Tests were run to the lesser of 20,000 cycles or to a permanent axial strain (PAS) of five percent. Specimens were tested at temperatures of 113ºF and 131ºF (45°C and 55°C). A typical RLT test setup is shown in Figure 2.9. A sample chart showing the relationship between PAS and repetitions is shown in Figure 2.10. The dimensions of the AMPT RLT specimens used in this study were 5.9 inches height and 3.9 inches diameter (150 mm height, 100 mm diameter).

The RLT test setup and equipment used in this project were originally developed for the Flow Number test, as described in AASHTO TP 79-13. The *flow number* is defined as "the number of load cycles corresponding to the minimum rate of change of permanent axial strain." The FN test is the same as the RLT performed in this study, except that the relationship of PAS to cycles was used to evaluate the permanent deformation characteristics of the mix rather than the flow number. As discussed in the introduction to this report, the FN was not used as the parameter to evaluate permanent deformation because of difficulty in defining it in the results for many mixes, and because there is doubt that it is a good indicator of permanent deformation resistance.

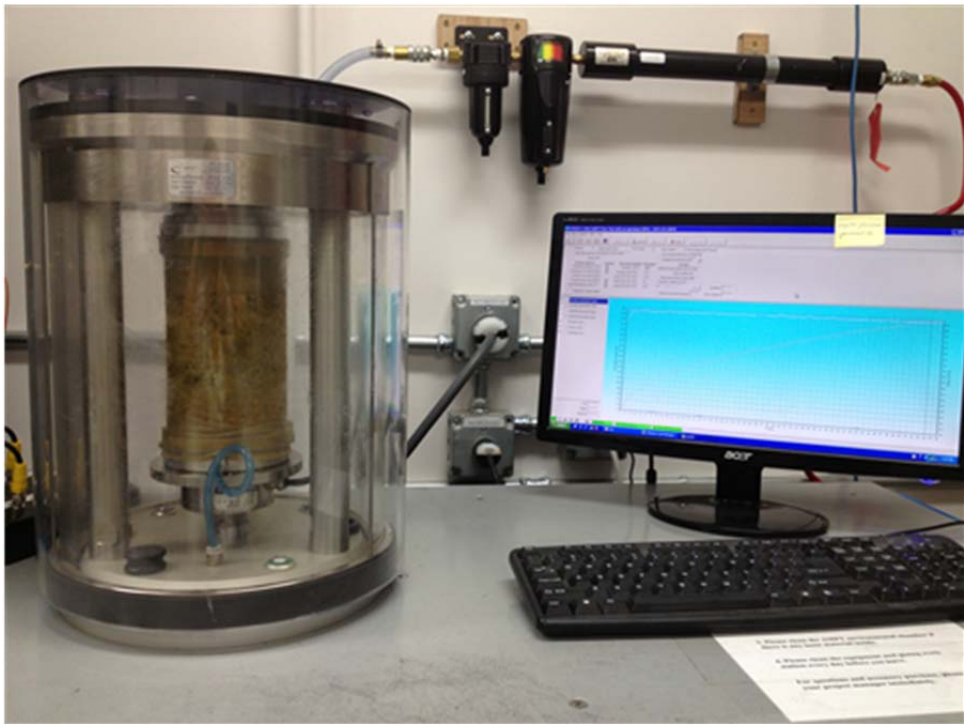

Figure 2.9: AMPT/RLT setup.

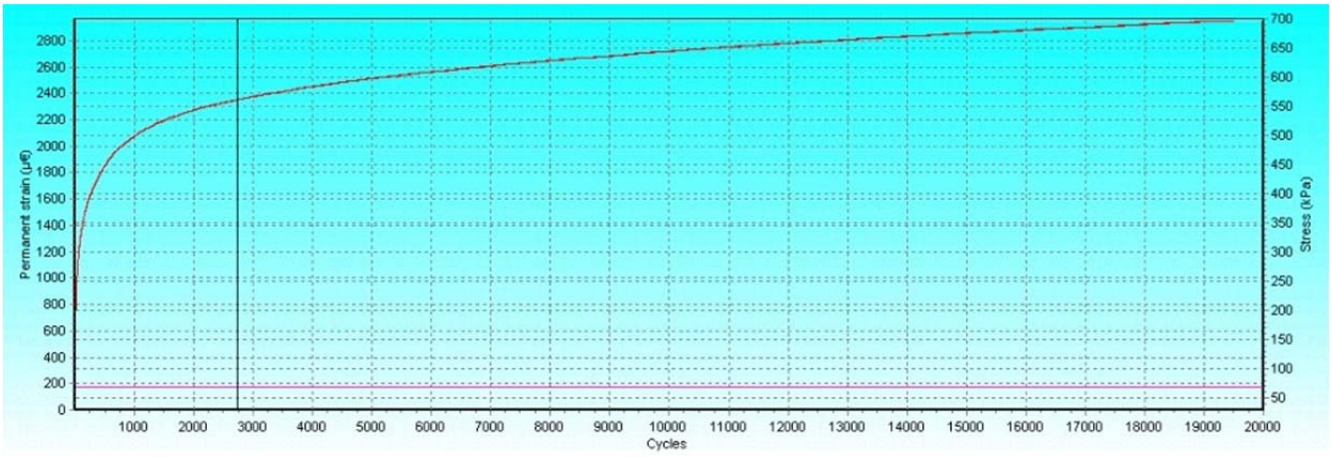

Figure 2.10: Sample output chart from AMPT/RLT showing permanent axial strain (PAS) versus cycles.

2.3.2 Dynamic Modulus (DM)

In the Dynamic Modulus (DM) test with the AMPT, an asphalt concrete specimen at a specified temperature is subjected to sinusoidal, stress-controlled compressive loading. A typical dynamic modulus test setup is shown in Figure 2.11. Both the applied stress and the resulting axial strain are recorded with time, as shown schematically in Figure 2.12. A difference in the specimen setup for the AMPT between RLT and DM testing is the use of three axial linear variable displacement transducers (LVDTs) mounted on the middle half of the specimen for the DM test, while axial strain is measured across the entire length of the specimen using an LVDT mounted on

the top cap for the RLT setup. Dimensions for AMPT DM specimens used in this study were 5.1 inches height and 3.9 inches diameter (130 mm height and 100 mm diameter).

Dynamic modulus is defined as the peak stress divided by the peak strain. It is the overall stiffness of the asphalt concrete mixture at a particular test temperature and loading frequency. Two replicates of each mix were tested at temperatures of 4.4, 21.1, 37.8 and 54.5°C (40, 70, 100, 130°F) for a frequency sequence of 25, 10, 5, 1, 0.5, and 0.1 Hz. The test was run without confining stress and the deviator stress was controlled by the software to maintain an axial peak-to-peak strain of 75 to 125 microstrain.

Figure 2.11: AMPT testing setup for HMA dynamic modulus with axial LVDTs mounted on the specimen.

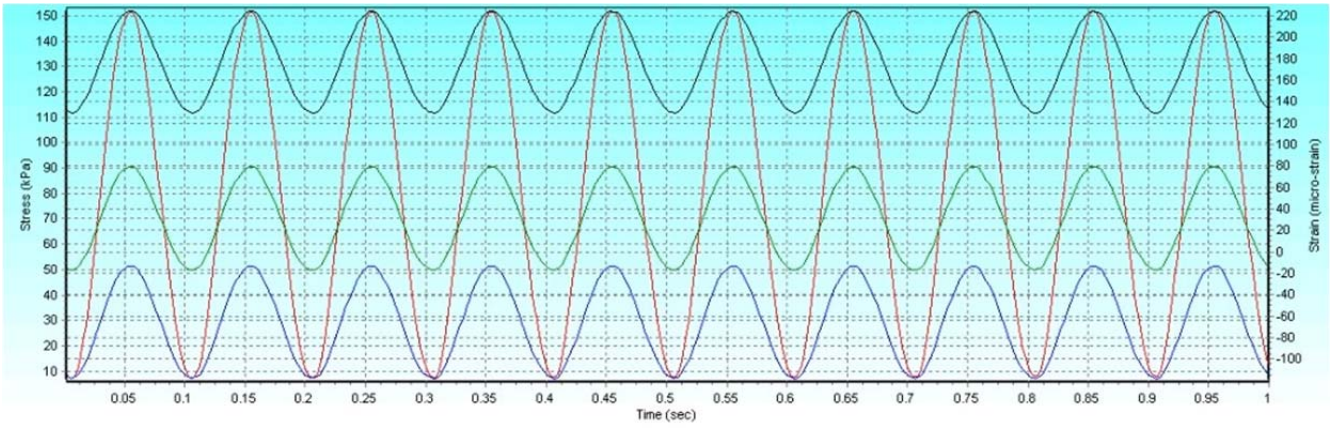

Figure 2.12: Sample output chart from AMPT dynamic modulus test showing stress and strain versus time.

2.3.3 Compression/Tension Fatigue (DT)

The test apparatus for the DT test, shown in Figure 2.13, was different from that used for the DM and RLT tests. The fatigue test consists of two parts: first, a dynamic modulus fingerprint test to estimate the stiffness of the specimen and then a cyclic fatigue test. The test process is controlled by the *S-VECD fatigue* program in the equipment software.

The test is run with a 10 Hz and 200 microstrain (peak to peak) waveform at 20°C. Tests were set to stop at 200,000 repetitions. Figure 2.14 shows the output charts from a typical fatigue test. Dimensions for AMPT DT specimens used in this study had 5.1 inches height and 3.9 inches diameter (150 mm height and 100 mm diameter).

Figure 2.13: AMPT direct tension fatigue test specimen and end caps (end caps glued to specimen).

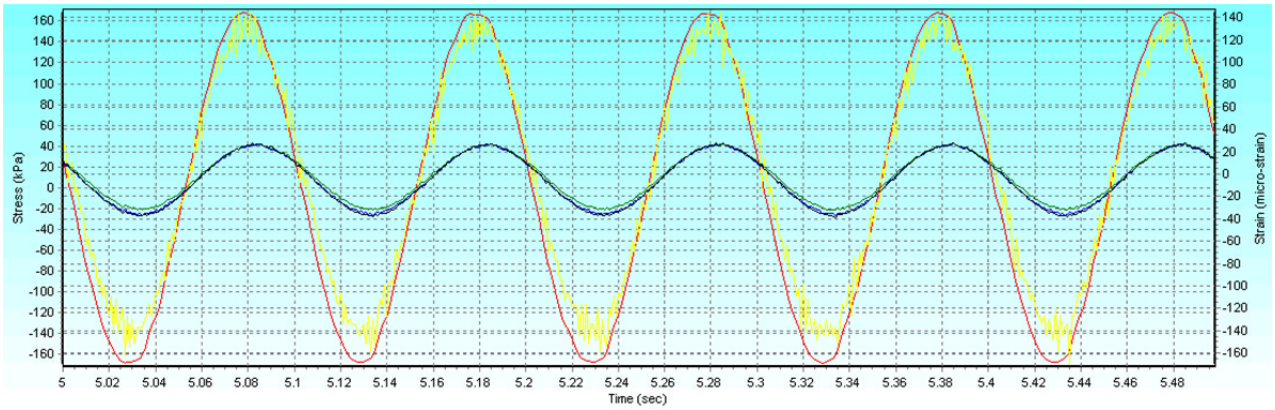

(a) Dynamic modulus fingerprint test output

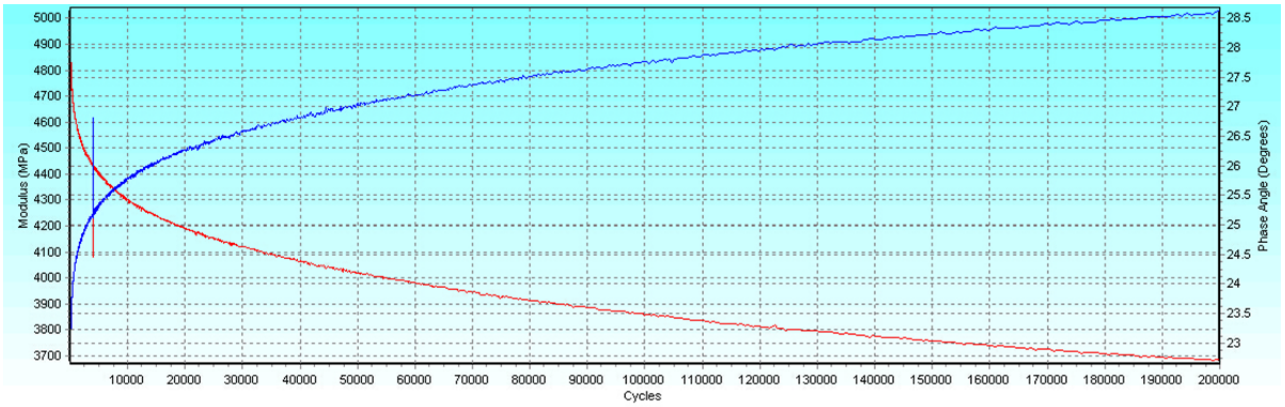

(b) S-VECD fatigue test output

Figure 2.14: Sample output chart from AMPT direct tension fatigue test.

2.4 Hamburg Wheel-Track Testing (HWTT)

Hamburg Wheel-Track Testing (HWTT) was used to assess mix rutting and moisture sensitivity performance. The test was run following AASHTO T 324. In this test, a 2 inch (52 mm) wide, 158 lb (77 kg) steel wheel is passed over HMA specimens submerged in 122°F (50°C) water for up to 20,000 passes (both directions). The HWTT is shown in Figure 2.15 and a typical specimen following testing is shown in Figure 2.16. Rut depths on the specimen were continually measured and both the rate of rutting and maximum rutting are recorded as test results. For data analysis, the depth versus number of cycles was plotted and the slope(s) of the curve were determined. In some mixes it has been observed that there is a bend (inflection point) at which the mix changes performance from the slow rut progression associated with rutting (creep slope) to the rapid rut progression associated with moisture damage (stripping slope). This idealized behavior is shown in Figure 2.17. Many mixes, including all of the mixes in this study, do not exhibit this behavior. Specimens were compacted using the SGC.

Figure 2.15: Hamburg Wheel-Track Tester.

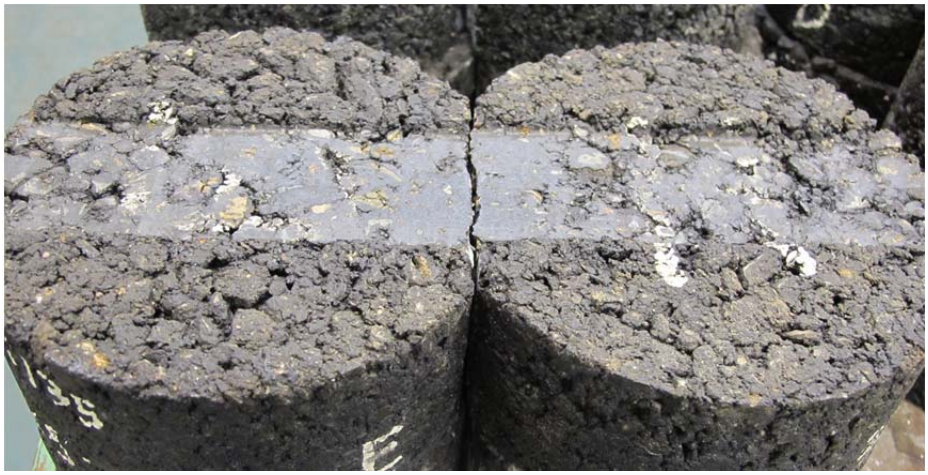

Figure 2.16: HMA cores following HWTT testing.

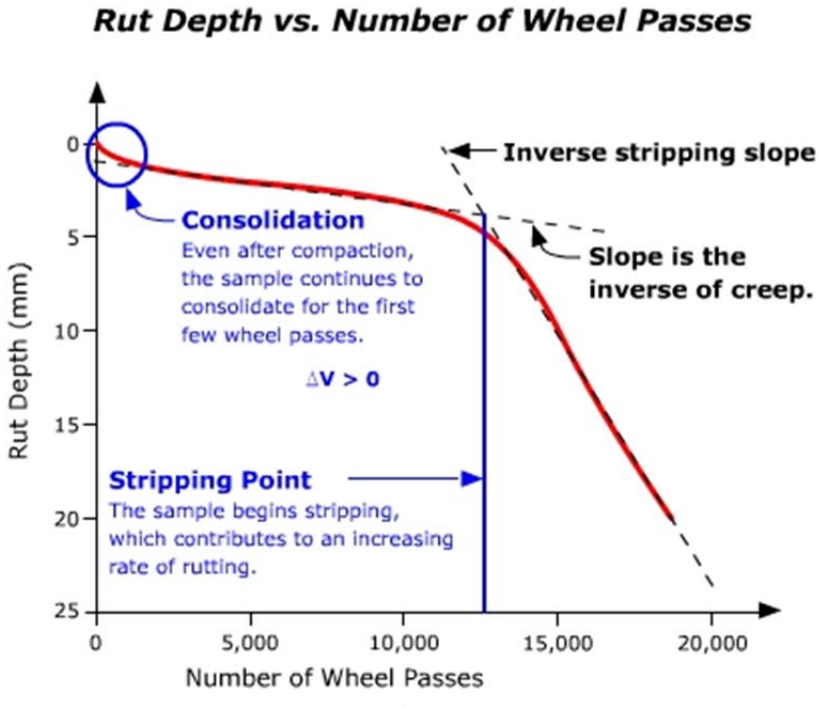

Figure 2.17: Idealized Hamburg Wheel-Track Test performance.
(Note: adapted from *Pavement Interactive)*

2.5 Tensile Strength Ratio (TSR)/Indirect Tensile Strength (IDT)

Moisture sensitivity was evaluated using the indirect tensile strength (IDT) apparatus. Both as-compacted (dry) and after conditioning (wet) specimens were tested following AASHTO T 283 in order to calculate the tensile strength ratio (TSR). The same apparatus was used to also measure indirect tensile strength on dry specimens for comparison with other cracking tests.

For these tests, specimens were compacted to 6 inches (150 mm) in diameter and 3.75 inches (95 mm) in height. Specimens were compacted using the SGC. The conditioning of the wet specimens consisted of partially saturating them, followed by moisture and freeze-thaw cycling per the AASHTO specification. Both sets of specimens were loaded diametrically at a constant rate of deformation, which resulted in an increasing tensile load on the specimen perpendicular to the direction of load, until the specimen failed in tension. The test apparatus is shown in Figure 2.18. An unconditioned specimen that broke in half after testing and exhibited fractured aggregates appears in Figure 2.19.

Caltrans specifications as of 2013 require that a mix specimen have a tensile strength ratio (TSR, ratio of conditioned strength to unconditioned strength) of 80 percent and that if this criterion is not met, the specimen must be treated. These Caltrans specifications differ somewhat from AASHTO T 283 in terms of the number of required replicates and in other details. To accommodate these differences, Caltrans has begun to consider eliminating the TSR from the specification and instead to specify minimum requirements for conditioned and unconditioned strength.

Figure 2.18 Indirect Tensile Strength (IDT) test device and specimen.

Figure 2.19 Post-test IDT specimen exhibiting fractured aggregate.

2.6 Semicircular Beam Test (SCB)

The Semicircular Beam (SCB) Test is a relatively new test that is being developed to quickly assess the fracture properties of HMA *(22, 23, 24).* Although an official standard procedure has not been developed yet, there are several references, including an AASHTO draft procedure, that contributed to the equipment setup and test procedure of this experiment. The test apparatus used is shown in Figure 2.20. HMA specimens that are 6 inches (150 mm) in diameter and 2.5 inches (63.5 mm) in height were compacted with the Superpave Gyratory Compactor and cut in half across the diameter. A 1 inch (25 mm) notch was cut in the center of the flat specimen face, perpendicular to it. At the center of that face, two square metal pieces with knife edges facing the notch were then glued to the specimen, 0.39 inches (10 mm) apart. Next, an LVDT was clipped to the metal pieces to monitor the notch opening.

After the specimen was turned onto its flat face within the test apparatus, with support on both sides of the notch, loading was applied on the center of the round face. During the test, loading was continually applied on the specimen to force the notch opening to crack at a constant rate of 3.9 (10^{-5}) inches per second (0.01 mm per second). Photos of test specimens pre- and post-testing are shown in Figure 2.21.

A graph of load versus vertical (load line) displacement was generated for each of the specimens tested. *Load line displacement* is the displacement measured in the direction (vertical) of the load application. An example load versus load line displacement graph is shown in Figure 2.22.

Three cracking properties were calculated and analyzed from the load displacement curve for each test. These properties are defined as *(25):*

- ***Secant Stiffness, S***: The slope of load versus deformation measured from the origin to the peak load.

$$S = \frac{\Delta y}{\Delta x} = \frac{Peak\ load}{Vertical\ deformation\ at\ Peak\ load}$$

- ***Fracture Energy, G_f***: The energy required to create a unit surface area of work. It is related to the work of fracture, which is the area under the curve in the generated graph.

$$G_f = \frac{W_f}{A_{lig}} = \frac{Work\ of\ Fracture}{Ligament\ Area} = \frac{Area\ under\ the\ P-u\ curve}{Ligament\ Area}$$

where:
$G_f = fracture\ energy\ (J/m^2)$
$W_f = work\ of\ fracture\ (J) = \int Pdu$
$P = applied\ load\ (N)$
$u = load\ line\ displacement\ (m)$
$A_{lig} = ligament\ area\ (m^2) = (r-a) \times t$
$r = specimen\ radius\ (m)$
$a = notch\ length\ (m)$
$t = specimen\ thickness\ (m)$

- ***Fracture toughness, K_{IC}***: A stress intensity factor at the peak load

$$K_{IC} = Y \times \frac{P_{peak}\sqrt{\pi a}}{2rt} \; where\; Y\; is\; normalized\; stress\; insensity\; factor$$

Figure 2.23 shows an illustration of secant stiffness (S) and work of fracture (W_f).

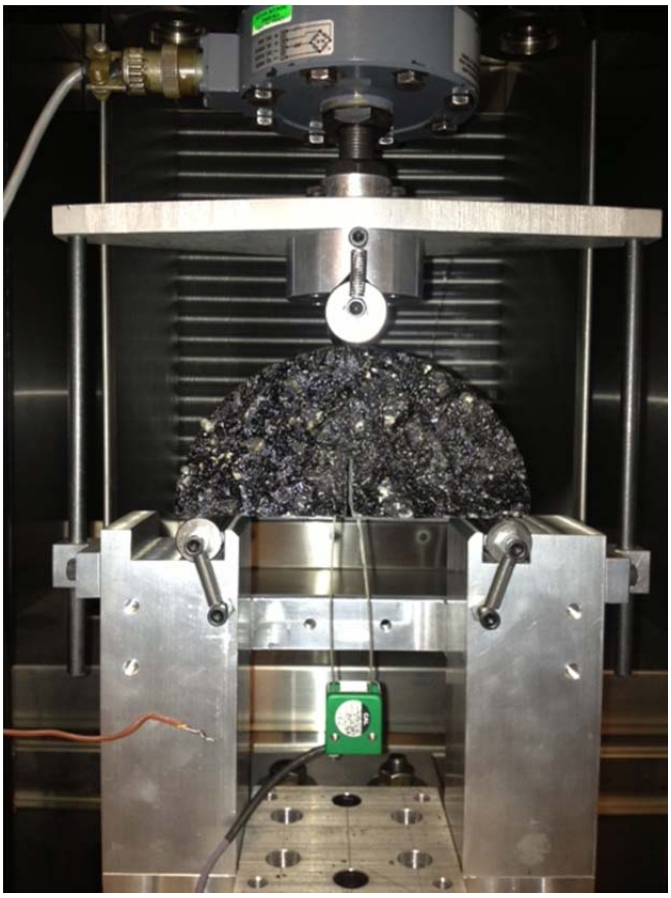

Figure 2.20: SCB test apparatus with specimen under test.

Figure 2.21: Semicircular beam (SCB) specimens before (top) and after (bottom) testing.

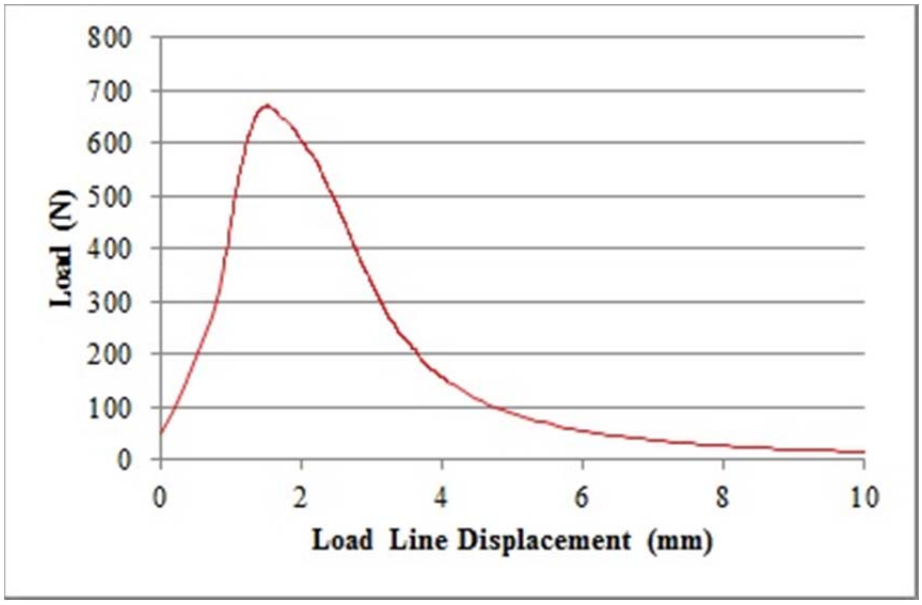

Figure 2.22: SCB actual load versus displacement example plot.

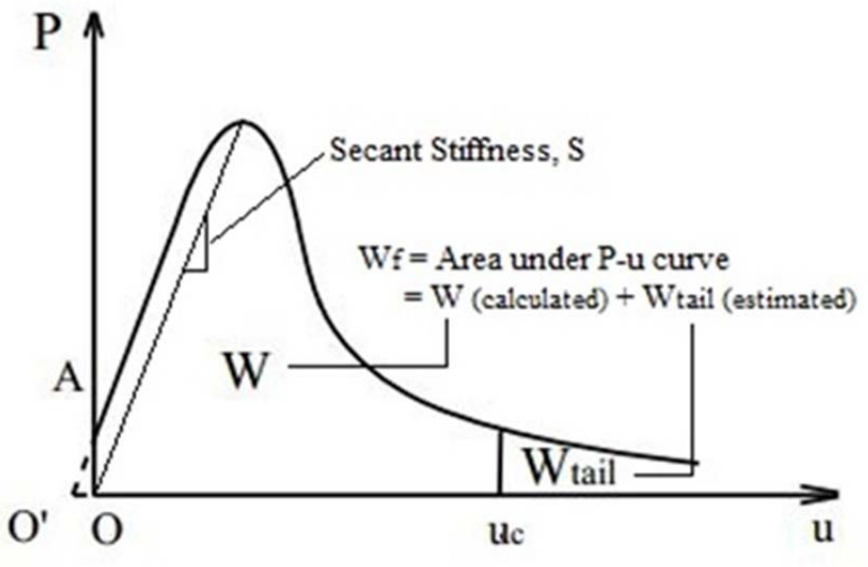

Figure 2.23: SCB performance parameter explanations *(25).*

2.7 HMA Mix Designs and Specimen Preparation

2.7.1 Batching, Mixing, and Short-Term Oven Aging

In Phase I, fifteen Hveem HMA mix designs selected from throughout California were prepared following draft Caltrans Superpave mix design procedures. In consultation with the Chief of the Office of Roadway Material Testing, Materials and Engineering Services, five mixes were selected for performance-related testing in Phase II. Table 2.1 shows the basic information for the Hveem and Superpave mix designs tested in Phase II. More details regarding the mix designs can be found in the Phase I technical memorandum *(19).*

The materials and preparation of specimens to evaluate the effects of testing conditions on RSCH and AMPT RLT results are discussed in Section 2.7.4.

For the Phase I mixes tested in Phase II, HMA specimens were produced from raw aggregates supplied to UCPRC by aggregate producers and with binder sourced from refineries. Aggregates were sieved, graded, and reblended to match the Superpave mix design from Phase I and to match the original Hveem mix design supplied by the mix producer. Binder contents used were those developed from Phase I (Table 2.1). Prior to producing aggregate batches for mixing, a sieve analysis was performed according to AASHTO T 11A (wet sieve) and AASHTO T 27 (dry sieve) to be sure that the target gradation was being produced. Aggregate batches corresponding to the appropriate specimen sizes for each test were mixed with heated binder and compacted by either the RW or SGC.

Mixing and compaction temperatures were determined from the temperature-viscosity charts provided by the binder supplier for each binder grade and type. A list of mixing, short-term oven-aging, and compaction temperatures is shown in Table 2.2.

The aggregate temperature was set 15°C higher than the binder-mixing temperature for neat binders as recommended in Asphalt Institute publication SP-2 *(26).* For polymer-modified and rubber-modified mixes, the aggregate was heated to the same temperature, which was determined from binder viscosity. After mixing, all mixtures were subjected to short-term oven-aging at 135°C for four hours *(26).*

Three additional plant-produced mixes that were not part of Phase I were added to the experiment after the initial evaluation of performance-related test results for the five Phase I mixes—designated Mixes A, B, I, J, and N—because it was difficult to compare results from the different tests with only five mixes. The additional mixes were designated Mixes R, S1, and S2. Mix R was a dense-graded mix with alluvial aggregate and a PG 64-16 asphalt binder. Mix S1 was a dense-graded mix with alluvial aggregate, 15 percent RAP, and a PG 64-28PM asphalt binder. Mix S2 was a dense-graded mix with alluvial aggregate, 25 percent RAP, and a PG 64-16 asphalt binder.

Fatigue, RSCH, and flexural stiffness results for the three additional mixes were available from another Caltrans/UCPRC study. Specimens were prepared with the three additional mixes for each of the other performance-related tests compared in Chapter 7 using plant-produced mix sampled during construction and Superpave gyratory compaction. Performance-related test results for the three additional mixes are included in the appendices.

Table 2.1: Superpave Phase II Mix Information *(19)*

Binder Type	Mix	Binder	Gradation	Aggregate Type	Hveem Design OBC (TWM)	SP Design OBC (TMW)	Hveem Design Air-Void Content	SP Design Air-Void Content	OBC Change (TWM)	Hveem Design Dust Proportion	SP Design Dust Proportion	Hveem VMA	SP VMA	Hveem VFA	SP VFA
Neat (Unmodified)	**A**	Refinery 1 PG 64-16	¾ inch Dense	Alluvial	4.8	5.2	4.0	4.0	+0.4	1.1	1.2	15.5	15.5	74.4	74.9
	B	Refinery 2 PG 64-16	¾ inch Dense	Basalt	4.9	5.9	4.0	4.5	+1.0	1.0	0.8	13.6	18.5	70.9	74.9
Rubber-modified	**I**	Refinery 2 PG 64-16 Rubber	½ inch Gap	Basalt	7.4	7.5	4.5	4.0	+0.1	0.5	1.0	19.1	18.7	76.0	78.8
	J	Refinery 3 PG 64-16 Rubber	¾ inch Gap	Granite	6.7	8.1	5.4	4.0	+1.4	0.5	1.0	18.8	18.7	71.3	78.8
Polymer-modified	**N**	Refinery 3 PG 64-28 PM	1 inch Dense	Granite	4.8	6.0	5.3	4.3	+1.2	0.7	1.0	15.1	17.6	64.5	74.9

Notes:

OBC is the Optimum Binder Content.

TWM is the Total Weight of Mix which is the basis for the percent binder.

Table 2.2: Phase II Materials Mixing and Compaction Temperatures

Binder Type	Mix Name	Mixing Temperature °F (°C) (Binder/Aggregate)	Short-Term Oven-Aging Temperature °F (°C)	Compaction Temperature °F (°C)
Neat (Unmodified)	A	293/320 (145/160)	275 (135)	284 (140)
	B	293/320 (145/160)	275 (135)	284 (140)
Rubber-modified	I	338/338 (170/170)	275 (135)	325 (163)
	J	338/338 (170/170)	275 (135)	325 (163)
Polymer-modified	N	331/331 (166/166)	275 (135)	302 (150)

2.7.2 Superpave Gyratory Compaction

The equipment used for SGC compaction was manufactured by the Pine Instrument Company. SGC specimens were produced following AASHTO T 312. The mass of HMA expected to produce the target air-void content was placed into the SGC and the machine was set to compact to a given height, depending on the specimen being made. Adjustments were made to the HMA weight placed in the mold if the desired air-void content was not achieved.

2.7.3 Rolling-Wheel Compaction

Rolling-wheel compaction was performed by passing a steel-wheel compactor back and forth over HMA placed in a metal ingot mold. The mix weight was calculated based on the volume of the mold and the desired air-void content of the specimens, and the mix was rolled until it was flush with the mold's surface to achieve the desired volume. Adjustments were made to the HMA weight placed in the mold if the desired air-void content was not achieved. The compaction roller and mold are shown in Figure 2.24. Caltrans specification LLP-AC2 and AASHTO PP3-94 describe this process in detail. Cores, beams, and AMPT specimens were cut from the large compacted HMA *ingots* as is shown in Figure 2.25.

2.7.4 Specimen Production for AMPT–RSCH Study

Specimens for this experiment were prepared using plant-mixed material from the I-5 Red Bluff Long-Life Asphalt project paved in 2012. The HMA material taken from this project included field cores and loose mix. The loose mix was used to prepare the following types of specimens using the RW and SGC:

- Field-mixed, field-compacted cores for RSCH and AMPT RLT
- Field-mixed, lab-compacted specimens prepared using SGC for RSCH and AMPT RLT
- Field-mixed, lab-compacted specimens prepared using RW for RSCH
- Field-mixed, lab-compacted specimens prepared using RW double lift for AMPT RLT

Figure 2.24: HMA specimen production by rolling-wheel compaction.

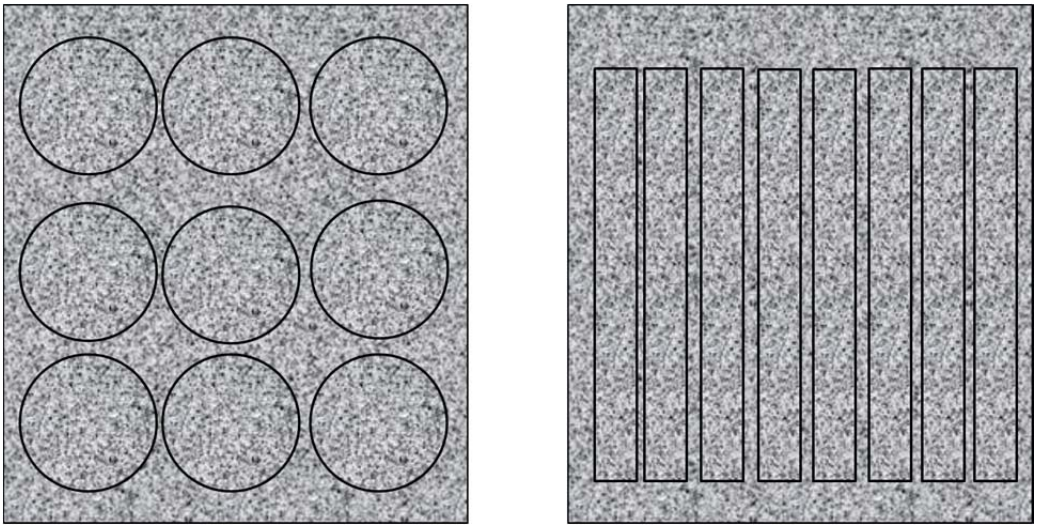

Figure 2.25: HMA specimen pattern for cutting cores and beams from compacted ingots.

Mix for the SGC and RW specimens was sampled at random locations during the construction of the project. Similarly, the field cores were randomly sampled as part of quality assurance for the project. Therefore, the variability of the results includes the variation of the mix in the field for the SGC and RW specimens, and of mix and field compaction for a given air-void content for the field cores.

Details of this mix design and the mix design process are given in Reference *(16).* Aggregates for all specimens were prepared from the Knife River quarry near Red Bluff, California. The virgin aggregate samples contained crushed granite rock, sand, and dust. The aggregate structure was dense-graded with a nominal maximum aggregate size of ¾ inch. The mix contained 25 percent RAP and 1.2 percent lime (based on the weight of the virgin aggregate) added using the lime marination process. The asphalt binder was a PG 64-16 conventional binder sourced from the Valero Refinery in Benicia, California. The asphalt content was 5.38 percent by weight of virgin aggregate plus lime. The mix design was prepared following the contractor's processes, and was required to meet RSCH, flexural fatigue, flexural stiffness, and other properties specified by Caltrans based on the mechanical-empirical pavement structural design.

The loose mix was oven-heated for two hours at 145°C prior to compaction using the RW and SGC. Compaction using the RW and SGC followed the procedures described previously. The SGC compaction parameters are shown in Table 2.3. Specimens were cut and/or cored to the final test specimen dimensions in the laboratory.

Table 2.3: Specimen Preparation Parameters

Specimen Preparation Parameters	
	E* / Flow Number
Target Air-void (via SSD*)	3%± 0.6%, 5%± 0.6%, 7% ± 0.6%
Gyratory compaction parameters	Pressure: 600 kPa
	Angle (internal): 1.16
	Mode: Height control
Compacted specimen diameter	150 mm
Compacted specimen height	170 mm
Cut specimen diameter	100 mm to 104 mm
Cut specimen height	147.5 mm to 152.5 mm
Standard Deviation of sample diameter	≤ 0.5 mm
End Flatness	≤ 0.5 mm
End perpendicularity	≤ 1.0 mm

*: SSD: saturated-surface-dry

AMPT RLT specimens prepared using the RW in the laboratory were compacted in a two-lift ingot mold. The first 4 inch high (100 mm) lift was compacted, and then a second mold was aligned and bolted to the lower mold. The assembly process took approximately five minutes to complete. The surface of the first lift was lightly scarified to facilitate bonding and the material for the second lift was placed on top. The top lift was then

compacted until the HMA was flush with the surface of the second mold to produce a specimen with a height of 8 inches (200 mm).

Field-compacted specimens were taken by extraction of 6 inch (152 mm) diameter full-depth cores with a mobile coring rig, which were then cut to test specimen dimensions by sawing in the laboratory.

Laboratory-compacted specimens were compacted to achieve three air-void contents, 3, 5, and 7 percent, and field cores were selected to meet the same criteria. Actual air-void contents were determined by the saturated-surface-dry (SSD) method according to AASHTO T 166A. Any specimen that did not meet the ±0.6% allowance of each target air-void was discarded.

(page blank)

3 TEST RESULTS FOR FIVE SUPERPAVE MIXES

3.1 Test Plan for Five Superpave Mixes

The factorial for Phase II testing for the five Superpave mixes selected from the Phase I experiment is shown in Table 3.1. Specific testing parameters for each test in Phase II are shown in Table 3.2.

Table 3.1: Phase II Number of Factor Levels and Specimens for Testing of Each Mix

	Compaction Method (Rolling Wheel—RW) (Superpave Gyratory—SGC)	Binder Contents	Temperatures	Replicates	Stress Strain Test Conditions	Number of Mixes	Total per Mix	Total
T 320 Shear RSCH RW	RW	2	2	3	1	5	12	60
T 321 Fatigue	RW	1	1	3	2	5	12	60
T 321 Fatigue Frequency Sweep	RW	1	1	2	1	5	4	20
AMPT Repeated Load Triaxial Confined	SGC	1	2	3	2	5	24	120
AMPT Dynamic Modulus	SGC	1	1	2	1	5	4	20
AMPT Fatigue	SGC	1	1	2	1	5	4	20
T 324 Hamburg Wheel-Track Test	SGC	1	1	2	1	5	4	20
T 283 IDT	SGC	1	1	3	2	5	12	60
SCB	SGC	1	1	3	1	5	6	30

Table 3.2: Specimen and Testing Parameters for Phase II

Test Type	Asphalt Binder Content and Dust Proportion	Air-Void Content	Test Variables
Beam Fatigue	1 OBC Superpave	6±0.5%	1 temperature (20°C); 2 strain levels (200 and 400 microstrain); 3 replicates
Beam Flexural Frequency Sweep	1 OBC Superpave	6±0.5%	3 temperatures (10, 20, 30°C); 1 strain level (100 microstrain at 10, 20ºC; 200 microstrain at 30ºC); 1 replicate
RSCH	2 OBC (Hveem and SGC)	3±0.5%	2 temperatures (45, 55°C), 1 stress level (70 kPa), 3 replicates
HWTT	1 OBC Superpave	7±1%	1 temperature (50°C); 1 bath condition (with water bath); 2 replicates
AMPT Repeated Load Triaxial (RLT)	1 OBC Superpave	4 or 7 ±1%	2 temperatures (45, 55°C); 1 deviator stress (70 psi [483 kPa]; 10 psi [69 kPa] confinement for confined test); 3 replicates
AMPT Direct Tension (DT)	1 OBC Superpave	7 ±1%	1 temperature (20°C); unconfined; 2 replicates
AMPT Dynamic Modulus (DM)	1 OBC Superpave	7±1%	1 temperature sequence (4, 21, 38, 55°C); 1 frequency sequence (25, 10, 5, 1, 0.5, 0.1 Hz); 1 stress level (deviator stress controlled by software to get 75 to 125 microstrain peak to peak axial strain); 2 replicates
SCB	1 OBC Superpave	6±0.5%	1 temperature (20°C), 6 replicates
CT 371 (T 283) IDT	1 OBC Superpave	7±1%	1 temperature (25°C); conditioned and dry conditions; 3 replicates

3.2 Flexural Fatigue and Flexural Frequency Sweep (AASHTO T 321)

3.2.1 Flexural Fatigue

Figure 3.1 shows the results of flexural fatigue tests at 200 microstrain. It can be seen that Mix A with a PG 64-16 binder from one source has a much higher initial stiffness than Mix B, which also has a conventional PG 64-16 binder but from another source. The two mixes have different aggregate sources; however, most of the difference in stiffness is from the binder rather than the aggregate. The rubberized mixes (Mixes I and J) have similar initial stiffnesses and the polymer-modified mix (Mix N) has the lowest initial stiffness, approximately one third that of Mix A. It can also be seen in the figure that the *rate of damage,* defined as loss of stiffness with repetitions, is highest for Mixes A and B with conventional binders, least for Mix N with the polymer-modified binder, and in between these extremes for the two rubberized binder mixes.

Figure 3.2 shows the same flexural fatigue data plotted in terms of *stiffness ratio,* which is the ratio of the stiffness at each repetition divided by the initial stiffness. The initial stiffness is defined as that occurring at the 50^{th} repetition. The results show that after approximately five million repetitions the average results for all of the mixes did not reach 50 percent loss of stiffness (stiffness ratio of 0.5). The relative rates of damage can also be seen on this normalized scale.

Figure 3.3 and Figure 3.4 show similar results for the five mixes at 400 microstrain. The relative performance of the five mixes is similar, although the damage rate is much faster as expected for the higher strain. In Figure 3.4 it can be seen that the two conventional PG 64-16 mixes (Mixes A and B) have a faster rate of damage after reaching a stiffness ratio of approximately 0.7 to 0.8, indicating that microcracks may be forming and propagating. On the other hand, the two rubberized mixes and the polymer-modified mix do not have an abrupt increase in their damage rate, indicating a slower rate of microcrack propagation.

Detailed results for each mix are presented in the appendices.

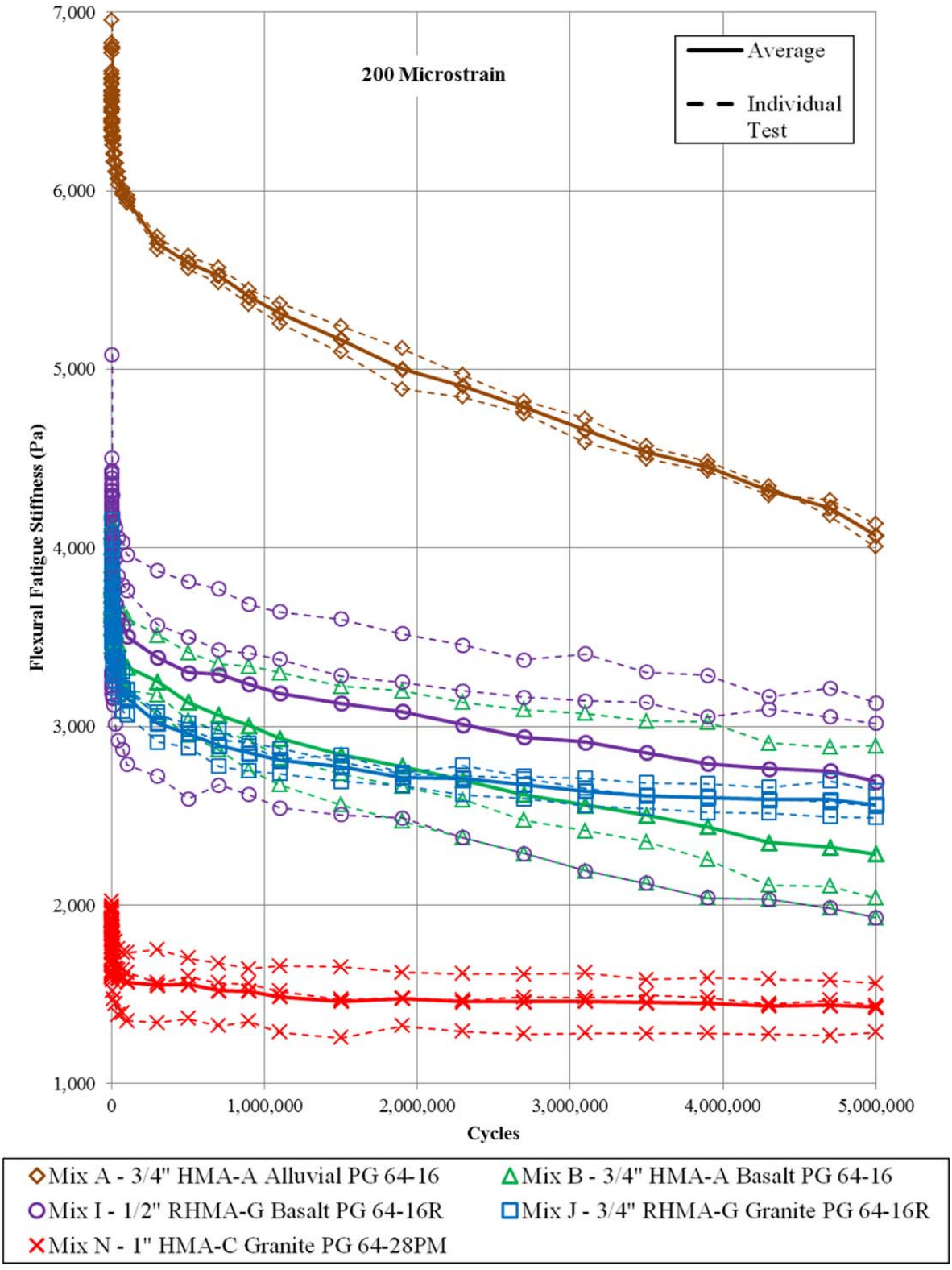

Figure 3.1: Comparison of flexural fatigue stiffness versus cycles (individual 200 microstrain tests with mix averages).

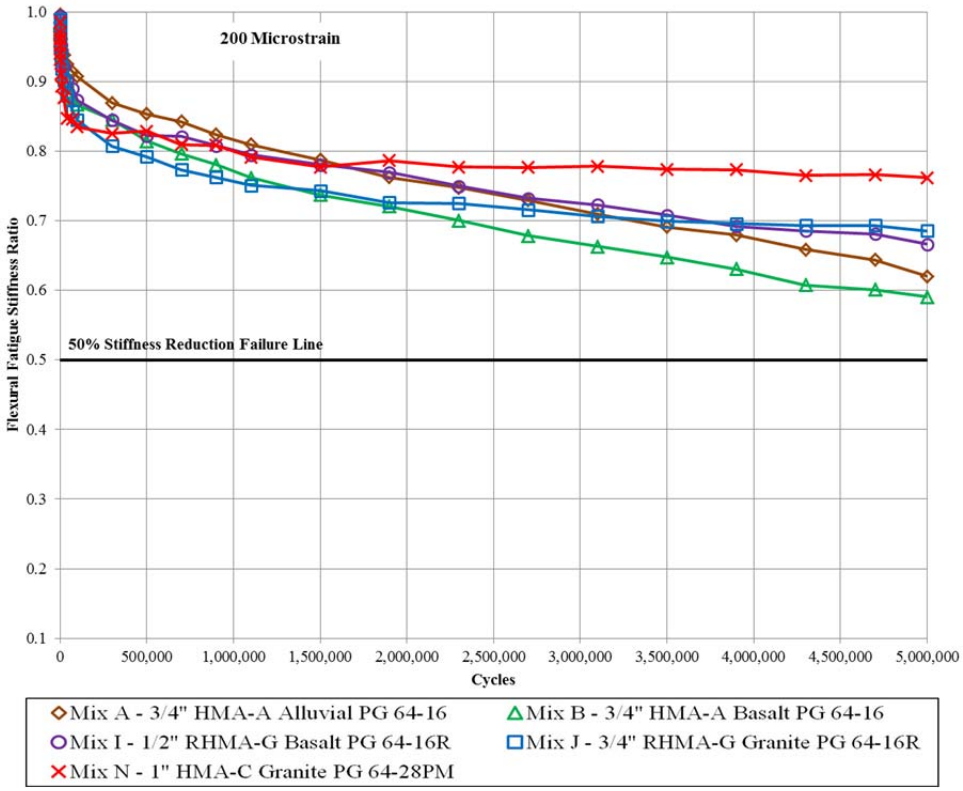

Figure 3.2: Comparison of flexural fatigue stiffness ratio versus cycles (200 microstrain test with mix averages).

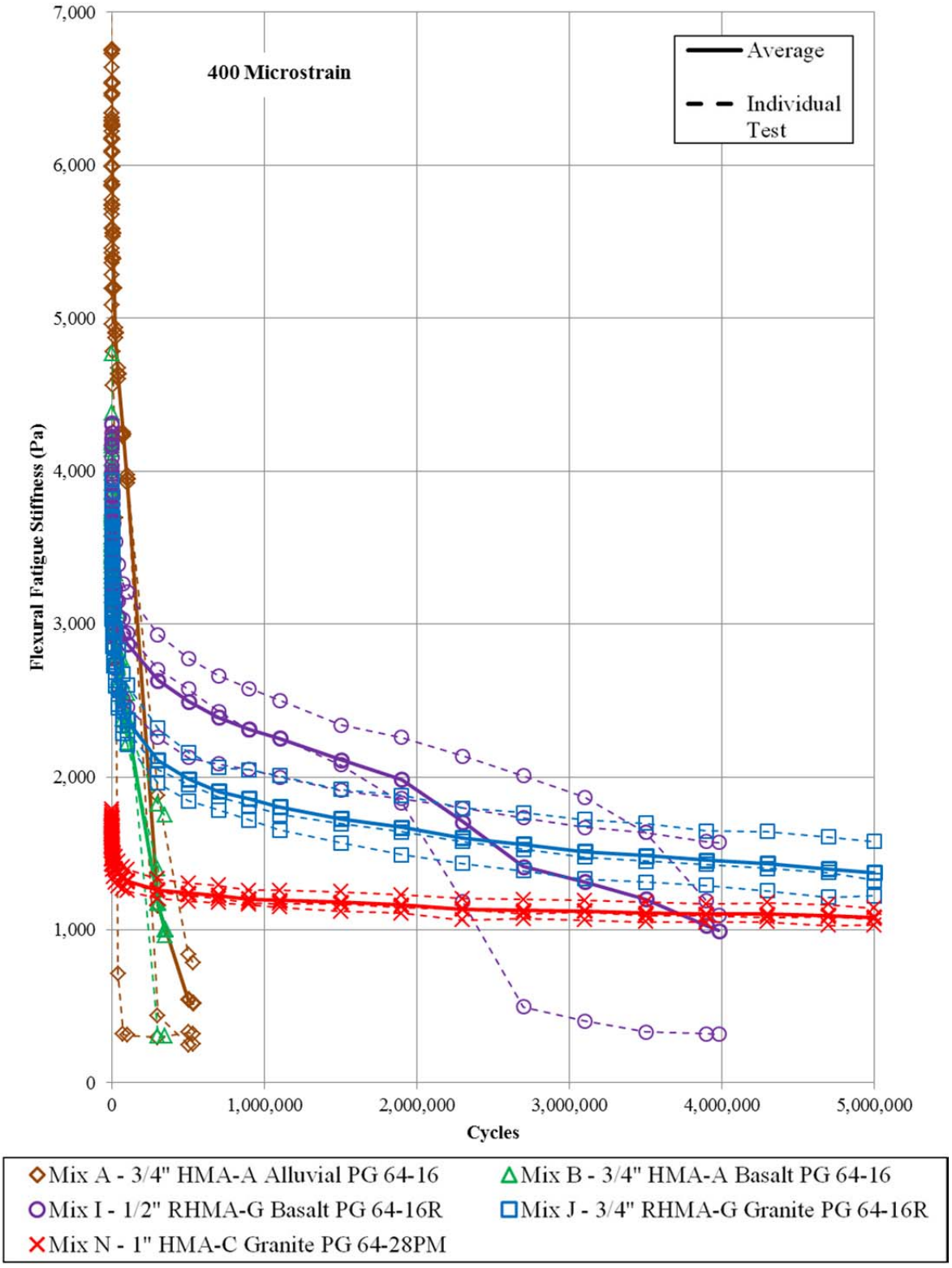

Figure 3.3: Comparison of flexural fatigue stiffness versus cycles (individual 400 microstrain test with mix averages).

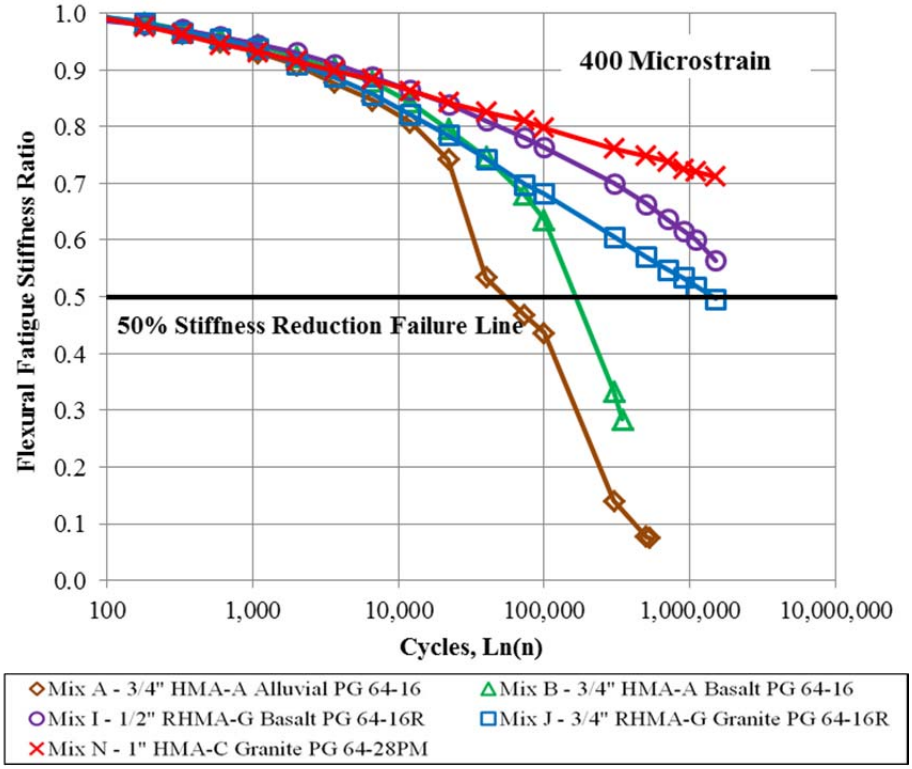

Figure 3.4: Comparison of flexural fatigue stiffness ratio versus cycles (400 microstrain tests with mix averages).

3.2.2 Flexural Frequency Sweep

Figure 3.5 shows the master curves in terms of *complex elastic modulus* (E*), also referred to as *complex stiffness,* versus the log of reduced time (time of loading relative to a frequency of 10 Hz at 20°C) produced from flexural frequency sweep tests for the five mixes. The results are similar to the initial stiffness at 10 Hz and 20°C seen in the flexural fatigue data. It can be seen from the master curve plot that Mix N is by far the softest at the standard test time and frequency but that under fast loading it has a stiffness similar to that of the stiff conventional binder Mix A. The other three mixes have similar stiffnesses across the entire master curve.

Figure 3.6 shows the flexural frequency sweep data plotted in terms of complex modulus versus the phase angle (Black diagram) for each of the frequency and temperature testing combinations included in the testing plan for the frequency sweep. A higher phase angle indicates more visoelastic behavior, while a lower phase angle indicates more elastic behavior. More viscoelastic behavior will tend to result in slower crack propagation. High stiffnesses and lower phase angles generally help in thick structural layers in asphalt pavements because they reduce bending and therefore reduce tensile strains at the bottom of the asphalt layers. Lower stiffnesses and higher phase angles generally result in slower reflective crack propagation when the material is used as a relatively thin overlay on cracked or jointed pavement. It can be seen that the phase angles are in the same ranges for all five mixes.

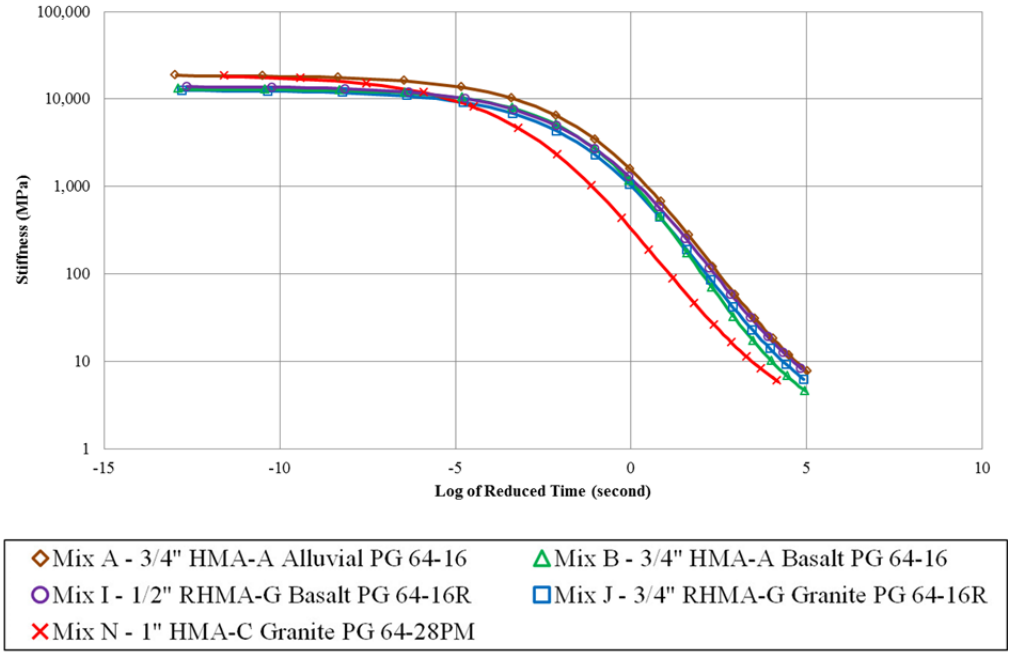

Figure 3.5: Comparison of flexural master curves for all five mixes.

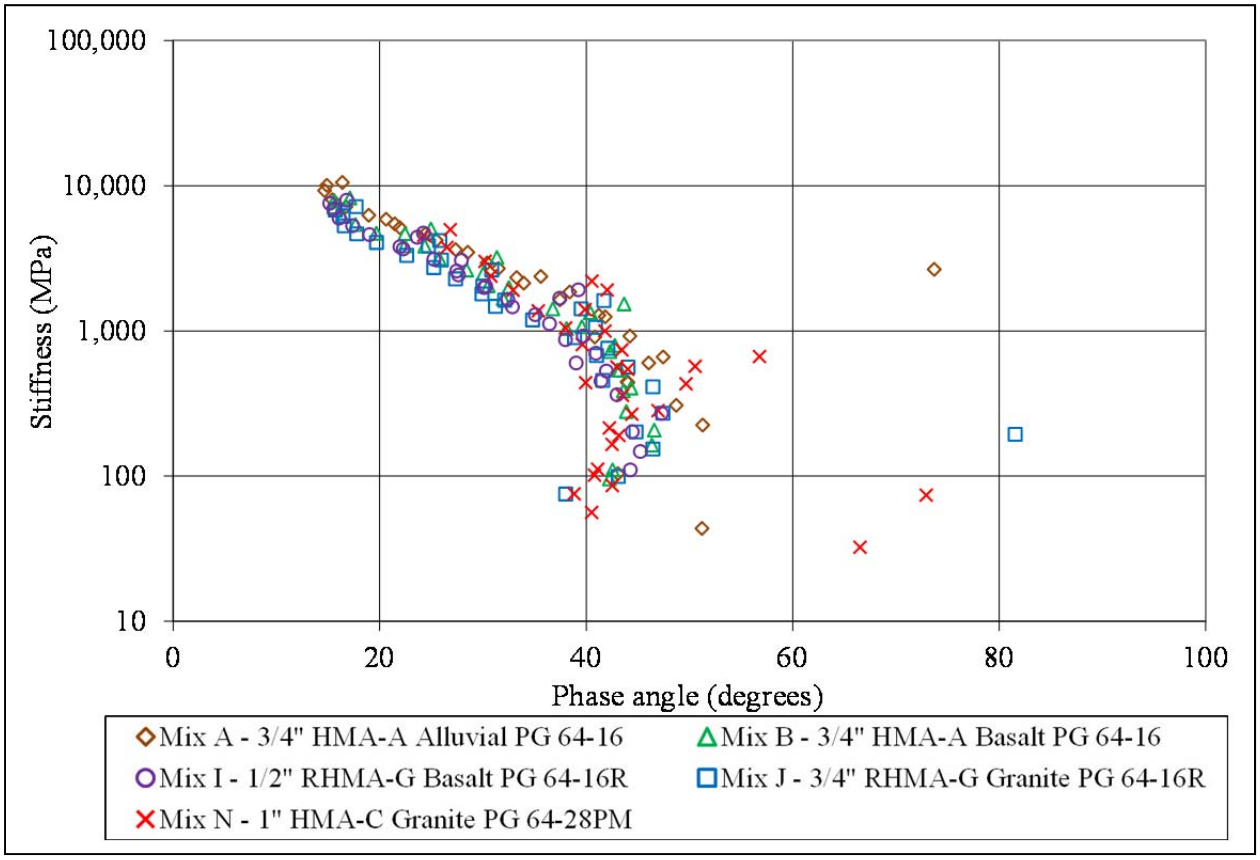

Figure 3.6: Black diagram from flexural frequency sweep for all five Superpave mix designs.

3.3 Repeated Shear Test at Constant Height (RSCH) (AASHTO T 320)

Figure 3.7 shows the averages of development of permanent shear strain (PSS) versus load repetitions (also referred to as "cycles") for the five mixes for each of the six combinations of shear stress (70, 100, and 130 kPa) and temperature (45 and 55°C). Five percent PSS has been correlated with a rut depth in the field of 0.5 inches (12.5 mm) *(27).* The plot shows that at the lowest stress at both temperatures, Mix A, which is the stiffest and has a conventional binder and a crushed alluvial aggregate, has the fastest rate of permanent deformation development, and that Mix B, which has a conventional asphalt binder from another source and an aggregate with 100 percent crushed faces, has the slowest rate of permanent deformation damage. It can also be seen that at the low stress (70 kPa [10 psi]) at both temperatures, the mix with polymer-modified binder and aggregate with 100 percent crushed faces (Mix N) is in the middle when it comes to permanent deformation, but at the higher stresses (100 kPa [14.3 psi], 130 kPa [18.6 psi]) it has the greatest permanent deformation. As the stress level and the temperature increase, the performance differences between the different mixes get proportionally smaller, with all of the mixes showing fairly rapid permanent deformation development at the highest stress and highest temperature.

Figure 3.8 shows the averages of development of permanent shear strain versus repetitions for each of the five mixes for the two test temperatures, sorted by stress level. The increase in permanent deformation can be seen as the stresses are increased, and as the temperature is increased. The RSCH results show a clear separation in average performance between the two temperatures at each of the three stress levels. The results indicate that the difference in performance between the two temperatures increases as the stress increases.

None of the RSCH results show *tertiary flow* behavior, which is defined as when there is a later increase in the rate of permanent deformation after the decrease in permanent deformation versus repetitions shown in the figures.

Detailed results and additional comparison figures between the mixes are presented in the appendices.

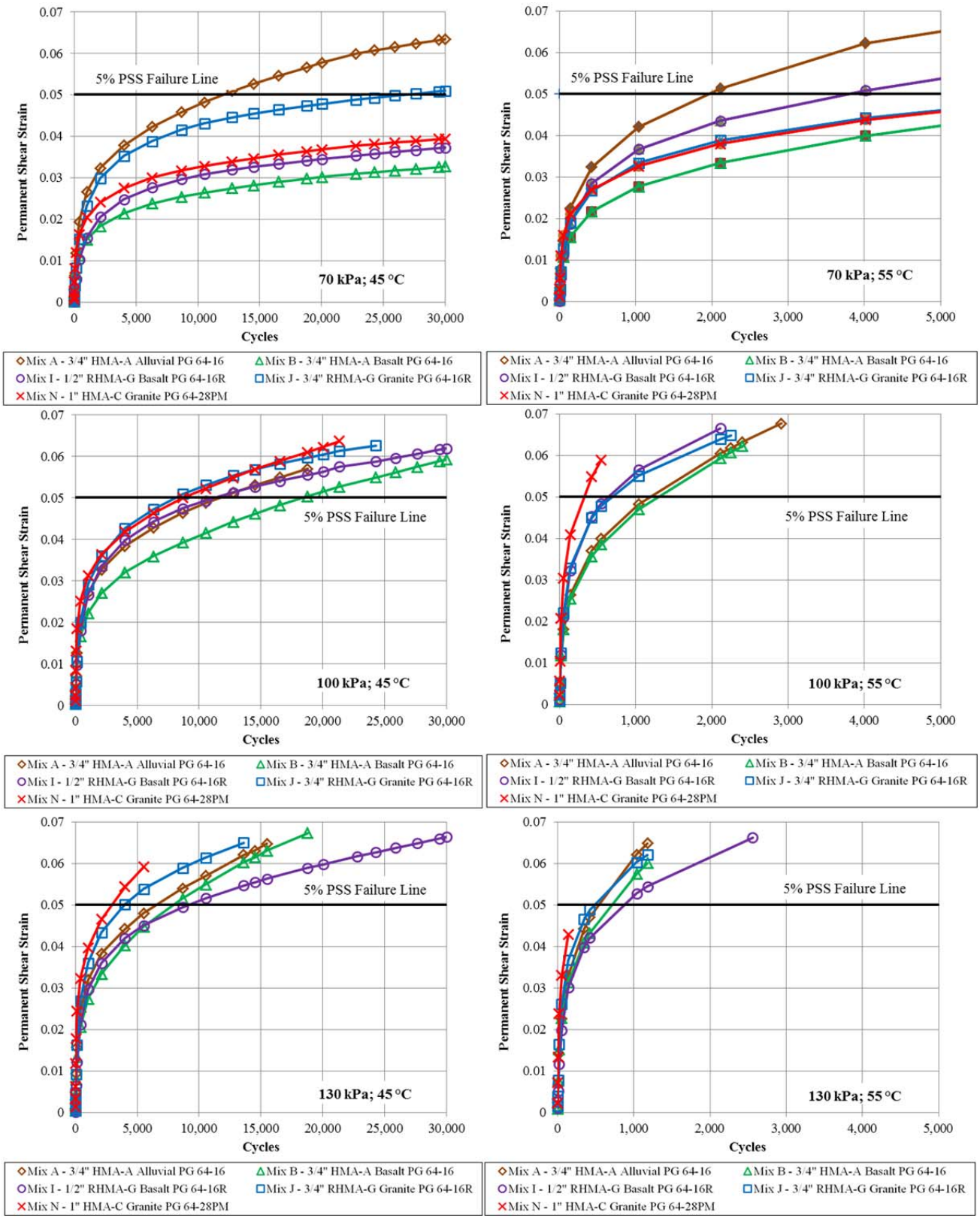

Figure 3.7: Permanent shear strain (PSS) versus cycles (RSCH tests with mix averages 70, 100, and 130 kPa at 45°C and 55°C).

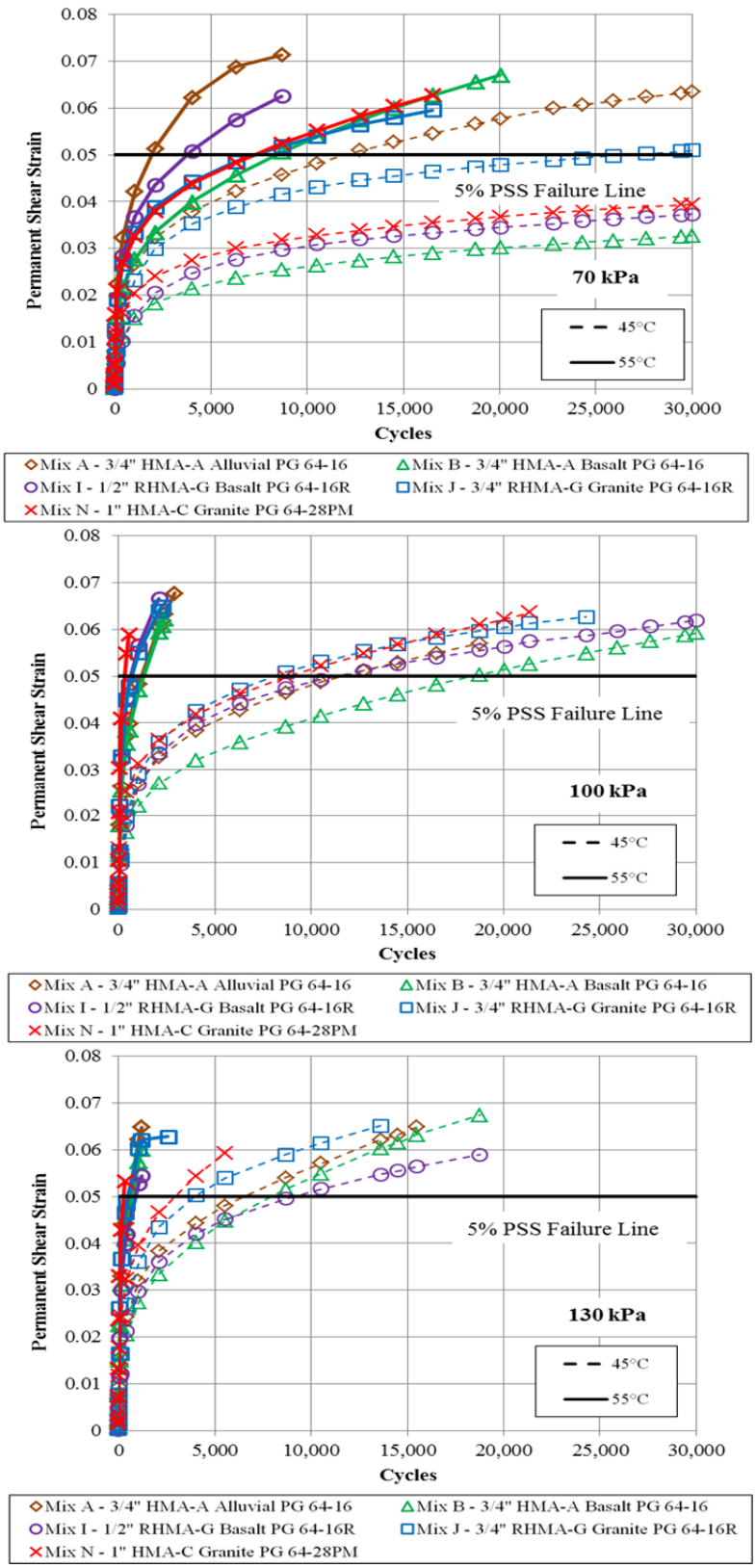

Figure 3.8: Comparison of permanent shear strain versus cycles for temperature effect (RSCH tests with mix averages 70, 100, and 130 kPa in 45°C and 55°C).

3.4 AMPT Repeated Load Triaxial

Figure 3.9 shows the averages of development of permanent axial strain (PAS) versus repetitions (cycles) for the five mixes at 45°C for the confined (483 kPa [70 psi] deviator stress, 30 kPa [4.3 psi] contact stress, 69 kPa [10 psi] confining pressure) and unconfined (no confined pressure, other stresses the same as confined test) conditions. Figure 3.10 shows the results for the same test conditions for the five mixes at 55°C. RLT tests were run to the lesser of 20,000 cycles or a PAS of 5 percent. No calibrated relationship has yet been developed between permanent axial strain in the RLT and rutting in the field.

As expected, the confined test condition results in much slower development of permanent deformation than does the unconfined test condition because the unconfined condition results in higher shear stresses in the specimen and also increases the mobilization of internal friction between aggregate particles inside the specimen. The unconfined test also appears to separate the performance of the different mixes to a greater degree than does the confined test, particularly at 45°C. The two mixes with conventional asphalt binders (Mix A and Mix B) have the best performance in the unconfined tests, while the mixes with rubberized binder (Mix I and Mix J) have the best performance in the confined test at 55°C. In the confined test results at 45°C, Mix I is the best and Mix J is the worst, although all of the mixes have similar performance.

It can be seen in both figures that the confined test results appear to approach an asymptotic permanent axial strain level at 45°C, and do the same to a lesser degree at 55°C, while the unconfined results show continued increases in permanent deformation with increased repetitions.

The RLT results do not appear to show much tertiary flow behavior, although there are slight increases in the rate of permanent axial deformation, such as can be seen for Mix A in Figure 3.9 and for Mix A and Mix B in Figure 3.10, but only for the unconfined results. The cycle in the RLT at which the increase occurs is called the *flow number* (FN). These results indicate that it would be impossible to identify an FN value for these five mixes under confined conditions, and it would be difficult to identify an FN value for most of the mixes in the unconfined test results.

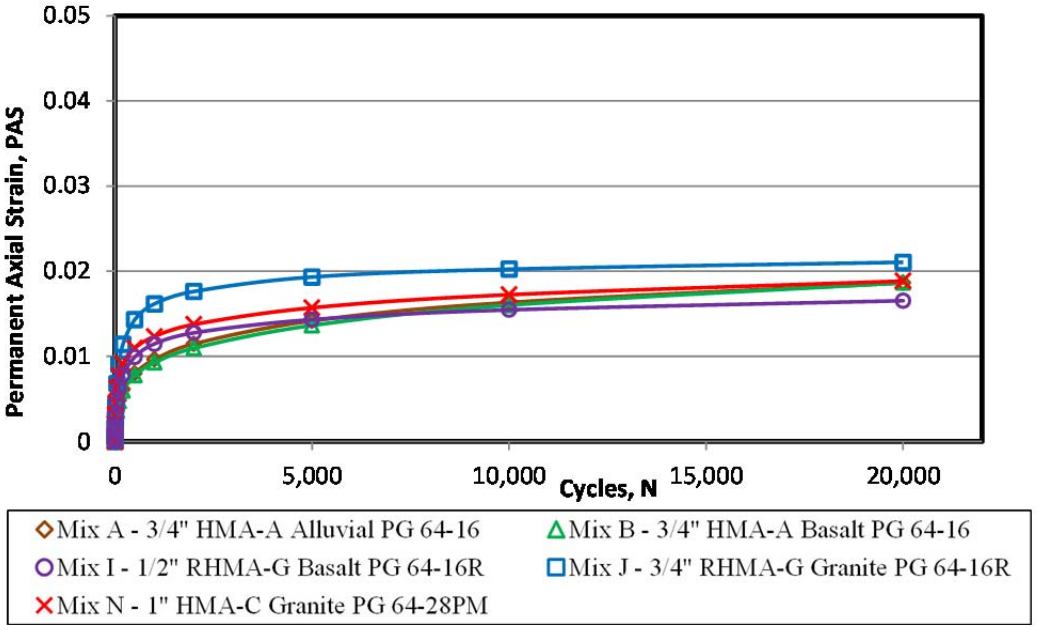

(a) Confined test

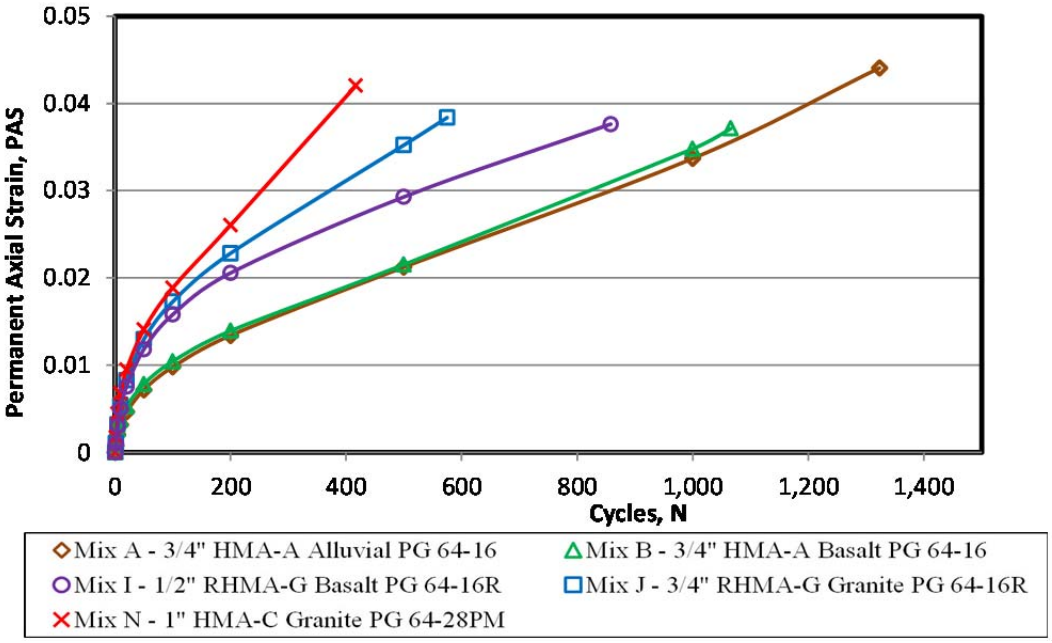

(b) Unconfined test

Figure 3.9: Average permanent axial strain versus cycles for the five mixes at 45°C.

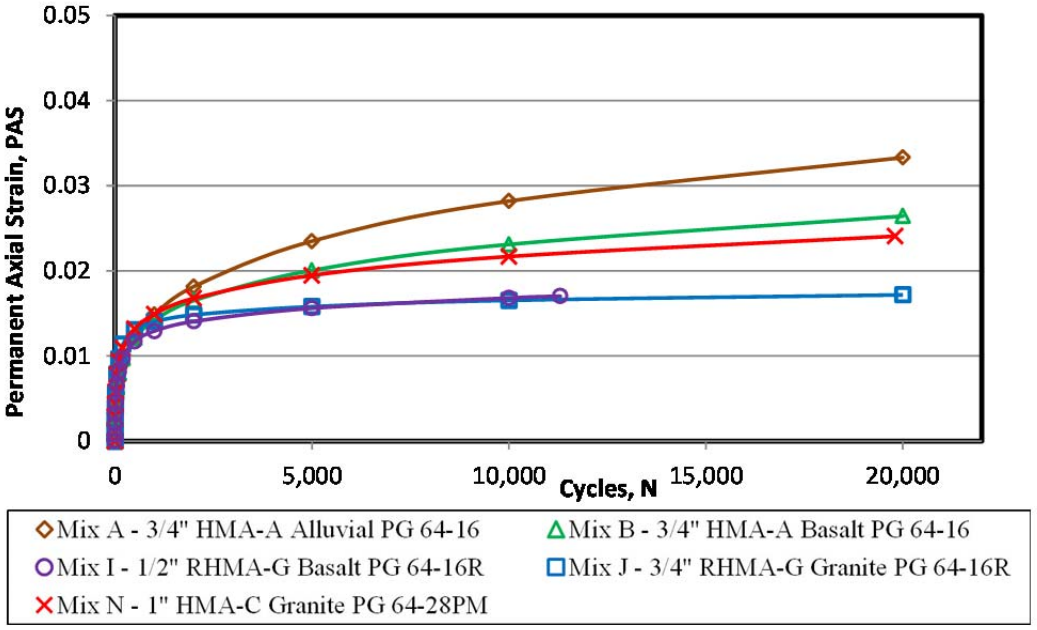

(a) Confined test

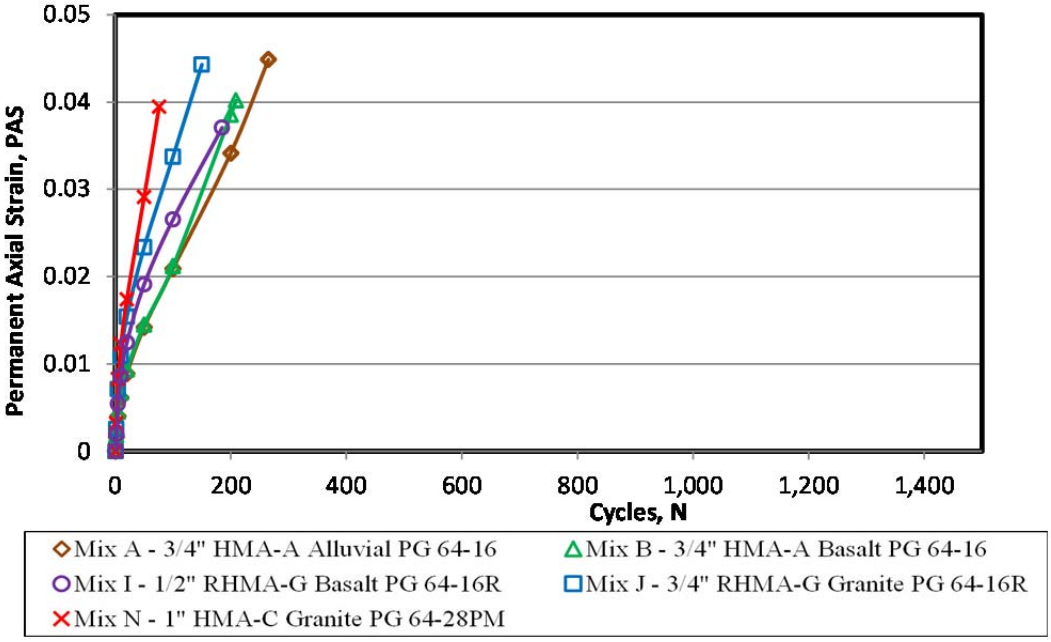

(b) Unconfined test

Figure 3.10: Average permanent axial strain versus cycles for the five mixes at 55°C.

3.5 AMPT Dynamic Modulus

Figure 3.11 shows the master curves for all five mixes. Figure 3.12 shows the relationship between stiffness and phase angle for each mix for all temperatures and frequencies in a Black diagram. It can be seen from the master curves that the two mixes (Mix A and Mix B) with the conventional PG 64-16 binders have the highest stiffnesses, although the two binders are from different refineries; an exception occurs at the coldest temperatures and fastest loadings (lowest reduced times) where the mix with the PG 64-28PM binder (Mix N) is the second stiffest.

It can be seen from the Black diagram that the rubberized mixes (Mix I and especially Mix J) have the highest phase angles (more delayed elastic and viscous behavior and less elastic behavior) compared with the conventional and polymer-modified mixes at higher temperatures and slower loading times when the stiffnesses are lowest. Low phase angles and high stiffnesses are desired at higher temperatures and slower loading times to minimize the risk of rutting. Mix B, with its conventional PG 64-16 binder, has high stiffnesses and the lowest phase angles under these conditions, indicating that it may have better resistance to rutting. Although stiffness and phase angle alone do not predict rutting performance, it can be seen from the previous RSCH and RLT results that Mix B had good permanent deformation performance in both of these tests.

In addition to their use in mechanistic-empirical pavement design, the results from performance-related tests such as the dynamic modulus provide insight into the best approaches for obtaining desired mix properties. For example, Mix N is interesting because polymers are generally added to reduce low temperature stiffnesses to minimize the risk of low-temperature cracking, and to increase high temperature stiffnesses to minimize the risk of rutting. However, it can be seen that Mix N has the lowest stiffness at high temperatures and slow loading (high reduced time) and the second highest stiffness at low temperatures (lowest reduced times). The rubberized binder used in Mix J is from the same refinery as the polymer-modified binder in Mix N, and exhibits similar high temperature susceptibility to stiffness, although not as much as the polymerized mix. The aggregate gradations of the two mixes are different and their aggregate source is the same, but the time and temperature susceptibility of stiffness is mostly controlled by the binder.

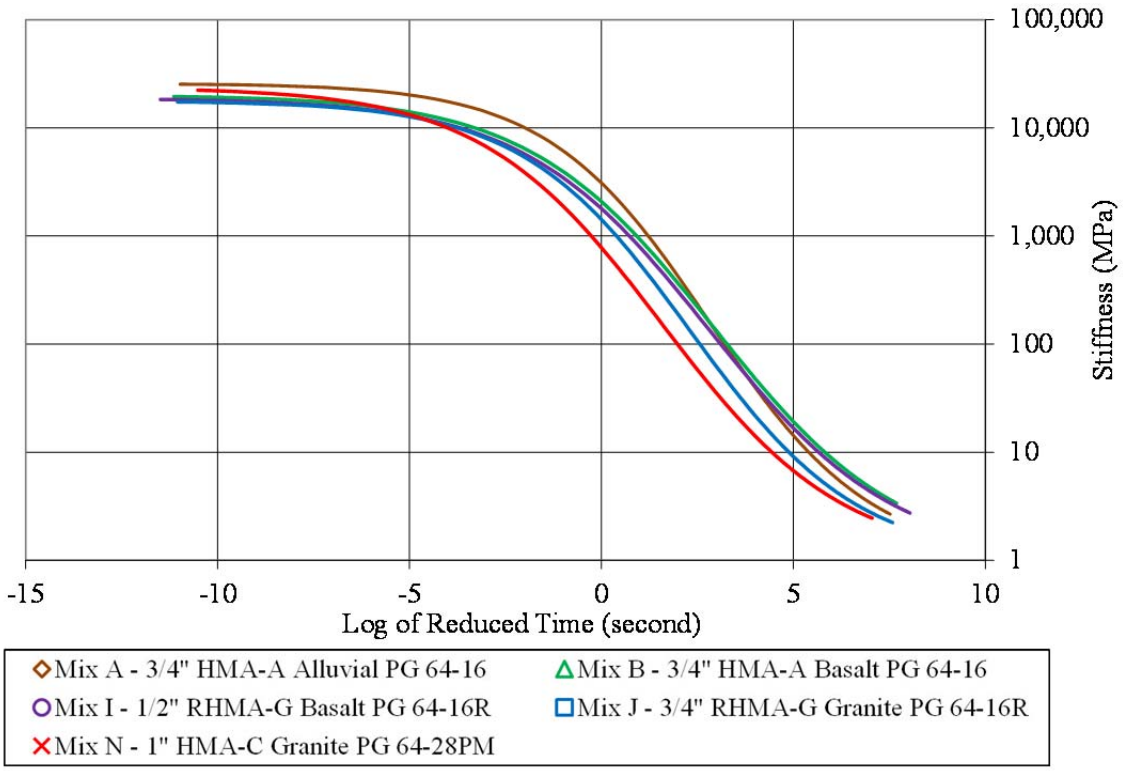

Figure 3.11: Comparison of dynamic modulus master curves for all five mixes.

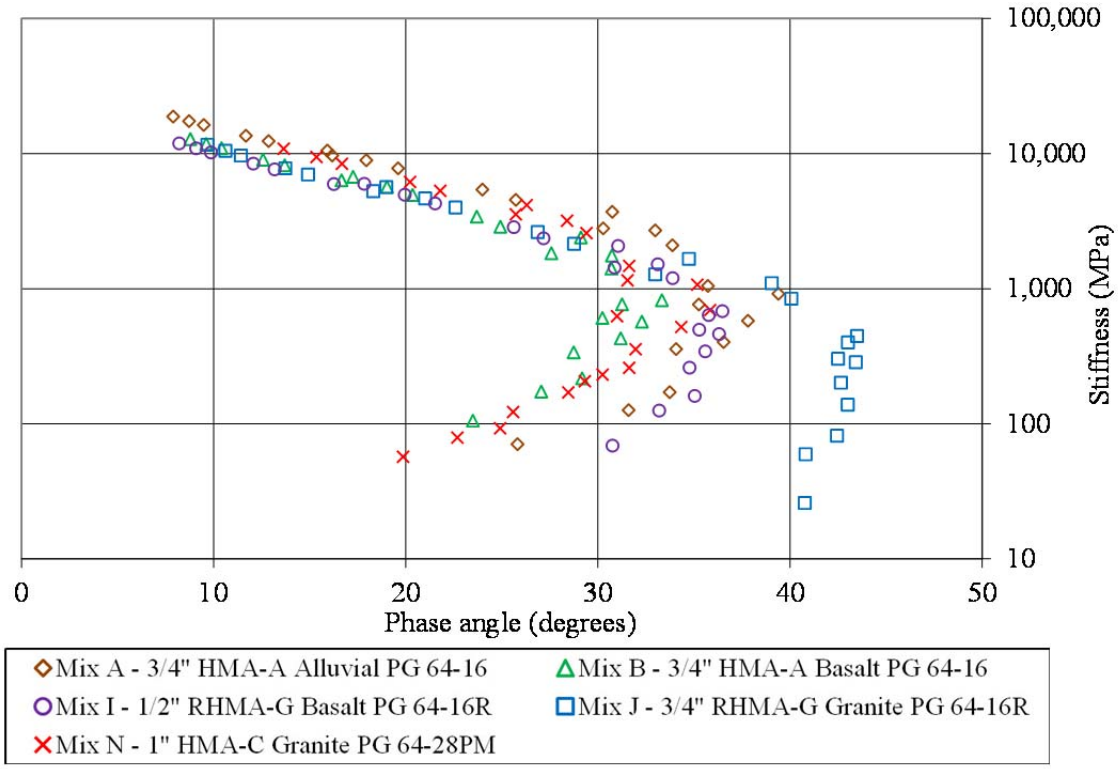

Figure 3.12: Black diagram from dynamic modulus for all five Superpave mix designs.

3.6 AMPT Direct Tension Fatigue (AASHTO TP 107)

Figure 3.13 shows average stiffness (dynamic modulus) versus load repetitions (cycles) for the direct tension test for the five mixes. Figure 3.14 shows the average phase angle versus load repetitions. Two replicates of each mix were tested but three out of ten tests did not providing meaningful results—the stiffness increased and decreased alternately and so did the phase angle. Despite the great care taken in preparing the specimens and mounting them in the test device, it is thought that the problems with the test resulted from misalignment of the top and bottom platens during the glueing process. Misalignment results in shear stresses in the specimens when the platens are locked into the AMPT loading apparatus.

The results for stiffness versus repetitions indicate that the polymer-modified mix (Mix N), which was the softest, had the slowest rate of damage, and was followed by the two rubberized mixes. Of the conventional mixes, Mix A had the fastest rate of damage and was also the stiffest mix under the test conditions. Both replicates of the second mix with conventional binder, Mix B, failed very quickly in the test for the reasons noted above. The results for phase angle versus repetitions indicate that the polymer-modified mix had the most delayed elastic and viscous behavior and that there was little change in phase angle after the initial heating of the mix in the first load repetitions. Conventional Mix B had limited results due to early failure, while Mix A showed a change in phase angle at that same time as a rapid change in the rate of damage (loss of stiffness). The rubberized mixes had similar performance with regard to phase angle change which was similar to the damage results.

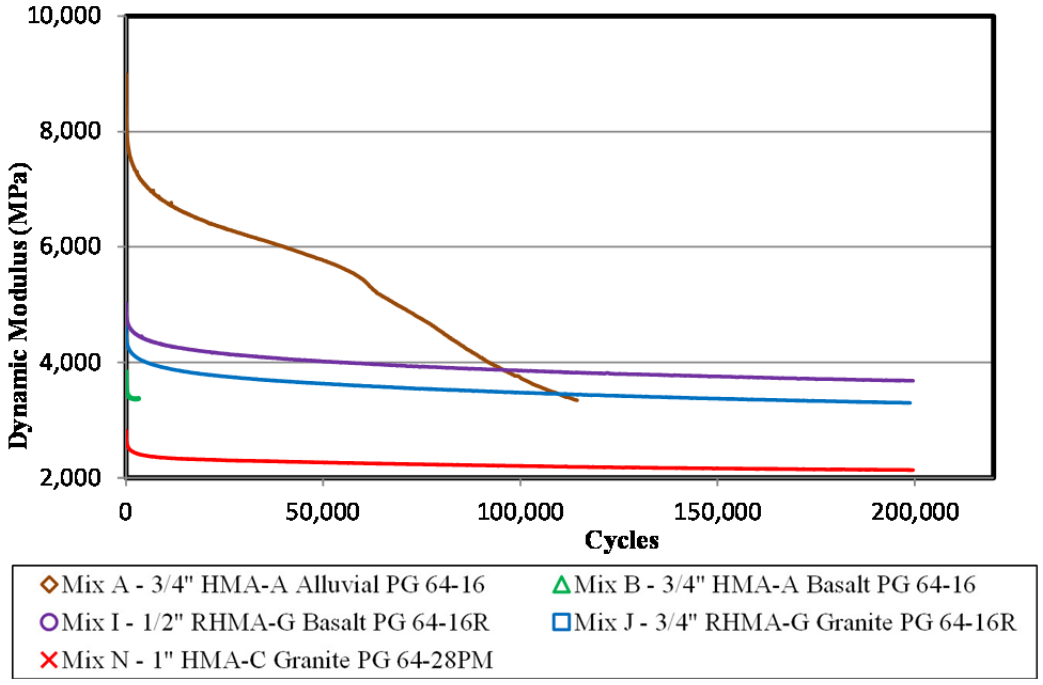

Figure 3.13: Comparison of direct tension fatigue stiffness versus cycles for the five mixes.

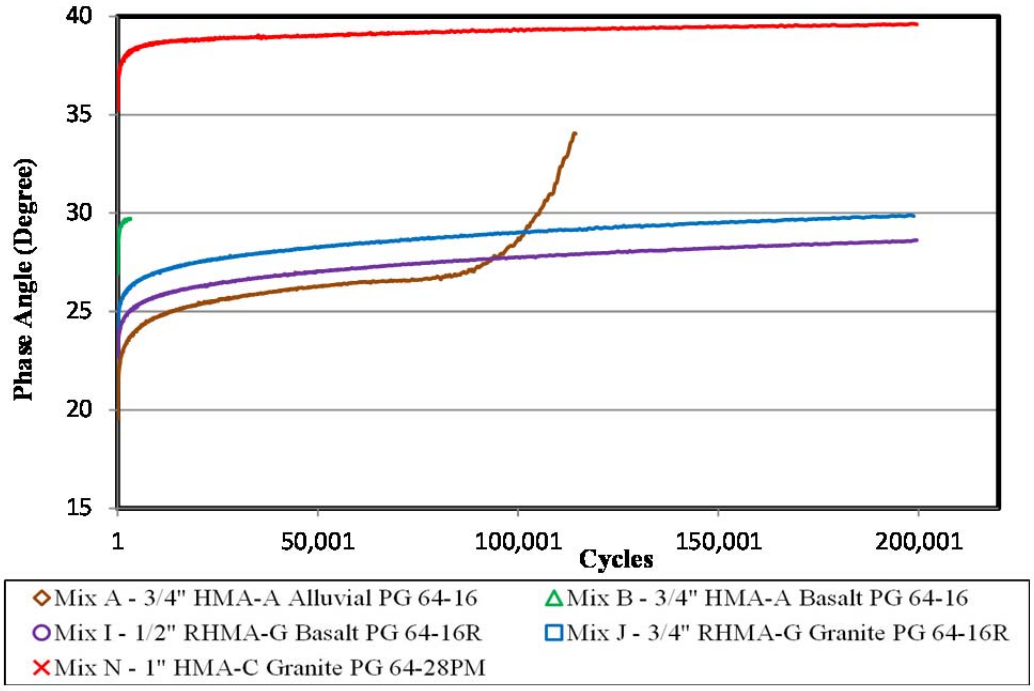

Figure 3.14: Comparison of direct tension fatigue phase angle versus cycles for the five mixes.

3.7 Hamburg Wheel-Track Testing (AASHTO T 324)

Figure 3.15 and Table 3.3 show the HWTT results for the five mixes. It can be seen that all five mixes show continuous rut increase after the initial embedment, and do not show a third stage of accelerated rutting that would indicate stripping. The two rubberized mixes (Mix I and Mix J) show the least amount of rutting while the two conventional mixes and the polymer-modified mix all show similar rutting performance in this test.

3.8 Indirect Tensile Test (AASHTO T 283)

Table 3.4 shows the indirect tensile test results for the five mixes. It can be seen from the results that the two conventional mixes and the polymer-modified mix have TSR values greater than 80 percent, while the two rubberized mixes have lower values. Caltrans is considering new specifications with minimum requirements for dry and wet strength of 100 psi and 70 psi (482 kPa and 689 kPa) respectively. The results indicate that the ability of the mixes to meet this unconditioned (dry) strength value do not appear to follow a pattern with regard to aggregate source or binder type. A mix with a conventional binder and alluvial aggregate (Mix A) and another with a rubberized binder and a crushed basalt aggregate (Mix I) pass, while the others do not. The conditioned (wet) strength results follow a clearer pattern, with the two mixes with the same granite aggregate source failing, although one has a rubberized binder (Mix J) and the other has a polymer-modified binder (Mix N).

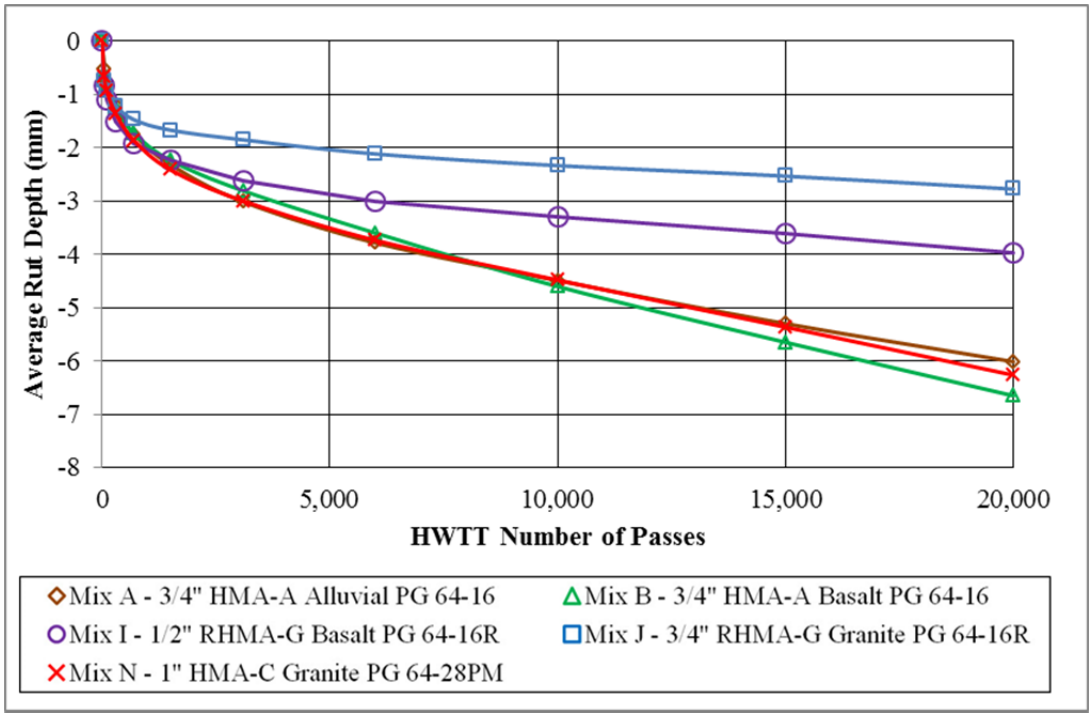

Figure 3.15: Comparison plot of average HWTT results for the five mixes.

Table 3.3: Average HWTT Results for the Five Mixes

Mix	Binder Type/ Grade	Aggregate Type	NMAS	Binder Content %	Average Rut Depth at 15,000 Cycles (mm)	Stripping Point[a]
A	PG 64-16	Alluvial	3/4"	5.5	5.37	N/A
B	PG 64-16	Basalt	3/4"	5.2	5.71	N/A
I	PG 64-16 RB	Basalt	1/2"	8.0	3.60	N/A
J	PG 64-16 RB	Granite	3/4"	7.2	2.44	N/A
N	PG 64-28 PM	Granite	1"	6.4	5.23	N/A

a. N/A indicates that there is no clear sign of stripping point.

Table 3.4: Indirect Tensile Test (AASHTO T 283) Results for All Five Mixes

Mix ID	Dry Tensile Strength (psi)		Wet Tensile Strength (psi)		Tensile Strength Ratio (%)
	Mean	Standard Deviation	Mean	Standard Deviation	
SSP 39 Spec[2]	**100**		**70**		**80**
Mix A	109.3	6.1	96.0	5.3	87.9
Mix B	90.4	6.4	75.1	1.8	83.1
Mix I	126.0	12.7	80.7	4.0	64.0
Mix J	94.6	9.9	45.9	0.9	48.5
Mix N	62.5	2.5	57.5	4.9	92.1

3.9 Semicircular Bending Test (SCB)

Table 3.5 shows results for the semicircular bending test. The results do not appear to show a distinct advantage for any binder type or aggregate source. As expected, the polymer-modified mix (Mix N) had the lowest secant stiffness, which matched the low stiffness measured with the other stiffness tests.

Table 3.5: Semicircular Bending Test Result for All Eight Mixes

Mix ID	Secant Stiffness S (kN/m)		Fracture Toughness K_{IC} (MPa x $m^{0.5}$)		Fracture Energy G_f (J/m^2)	
	Average	CV	Average	CV	Average	CV
Mix A	750.1	0.18	0.232	0.13	0.993	0.15
Mix B	412.2	0.19	0.147	0.13	0.729	0.15
Mix I	747.2	0.41	0.209	0.11	0.909	0.15
Mix J	563.3	0.37	0.176	0.17	0.961	0.11
Mix N	236.9	0.51	0.088	0.22	0.510	0.19

4 COMPARISON OF HVEEM MIX DESIGN AND SUPERPAVE MIX DESIGN TEST RESULTS

The next part of this study examined samples of mixes prepared with the same materials but with the different design methods, Hveem and Superpave, in order to anticipate what performance changes might result with a transition from the former to the latter. Samples of two conventional mixes (Mixes A and B) and one rubberized mix (Mix I) were prepared following each design method, and each sample was tested using the flexural frequency sweep test (to evaluate stiffness), the flexural fatigue test (to evaluate fatigue performance), and the repeated shear test at constant height (to evaluate permanent deformation performance).

The expectation was that the higher binder contents and consideration of the dust-to-asphalt ratio in the Superpave mix designs would result in slightly reduced stiffness, improved fatigue performance, and some reduction in permanent deformation resistance. This change was desired since the Hveem mix design method has traditionally been considered overly risk averse with regard to permanent deformation and not risk averse enough for fatigue cracking for the designs for most segments on the state highway network—with potential exceptions where there is heavy slow traffic in very hot environments.

4.1 Flexural Frequency Sweep

Flexural frequency sweep test results for the two mix design methods for Mixes A, B, and I for each set of materials show that in general the Hveem mix designs have somewhat higher stiffnesses than the Superpave mix designs, particularly at lower temperatures, and similar phase angles. Figure 4.1, Figure 4.2, and Figure 4.3 show that across all frequencies and temperatures the master curves display little difference between the two mix designs. Figure 4.4, Figure 4.5, and Figure 4.6 show a Black diagram for the two mix designs for each of the three mixes. These results show that the stiffnesses as well as the phase angles are very similar for the two mix designs.

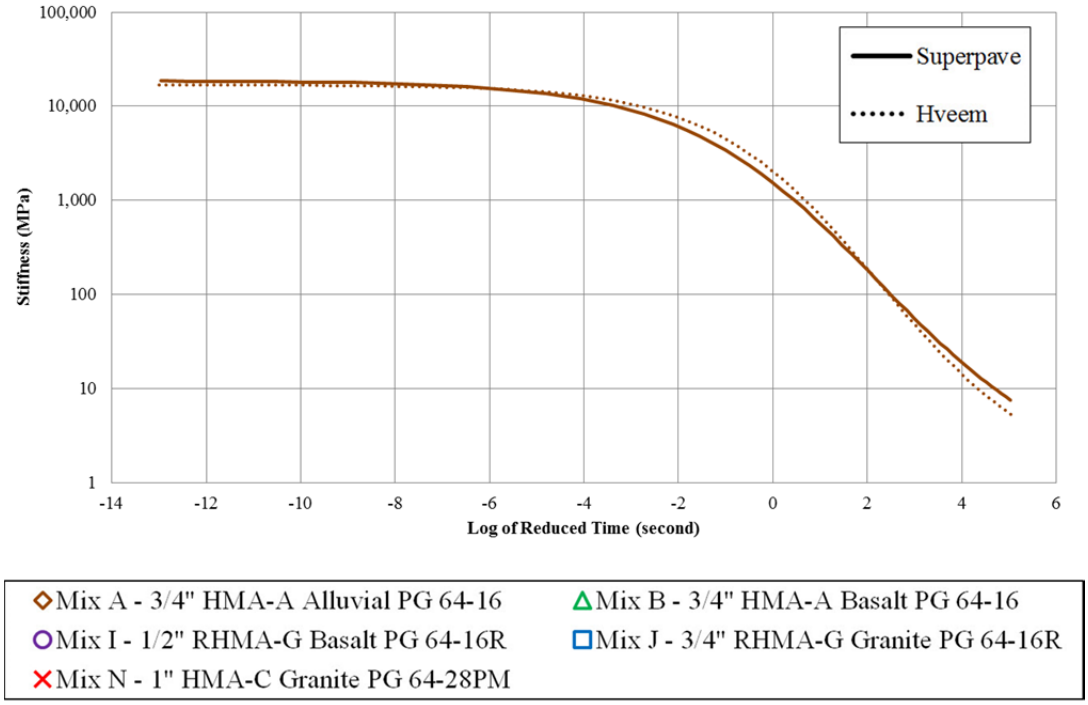

Figure 4.1. Comparison of Superpave and Hveem mix design master curves, stiffness versus reduced time (log scale) for Mix A.

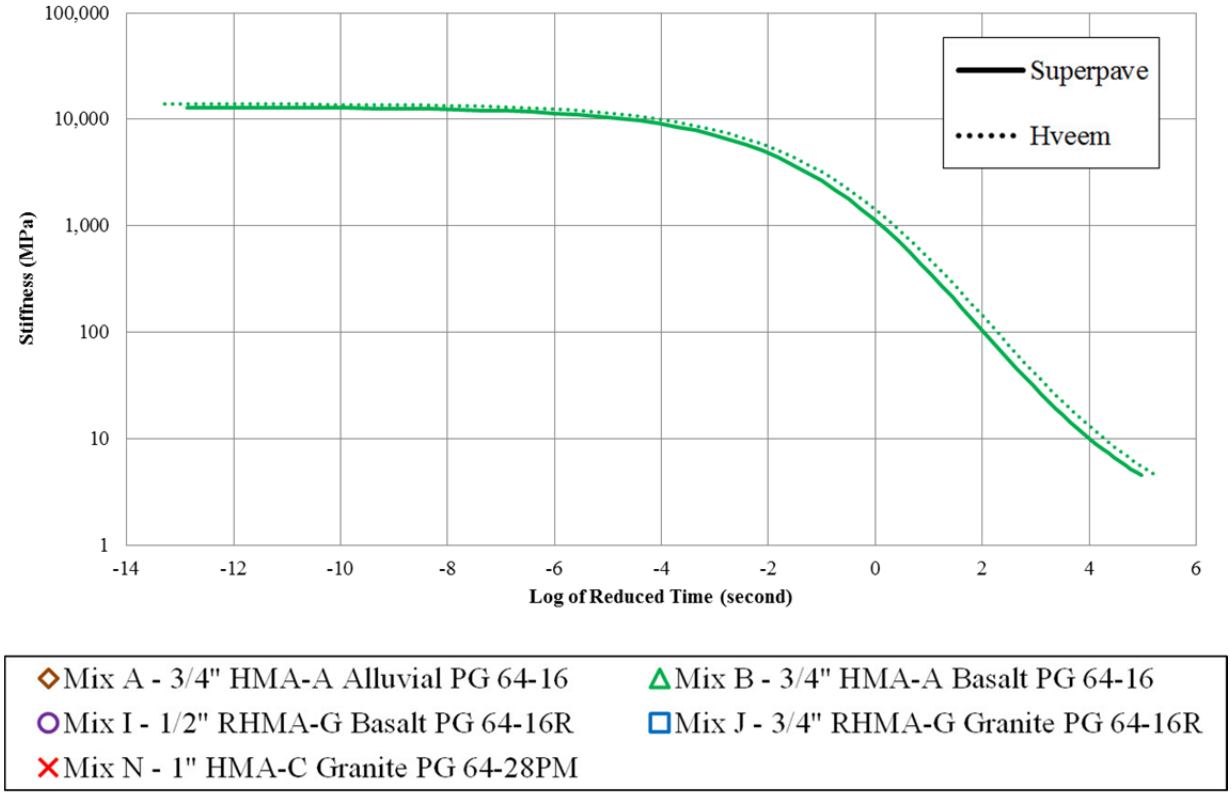

Figure 4.2. Comparison of Superpave and Hveem mix design master curves, stiffness versus reduced time (log scale) for Mix B.

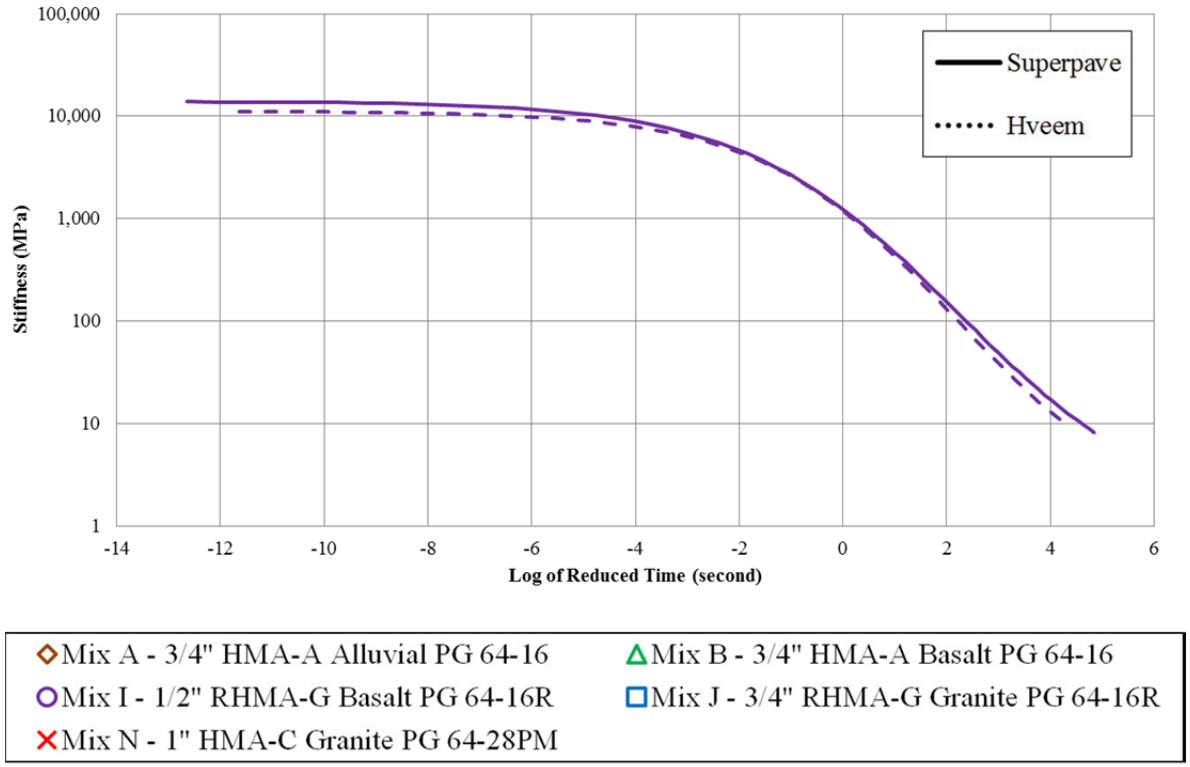

Figure 4.3. Comparison of Superpave and Hveem mix design master curves, stiffness versus reduced time (log scale) for Mix I.

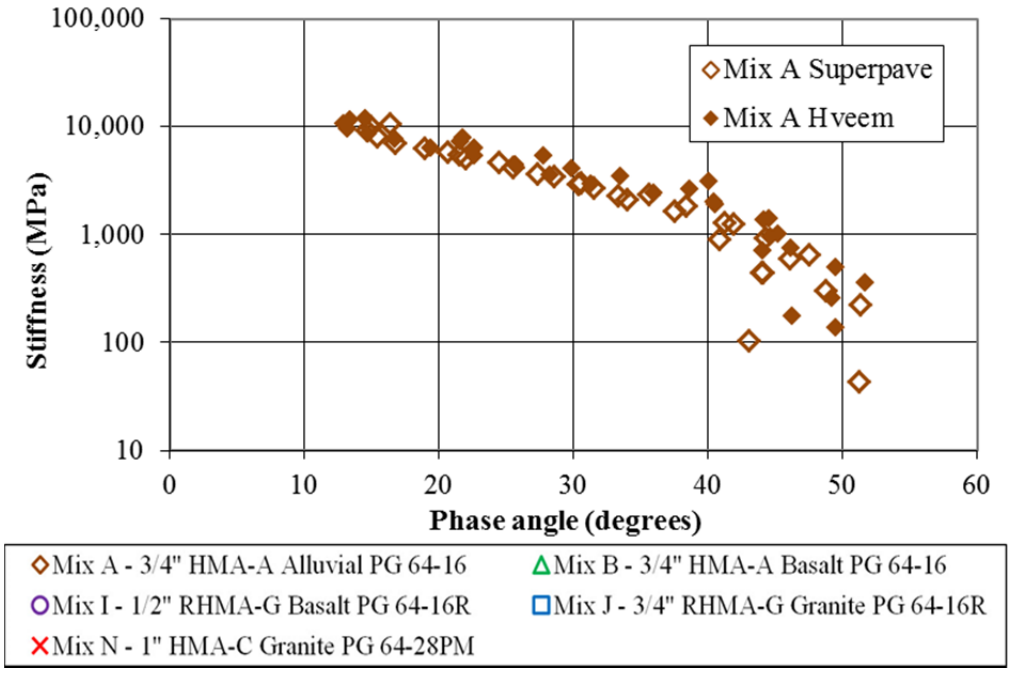

Figure 4.4: Comparison of Superpave and Hveem mix designs: Black diagram for Mix A.

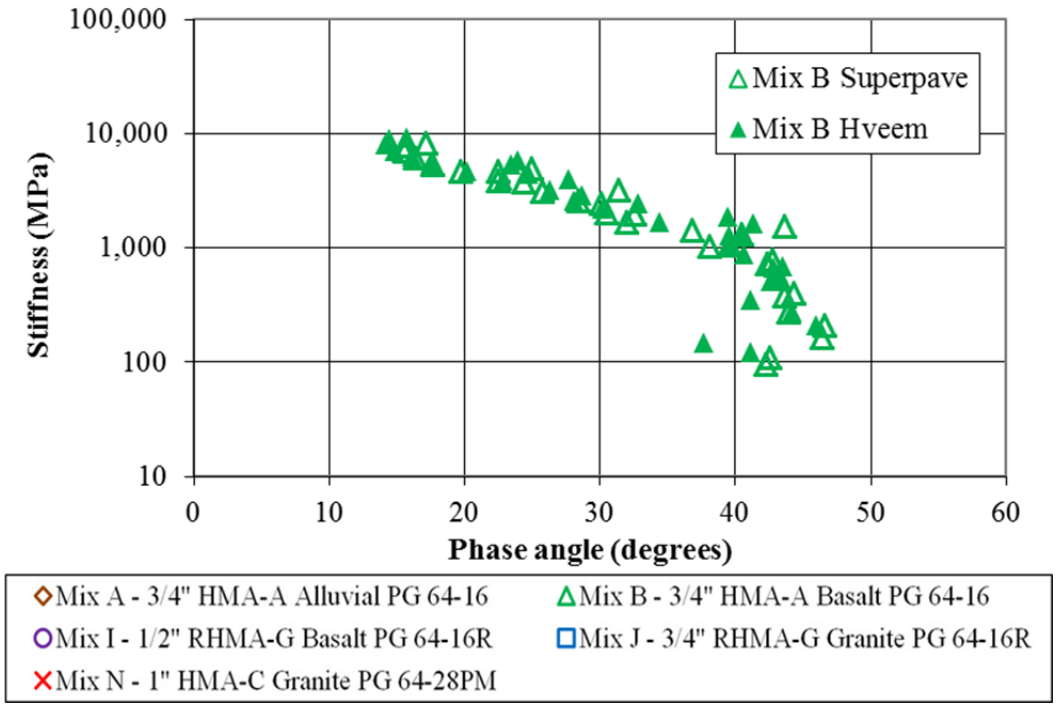

Figure 4.5: Comparison of Superpave and Hveem mix designs: Black diagram for Mix B.

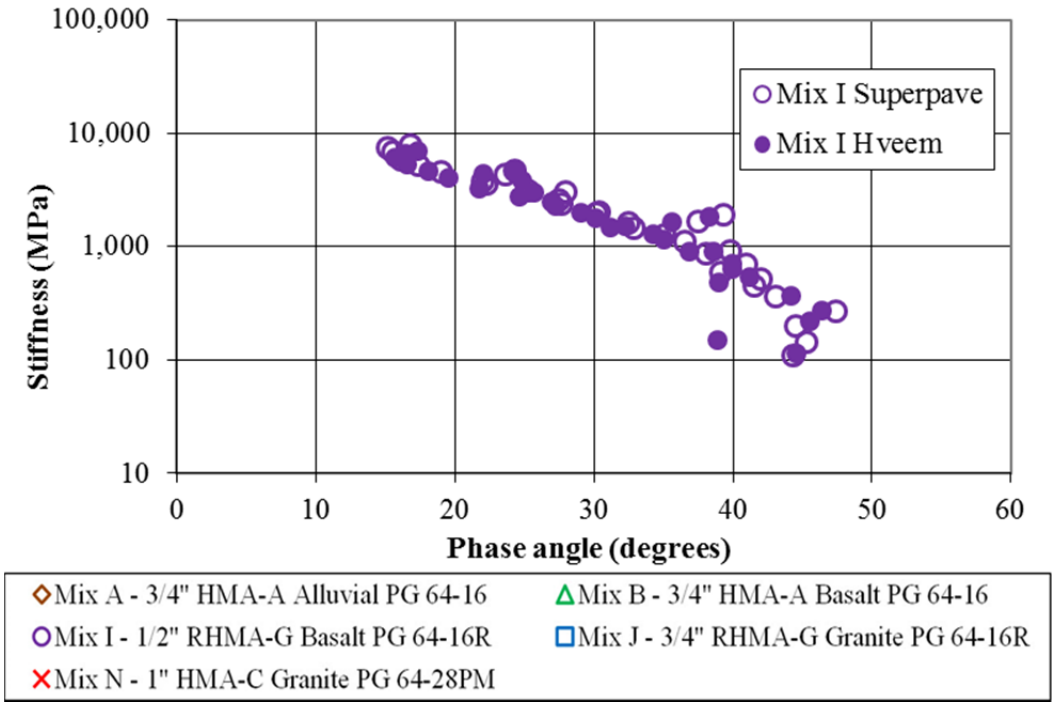

Figure 4.6: Comparison of Superpave and Hveem mix designs: Black diagram for Mix I.

4.2 Flexural Fatigue

Table 4.1 summarizes the flexural fatigue test results for the Superpave and Hveem mix designs for the three mixes and shows the other two mixes for comparison. The results indicate that for the two conventional mixes (Mix A and Mix B) the Superpave mix design has an approximately 400 percent longer fatigue life than the Hveem mix design. However, the rubberized mix (Mix I) shows similar fatigue results for both mix designs. Mix I also has the least difference in binder content between the two mix designs, which likely explains the similar results. Figure 4.7 and Figure 4.8 show the average damage process (loss of stiffness versus load repetitions) for the two mix designs (Hveem and Superpave) for the three mixes as well as the Superpave results for the two other mixes for the 200 and 400 microstrain testing respectively. It can be seen that the initial stiffnesses at the two fatigue test strain levels are not the same in all cases, which is different from the flexural frequency sweep results which use a much smaller strain. This indicates that the two mix designs can produce different stiffnesses, at least at 10 Hz and 20°C, at higher strain levels, with the stiffness of Mix B showing the greatest strain sensitivity and the Hveem mix having higher stiffness at both high strain levels. The other two mixes have approximately similar initial stiffness.

Looking at the change of stiffness versus repetitions, it can be seen that the damage rate is considerably faster for the Hveem mix designs for the two conventional mixes at both strain levels. For the rubberized mix the damage rates are similar for the two mix designs, with the Superpave mix having a slightly more rapid damage rate at the very end of the test. It is interesting to note that the dust proportion is similar between the Superpave and Hveem mix designs for the two conventional mixes, with all dust proportions between 0.8 and 1.2. For the rubberized mix the dust proportion is 0.5 for the Hveem mix design, which is low, and it is 1.0 for the Superpave mix design. This indicates that increasing the binder contents of the conventional mixes while maintaining approximately the same dust ratios substantially improved fatigue life, and that slightly increasing the binder content of the rubberized mix while increasing the dust proportion to within Superpave specifications did not have much effect on fatigue life. These results indicate that increases in binder content may be more important than bringing dust proportion into the specification, although the results are for very few mixes and the interaction with binder type cannot be considered. Detailed results are presented in the appendices.

Table 4.1: Superpave and Hveem Mix Design (where applicable) Fatigue Life Averages at 200 and 400 Microstrain for Mixes A, B, I, J, and N

Mix	Binder Type/ Grade	Aggregate Type	NMAS	Micro-strain	Superpave				Hveem			
					AC %	Average Initial Stiffness (MPa)	Average Initial Stiffness (psi)	Fatigue Life N_f	AC %	Average Initial Stiffness (MPa)	Average Initial Stiffness (psi)	Fatigue Life N_f
A	PG 64-16	Alluvial	3/4	200	5.5	5,952	863,265	7,220,644	5.0	6,549	949,821	1,683,271
				400		5,863	850,383	133,922		6,405	928,998	33,331
B	PG 64-16	Basalt	3/4	200	6.3	3,846	557,788	17,118,276	5.2	4,814	698,201	3,613,226
				400		3,733	541,394	226,478		4,583	664,715	68,510
I	PG 64-16RB	Basalt	1/2	200	8.3	4,000	580,137	59,065,825	8.0	3,623	525,448	355,346,670
				400		3,758	544,979	2,868,462		3,629	526,314	2,693,669
J	PG 64-16RB	Granite	3/4	200	8.8	3,745	543,203	122,773,034				
				400		3,478	504,416	1,465,472				
N	PG 64-28PM	Granite	1	200	6.4	1,876	272,026	827,309,038,768				
				400		1,656	240,218	119,139,416				

*Note: Hveem mix designs not subjected to performance-related testing for Mixes J and N.

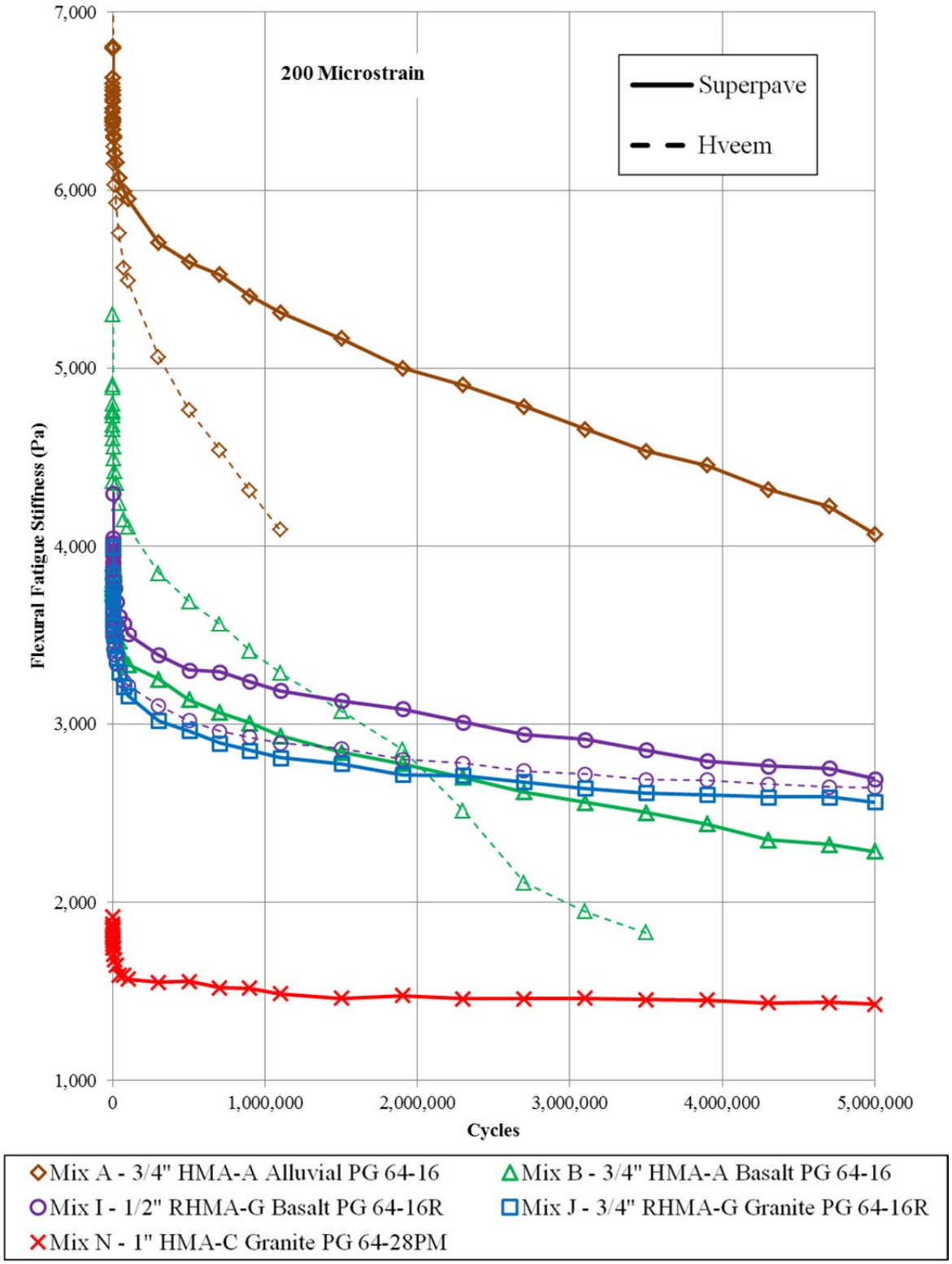

Figure 4.7: Comparison of Superpave and Hveem mix designs, 200 microstrain fatigue test, flexural fatigue stiffness versus cycles.
(Note: Hveem mix design shown with dashed line, Superpave mix design shown with solid line.)

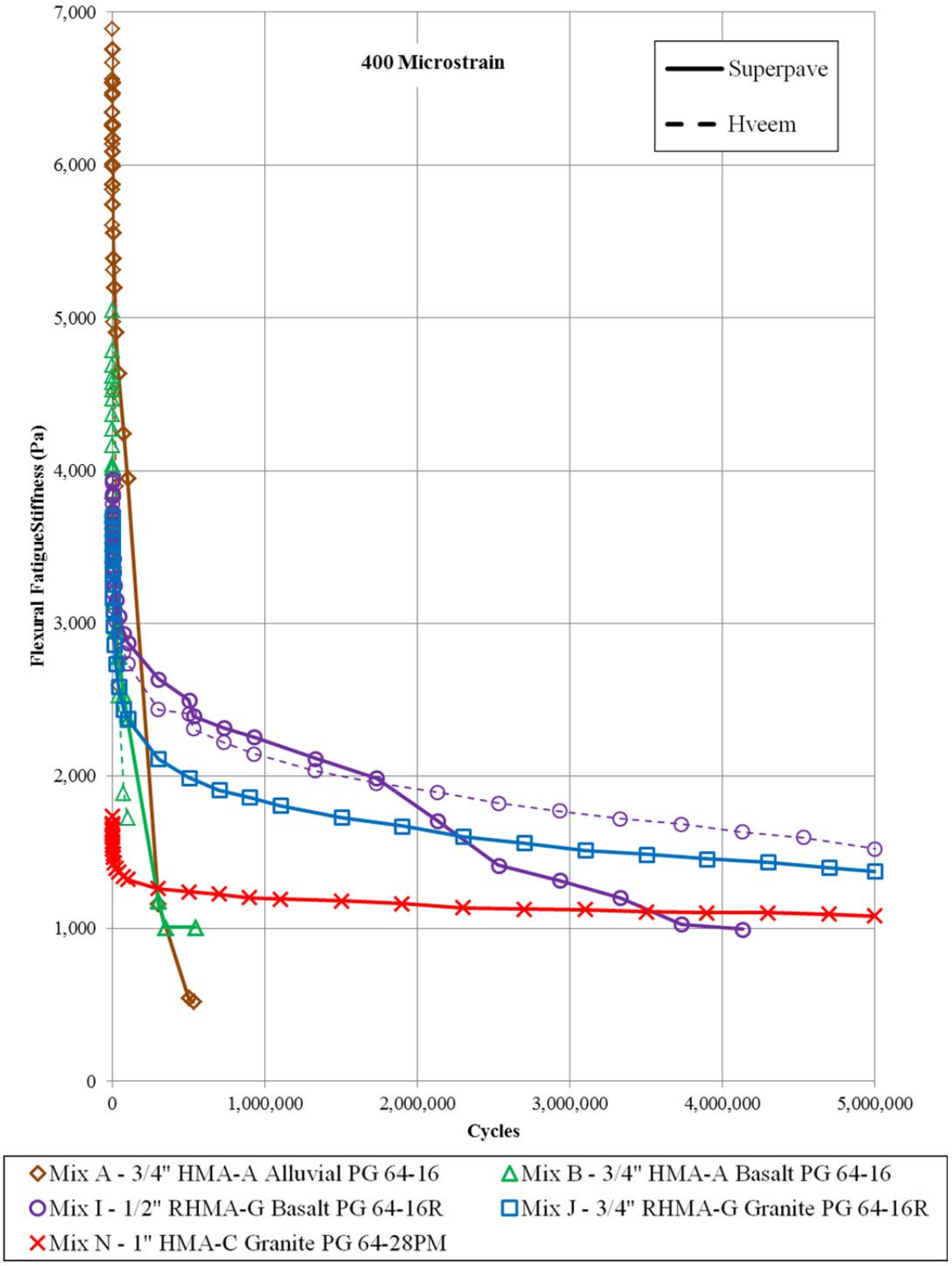

Figure 4.8: Comparison of Superpave and Hveem mix designs, 400 microstrain fatigue test, flexural fatigue stiffness versus cycles.
(Note: Hveem mix design shown with dashed line, Superpave mix design shown with solid line.)

4.3 Repeated Shear Constant Height

Figure 4.9 and Figure 4.10 show a permanent deformation performance comparison between the two mix designs at 45°C and 55°C respectively. The results indicate that the three Hveem mixes have a considerably higher resistance to rutting than the three Superpave mixes. Using the mix design criteria of repetitions to 5 percent permanent shear strain, it can be seen that the Hveem mixes outperformed the Superpave mixes by approximately three orders of magnitude (extrapolated for the Hveem mixes) at 45°C with the result indicating that the Hveem mixes are unlikely to reach the failure shear strain at that temperature. The Hveem mixes outperformed the Superpave mixes by a factor of five to ten at 55°C.

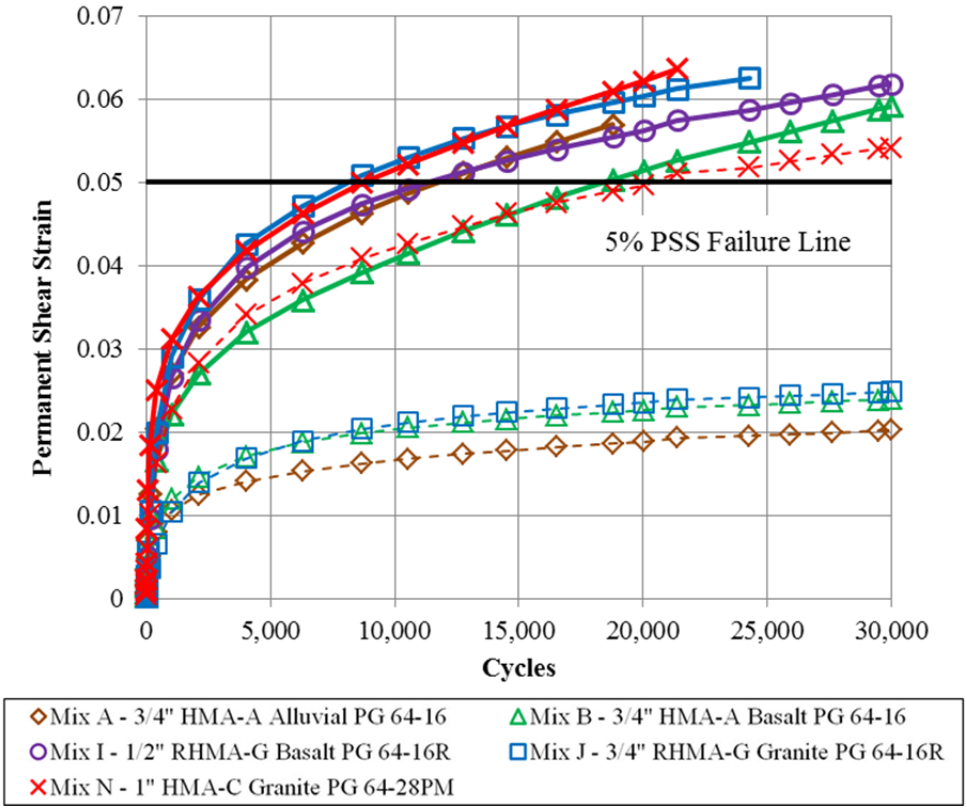

Figure 4.9: Comparison of Superpave and Hveem mix design average RSCH test results at 100 kPa and 45°C, permanent shear strain versus cycles.
(Note: Hveem mix design shown with dashed line, Superpave mix design shown with solid line.)

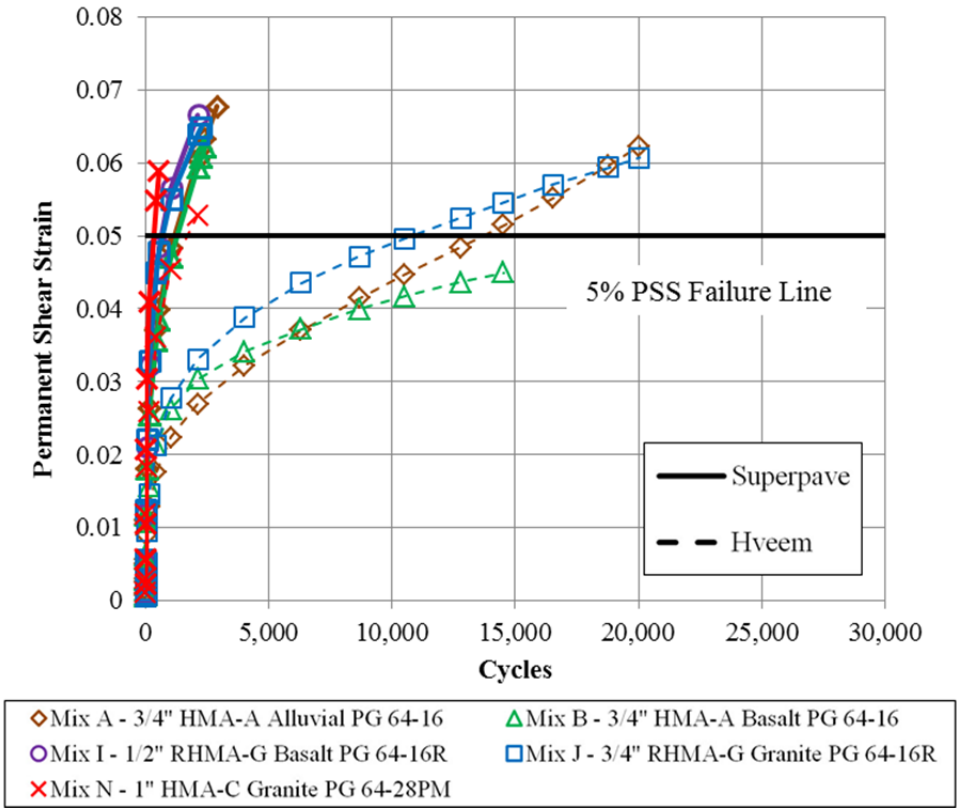

Figure 4.10: Comparison of Superpave and Hveem mix design average RSCH test results at 100 kPa and 55°C, permanent shear strain versus cycles.
(Note: Hveem mix design shown with dashed line, Superpave mix design shown with solid line.)

4.4 Findings

The results for the three mixes confirmed the expectation that the higher binder contents and consideration of the dust-to-asphalt ratio of the Superpave mixes would result in slight reductions in stiffness and improved fatigue resistance. And, the extent of the reduction in permanent deformation resistance was greater than expected. However, looking at test results alone without considering the context of traffic loading and climate does not answer the question as to how the change in mix design affects the expected performance of the pavement under different conditions and whether the reduction in rutting resistance puts the pavement at significant risk of rutting. Mechanistic-empirical simulations were performed in order to provide a more complete analysis of the impacts of the differences between the Superpave and Hveem mix designs and are presented in the next chapter.

5 COMPARISON OF FIELD RUTTING AND CRACKING PERFORMANCE ESTIMATES FOR HVEEM AND SUPERPAVE MIX DESIGNS UTILIZING *CALME* MECHANISTIC ANALYSIS

5.1 Introduction

The flexural stiffness, flexural fatigue, and repeated shear test results for Mixes A, B, and I were used to produce materials coefficients for use with *CalME* mechanistic-empirical models *(6, 7)* to simulate pavement performance. These mixes were used to analyze the performance of three structures:

- A flexible pavement analyzed for rutting and cracking,
- A flexible structure with a thin rubberized overlay, analyzed for cracking when built as a new pavement, and when the overlay is placed after the underlying asphalt has already cracked, and
- A composite structure of asphalt on concrete, analyzed for cracking when built as a new pavement and when the overlay is placed after the concrete has already cracked.

The purpose of the simulations was to evaluate the expected effect on pavement performance of the change from Hveem mix designs to Superpave mix designs for the same three materials (Mixes A, B, and I). The analyses shown were deterministic, indicating 50 percent reliability. *CalME* uses Monte Carlo simulation for reliability calculations; however that feature was not used for this study to keep the presentation of the results relatively simple to follow.

5.2 Rutting Performance of Flexible Pavements

The factorial that was used for the *CalME* runs is summarized in Table 5.1. A total of seventy-two cases were simulated with *CalME* to evaluate the effect of mix design method on rutting performance. The three climate regions included in this analysis are among the hottest of the six Caltrans uses for pavement design and PG specification that use PG 64-XX as the typical binder, which is the binder grade used in Mixes A and B. The hottest district (Mojave Desert) was not included because it requires a PG 70-10 binder.

Table 5.1: Factorial of Structures and Climates for Rutting Performance Evaluation: Hveem versus Superpave Mix Design

Mix	Mix Design	Structure	Traffic	Climate Region
Mix A Mix I Mix B	Hveem Superpave	Structure #1[1] Structure #2	Traffic #1[2] Traffic #2	Inland Valley High Desert Low Mountain

Notes:

[1] Structure #1: 125 mm thick AC layer on top of 300 mm thick AB (E_{ab}=250 MPa) and a subgrade with 150 MPa stiffness; Structure #2: 175 mm thick AC layer on top of 300 mm thick AB (E_{ab}=250 MPa) and a subgrade with 150 MPa stiffness

[2] Traffic #1: 1st year = 3 million axles with a 5% growth rate; Traffic #2: 1st year = 6 million axles with a 5% growth rate; typical axle load spectra for California used

5.2.1 General Procedure

The mechanistic-empirical (ME) approach to pavement design makes use of fundamental physical properties and a theoretical model to predict stresses, strains, and deflections, i.e., the pavement response, caused by a load on the pavement. *CalME* uses a modified version of the shear-based procedure developed by Deacon et al. *(28)* to predict accumulated rut depth in HMA layers and also considers the effects of temperature, material properties, load levels, and vehicle speed. *CalME* follows an increment-recursive (IR) procedure when simulating pavement performance where material properties in terms of damage (change in stiffness) and permanent deformation are updated for each time increment by considering the changes in environmental conditions, traffic characteristics, and HMA stiffness. Calculated damage for each time increment is recursively accumulated to be able to predict the pavement condition at any point in time.

The gamma function used to calculate permanent shear strain is given as follows in Ullidtz *(6):*

$$\gamma^i = \exp\left(A + \alpha \times \left[1 - \exp\left(-\ln(N)/\gamma \right) \times \left(1 + \ln(N)/\gamma \right) \right] \right) \times \exp\left(\beta \times \tau / \tau_{ref} \right) \times \left(\gamma^e \right)^{\delta} \qquad \textbf{(1)}$$

where:

γ^i = permanent shear strain

γ^e = elastic shear strain

τ = shear stress

N = number of load repetitions

τ_{ref} = reference shear stress (0.1 MPa = atmospheric pressure)

A, α, β, γ, and δ are model coefficients determined from the RSCH (AASHTO T 320) results.

Calculated model coefficients for the three mixes are presented below in Table 5.2.

Table 5.2: Model Coefficients for *CalME* Rutting Model

Mixes	Mix Design	A	α	τ_{ref}	β	γ	δ
Mix A	Hveem	0.8051	3.4002	0.1000	0.0000	2.9889	1.0000
Mix B	Hveem	0.0000	4.2703	0.1000	0.0000	2.2788	1.0000
Mix I	Hveem	0.0000	3.8648	0.1000	0.0000	2.1627	1.0000
Mix A	Superpave	0.6712	3.5988	0.1000	0.0000	2.2451	1.0000
Mix B	Superpave	1.2356	3.1455	0.1000	0.0000	2.6675	1.0000
Mix I	Superpave	0.0000	4.3135	0.1000	0.0000	2.0478	1.0000

Shear stresses at 50 mm (2 in.) depth at the edge of the tire were calculated by using the calculated stiffnesses, traffic-vehicle characteristics, and material properties as inputs to a layered elastic program. Elastic shear strain values for each repetition interval are calculated by using the following Equation (2):

$$\gamma^e = \frac{\tau}{E_i / (1 + \nu_i)} \quad \textbf{(2)}$$

where:
τ = shear stress calculated from layer elastic theory
E_i = modulus of layer i
ν_i = Poisson's ratio for layer i (assumed to be 0.35 for all layers)

The calculated elastic shear strain value for the corresponding repetition interval and each axle load are used in Equation (1) to calculate the corresponding permanent shear strain (PSS). For the calibration of the model, the coefficient for the shear stress variable (β) was assumed to be equal to zero for all material types because the effect of shear stress on accumulated PSS was simulated using the elastic shear strain variable. *CalME* assumes that rutting is confined to the upper 100 mm of the asphalt layers *(7),* therefore calculated PSSs (from Equation [1]) for each repetition interval are multiplied by 100 mm to calculate the corresponding rutting deformation. Calculated rut depths for each repetition interval are accumulated based on the IR procedure to develop the final rutting-versus-time curve.

The calculated PSS values are related to measured downward rut depths using the following equation:

$$dpi = K \times hi \times \gamma^i \quad \textbf{(3)}$$

where:
K= calibration coefficient, calibrated based on Heavy Vehicle Simulator and WesTrack data (2 for HMA, 0.5 for RHMA)
h_i= thickness of layer i (up to 100 mm, assumed to be 100 mm for thicker asphalt layers)
dp_i = rut depth

5.2.2 Results

In this study, rutting at Year 40 was used as a parameter to evaluate the effect of mix design method on predicted rutting performance. As an example, Figure 5.1 shows the *CalME*-predicted surface rutting accumulation for Mix A under Traffic Level #1 (1st year = 3 million axles with a 5 percent growth rate) for different climate regions and structures.

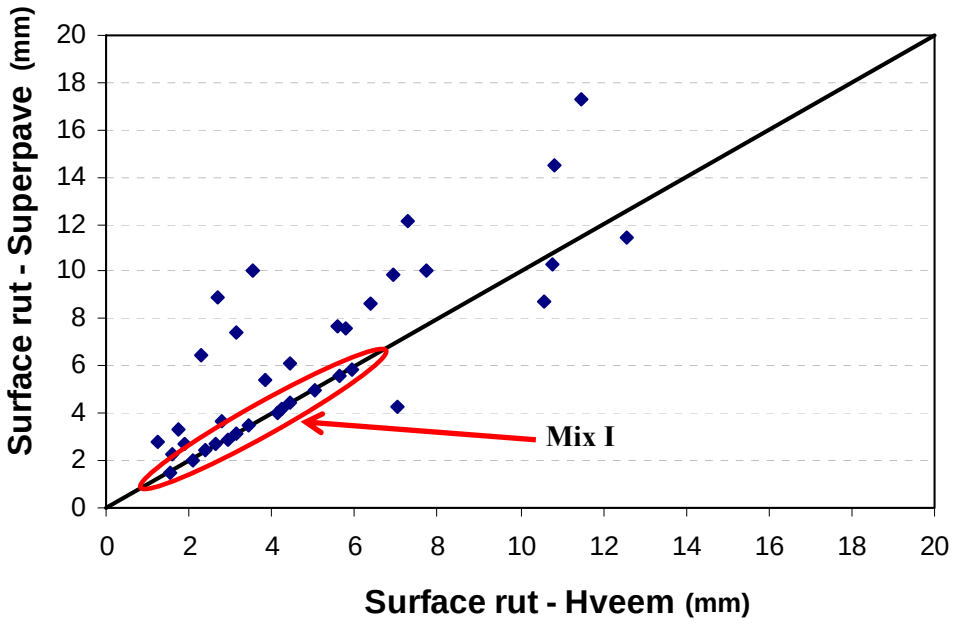

Figure 5.1: Comparison of *CalME*-predicted surface rutting at Year 40 for mixes designed with Hveem and Superpave methods for Mixes A, B, and I.
(Note: The points in the red ellipsoid are the predictions for Mix I. No significant asphalt layer rutting was observed for Mix I.)

Figure 5.2 shows the comparison of calculated surface rut for the same structure with the two mix designs. It can be seen that for Mixes A and B, the Hveem design had less rutting more often than the Superpave design, while Mix I showed almost identical results for the two mix designs. It can also be seen that all of the Hveem mix designs had simulated rut depths less than the Caltrans design criteria of 12.5 mm (1/2 inch) and most were less than 8 mm. Despite the difference in the laboratory RSCH results and the simulated rutting performance between the Superpave and Hveem mix designs, only two of the thirty-six Superpave simulations had predicted rutting greater than the Caltrans criteria. This indicates that for these cases, the results support the hypothesis that the rutting performance obtained from the Hveem procedure could be safely reduced, with the intention of increasing cracking performance. These results are based on 50 percent reliability, which is lower than would be acceptable for pavement design.

In order to determine the statistical significance of the rutting performance difference between the Hveem and Superpave mix design methods, the Welch-modified two sample t-test was used. F_1 and F_2 are two distributions, and the possible hypotheses and alternatives concerning these distributions are:

H_0: $F_1(x) = F_2(x)$ (There is no difference in the rutting performance between the Hveem and Superpave mix design methods)

H_A: $F_1(x) \neq F_2(x)$ (There is a significant difference in the rutting performance between the Hveem and Superpave mix design methods)

Decision rule: Reject H_0 if p-value < 0.10; fail to reject H_0 if p-value ≥ 0.10

The calculated p-value for the distributions of predicted rutting for the Hveem and Superpave methods was 0.09, indicating that the null hypothesis can be rejected and that the mix designs produce rutting that is significantly different. Further analysis of the data by finding the shift factor that minimized the difference between the rutting distributions indicated that the predicted surface rutting for the Superpave mixes is 20 percent higher than the surface rutting of Hveem mixes. Condidering that surface rutting is seldom a trigger for treatment on the Caltrans network, this indicates that in general the Superpave mix designs should still provide acceptable performance despite the increase in rutting susceptibility compared with the Hveem designs. Considering that most mix rutting appears within the first five years of construction, monitoring should be performed on projects using Superpave mix designs each year over the next five years using Caltrans Automated Pavement Condition Survey data as it becomes available each year.

Differences in surface rut for the two structures are primarily due to differences in rutting of the asphalt layer, and show that most of the rutting occurred in the asphalt layers. Figure 5.3 shows the *CalME*-predicted rutting accumulation only in the asphalt layer for the same cases for Mix A. The same Welch-modified two sample t-test was used to evaluate the statistical significance in the asphalt rutting predictions, and returned a p-value of 0.05, suggesting that the asphalt rutting is significantly different. Further analysis of the data by finding the shift factor that minimized the difference between the rutting distributions indicated that the predicted asphalt rutting for the Superpave mixes is 56 percent higher than the asphalt rutting of Hveem mixes.

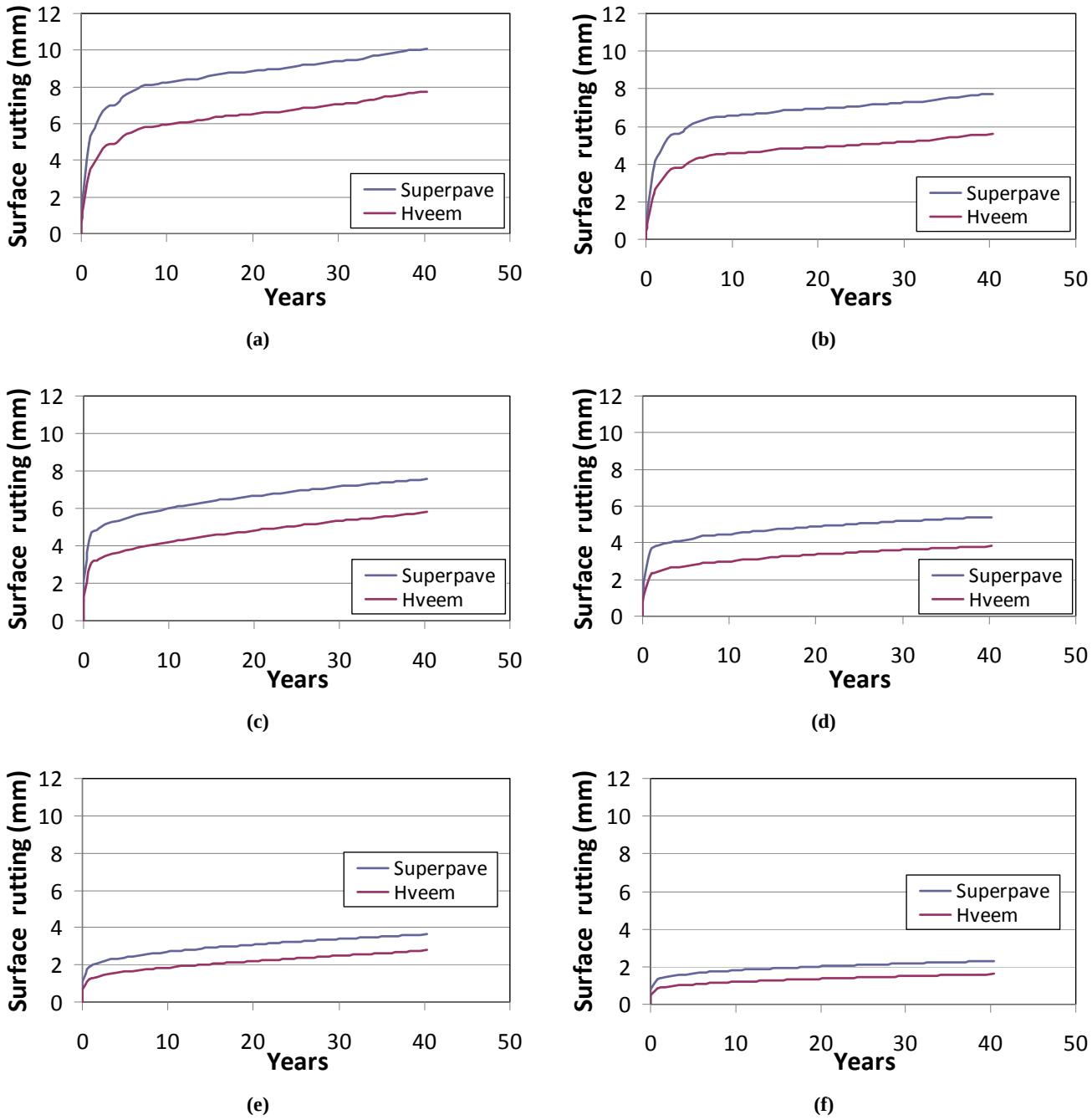

Figure 5.2: *CalME*-predicted surface rutting for Mix A under Traffic Level #1: (a) High Desert – Structure #1 (125 mm AC layer); (b) High Desert – Structure #2 (175 mm AC layer); (c) Inland Valley – Structure #1 (125 mm AC layer); (d) Inland Valley – Structure #2 (175 mm AC layer); (e) Low Mountain – Structure #1 (125 mm AC layer); (f) Low Mountain – Structure #2 (175 mm AC layer).

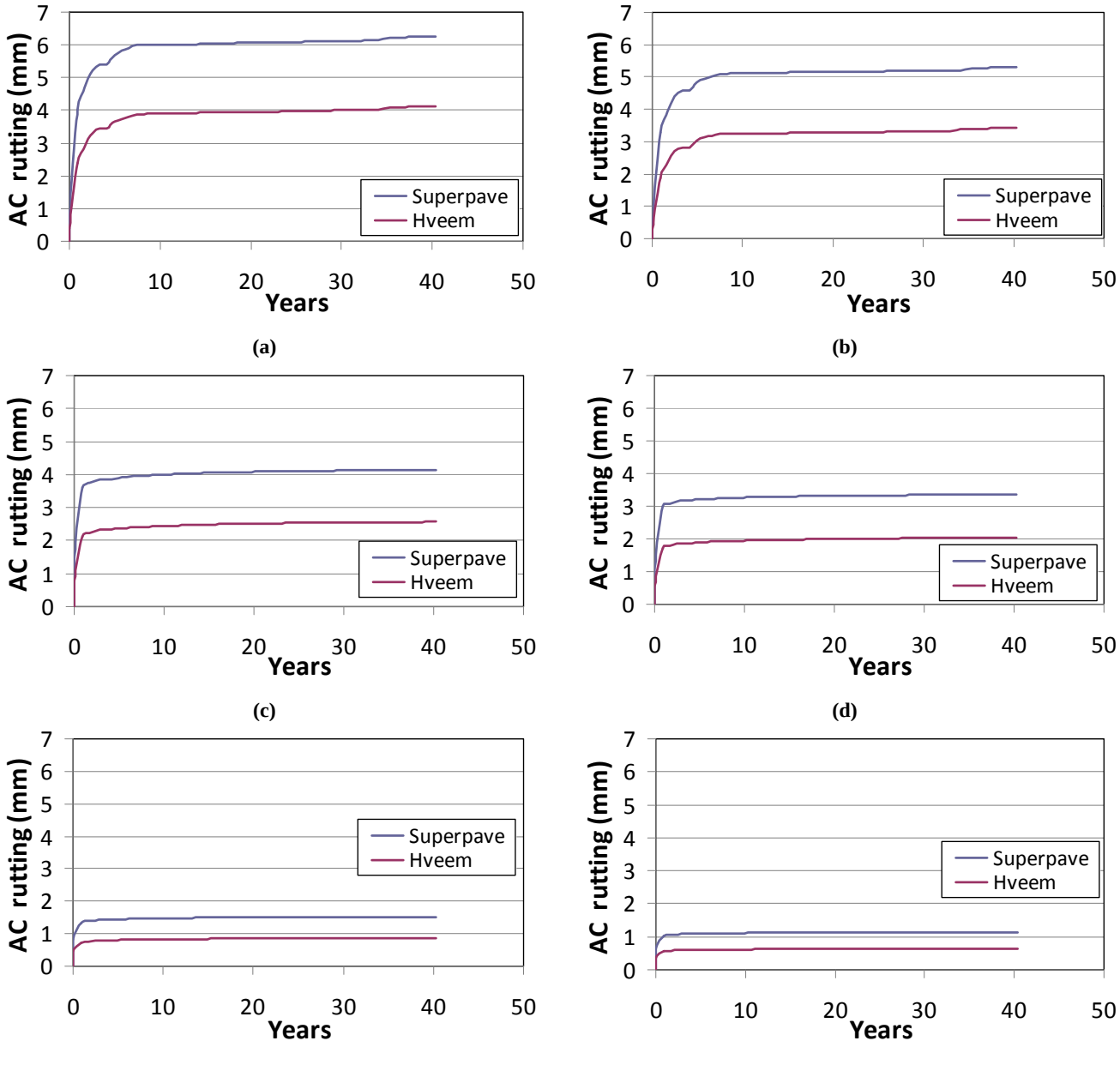

Figure 5.3: *CalME*-predicted asphalt layer rutting for Mix A under Traffic Level #1: (a) High Desert – Structure #1 (125 mm AC layer); (b) High Desert – Structure #2 (175 mm AC layer); (c) Inland Valley – Structure #1 (125 mm AC layer); (d) Inland Valley – Structure #2 (175 mm AC layer); (e) Low Mountain – Structure #1 (125 mm AC layer); (f) Low Mountain – Structure #2 (175 mm AC layer).

5.3 Cracking Resistance of Thin Rubberized HMA Layer (Mix I) Constructed on Top of Mix A Layer

Caltrans uses rubberized gap-graded HMA (RHMA-G) overlays extensively—as a surface layer in rehabilitation projects using thick overlays or all new asphalt layers, and as a thin overlay on existing cracked asphalt pavement. The hypothesis that the Superpave mix designs might provide better cracking resistance was evaluated using *CalME* following the factorial shown in Table 5.3. A total of twenty-four cases were simulated with *CalME* to evaluate the effect of mix design method on cracking performance.

Table 5.3: Factor Levels for Mix I Cracking Performance Evaluation: Hveem versus Superpave Mix Design

Mix Design	Structure	Traffic	Climate Region	Analysis
Hveem Superpave	Structure #1[1] Structure #2	Traffic #1[2]	Inland Valley High Desert Low Mountain	With reflective cracking Without reflective cracking

Note:

[1]: Structure #1: 60 mm thick Mix I layer on top of 125 mm thick Mix A layer on a 100 mm thick AB (E_{ab}=200 MPa) and a subgrade with 100 MPa stiffness; Structure #2: 60 mm thick Mix I layer on top of 175 mm thick Mix A layer on a 100 mm thick AB (E_{ab}=200 MPa) and a subgrade with 100 MPa stiffness.

[2] Traffic #1: 76 million ESALs over 20 years using a typical California axle load spectrum

5.3.1 General Procedure

Stiffness Model for Asphalt-Bound Materials

The asphalt-bound material modulus was modeled in *CalME* as a function of temperature and loading time, using the NCHRP 1-37A Design Guide model *(29)*

$$\log(E) = \delta + \frac{\alpha}{1+\exp(\beta+\gamma\log(tr))} \quad \textbf{(4)}$$

where:

E is the modulus in MPa,
tr is reduced time in sec,
α, β, γ, and δ are constants, and
logarithms are to base 10.

Reduced loading time *tr* was found from:

$$tr = lt \times \left[\frac{\eta(T_{ref})}{\eta(T)}\right]^{aT} \quad \textbf{(5)}$$

where:

lt is the loading time (in sec),
$\eta(T_{ref})$ is the binder viscosity at the reference temperature,
$\eta(T)$ is the binder viscosity at the actual temperature, and
aT is a constant.

The viscosity (cPoise) is found from:

$$\log(\log(\text{viscPoise})) = A + VTS \times \log(t_k) \quad (6)$$

where t_k is the temperature in °K and A and viscosity temperature susceptibility (VTS) are constants.

The master curve coefficients for the three asphalt mixes are shown in Table 5.4.

Table 5.4: Model Coefficients for *CalME* HMA Modulus Model (Eqs. 4 and 5)

Mixes	Design method	δ	β	γ	aT	E_{ref}	T_{ref}	α
Mix A	Superpave	2.3010	0.2316	0.7756	1.2086	4999	21.4	1.8261
Mix B	Superpave	2.3010	0.3809	0.8298	1.1977	3990	21.4	1.7188
Mix I	Superpave	2.3010	0.3007	0.7578	1.1894	3899	21.4	1.7274
Mix A	Hveem	2.3010	-0.0014	0.8132	1.2390	6495	21.4	1.8541
Mix B	Hveem	2.3010	0.2780	0.7990	1.2995	4454	21.4	1.7622
Mix I	Hveem	2.3010	0.2791	0.8631	1.1002	3825	21.4	1.6327

Note:
In Equation (6), A=9.6307, VTS=-3.5047,
In Equation (5), lt=0.015 for all mixes

Fatigue Cracking Model

Fatigue causes damage in asphalt-bound materials and in composite pavements the damage appears as surface cracking. In *CalME*, the density of surface cracking caused by fatigue is a function of the damage in an asphalt-bound layer. The fatigue damage, in turn, is accumulated at a rate that is determined by the tensile strain caused by traffic loading, which is determined using either layer elastic theory if there are no existing cracks or a regression model for tensile strain based on finite element analysis results if there is existing cracking *(30, 31)*. Fatigue damage determines the residual stiffness of asphalt-bound materials. Specifically, the stiffness for asphalt-bound material with damage ω becomes:

$$\log(E) = \delta + \frac{\alpha \times (1-\omega)}{1+\exp(\beta + \gamma \log(tr))} \quad (7)$$

where the variables are defined in Equation (7) and the damage ω was calculated from:

$$\omega = \left(\frac{MN}{FSF \cdot MN_p} \right)^{\alpha} \quad (8)$$

where *MN* was the number of load applications in millions, MN_p was the allowable number of load repetitions in millions, *FSF* was the fatigue shift factor, and α was a material-dependent exponent. α was calculated using the following equation:

$$\alpha = \exp\left(\alpha_0 + \alpha_1 \times \frac{t}{1°C}\right) \quad \textbf{(9)}$$

where:

t = material temperature in °C, and

α_0 and α_1 are material constants

while MN_p was calculated using the following equation:

$$MN_p = A \times \left(\frac{\varepsilon}{\varepsilon_{ref}}\right)^{\beta} \times \left(\frac{E}{E_{ref}}\right)^{\gamma} \times \left(\frac{E_i}{E_{ref}}\right)^{\delta} \quad \textbf{(10)}$$

where:

ε = bending strain at the bottom of the asphalt layer, με,

ε_{ref} = reference bending strain, με,

E_i = intact modulus for the current temperature and loading time,

E_{ref} = reference modulus, and

A, β, γ, and δ are material constants.

The model parameters for Equations (8), (9), and (10) were determined by fitting the stiffness reduction curves from the flexural fatigue tests conducted at 20°C for the three mixes. In the current use of *CalME,* values of α_1=0, δ=0, and γ = β/2 are used to be consistent with the concept of damage driven by strain energy, since the energy of bending the beam is related to strain squared times stiffness.

Calculated model coefficients for the three mixes are given in Table 5.5.

Table 5.5: Model Coefficients for *CalME* HMA Cracking Model (Eqs. 8 and 9)

Mixes	Design method	A	α_0	ε_{ref}	β	E_{ref}	γ
Mix A	Superpave	651.3	-0.2925	200	-7.741	3000	-3.8706
Mix B	Superpave	30.8	-0.2415	200	-5.367	3000	-2.6836
Mix I	Superpave	1302.9	-0.9251	200	-4.730	3000	-2.3648
Mix A	Hveem	29.12	0.0305	200	-5.992	3000	-2.9959
Mix B	Hveem	13.9	-0.0245	200	-5.021	3000	-2.5105
Mix I	Hveem	1511.8	-0.9738	200	-4.656	3000	-2.3277

The laboratory-to-field fatigue shift factor (FSF) was determined from a reference factor accounting for the difference between laboratory fatigue tests and full-scale testing, and includes the effects of rest periods:

$$FSF = \left\{ 1 + \left[\frac{RP}{RP_{ref}} \times \left(\frac{\eta(T_{ref})}{\eta(T)} \right)^{aT} \right]^{\varphi} \right\} \times FSF_{ref} \quad \textbf{(11)}$$

where:

RP = rest period for traffic loading,

$\eta(T_{ref})$, $\eta(T)$ and aT = stiffness master curve parameters,

RP_{ref} = 10 seconds is the reference rest period,

φ = 0.4 is a constant model parameter, and

FSF_{ref} is the laboratory-to-field fatigue shift factor without accounting for rest periods.

Once the fatigue damage for the asphalt surface layer has been determined, the surface crack density can be calculated. The amount of cracking at crack initiation must be assumed (in calibration studies, values of 5 percent of the wheelpath or 0.5 m/m^2 have been used).

$$CR = \frac{CR_{\max} \times \left(\omega_{initiation}^{\alpha} - 1 \right)}{\omega_{initiation}^{\alpha} - \frac{CR_{\max}}{CR_i} + \left(\frac{CR_{\max}}{CR_i} - 1 \right) \cdot \omega^{\alpha}} \quad \textbf{(12)}$$

where:

CR_{max} = 100% or 10 m/m^2 is the maximum surface crack density,

CR_i = 5% or 0.5 m/m^2 is the surface crack density corresponding to crack initiation,

ω = damage in asphalt-bound material,

$\omega_{initiation}$ = damage corresponding to crack initiation, calculated separately, and

α is a model constant determined from field calibration.

The crack initiation damage $\omega_{initiation}$ was calculated using the following equation:

$$\omega_{initiation} = \frac{A_i}{1 + \left(\frac{h_{AC}}{h_{ref}} \right)^{a_i}} \quad \textbf{(13)}$$

where:

h_{AC} = combined asphalt concrete overlay thickness

h_{ref} = 250 mm is the reference overlay thickness

a_i = -2.0 is a model parameter determined from field calibration

A_i =1.0 is a another model parameter determined from field calibration

Cracking density is given in m/m^2.

Reflective Cracking Model

Reflective cracking damage was calculated the same way as fatigue cracking damage. The difference was that the strain in Equation (10) for reflective cracking strain was calculated differently, based on a method developed by Wu *(30, 31)* that is a regression equation based on finite element runs. Once reflective cracking damage was calculated, surface crack density was calculated using Equations (12) and (13) but with different values for A_i and a_i, specifically $A_i = 0.54$ and $a_i = -0.90$.

5.3.2 Results

The cases outlined in Table 5.3 were simulated in *CalME* to evaluate the cracking resistance of thin Mix I (RHMA) layers constructed on top of thicker cracked and uncracked Mix A (HMA) layers. Results of the bottom-up fatigue-cracking simulations (60 mm RHMA on uncracked 125 or 175 mm HMA) are shown in Figure 5.4**.** It can be observed that Structure #1 with a 125 mm Mix A layer designed with the Hveem method (a) fails at around Year 25 (for a 1.6 m/m^2 cracking limit) for the climate regions used in this study. For the same structure, climate, and traffic level, the Superpave designed mix (c) did not show any cracking during the 40-year design period. Structure #2 with a 175 mm Mix A layer (b and d), did not show any cracking for both mix design methods.

For the reflective cracking cases outlined in Table 5.3 (60 mm RHMA on cracked 125 mm or 175 mm HMA), a crack spacing of 200 mm in the underlying asphalt was used for the analyses. Results are given in Figure 5.5.

It can be observed that Structure #1 with the RHMA-G overlay designed with the Hveem method on a cracked 125 mm Mix A layer (a) fails at around Year 30 (for a 1.6 m/m^2 cracking limit) for the climate regions used in this study. For the same structure, climate, and traffic level, the RHMA-G overlay designed with the Superpave method (c) shows a very low level of cracking at the end of the 40-year design period. Structure #2 with a 175 mm Mix A layer did not show any cracking for both mix design methods.

These results indicate that the hypothesis that Superpave mixes may improve both bottom-up and reflective fatigue-cracking performance was validated.

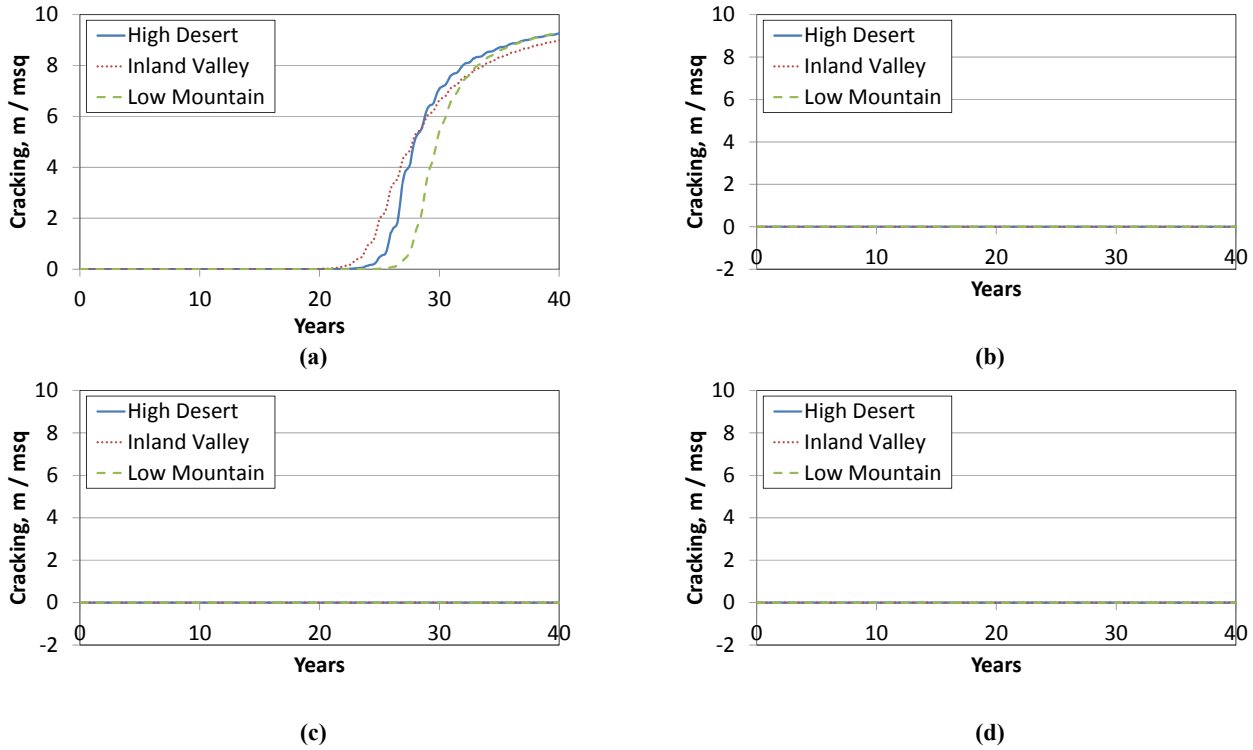

Figure 5.4: *CalME*-predicted surface cracking from bottom-up fatigue (reflective cracking was not simulated) for Hveem and Superpave designs: (a) Structure #1 with 125 mm Mix A layer; Hveem mix design; (b) Structure #2 with 175 mm Mix A layer; Hveem mix design; (c) Structure #1 with 125 mm Mix A layer; Superpave mix design; (d) Structure #2 with 175 mm Mix A layer; Superpave mix design.

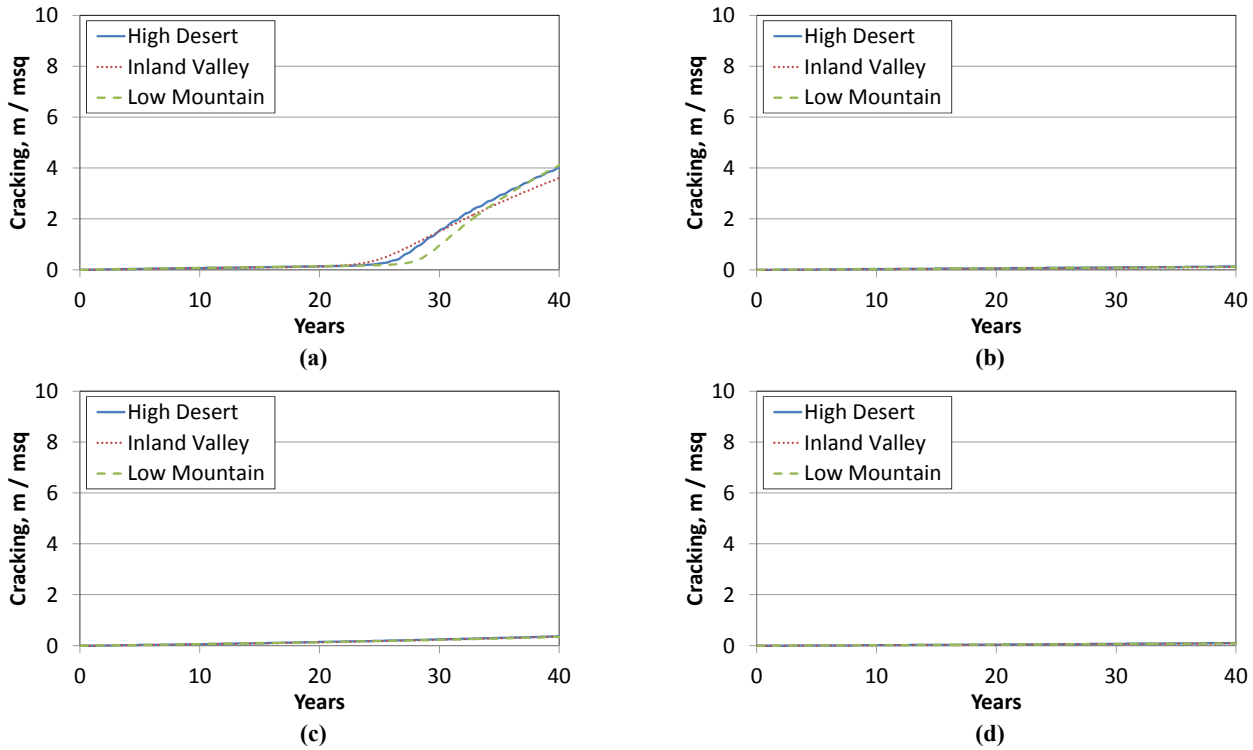

Figure 5.5: *CalME*-predicted surface cracking (reflective cracking was simulated) for Hveem and Superpave designs: (a) Structure #1 with 125 mm Mix A layer; Hveem mix design; (b) Structure #2 with 175 mm Mix A layer; Hveem mix design; (c) Structure #1 with 125 mm Mix A layer; Superpave mix design; (d) Structure #2 with 175 mm Mix A layer; Superpave mix design.

5.4 Reflective Cracking Resistance of Thin Overlays on Concrete

Reflective cracking was simulated for thin HMA (Mix A, Mix B), and RHMA (Mix I) overlays constructed on top of concrete pavement (note that the slab thicknesses for the concrete are less than typically used for Caltrans, and come from the SHRP R21 study on composite pavement), however the results indicate the expected trend for cracking for the different mix design procedures. A crack and joint spacing of 1.2 m (4 ft) was assumed for the cracked and seated concrete. The factorial with a total of twenty-four cases that was used for *CalME* runs is summarized in Table 5.6.

Table 5.6 Factorial for Thin AC Layer Cracking Performance Evaluation (AC Layer on Cracked PCC): Hveem versus Superpave Mix Design

Mix	Mix Design	Structure	Traffic	Climate	Analysis
MixA Mix B Mix I	Hveem Superpave	Structure #1[1] Structure #2	Traffic #1[2]	High Desert Low Mountain	With reflective cracking

Notes:

[1]: Structure #1: 60 mm thick overlay on top of 125 mm thick cracked concrete layer (E_{PCC}=35,000 MPa) on a 100 mm thick AB (E_{ab}=200MPa) and a subgrade with 100 MPa stiffness; Structure #2: 60 mm thick AC layer on top of 175 mm thick cracked concrete layer on a 100 mm thick AB (E_{ab}=200MPa) and a subgrade with 100 MPa stiffness

[2] Traffic #1: 3.2 million ESALs per year for 20 years

Results are shown in Figure 5.6 and Figure 5.7 for the Low Mountain and High Desert climates, respectively. Results for other climate regions showed very similar trends. It can be observed that cracking resistance of Mix A was highly sensitive to the mix design type. Mix A overlays designed with the Superpave method show significantly better cracking resistance than Mix A layers designed with the Hveem method. On the other hand, mix design method does not appear to have a significant effect on the cracking performance of Mix I and Mix B overlays. It can also be seen that the RHMA-G (Mix I) overlay shows significantly better reflective cracking resistance, as expected. For a 1.6 m/m^2 cracking design limit, Mix B fails at around Year 10 while Mix I layers do not reach the design limit even at Year 40 for any of the climate regions or structure types (note that the model does not consider block cracking caused by aging). As with the simulations of cracking on flexible pavements, the use of Superpave mix designs showed improvement of reflective cracking performance for thin overlays on concrete pavement compared with the same pavements with Hveem mix designs, with some mixes showing a large difference in simulated performance while other showed small changes.

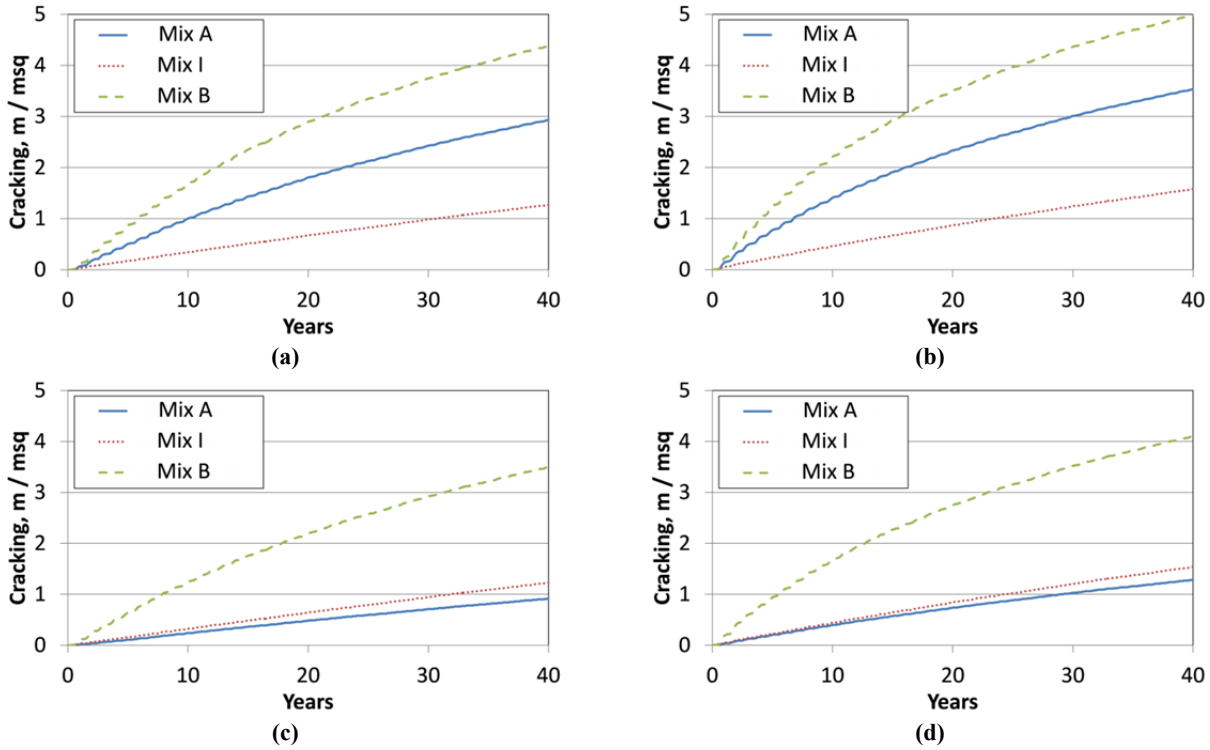

Figure 5.6: High desert climate−*CalME*-predicted surface cracking (reflective cracking was simulated) for Hveem and Superpave designs: (a) Structure #1 with 125 mm concrete layer; Hveem mix design; (b) Structure #2 with 175 mm concrete layer; Hveem mix design; (c) Structure #1 with 125 mm concrete layer; Superpave mix design; (d) Structure #2 with 175 mm concrete layer; Superpave mix design.

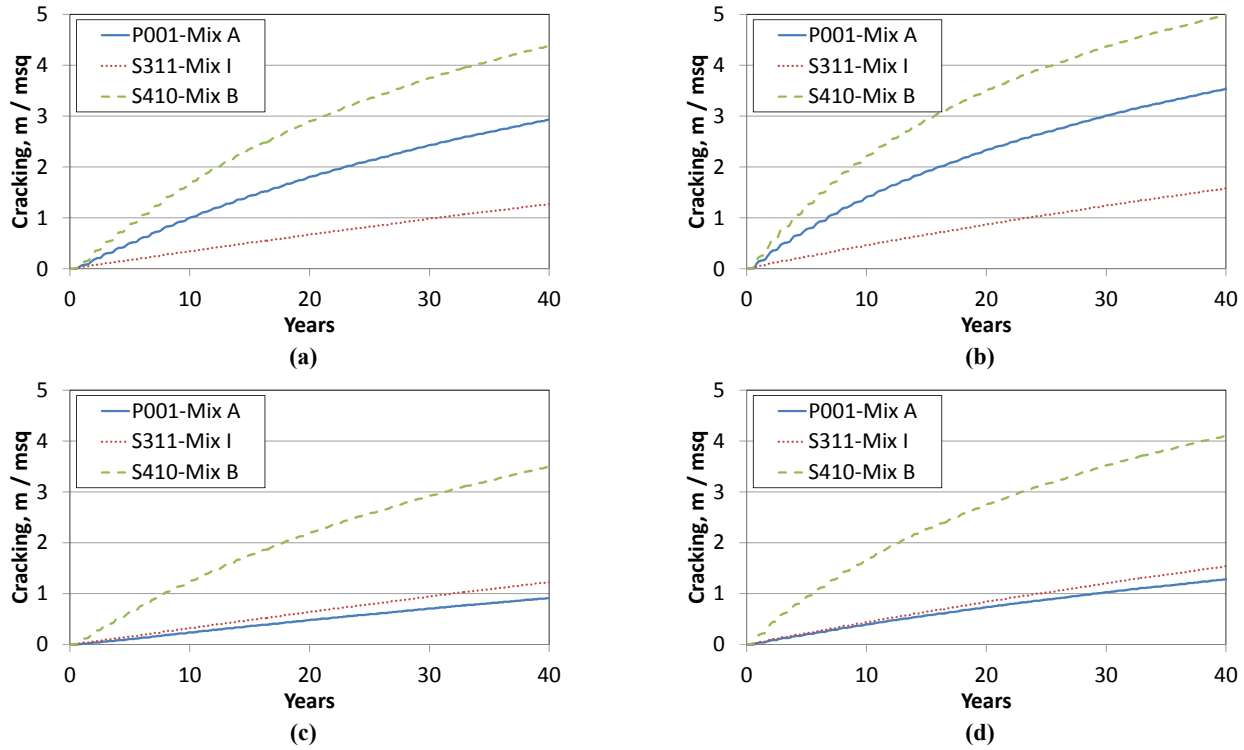

Figure 5.7: Low mountain climate−*CalME*-predicted surface cracking (reflective cracking was simulated) for Hveem and Superpave designs: (a) Structure #1 with 125 mm concrete layer; Hveem mix design; (b) Structure #2 with 175 mm concrete layer; Hveem mix design; (c) Structure #1 with 125 mm concrete layer; Superpave mix design; (d) Structure #2 with 175 mm concrete layer; Superpave mix design.

5.5 The Effect of Mix Design Method on Design Layer Thicknesses

In order to evaluate the effect of mix design method on design layer thicknesses for simple flexible pavements consisting of asphalt concrete on a Class 2 aggregate base on a clay subgrade, asphalt layer design thicknesses for two traffic levels were determined by evaluating the cracking and rutting resistance of Mix A. The factorial for Mix A thickness designs is given in Table 5.7. The pavements were designed for Traffic Index values of 10 and 14 which represent 2.4 and 41 million equivalent single axle loads in the design period, respectively, and a reliability of 50 percent, for the purposes of illustration. By using optimization, design layer thicknesses for Hveem and Superpave mixes for Traffic #1 were determined to be 103 mm and 84 mm, respectively. Design layer thicknesses for Hveem and Superpave mixes for Traffic #2 were determined to be 162 mm and 122 mm, respectively. The Superpave mix design resulted in a reduction in required asphalt thickness of 23 percent for the Traffic #1 (TI=10) pavement and 33 percent for the Traffic #2 (TI=14) pavement. In all the simulated cases, cracking appears to be the distress type that controls the design. Rut depths for the design thicknesses are shown in Figure 5.8.

Typically, the largest environmental and cost impacts from the materials production and construction phases of the example pavements are from the asphalt binder in the asphalt mix. In order to determine the amount of binder used for the Hveem and Superpave designs, a simple case study was prepared that considered the binder content in each mix, which was less for the Hveem mix design, and the required thickness of the mix, which was greater for the Hveem mix design. The amount of binder required to pave a one-mile long, twelve-foot wide (3.66 m) asphalt layer was calculated for both Hveem and Superpave mixes, and the results are presented in Table 5.8. For Traffic #1, the amount of binder required to construct the hypothetical section is about 11.5 percent larger for the Hveem mix design method. For Traffic #2, this number increases to 20.7 percent. This result suggests that Superpave mixes might become more economical alternatives if the materials properties of the different mix designs are considered in the structural design, especially at high traffic levels. However, these results are only for a specific structure and climate region. A variety of cases should be analyzed to evaluate the economic benefits of each design method. For warmer climates and softer mixes, the Hveem mix design method might be more economical due to its better rut resistance. For this reason, a larger factorial analysis should be performed to better evaluate the economic benefits.

Table 5.7: Factorial for Mix A Thickness Design−Hveem versus Superpave

Mix	Mix Design	Structure	Traffic	Climate
Mix A	Hveem Superpave	Structure #1[1]	Traffic #1[2] Traffic #2	Inland Valley

Notes:

[1] Structure #1: Mix A layer on top of a 150 mm thick AB (E_{ab}=200MPa) and a subgrade with 100 MPa stiffness

[2] Traffic #1: 2.5 million ESALs for 20 years: TI10; Traffic #2: 40 million ESALs for 20 years: TI14

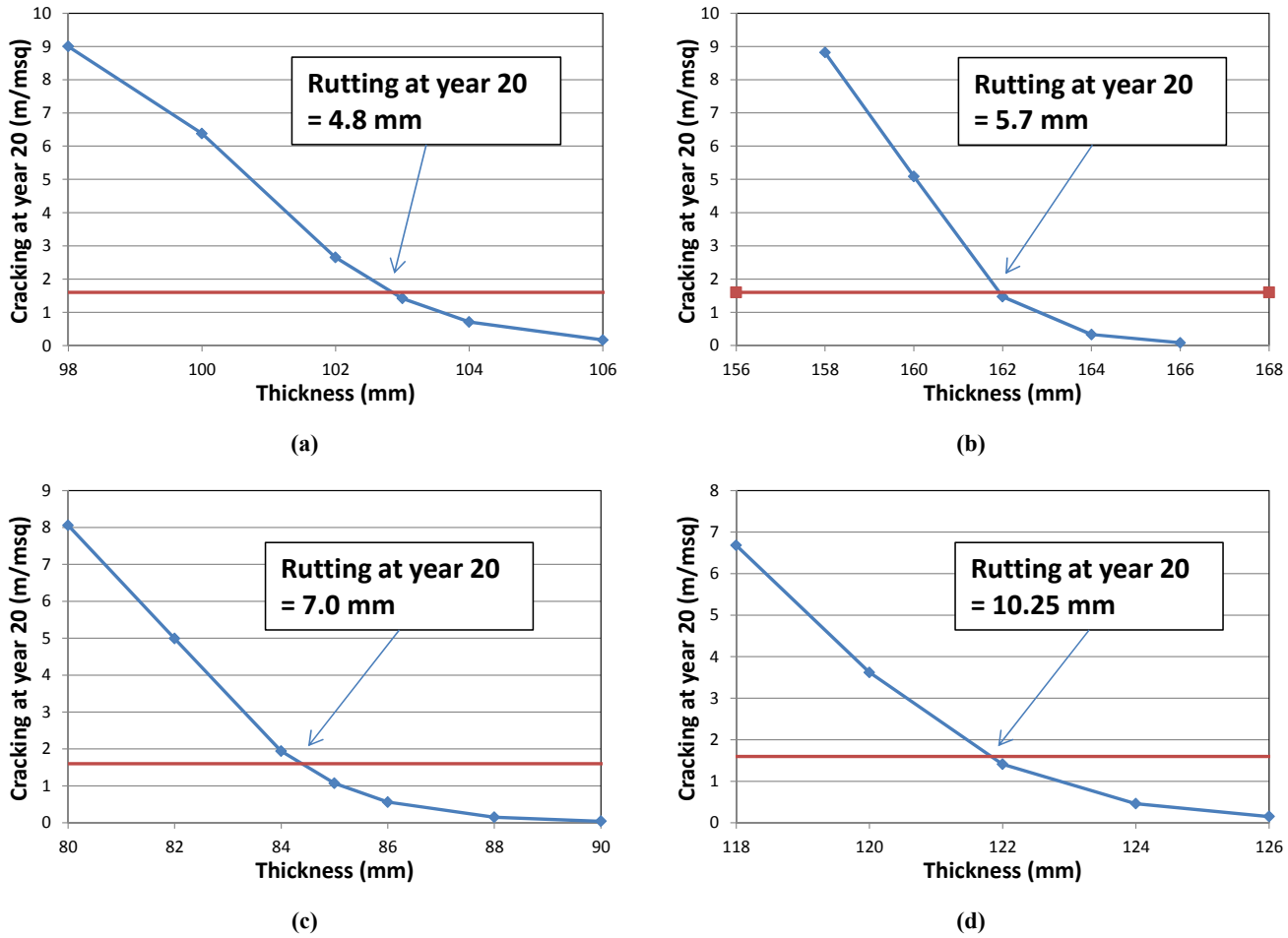

Figure 5.8: Deterimination of design asphalt layer thickness based on cracking (blue line) and rutting (text box) for (a) Hveem mix design – Traffic #1 (103 mm), (b) Hveem mix design – Traffic #2 (162 mm), (c) Superpave mix design – Traffic #1 (84 mm), (d) Superpave mix design – Traffic #2 (122 mm).

Table 5.8: Simple Case Study to Evaluate the Amount of Binder Used for Hveem and Superpave Mixes

	T#1[1] V_{mix}[2] (m^3)	T#2[3] V_{mix} (m^3)	Design AC (%)	T#1 $mass_{binder}$[4] (metric tonnes)	T#2 $mass_{binder}$ (metric tonnes)
Hveem	606	953	5.00	30.9	48.5
Superpave	494	718	5.50	27.7	40.3

Notes:
[1]: T#1: Traffic level 1 – TI_10
[2]: V_{mix} : Volume of asphalt mix used for a 1 mile section for a 12 ft (3.66 m) lane width
[3]: T#2: Traffic level 2 – TI_14
[4]: $mass_{binder}$: mass of asphalt binder used for a 1 mile section for a 12 ft lane width

5.6 Findings

The following findings are based on the mechanistic-empirical comparison of simulated performance for rutting, bottom-up fatigue, and reflective cracking performance for Hveem and Superpave mix designs using the same materials:

- For rutting, it was observed that mix design method was an important factor affecting the simulated rutting in the asphalt layers. Statistical analysis indicated that the mean predicted asphalt layer rutting for Hveem mixes is significantly less than that of Superpave mixes. However, the Superpave mix designs still met Caltrans design criteria for rutting performance in thirty-four of thirty-six scenarios analyzed at the 50 percent reliability level, indicating that the Hveem mix designs may have been overly conservative for rutting.
- For fatigue and reflective cracking, some improvement was shown when using the Superpave mix design as compared to the Hveem mix design in simulated cracking performance, with one of three mixes showing a large improvement and the other two showing lesser improvement. These results indicate that for the cases simulated, the hypothesis that Superpave mix designs would show poorer, but likely still sufficient, rutting performance, while improving cracking performance is reasonable.
- Based on these findings, it is recommended that construction projects with Superpave and Hveem mix designs be evaluated annually using Automated Pavement Condition Survey data over the next five years to compare actual field performance of the two mix design approaches.

6 INTERACTIONS WITH SPECIMEN PREPARATION AND TEST VARIABLES AND DEVELOPMENT OF INITIAL RSCH-RLT SHIFT FACTORS

6.1 Introduction

This chapter presents the results of the comparison of permanent strain versus repetitions for the repeated load triaxial (RLT) test using the AMPT and the repeated shear test at constant height (RSCH) for a single field mix. The purpose of the comparison was to determine the best approach for using RLT results for specimens compacted using Superpave gyratory compaction (SGC) to replicate RSCH results for specimens compacted in the field or with rolling-wheel compaction. The two tests were compared using:

- Superpave gyratory-compacted and field-compacted (and rolling-wheel as field surrogate) specimens
- Specimens compacted to different air-void contents
- Different test temperatures
- In the confined and unconfined conditions in RLT testing (i.e., with and without confining stress)

RLT results for permanent axial strain (PAS) using cap-to-cap measurements and measurements on the middle half of the specimen were also compared to determine whether the cap-to-cap measurements produced the same results as the measurements on the middle half of the specimen. Cap-to-cap measurements are simpler to use but do not eliminate the potential effects of friction at the caps.

The SHRP A-003A study found that RSCH testing specimens produced by rolling-wheel compaction best matched those produced by field compaction *(10, 32).* The RSCH uses specimens compacted to 3 percent air-void content, assuming that this is close to a "refusal" density for most mixes and that they will densify toward this value under initial traffic. The RSCH test does not allow further densification (constant volume), seeking to isolate the effects of shear from those of densification (volume change) by minimizing compressive stresses and attempting to keep most of the specimen subject to shear stresses only. In the RSCH test, increasing the air-void content generally causes significant increases in permanent deformation.

The RLT test allows both densification and shearing by applying compressive and shear stresses. The typical test is recommended to be conducted on a Superpave gyratory cylindrical specimen compacted to 7 percent air-void content and cored and cut from the larger compacted specimen following AASHTO TP 79-12 *(3)* and AASHTO PP 60-11. Gibson et al. *(33)* compared the permanent deformation of RLT test specimens that were compacted by SGC with those compacted with a field roller compactor and found that field-compacted cores were initially less resistant to rutting than the SGC specimens but that they also had less binder aging than the

SGC specimens (due to the reheating of the mix required to produce the SGC specimens). NCHRP 9-30A tried to compare RSCH results using rolling-wheel specimens and AMPT/RLT results using SGC-prepared specimens, and did not find a good correlation *(13)*.

The normal axial deformation measurement device configuration for the AMPT uses the linear variable differential transducer (LVDT) in the actuator, which assumes the entire height of the sample (150 mm [6 inches]) as the gauge length. Following AASHTO TP 79, the specimen assembly procedure requires "greased double latex" friction reducers to be placed between the platens and test specimens. Most RLT testing also includes measurement of axial deformation over a smaller gauge length in the middle of the specimen in order to reduce the influence of end effects. Since data accuracy might be affected, it was necessary to verify the default AMPT deformation measurement method and develop a new system if the normal test setup did not provide acceptable results.

The effects of SGC and field compaction on dynamic modulus master curve results were compared using the same mix, in addition to the comparison of compaction effects on permanent deformation test results.

This chapter answers the following key questions:

1. How does compaction method affect test results?
2. How does air-void content affect test results?
3. How does temperature affect test results?
4. Do on-specimen LVDT results match RLT actuator LVDT results?
5. Is it possible to relate typical RLT and RSCH test results? And if yes, how?

The chapter also provides a preliminary evaluation of the effects of performing the RLT in the confined state and in the unconfined state, using SGC-compacted specimens at two temperatures.

6.2 Experimental Plan and Test Conditions

The experiment design is shown in Table 6.1 for the RLT specimens and in Table 6.2 for the RSCH specimens. One mix was used for this study. The mix design was developed based on a performance-related "long-life asphalt" specification that required a minimum rutting resistance based on the RSCH test, a minimum fatigue resistance based on the flexural fatigue test (AASHTO T 321), and a minimum stiffness at 20°C also based on flexural beam testing. Aggregate was sourced near Red Bluff, California. The aggregate structure was dense-graded with a nominal maximum aggregate size of ¾ inch; 1.2 percent lime (based on the weight of the virgin aggregate) was added using the process of lime marination. The gradation curve is shown in Figure 6.1. A PG 64-16 conventional asphalt binder was used. The target binder content for the mix was 5.38 percent by dry weight of aggregate from the job mix formula. The mix contained 25 percent RAP by dry weight of aggregate.

Table 6.1: Repeated Load Triaxial and Dynamic Modulus (AMPT) Test Plan

Confined Repeated Load Triaxial Test (10 psi [68.9 kPa] confining stress, 70 psi [483 kPa] deviator stress)				
Rolling-Wheel				
Target Air Voids	**Minimum Replicates[1]**	**# Tested**	**Replicates and Test Temperatures[2]**	
3%	6	12	6 at 45°C, 6 at 55°C	
5%	6	12	6 at 45°C, 6 at 55°C	
7%	6	None	No cores	
Superpave Gyratory				
Target Air Voids	**Minimum Replicates**	**# Tested**	**Replicates and Test Temperatures**	
3%	6	12	6 at 45°C, 6 at 55°C	
5%	6	8	4 at 45°C, 4 at 55°C	
7%	6	12	6 at 45°C, 6 at 55°C	
Field				
Target Air Voids	**Minimum Replicates**	**# Tested**	**Replicates and Test Temperatures**	
3%	6	10	5 at 45°C, 5 at 55°C	
5%	6	12	6 at 45°C, 6 at 55°C	
7%	6	7	3 at 45°C, 4 at 55°C	
Unconfined Repeated Load Triaxial Test (no confining stress, 70 psi [483 kPa] deviator stress)				
Air Void %	**Compaction**	**# Tested**	**Replicates and Test Temperatures**	
7	SGC	6	3 at 45°C, 3 at 55°C	
Dynamic Modulus Test				
Air Void %	**Compaction**	**Replicates[3]**	**Temperature (°C)[2]**	Comments
5	SGC	2	4, 20, 40	Unconfined test at 4°C and 20°C. Confined test at 40°C (10 psi [68.9 kPa] confining stress)
	Field	2		

Notes:
[1]: Three replicate RLT tests are recommended according to AASHTO TP 79.
[2]: 45°C = 113°F, 55°C = 131°F, 4°C= 39°F, 20°C = 68°F, 40°C = 104°F
[3]: Two replicated dynamic modulus tests are recommended according to AASHTO TP 79.

Table 6.2: Repeated Shear Test at Constant Height Test Plan

Rolling-Wheel*		
Target AV	# Tested	Test Temperatures
3%	6	3 at 45°C, 3 at 55°C
5%	10	5 at 45°C, 5 at 55°C
Field		
Target AV	# Tested	Test Temperatures
3%	12	5 at 45°C, 7 at 55°C
5%	9	4 at 45°C, 5 at 55°C

Notes:
45°C = 113°F, 55°C = 131°F
* Five second rest period used for rolling wheel-specimen tests instead of standard six second rest period.

Details of the requirements for the specimen preparation are shown in Table 6.3. Specimens were prepared at two or three air-void contents for each method of laboratory compaction and selected for the same air-void contents from field cores. Mix for the SGC and RW specimens was sampled at random locations during construction of the project. Similarly, field cores were randomly sampled as part of quality assurance for the field construction project. Therefore, the variability of the results includes the variation of the mix in the field for the SGC and RW specimens, and of mix and field compaction for a given air-void content for the field cores.

Laboratory-compacted specimens were fabricated upon receipt of the loose mix soon after construction. Mix was laboratory oven-heated for two hours at 145°C prior to compaction. SGC specimens were fabricated in compliance with AASHTO T 312-12 and AASHTO PP 60-11. The gyratory compactor was set at 600 kPa (87 psi) compaction pressure and 1.16° internal angle to fabricate specimens that were 170 mm in height and 150 mm in diameter. Tested specimens (150 mm in height and 100 mm in diameter) were then cored and cut from the original compacted specimens. The procedures to fabricate RW specimens followed AASHTO PP 3-94, except that specimens were compacted using two lifts to provide sufficient height for RLT specimens. RW specimens were then cored and cut to the final dimensions. RW specimens were not compacted at 7 percent air-void content since the main focus of the study was on field- and SGC-compacted specimens. The field cores were taken in the vertical direction, cut to final dimensions, and selected to match air-void requirements.

Actual air-void contents were determined by the saturated-surface-dry (SSD) method according to AASHTO T 166A-12. Any specimen that did not meet the ±0.6% allowance of each target air-void was discarded.

In the AMPT/RLT test, the compression loading was applied in the form of haversine with a loading time of 0.1 seconds and rest period of 0.9 seconds. A 30 kPa (4.4 psi) contact stress was used as recommended in NCHRP Report 719 *(13)*. Tests were run to the lesser of 20,000 cycles or a PAS of 5 percent. Specimens of each compaction type were tested at two elevated temperatures, 45°C and 55°C. In the unconfined test the contact stress was the same as in the confined test.

In the RSCH test, the RW-compacted specimens were inadvertently tested with a 0.5 second rest period instead of the normal 0.6 second rest period. Four of the twenty-one field-compacted specimens were also tested with the shorter rest period. The shorter rest period will make the RW specimens accumulate permanent deformation faster by not permitting as much recovery. Review of the results from the field-compacted specimens indicates that the small number of specimens tested this way did not affect the results or conclusions. The RW specimens shown in the plots in this chapter should be expected to have somewhat better performance than shown if tested with the 0.6 second rest period; however, since the RW results are not the main focus of the study, this does not affect the conclusions and recommendations.

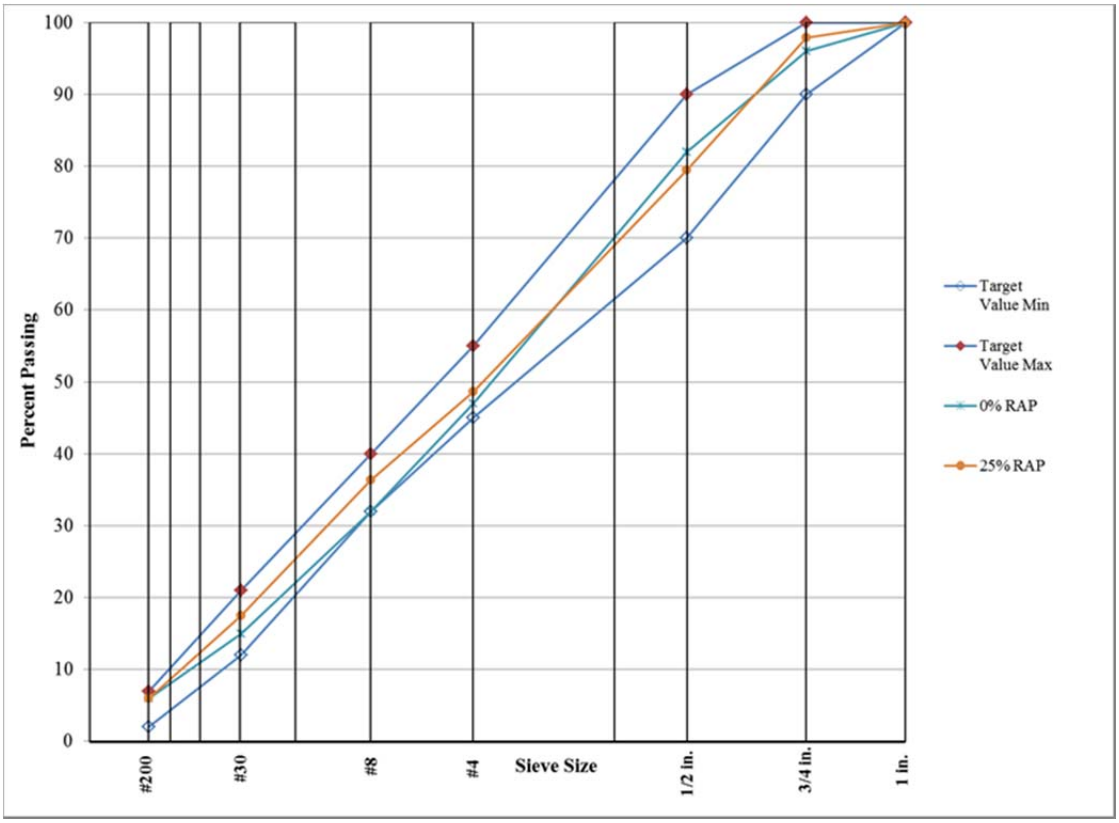

Figure 6.1: Aggregate gradation curve.

Table 6.3: Specimen Preparation Parameters

Specimen Preparation Parameters	
Target Air-void Content (via SSD)	3%± 0.6%, 5%± 0.6%, 7% ± 0.6%
Compacted Specimen Diameter	150 mm
Compacted Specimen Height	170 mm
Cut Specimen Diameter	100 mm to 104 mm
Cut Specimen Height	147.5 mm to 152.5 mm
Standard Deviation of Sample Diameter	≤ 0.5 mm
End Flatness	≤ 0.5 mm
End Perpendicularity	≤ 1.0 mm

In order to evaluate the AMPT actuator versus on-specimen deformation results, the UCPRC created a new deformation measurement system for the AMPT RLT by mounting three long-travel linear variable differential transducers onto each specimen to measure the deformation of its center part (gauge length 70 mm [2.76 inches]) (see Figure 6.2). Each of the LVDTs ranges from -2.5 mm to 2.5 mm. They are manufactured by Solartron Metrology Ltd. and certified by IPC Global. The gauges were mounted using IPC Global's AMPT Gauge Point Fixing Jig.

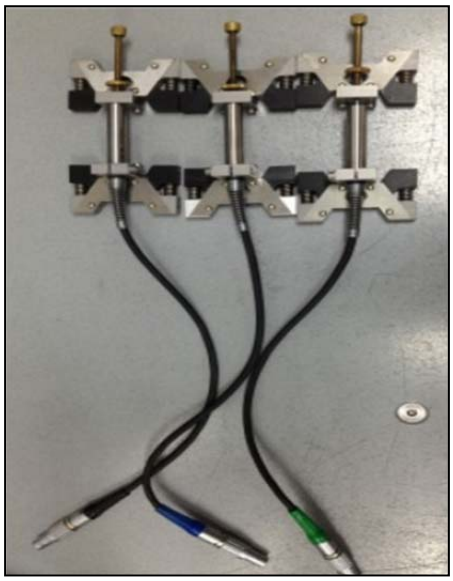

(a) LDVTs

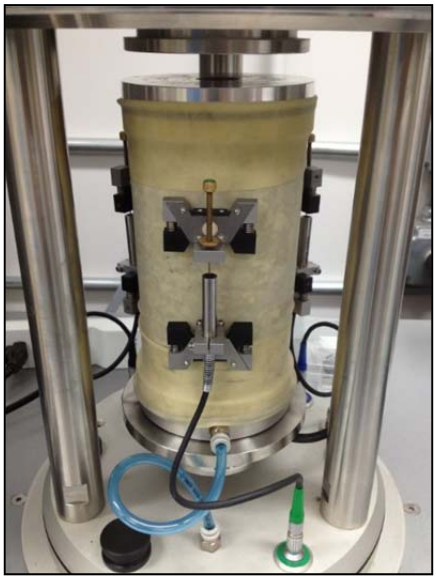

(b) Test specimen with mounted LVDTs

Figure 6.2: Configuration of on-specimen LVDTs.

6.3 Results of Repeated Load Triaxial Tests with Confinement

6.3.1 Detailed Results

Specimens were sorted prior to testing so that the average air-void contents for specimens tested at 45°C and 55°C were equal and well distributed between the two temperatures. Test results are shown in Figure 6.3(a) through (h) below. Outliers were identified by visual observation (when curve shape is very different than the others) and were excluded from the analysis. Outliers were primarily caused by slippage of the LVDTs.

(a) SGC-3% Air-void

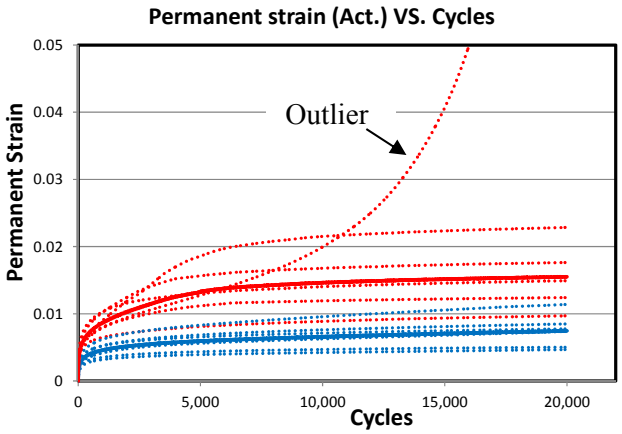

(b) Field-3% Air-void

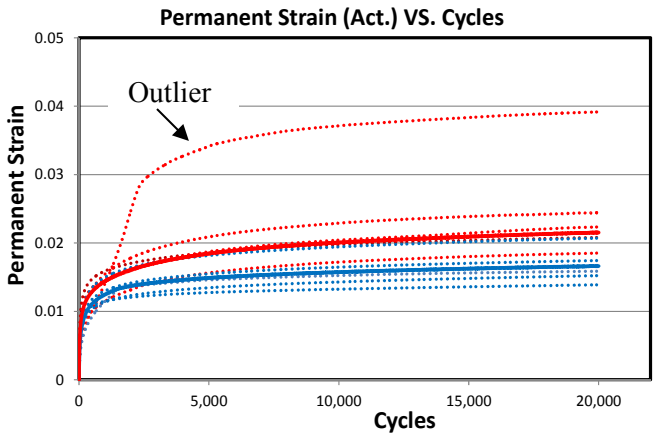

(c) SGC-5% Air-void

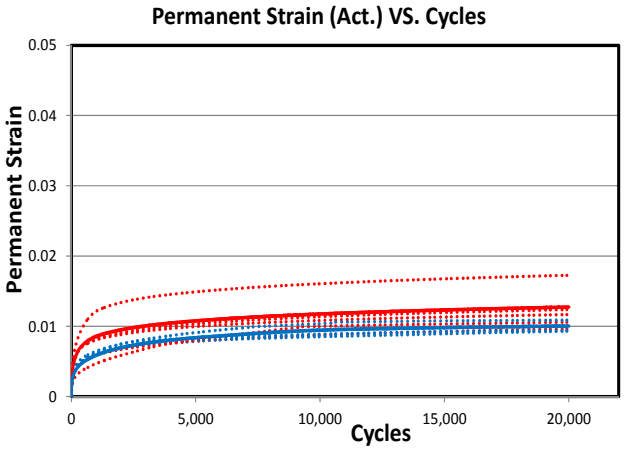

(d) Field-5% Air-void

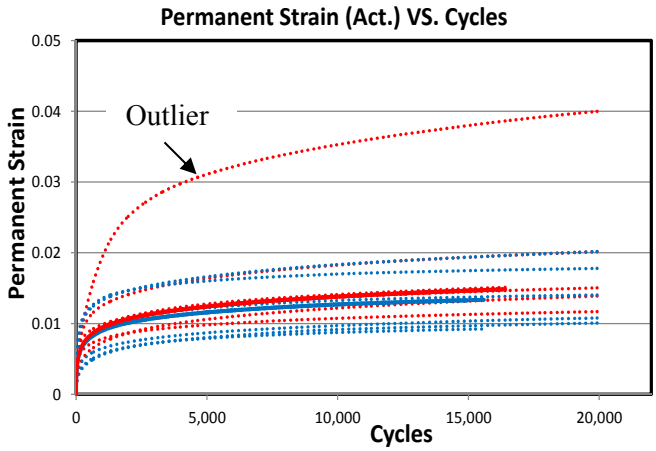

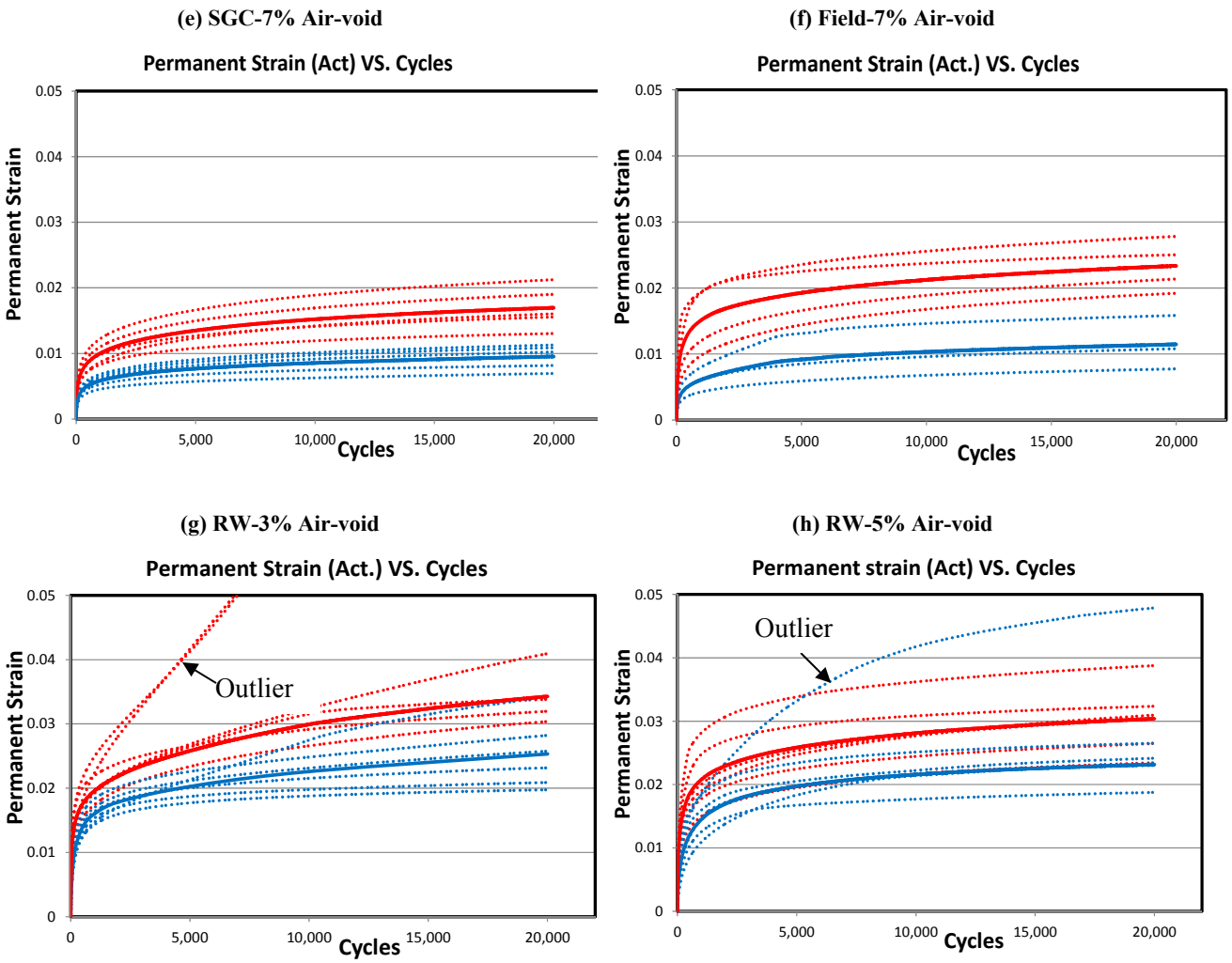

Figure 6.3: RLT test results for field cores and SGC-compacted specimens at two temperatures and three air-void contents: horizontal axis is test repetition; vertical axis is permanent axial strain measured by actuator LVDT (PAS).
(Note: red lines indicate tests conducted at 45°C and blue lines tests conducted at 55°C; dashed lines show each individual test and solid lines show the average value for all replicates.)

Table 6.4 shows the values of test variance. μ is the average for permanent axial strain at the 10,000th repetition; σ, standard deviation for PAS at the 10,000th repetition. It can be seen that the variability is low when shown in terms of permanent axial strain at a given number of repetitions.

Table 6.4: Variance between Replicates for Permanent Axial Strain at 10,000 Repetitions

Test (Air Voids)	n		μ (%)		σ	
	45°C	55°C	45°C	55°C	45°C	55°C
SGC-3%	6	6	0.7	1.5	0.00197	0.00482
SGC-5%	4	4	0.9	1.2	0.00088	0.00308
SGC-7%	6	6	0.9	1.5	0.00146	0.00243
FIELD-3%	5	5	1.6	2.0	0.00238	0.00234
FIELD-5%	6	6	1.3	1.4	0.00419	0.00282
FIELD-7%	3	4	1.0	1.7	0.00396	0.01018
RW-3%	6	6	2.3	3.0	0.00325	0.00262
RW-5%	6	6	2.2	2.8	0.00265	0.00506

6.3.2 Effect of Compaction Type

The test results shown in Figure 6.4 compare results for the three compaction methods grouped by air-void content and temperature. The curves were drawn by taking the average value of the replicates for each condition. The plots show that the SGC-compacted specimens generally exhibit the least permanent axial strain, compared with the field- and rolling wheel-compacted specimens. For the 3 percent and 5 percent air-void content specimens, the curves of field-compacted cores lay between those of the SGC- and RW-compacted specimens. It can also be seen that the differences in permanent axial deformation resistance between the SGC specimens and the field cores diminish as lighter compactive efforts are applied, and are very similar for the 7 percent air-void specimens. Similar response characteristics are exhibited at both test temperatures (45°C and 55°C) for each of the air-void content groups.

As noted previously, the loose mix samples used to fabricate the SGC and RW specimens were all reheated before compaction. Therefore, reheating does not influence the differences between SGC and RW results, while the field cores can be expected to have less aging than both the SGC and RW specimens. If similar heating histories were applied, it would be expected that the field cores would have increased permanent deformation resistance and shift closer to the SGC curves, although the amount of shifting cannot be determined from these results.

6.3.3 Effect of Air-Void Content/Compaction Type

The test results shown in Figure 6.5 compare results for the different air-void contents, grouped by compaction type and temperature. In general, the results show less effect from air-void content than from compaction method. The results indicate that compaction level had somewhat more of an effect on field specimens at 45°C than at 55°C, and had more of an effect on field specimens than on SGC- and RW-compacted specimens at both temperatures. It can also be seen that the better-compacted field cores had the worst performance at 45°C, which was unexpected.

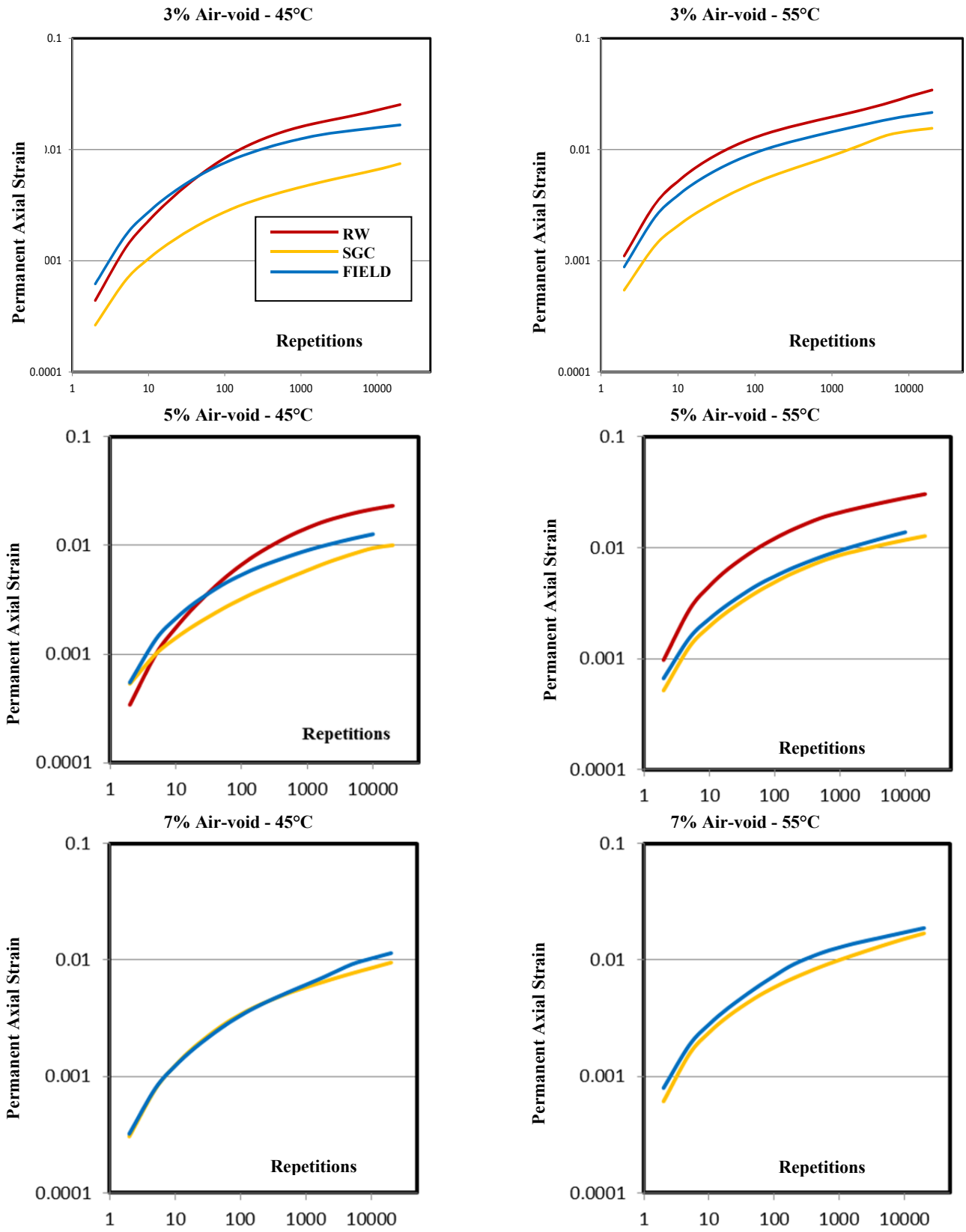

Figure 6.4: Average compaction-type effect on RLT test.
(Note: the red line indicates rolling-wheel compaction; the yellow line, gyratory compaction; and the blue line, field compaction. Plots are in logarithmic scale.)

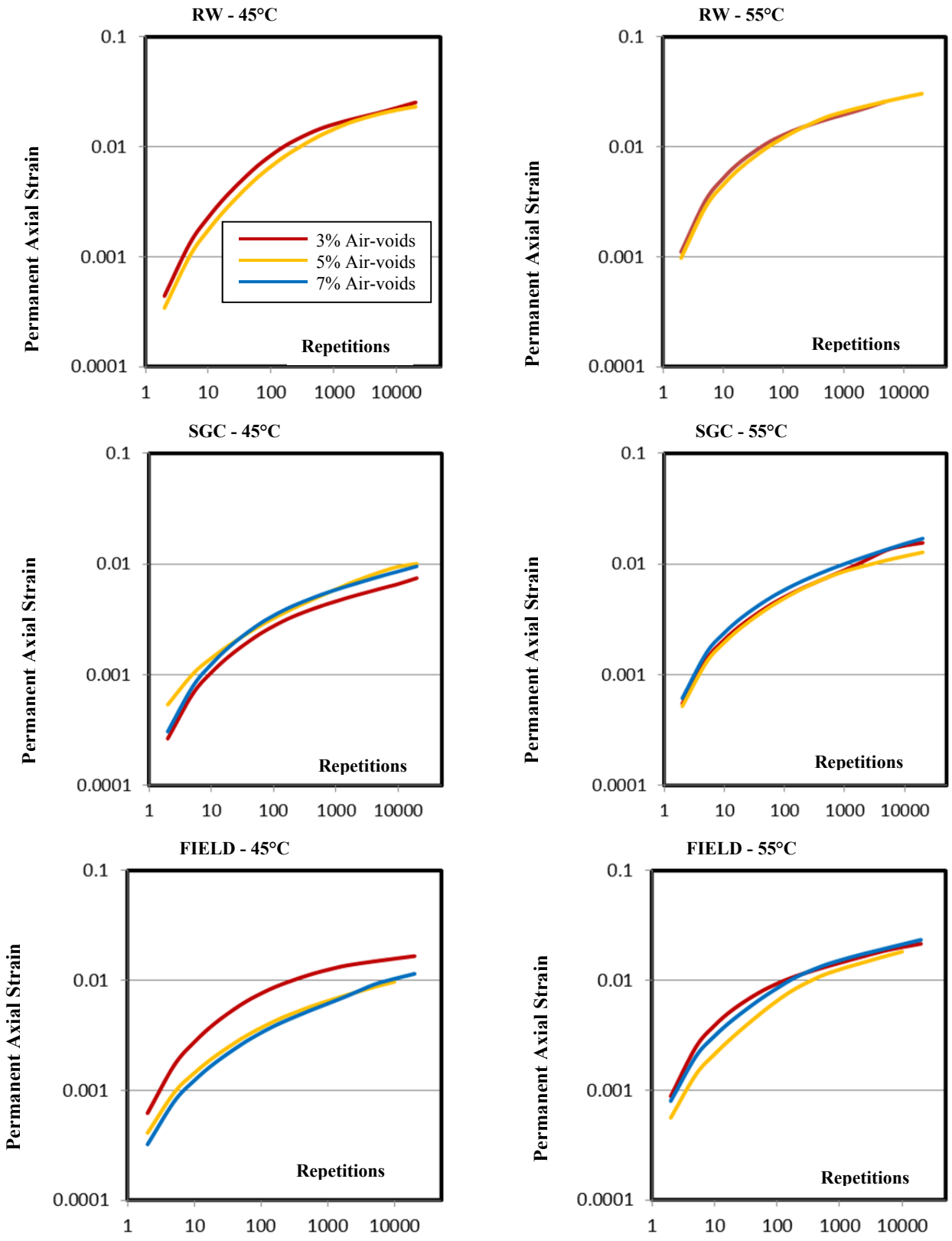

Figure 6.5: Average effect of air voids on RLT test: horizontal axis is test repetitions; vertical axis is permanent axial strain (PAS) measured by actuator LVDT.
(Note: the red line indicates 3% air voids; the yellow line, 5% air voids; and the blue line, 7% air voids. Plots are in logarithmic scale.)

6.3.4 Effect of Temperature

The test results shown in Figure 6.6 compare test temperatures and are grouped by compaction type and air-void content. Generally, it can be concluded that higher test temperatures resulted in higher permanent axial deformation, as expected. The plots demonstrate that there are very clear differences between the 45°C curve and 55°C curves for RW- and SGC-compacted specimens. However, for field-compacted 3 percent and 5 percent air-void specimens, the differences between the curves are smaller than in the other plots, which indicates that the effect of test temperature was less.

6.3.5 Statistical Analysis

The discussion above is based on a visual examination of the graphs. A more rigorous analysis of the data using statistical tools was also performed.

The ANOVA (ANalysis Of VAriance) approach was used to identify the crucial factors for AMPT RLT testing. The ANOVA analyses were performed by using the permanent axial strain (PAS) after 1,000, 2,000, and 5,000 repetitions (notated as PAS_{1000}, PAS_{2000}, and PAS_{3000}, respectively) as the dependent variables and by using compaction type, air-void content, and test temperature as the independent variables. The reason for choosing PAS_{1000}, PAS_{2000}, and PAS_{3000} as the dependent variables is to be certain that the same effects are noted for different levels of permanent deformation.

The ANOVA approach was used to test the null hypothesis that the mean PAS is the same for all independent variable categories (i.e., the sample means of PAS_{1000} are equal no matter what compaction type was used). A significance level of 0.01 was used. Therefore, any independent variable with p-value larger than 0.01 can be regarded as an insignificant variable.

The results of the ANOVA for PAS_{1000}, PAS_{2000}, and PAS_{5000} are listed in Table 6.5. On the basis of this decision rule, it can be concluded that compaction type, compaction level, and test temperature all appear to be significant variables, as expected. By looking at the F-values, it can be seen that compaction type affects the rutting predictions the most, temperature affects them less, and air-void content has the smallest effect. The same conclusion can be drawn from the datasets for the permanent axial strain at all three load repetition levels.

At the proposed significance level (0.01), none of the interactions among compaction type, air-void content, and test temperature were statistically significant. However, the interaction between compaction type and air-void content has more effect than other interactions because its p-value is the least at all three load repetition levels.

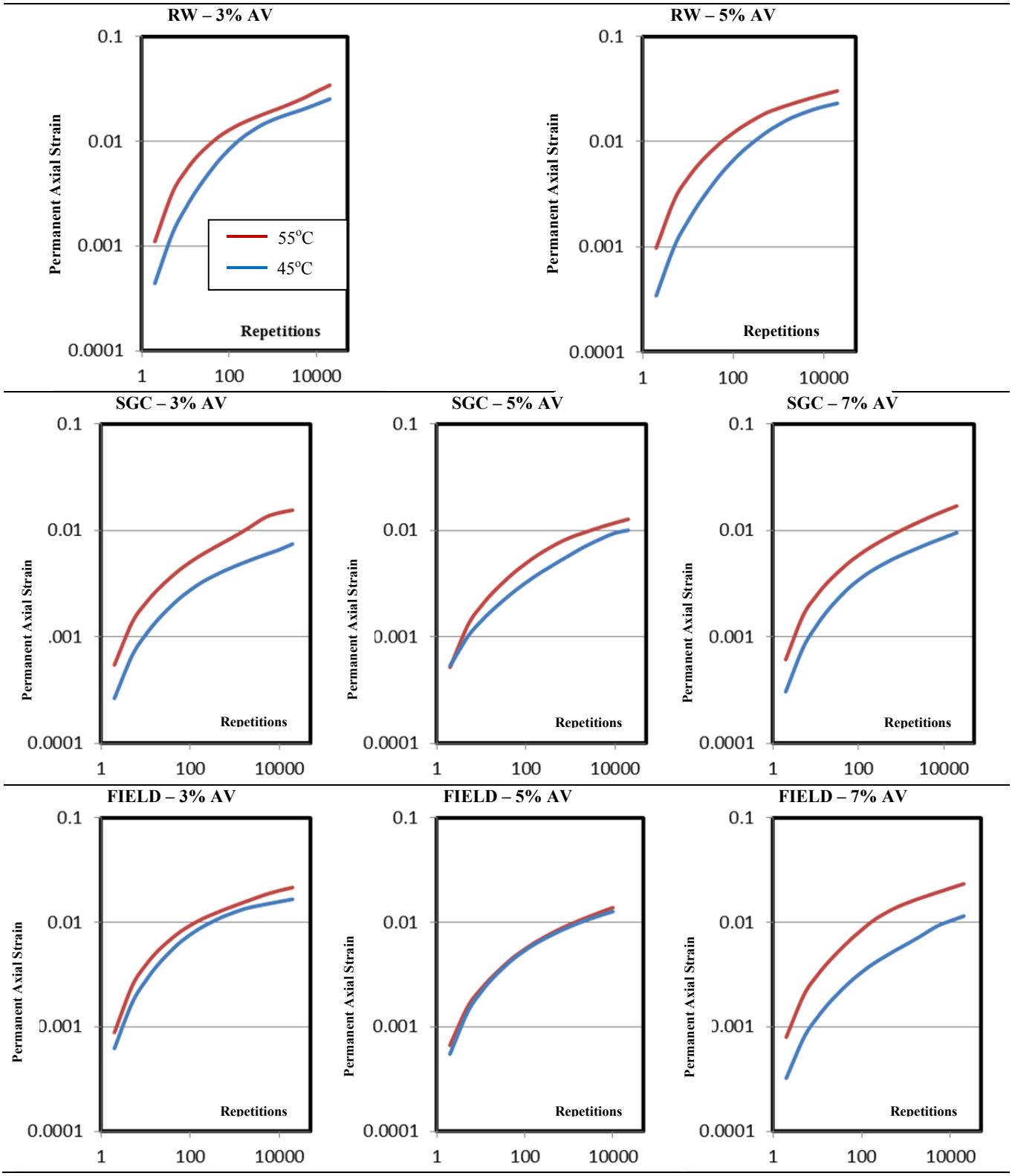

Figure 6.6: Average effect of temperature on RLT test (horizontal axis is test repetition; vertical axis is permanent axial strain [PAS]) measured by actuator LVDT.
***(Note:* the red line indicates a test temperature of 55°C and the blue line, a test temperature of 45°C. Plots are in logarithmic scale.)**

Table 6.5: ANOVA Results for the Complete PAS_{1000}, PAS_{2000}, and PAS_{5000} Dataset

Variable	Type	DOF	PAS_{1000}			PAS_{2000}			PAS_{5000}		
			SS	F-value	p-value	SS	F-value	p-value	SS	F-value	p-value
Comp	RW, SGC, Field	2	0.00126	95.78	<2.2E-16	0.00145	58.0343	5.12E-15	0.00181	54.8676	1.59E-14
AV	3%, 5%, 7%	2	0.00012	9.17	0.00032	0.00022	8.9007	0.000394	0.00028	8.417	0.000576
Temp	45°C and 55°C	1	0.00031	47.82	2.81E-09	0.00038	30.6255	6.46E-07	0.00055	33.431	2.48E-07
AV: Temp	Interaction	2	0.00002	1.78	0.177004	0.00001	0.297	0.744068	0.00001	0.3023	0.740169
AV: Comp	Interaction	3	0.00007	3.68	0.016505	0.00008	2.2064	0.096054	0.00007	1.4809	0.228266
Temp: Comp	Interaction	2	0.00003	1.91	0.156534	0.00001	0.4327	0.650676	0.00001	0.2671	0.766483
AV:Temp:Comp	Interaction	3	0.00006	2.8	0.047333	0.00002	0.63	0.598657	0.00003	0.54	0.655965
Residuals		63	0.00041			0.00079			0.00104		

Note: Comp, Compaction; AV, air-void content; Temp., Temperature; RW, Rolling-Wheel Compaction, SGC, Superpave Gyratory Compaction; Field, Field Compaction; DOF, degrees of freedom; SS, sum of squares.

6.3.6 Comparison of Deformation Measurement Devices

Figure 6.7 shows the comparison of AMPT actuator LVDT and on-specimen LVDT results. Each point shown in the figure represents an individual test. It can be seen that the points for both temperatures are very close to the line of equality. Table 6.6 further shows the correlations by calculating Pearson's r value. Figure 6.8 shows that for some tests the three on-specimen LVDTs had similar results, indicating uniform compression of the specimen, while in some other cases they did not, indicating that there was widely variable compression around the specimen. Overall, the results show that the on-specimen LVDTs provide almost the same average permanent axial strain as the actuator does. This provides confidence for the assumption that LVDT results from the actuator LVDT are similar to those from the on-specimen LVDTs. The actuator LVDT setup is much easier and faster to use.

Table 6.6: Correlations of Actuator and LVDT Results

TEST	Pearson's r between Actuator and On-Specimen LVDTs	
	45°C	55°C
RW-3%	0.999652	0.999120
RW-5%	0.999457	0.999682
SGC-3%	0.998064	0.999438
SGC-5%	0.999399	0.999921
SGC-7%	0.999993	0.999961
FIELD-3%	0.999978	0.999683
FIELD-5%	0.999700	0.999845
FIELD-7%	0.995912	0.999744

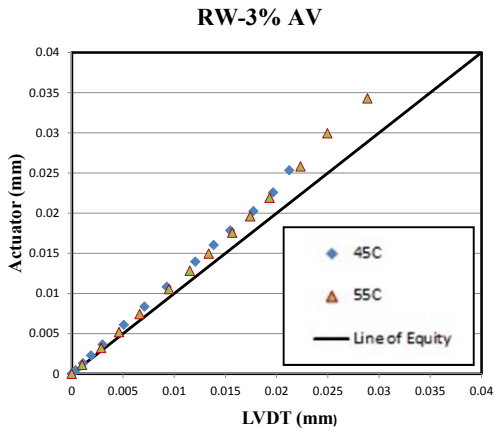
RW-3% AV
Actuator (mm)
LVDT (mm)
45C
55C
Line of Equity

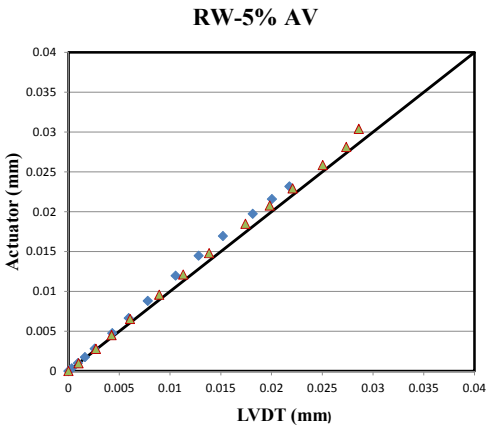
RW-5% AV
Actuator (mm)
LVDT (mm)

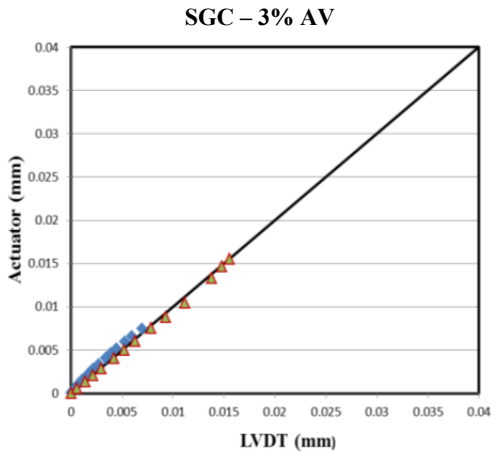
SGC – 3% AV
Actuator (mm)
LVDT (mm)

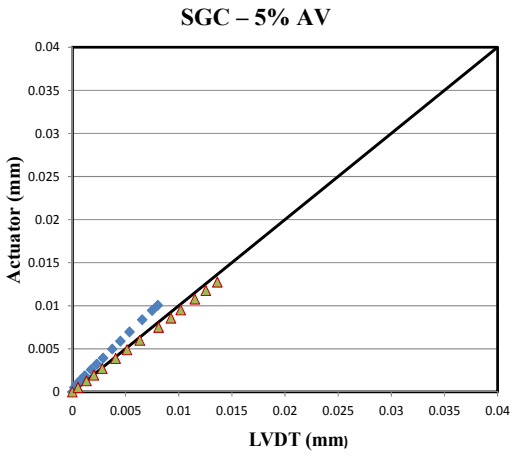
SGC – 5% AV
Actuator (mm)
LVDT (mm)

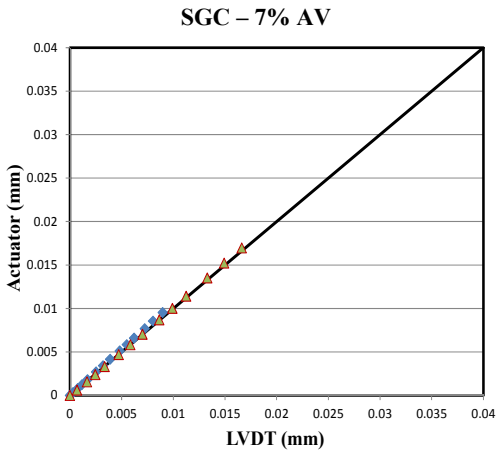
SGC – 7% AV
Actuator (mm)
LVDT (mm)

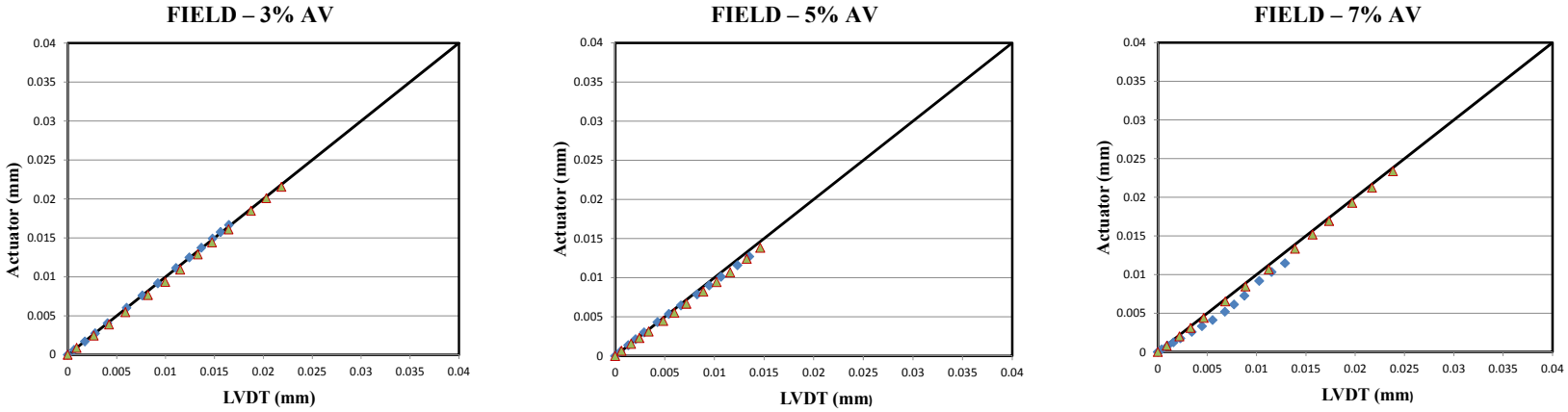

Figure 6.7: AMPT Actuator result versus average on-specimen LVDT results (on Permanent Axial Strain).
(Note: blue diamond-shaped dot, tests conducted at 45°C; red triangle-shaped dot, tests conducted at 55°C; black solid line, line of equity; horizontal axis is LVDT data; vertical axis is actuator data.)

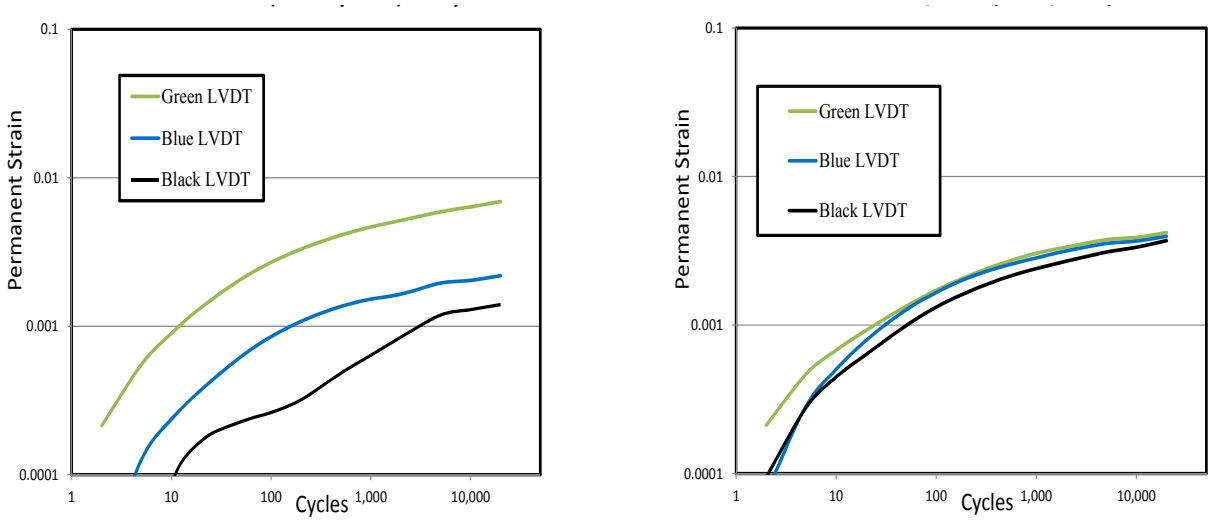

(a) PAS around specimen is not equal. **(b) PAS around specimen is very close.**

Figure 6.8: Example on-specimen LVDT results showing an example of non-uniform deformation (a) and relatively uniform deformation (b).

6.4 Results of Unconfined Repeated Load Triaxial Tests

Unconfined RLT results on SGC-prepared specimens are shown in Figure 6.9. Comparing the results in Figure 6.9 with those for the confined RLT test on similar specimens shown in Figure 6.3, it can be seen that the effect of temperature is much larger for the unconfined test than for the confined test. These results indicate that the unconfined test may be more sensitive to important variables affecting permanent deformation than the confined test.

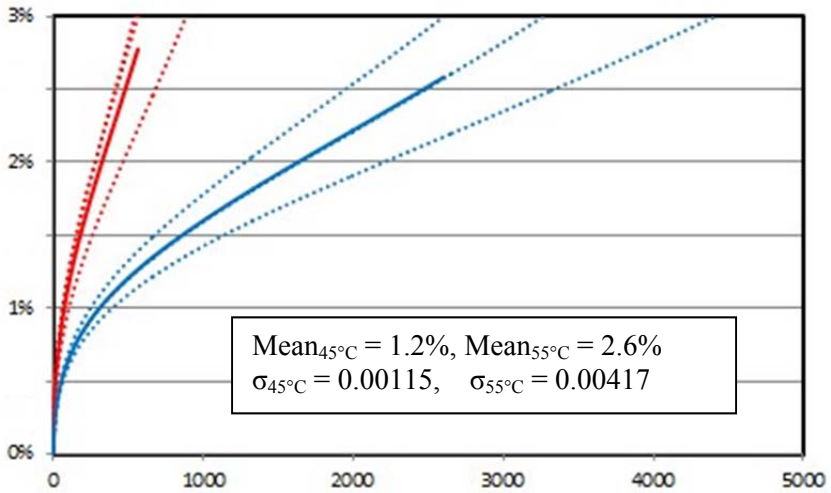

Figure 6.9: Unconfined RLT test results.
(Note: the red line indicates test temperature of 55°C and the blue line, test temperature of 45°C; mean and standard devaluation of PAS is at the 500th repetition.)

6.5 RSCH Test Results

Test results for the RSCH are shown in the following plots, separated by compaction method and target air-void content. Plots for rolling wheel-compacted (RW) and field-compacted tests are shown in Figure 6.10 and Figure 6.11, respectively. The plots show the high sensitivity to temperature and the typical variance of the results.

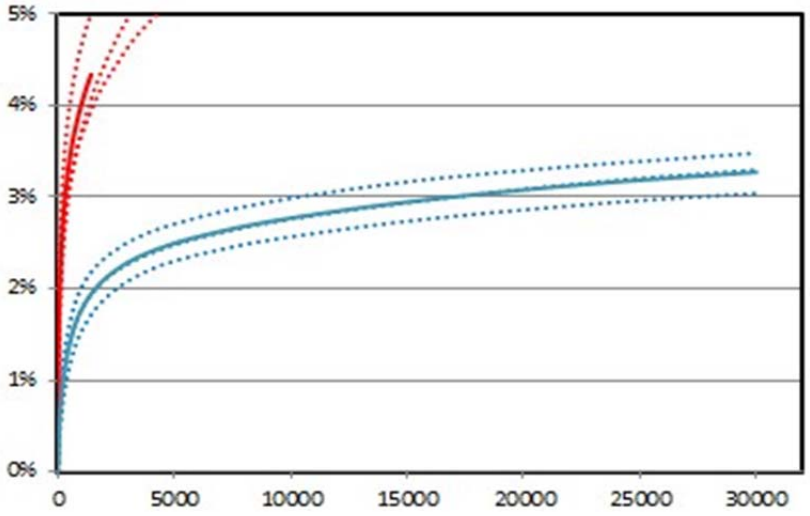

(a) RW-3% Air-void

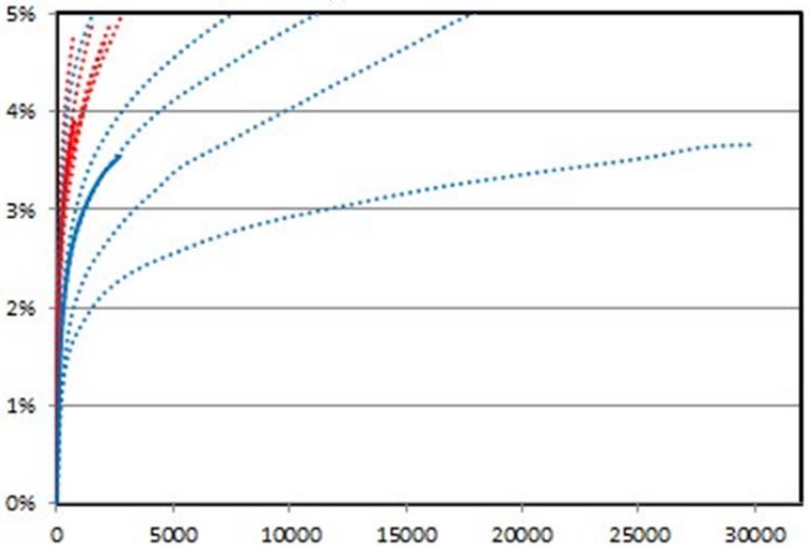

(b) RW-5% Air-void

Figure 6.10: RSCH test results of RW specimens.

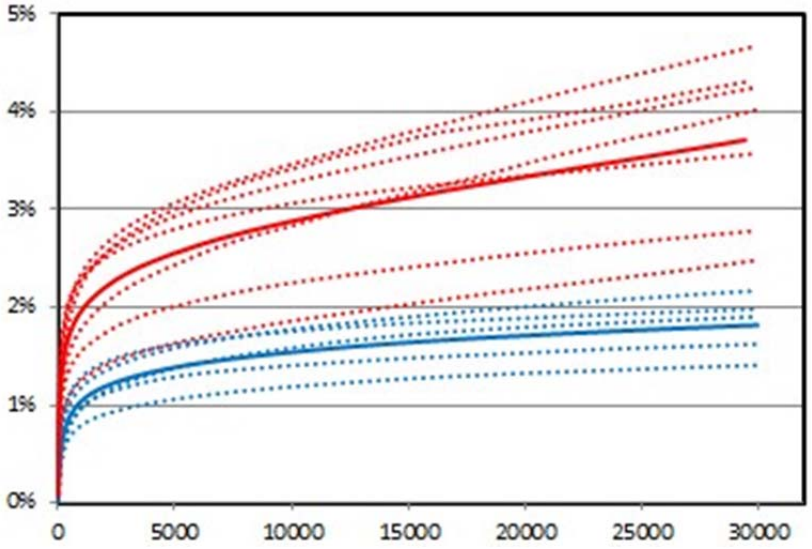

(a) FIELD-3% Air-void

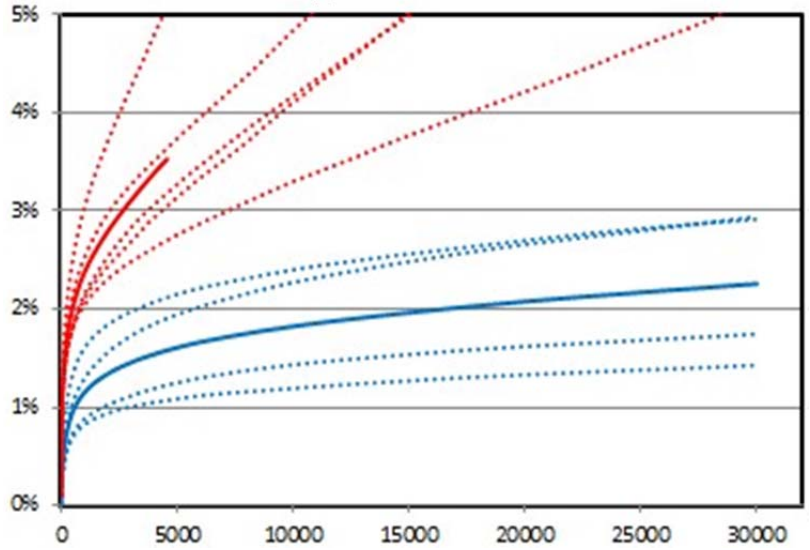

(b) FIELD-5% Air-void

Figure 6.11: RSCH test results of field specimens.

(Note: horizontal axis is test repetition; vertical axis is permanent shear strain (PSS); the red line indicates test temperature of 55°C; the blue line, test temperature of 45°C.)

Table 6.7 shows the values of test variance. μ is the average for permanent shear strain at 3,000 repetitions; σ, standard deviation for PSS at 3,000 repetitions. It can be seen that the variability is low when considered in terms of permanent shear strain at a given number of repetitions. The results also show that the field-compacted specimens had greater resistance to permanent deformation in the RSCH than did the rolling wheel-compacted specimens, which was also true for the RLT results shown previously.

Table 6.7: Variance of Permanent Shear Strain at 3,000 Repetitions between RSCH Number Test Replicates

Test (Air Voids)	μ (%)		σ	
	45°C	55°C	45°C	55°C
RW-3%	2.3	4.8	0.00211	0.00233
RW-5%	3.2	5.0	0.00763	*
Field-3%	1.3	2.4	0.00219	0.00515
Field-5%	1.5	3.1	0.00473	0.00719
*All tests terminated before the 3,000th repetition for RW-5% air-void specimens tested at 55°C.				

6.6 Development of Preliminary Shift Factor between RSCH and Confined RLT Results

A preliminary shift factor for the permanent deformation versus load repetitions relationship across the entire test was developed for confined RLT results from 7 percent air-void content, gyratory-compacted specimens and RSCH results from 3 percent air-void content, field-compacted specimens. This preliminary shift factor is based on the results from the single field mix used in the tests presented in this chapter.

To prepare the shift factors, the difference between the permanent deformation relations for each potential pair of RLT and RSCH tests was minimized using all the results of permanent strain versus repetitions (the full curve) from each test for each temperature. The estimated RSCH repetitions to a given permanent strain (shear strain) result was calculated by multiplying the RLT permanent strain (axial strain) at the same number of repetitions by the shift factor. Table 6.8 and Table 6.9 summarize the shift factors at 45°C and 55°C, as well as the mean shift factors for each temperature.

It can be seen in the tables that the shift factor ranges from 1.2 to 2.8 for the 45°C tests, and from 1.0 to 3.0 for the 55°C tests. Based on these results it appears that a preliminary shift factor of approximately 2.0 can be used to convert RLT results to RSCH results.

Table 6.8: Summary of Shift Factors for 45°C Tests

		S.F.	Confined RLT-SGC-7%-45C						
			Replicate No.						
			1	2	3	4	5	6	mean
RSCH-FIELD-3%-45C	Replicate No.	1	1.6	1.7	1.6	2.5	1.8	2.1	
		2	1.4	1.5	1.4	2.2	1.6	1.9	
		3	1.2	1.3	1.2	1.9	1.4	1.6	
		4	1.8	1.9	1.8	2.8	2.1	2.4	
		5	1.8	1.9	1.8	2.8	2.0	2.4	
		mean							1.8

Table 6.9: Summary of Shift Factors for 55°C Tests

		S.F.	RLT-SGC-7%-55C						
			Replicate No.						
			1	2	3	4	5	6	mean
RSCH-FIELD-3%-55C	Replicate No.	1	1.6	1.1	1.0	1.3	1.3	1.4	
		2	1.9	1.3	1.2	1.5	1.6	1.6	
		3	2.4	1.7	1.5	1.9	2.1	2.1	
		4	2.8	2.0	1.8	2.2	2.4	2.4	
		5	3.0	2.1	1.9	2.3	2.5	2.5	
		6	2.6	1.8	1.6	2.0	2.1	2.2	
		7	2.8	2.0	1.8	2.2	2.3	2.4	
		mean							1.9

6.7 Comparison of Results of Dynamic Modulus Test for SGC and Field Compaction

The effects of specimen compaction method on dynamic modulus master curves were also investigated. Summary results are shown in Table 6.10a for the SGC-compacted specimens and Table 6.10b for the field-compacted specimens. Both sets of specimens had target air-void contents of five percent. Master curves were generated by *Mastersolver* Version 2.2 (which is used in conjunction with the AMPT), which was developed by Dr. Ramon Bonaquist of Advanced Asphalt Technologies LLC. Master curves of gyratory specimens and field specimens are shown in Figure 6.12 and Figure 6.13, respectively.

The master curves for the two compaction methods are compared in Figure 6.14. It can be seen that the two sets of specimens have similar master curves at high frequencies, and therefore also at low temperatures, while at low frequencies, which also correspond to higher temperatures, the SGC-compacted specimens are stiffer. Based on the average results in the tables, at 40°C and 0.1 Hz the SGC-compacted specimen is 30 percent stiffer than the field-compacted specimen. The difference can be attributed in part to the reheating of the mix to produce the SGC specimen; however, it is interesting to note that this would be expected to produce similar stiffness results at higher frequencies and lower temperatures as well, which does not appear to have occurred. It can also be seen that the phase angles are similar between the two sets of specimens, indicating that there has not been a great deal of aging in the SGC binder. Therefore, the difference is most likely due to differences in aggregate structure that become more apparent when the binder is softer at low frequencies and high temperatures. This result is only based on this one mix from one project, and should be seen as only an indicator of potential differences in measured stiffness that would influence pavement structural design.

Table 6.10: Summary Table of Dynamic Modulus Test

(a) SGC-5% Air-void

		Specimen T15		Specimen T17		Average	Average	Fitted
Temp	Frequency	Modulus	Phase Angle	Modulus	Phase Angle	Modulus	Phase Angle	Modulus
°C	Hz	ksi	Degrees	ksi	Degrees	ksi	Degrees	ksi
4	0.1	1654.6	16.1	2457.4	11.2	2056.0	13.7	1963.8
4	1	2294.5	11.8	3135.6	7.7	2715.0	9.8	2571.6
4	10	2889.9	8.5	3622.0	5.9	3256.0	7.2	2969.2
20	0.1	530.5	27.4	643.7	27.3	587.1	27.3	585.3
20	1	1002.9	22.5	1190.2	21.4	1096.6	22.0	1172.7
20	10	1610.6	17.3	1878.7	16.1	1744.7	16.7	1898.3
40	0.01	78.1	19.3	57.7	20.5	67.9	19.9	67.8
40	0.1	111.4	24.1	96.1	28.5	103.7	26.3	105.8
40	1	194.2	22.5	222.3	33.1	208.3	27.8	205.2
40	10	419.4	30.8	528.4	31.3	473.9	31.0	455.6

(b) FIELD-5% Air-void

		Specimen F19		Specimen F27		Average	Average	Fitted
Temp	Frequency	Modulus	Phase Angle	Modulus	Phase Angle	Modulus	Phase Angle	Modulus
°C	Hz	ksi	Degrees	ksi	Degrees	ksi	Degrees	ksi
4	0.1	1427.8	16.5	1689.8	15.2	1558.8	15.9	1507.8
4	1	2019.1	12.0	2251.7	10.7	2135.4	11.4	2152.7
4	10	2609.7	8.7	2783.0	7.7	2696.4	8.2	2656.5
20	0.1	330.5	30.7	577.4	28.7	454.0	29.7	444.6
20	1	685.6	26.1	1107.8	21.6	896.7	23.9	916.9
20	10	1195.4	18.8	1711.7	15.9	1453.6	17.4	1562.1
40	0.01	31.5	19.8	68.7	17.0	50.1	18.4	48.2
40	0.1	50.7	27.7	108.4	25.8	79.6	26.7	84.2
40	1	115.5	26.1	228.6	32.4	172.1	29.2	177.0
40	10	308.9	33.5	555.1	31.0	432.0	32.2	402.6

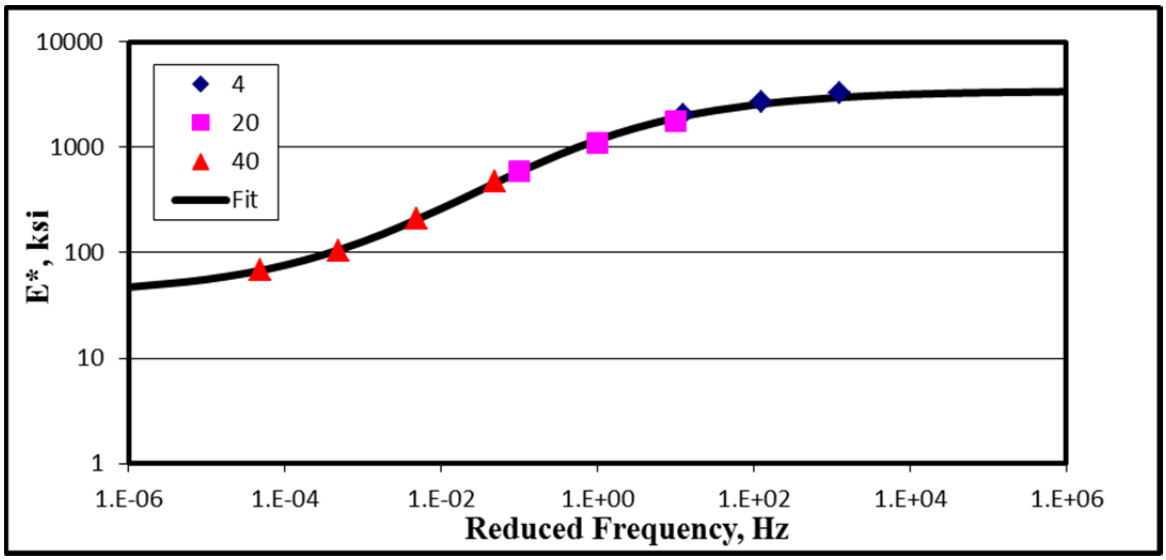

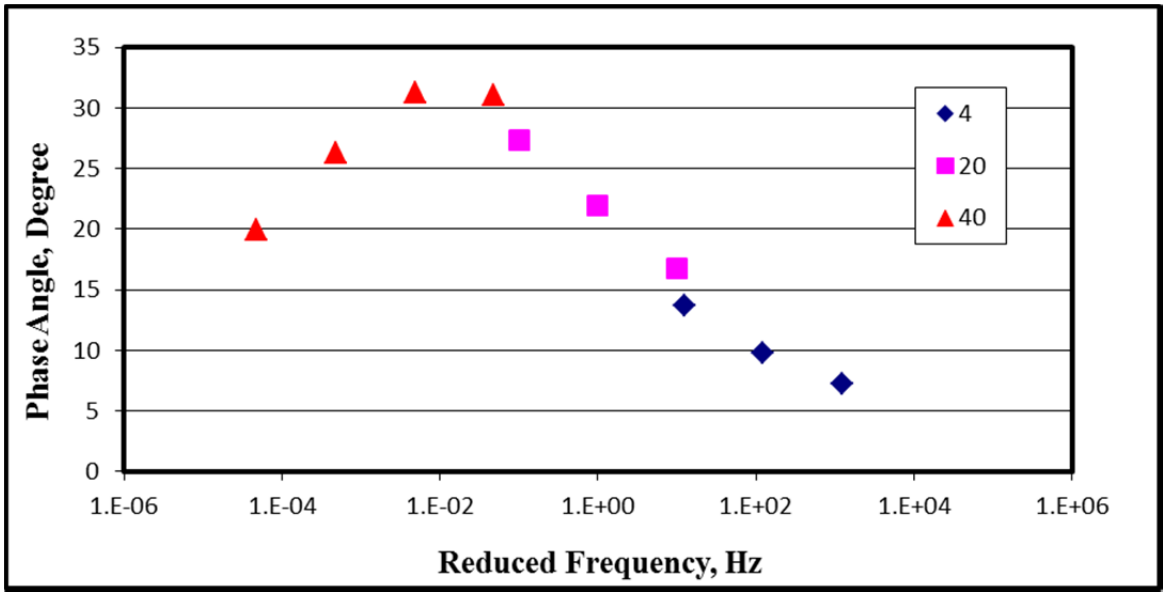

$$\log [a(T)] = \frac{203582}{19.14714}\left(\frac{1}{T} - \frac{1}{T_r}\right)$$

$$\log |E^*| = \log 39.9 + \frac{log\ 3425.6 - \log 39.9}{1 + e^{-1.14875 - 0.72977 \log \omega_r}}$$

Goodness of Fit: $R^2 = 0.9952$, $S_e/S_y = 0.05$

Figure 6.12: Master curve of gyratory specimens.

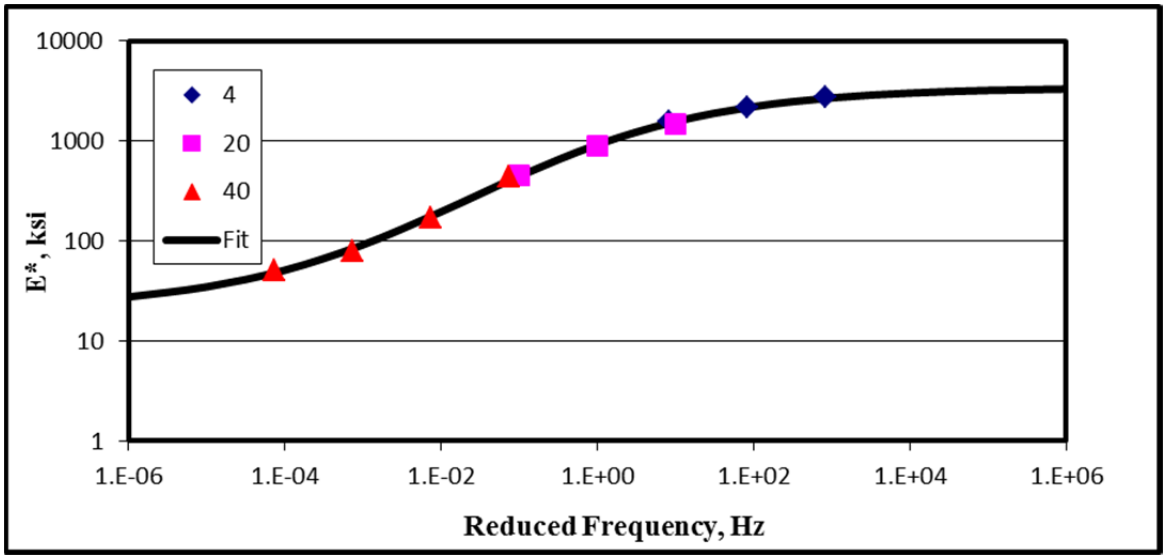

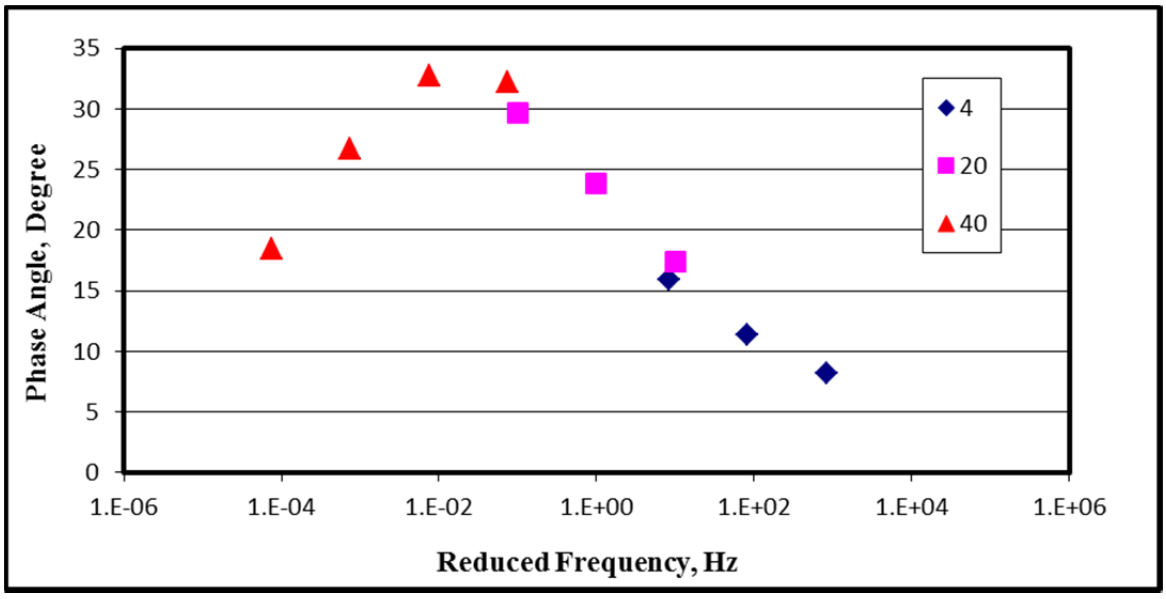

$$\log [a(T)] = \frac{186680}{19.14714}\left(\frac{1}{T} - \frac{1}{T_r}\right)$$

$$\log |E^*| = \log 20.9 + \frac{log\ 3418.5 - \log 20.9}{1 + e^{-1.05532 - 0.65086 \log \omega_r}}$$

Goodness of Fit: $R^2 = 0.9969$, $S_e/S_y = 0.04$

Figure 6.13: Master curve of field specimens.

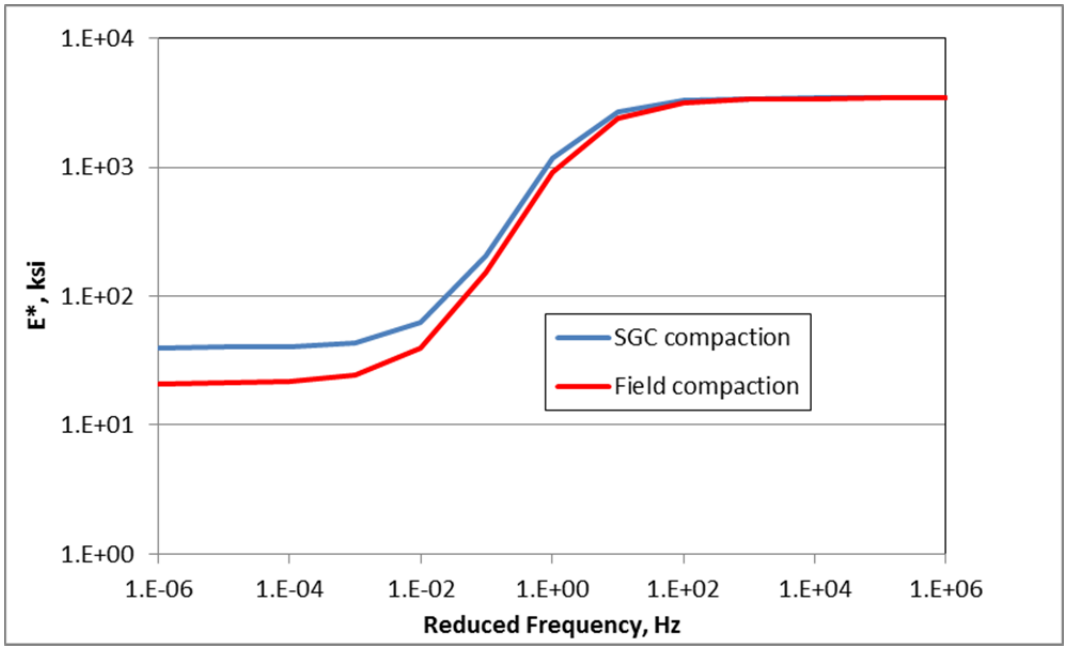

Figure 6.14: Master curves of SGC and field specimens plotted from equations.

6.8 Findings

The following findings are based on the results from this pilot study using one mix:

- Based on results from testing up to 3 percent permanent axial strain or 20,000 axial load repetitions for the confined RLT test and 5 percent permanent shear strain or 30,000 shear load repetitions for the RSCH test, a preliminary indication is that a shift factor of approximately 2 provides the best fit to convert the relationship between load repetitions versus permanent axial strain from the confined RLT test (7 percent air-void content, Superpave gyratory compaction [SGC]) to a relationship between load repetitions and permanent shear strain from the RSCH test (3 percent air-void content, field compaction).
- Through visual observation and statistical analysis, compaction type, compaction level, and temperature all appear to be significant variables in the confined RLT test. Compaction type affects permanent axial deformations the most, temperature has less effect, and air-void content has the least effect. The low sensitivity to temperature was surprising.
- The permanent axial deformation of Superpave gyratory-compacted specimens is less than that of rolling-wheel–compacted specimens and field-compacted specimens. These differences in compaction method need to be accounted for in evaluating confined RLT/SGC test results for construction compliance, mix design, and pavement design. However, if SGC specimens are used in the RLT rutting test, the predicted repetitions to failure would be larger than those expected for the same mix compacted in the field. This conclusion is somewhat biased by differences in heating time

for the SGC and field specimens used in this experiment. This finding regarding compaction method effects is similar to that from previous observations on RSCH tests documented in Reference *(10)*.

- In general, as the test temperature increased, the permanent strain also increased for both confined RLT and RSCH tests, as expected. However, the temperature effect was observed more on RSCH test results than on confined RLT test results.
- The confined RLT test results are also statistically sensitive to compaction level, although to a much lesser degree than compaction method and test temperature. The results did not show consistent trends for permanent deformation resistance relative to air-void content. For RW and SGC cores, the lower the air-void content, the greater the permanent deformation resistance; for field-compacted cores, the opposite relation was found, which was unexpected. It is not certain why this occurred, although greater variability would be expected from the field cores, which were sampled at various locations across a large project, and the laboratory-compacted specimens, which were made with material sampled in a few locations.
- Use of the LVDT in the actuator for permanent axial strain measurement in the RLT provides very good data quality. It is recommended to use the actuator LVDT because it provides similar results to on-specimen LVDT measurement and is much easier to use.
- A preliminary indication was that the unconfined RLT test has much greater sensitivity to temperature than the confined RLT test. Because rutting in the field is known to be extremely sensitive to temperature, the indication is that the unconfined test configuration may produce better results than the confined configuration.
- Comparison of dynamic modulus master curves from the AMPT device for field and SGC specimens compacted to the same air-void contents indicates that both specimens have similar results at higher frequencies and lower temperatures. SGC specimens can have on the order of 30 percent greater stiffness at low frequencies and high temperatures, which can have a large influence on pavement structural design.

(page blank)

7 COMPARISON OF DIFFERENT PERFORMANCE-RELATED TESTS AND RLT TO RSCH SHIFT FACTORS

7.1 Introduction

This chapter compares the performance-related tests currently used in California—the flexural fatigue, flexural frequency sweep, repeated shear at constant height (RSCH) and Hamburg Wheel-Track Testing (HWTT)—with the following alternative tests for mix design and quality assurance: semicircular beam (SCB), indirect tensile strength (IDT), and the tests that can be performed using the AMPT, that is, the repeated load triaxial (RLT), dynamic modulus (DM), and direct tension (DT) tests. Comparisons are made with regard to fatigue, shear, stiffness, and moisture sensitivity. Shift factors are also developed to convert the RLT results for both the confined and unconfined tests to RSCH results at different stress levels, improving the shift factors from the preliminary study presented in Chapter 6.

These tests were evaluated and compared using results from the five mixes discussed in Chapter 2. Some additional testing was performed using three mixes from a long-life asphalt concrete rehabilitation on Interstate 80 in Solano County. These three mixes, which are identified as Mixes R, S1, and S2 all had dense gradations with either a ½ or ¾ inch maximum aggregate size gradation, as indicated on the plots, and all were made from the same crushed alluvial aggregate as Mix A. Mixes R and S1 had a PG 64-28PM polymer-modified binder, while Mix S2 had a conventional PG 64-16 binder.

7.2 Fatigue

7.2.1 Flexural Fatigue versus Semicircular Bending Parameters

A two-way scatter box plot is used to compare the flexural fatigue testing results with the semicircular beam test. Each of these tests assesses a different physical property of HMA: crack propagation for the SCB test and stiffness loss for flexural fatigue. Figure 7.1 through Figure 7.8 present comparison plots of three different properties from the SCB test—secant modulus, fracture energy, and fracture toughness—versus flexural fatigue life, with *flexural fatigue life* defined as repetitions to 50 percent loss of stiffness. In these plots, the horizontal line is the box plot for the laboratory test data on the horizontal axis and the vertical line is the box plot for the test data on the vertical axis. The intersection of the horizontal line with the vertical line represents the mean value for both data sets. The vertical and horizontal "hash lines" represent the interquartile range (IQR, a statistical range from 25th percentile to 75th percentile) which measures the spread of the data. SCB test results are summarized in Table 7.1.

Table 7.1: Summary of Semicircular Beam Test Results

Mix ID	Secant Stiffness S (kN/m)		Fracture Toughness K_{IC} (MPa x $m^{0.5}$)		Fracture Energy G_f (J/m^2)		Fracture Energy Index	
	Average	CV	Average	CV	Average	CV	Average	CV
Mix A	750.1	0.18	0.232	0.13	0.993	0.15	1.369	0.27
Mix B	412.2	0.19	0.147	0.13	0.729	0.15	1.838	0.28
Mix I	747.2	0.41	0.209	0.11	0.909	0.15	1.388	0.41
Mix J	563.3	0.37	0.176	0.17	0.961	0.11	1.946	0.44
Mix N	236.9	0.51	0.088	0.22	0.51	0.19	2.627	0.46
Mix R	462.7	0.17	0.119	0.08	0.602	0.09	1.333	0.20
Mix S1	483.8	0.49	0.149	0.10	0.696	0.12	0.564	0.33
Mix S2	1392.2	0.20	0.227	0.12	0.748	0.18	1.732	0.42
Note: CV = coefficient of variation = standard deviation/mean								

Figure 7.1 and Figure 7.2 present the comparison scatter plots of the log of flexural fatigue life at 200 and 400 microstrain versus SCB secant stiffness, respectively. It can be seen that there is a general but very weak trend of increased fatigue life with lower secant stiffness for both flexural fatigue strain levels. Secant stiffness, or any other type of stiffness, generally shows a trend of increased controlled-deformation flexural fatigue life.

Figure 7.3 and Figure 7.4 present comparison scatter plots between flexural fatigue life at 200 and 400 microstrain and SCB fracture energy, respectively. It can be seen that there is very little correlation between fracture energy and the log of flexural fatigue life for either fatigue strain level.

The fracture energy parameter has been used for low-temperature, reflective, and fatigue-cracking characterization. The SCB configuration used for this project has been criticized for potentially constricting the later stages of crack propagation and having higher variability than some other configurations for testing fracture energy of asphalt mixes *(22).* The coefficient of variation of the fracture energy test from the tests done for this project is within the range of 15 to 34 percent found by other researchers for the same test *(23).* Walubita et al. also identified a lack of correlation between flexural fatigue life and fracture energy and indicated that a *fracture energy index* (FEI), defined as the fracture energy divided by the tensile modulus when testing using a direct tension device, might provide a better correlation. For this study, the fracture energy from the SCB configuration was divided by the secant modulus, which should be similar to the tensile modulus, to produce a fracture energy index that was plotted against flexural fatigue life as shown in Figure 7.5 and Figure 7.6 for the two flexural fatigue strains. From the results it can be seen that the FEI aligns better with the flexural fatigue

lives at 200 microstrain, but shows much less correlation with the 400 microstrain results. The FEI also moves in the same direction as fatigue life, with higher index values corresponding to longer fatigue lives.

Figure 7.7 and Figure 7.8 present comparison scatter plots between flexural fatigue life at 200 and 400 microstrain versus SCB fracture toughness (K_{IC}), respectively. As with the other SCB tests, there is a general trend for reduced controlled-deformation fatigue life and increased fracture toughness. The relationship between SCB fracture toughness and flexural fatigue life at 200 microstrain appears to be stronger than it does with fatigue life at 400 microstrain, which is true for all of the SCB parameters.

Overall, of the SCB parameters considered in this study, fracture toughness and FEI appear to provide the clearest relationship with fatigue life. However, the trend for fracture toughness appears to be the opposite of what would be expected, with the highest fracture toughnesses corresponding to the lowest fatigue lives, while the FEI has a positive relation with fatigue life.

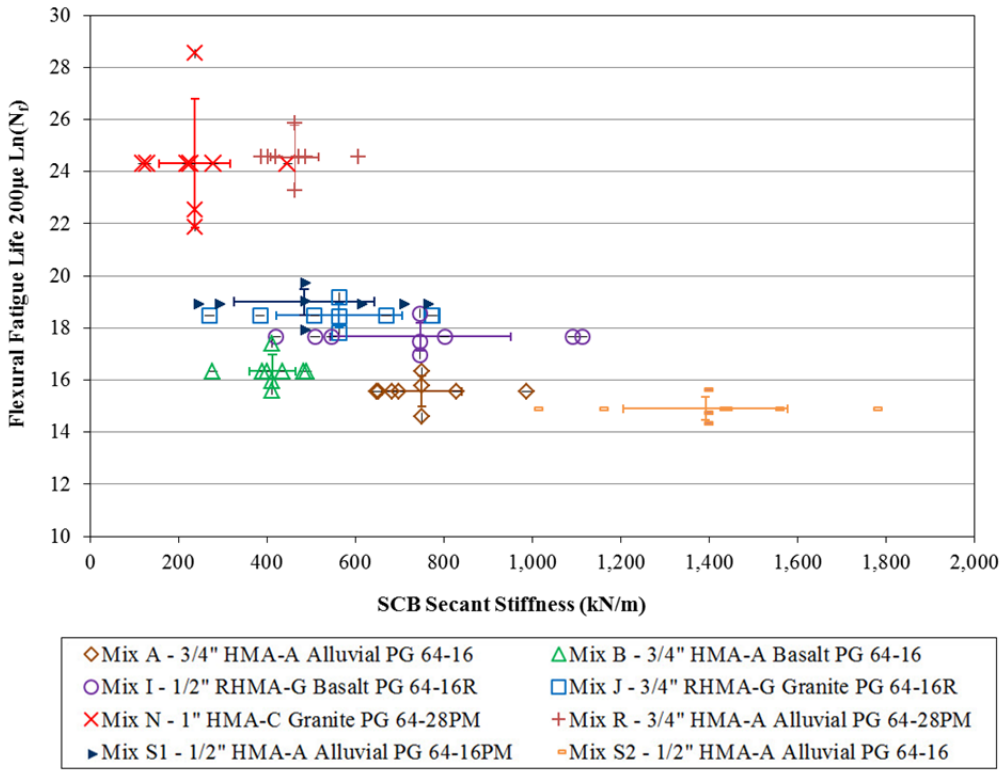

Figure 7.1: Flexural fatigue life (200 με) versus SCB secant stiffness.

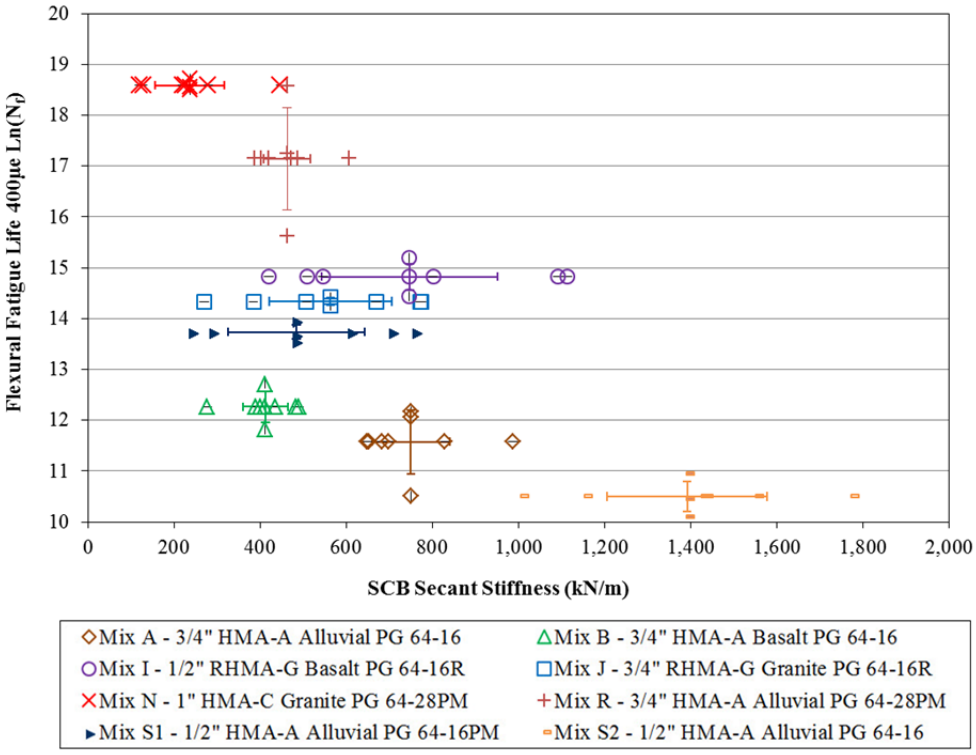

Figure 7.2: Flexural fatigue life (400 με) versus SCB secant stiffness.

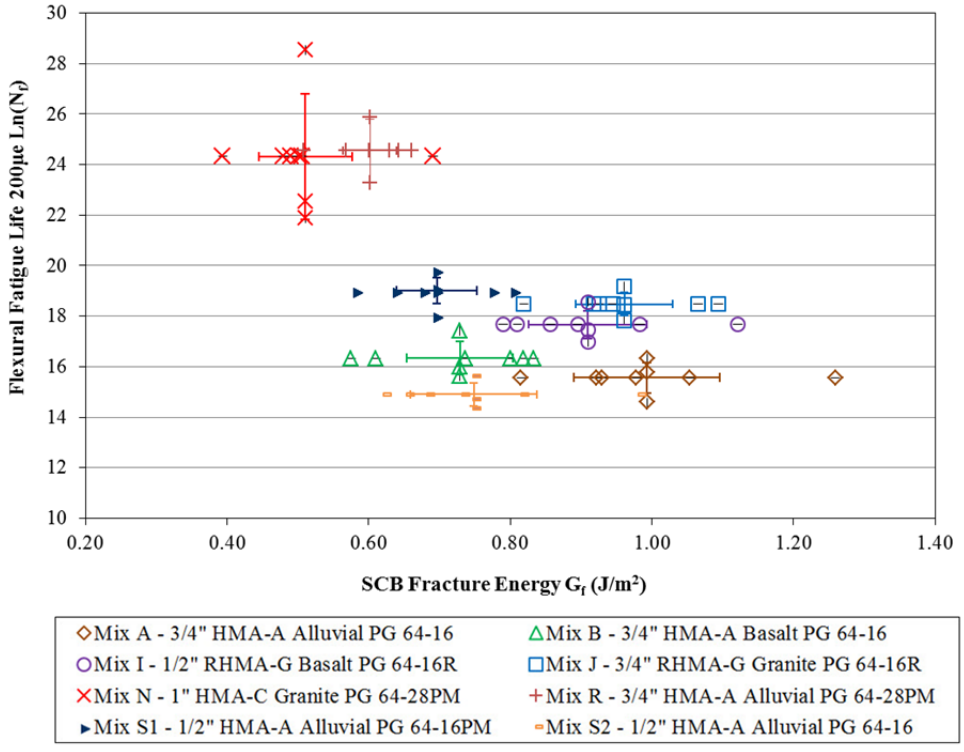

Figure 7.3. Flexural fatigue life (200 με) versus SCB fracture energy.

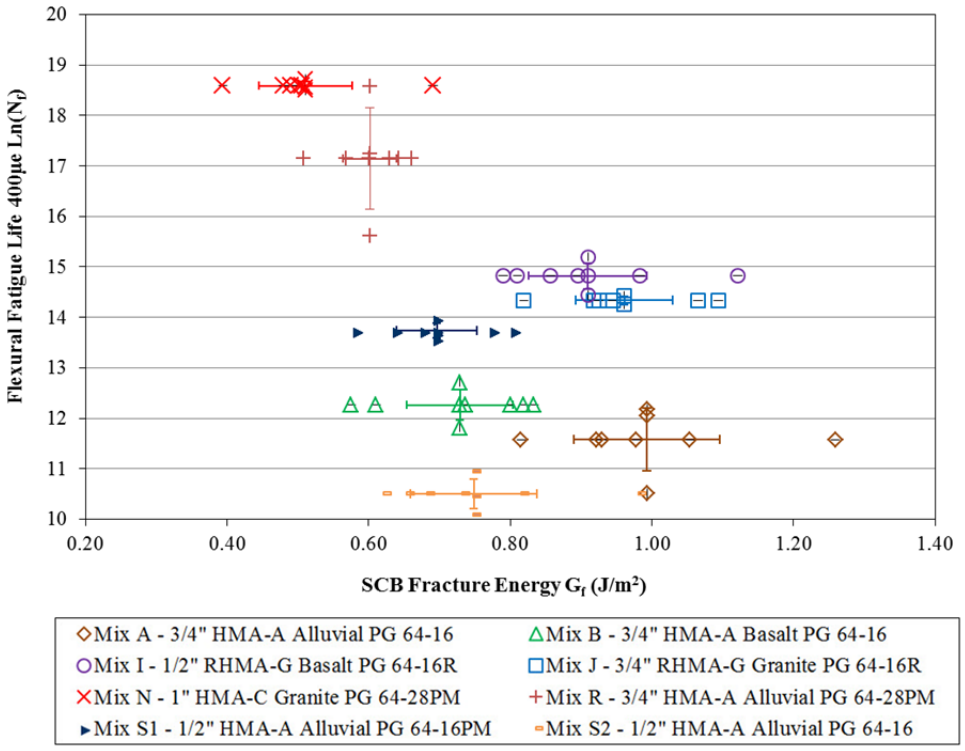

Figure 7.4: Flexural fatigue life (400 με) versus SCB fracture energy.

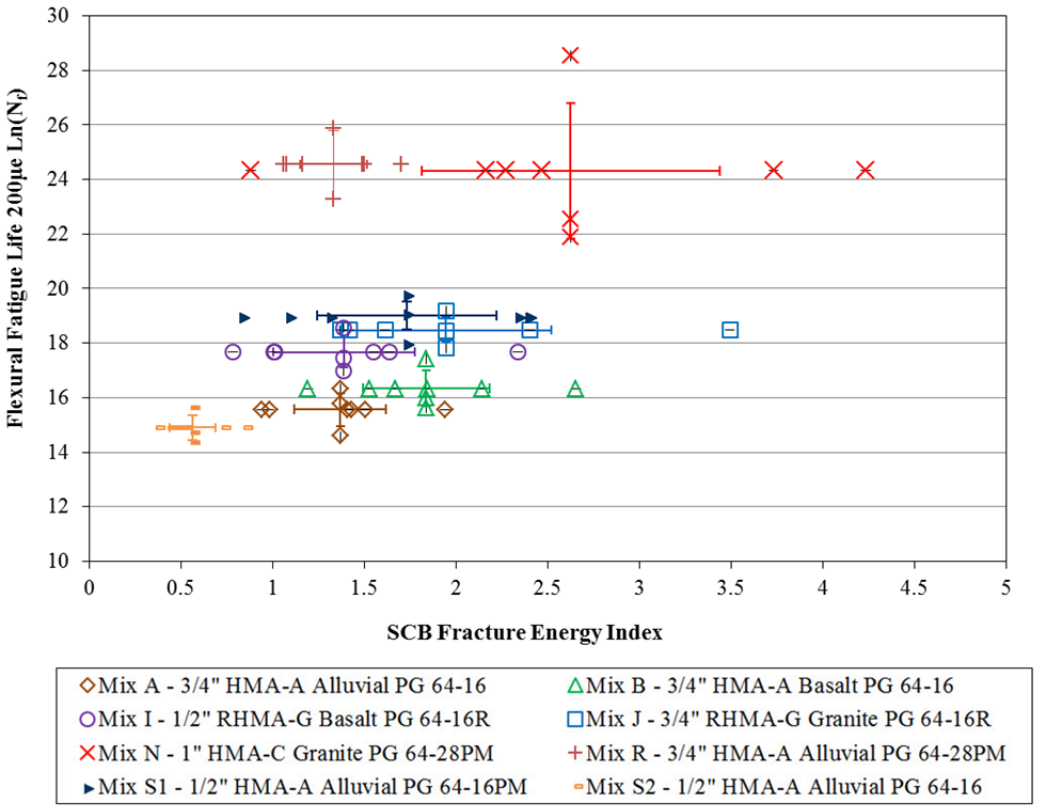

Figure 7.5: Flexural fatigue life (200 με) versus SCB fracture energy index (FEI).

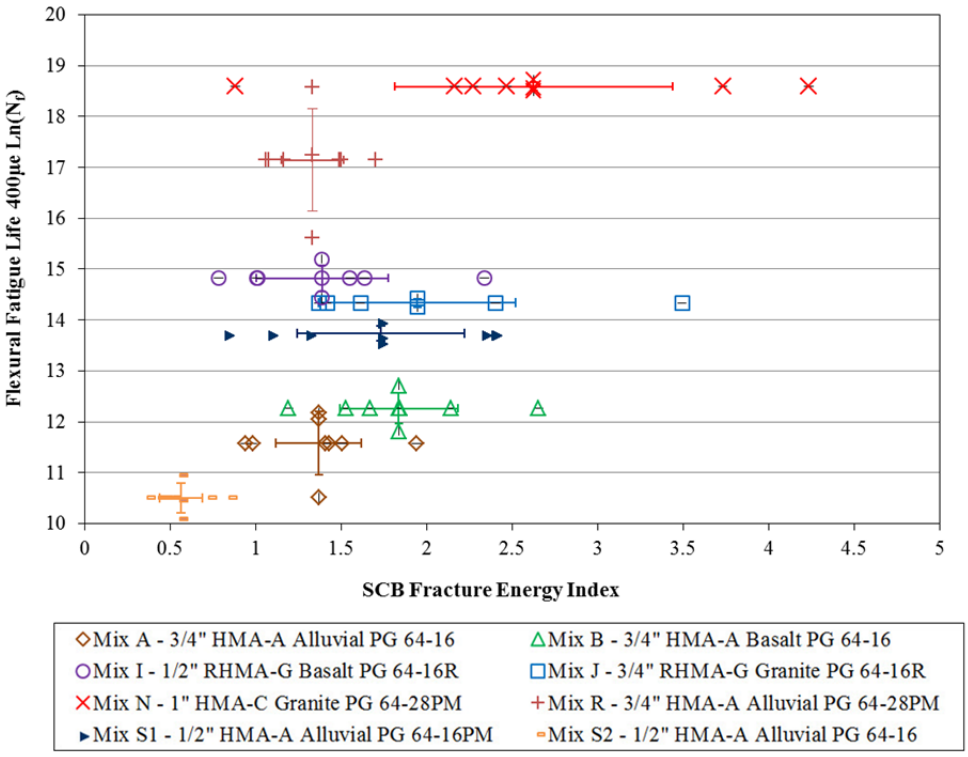

Figure 7.6: Flexural fatigue life (400 με) versus SCB fracture energy index (FEI).

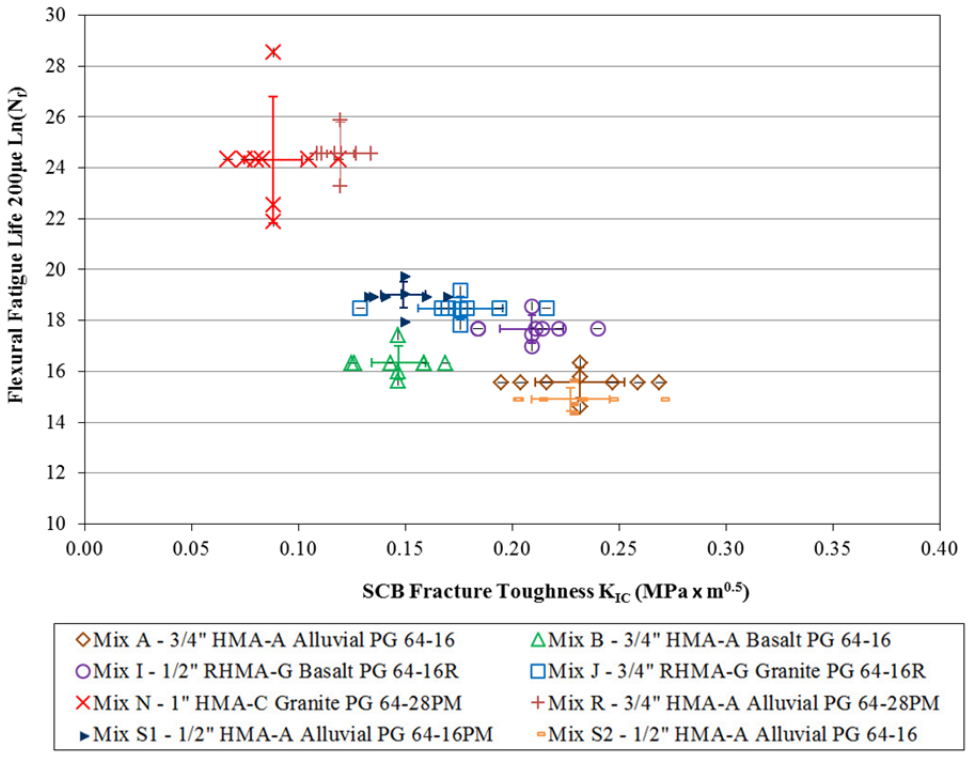

Figure 7.7: Flexural fatigue life (200 με) versus SCB fracture toughness (K_{IC}).

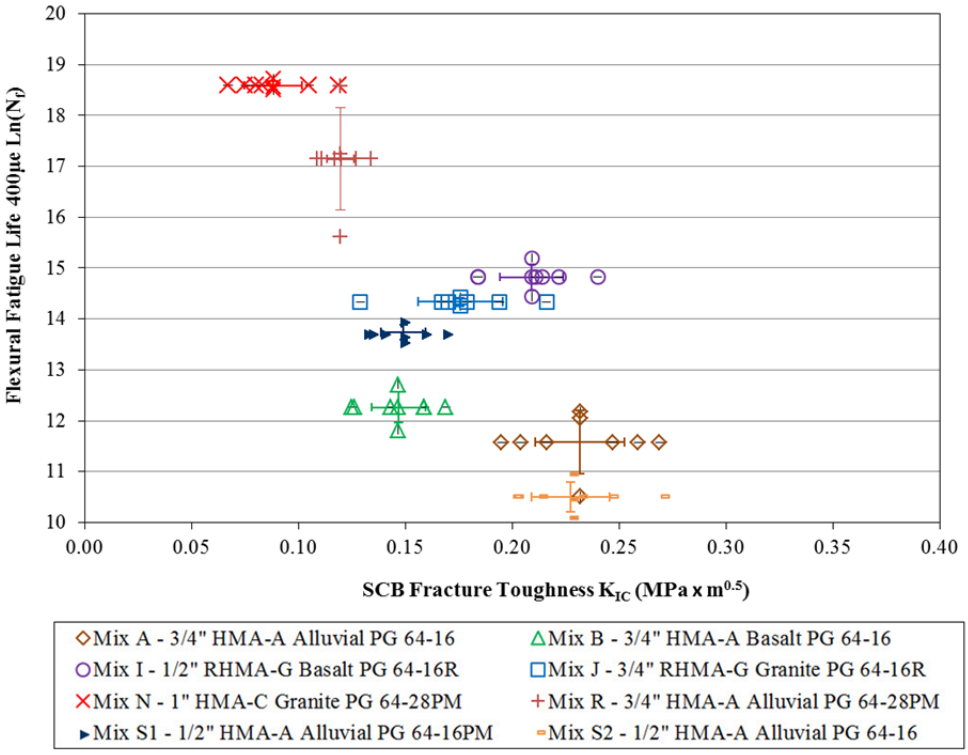

Figure 7.8: Flexural fatigue life (400 με) versus SCB fracture toughness (K_{IC}).

7.2.2 Flexural Fatigue versus Indirect Tensile Strength (Dry Strength)

Flexural fatigue life tests at 200 and 400 microstrain and dry IDT tests are compared through scatter plots in Figure 7.9 and Figure 7.10, respectively. The results indicate almost no correlation between the flexural results and the dry IDT results, except that the polymer-modified mix has high controlled-deformation flexural fatigue resistance and low IDT strength.

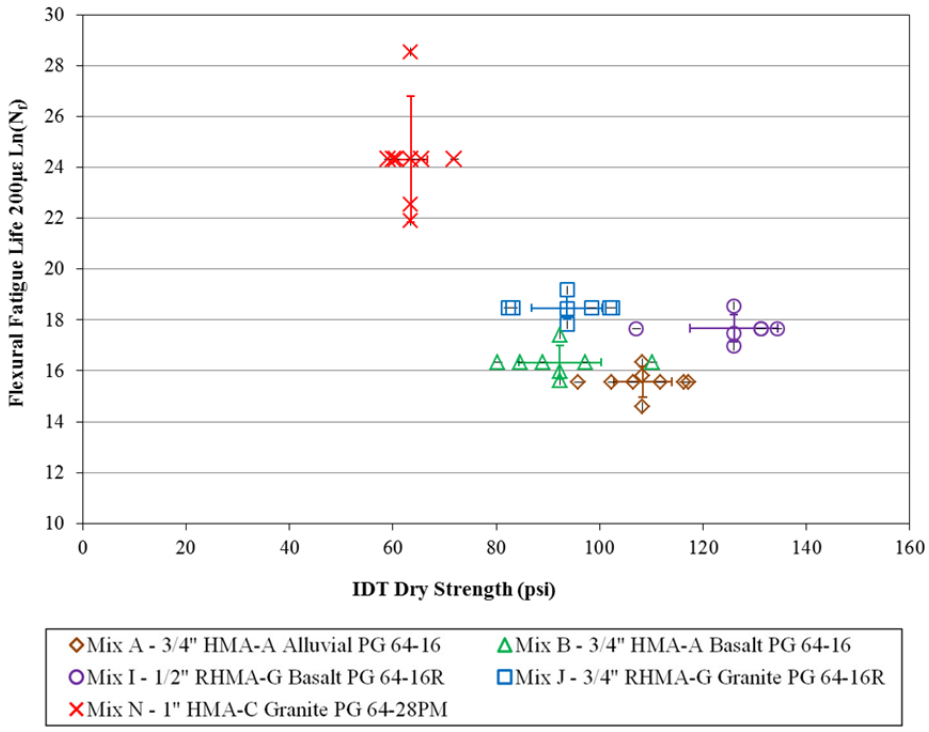

Figure 7.9: Flexural fatigue life (200 με) versus IDT dry strength.

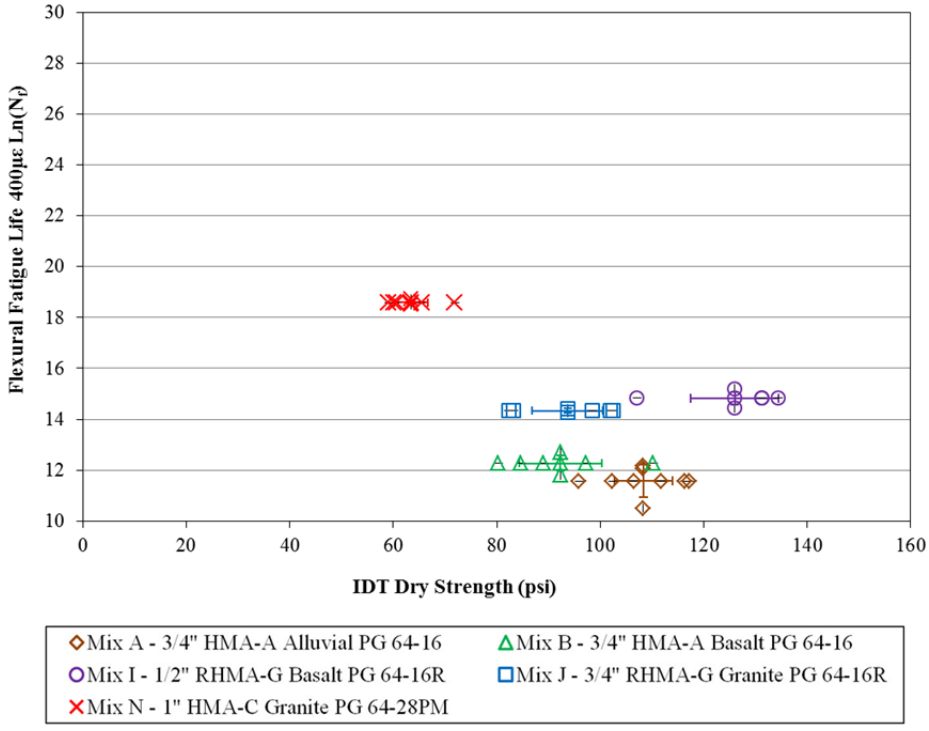

Figure 7.10: Flexural fatigue life (400με) versus IDT dry strength.

7.2.3 Flexural Fatigue versus Direct Tension Fatigue

Figure 7.11 and Figure 7.12 show the average relationship for the five mixes between stiffness ratio, beginning with the 100th repetition, for the flexural fatigue and direct tension tests, respectively. The strain levels are 200 microstrain for both tests. It can be seen that the overall trends are similar, and both tests show Mix A with the worst performance and Mix N with the best performance toward the end of the tests. The flexural fatigue tests for the mixes other than Mix A appear to reach 30 percent loss of stiffness (0.7 stiffness ratio) at very different rates, while the direct tension tests appear to have very similar performance although none reached 0.7 stiffness ratio because they were stopped at 200,000 repetitions due to time constraints on the testing.

Figure 7.13 through Figure 7.17 show the comparison of flexural fatigue and AMPT direct tension for each of the five individual mixes. The similarity of the trends can be seen, which is partly accentuated by the more rapid damage rate in the direct tension tests in the first 100 repetitions.

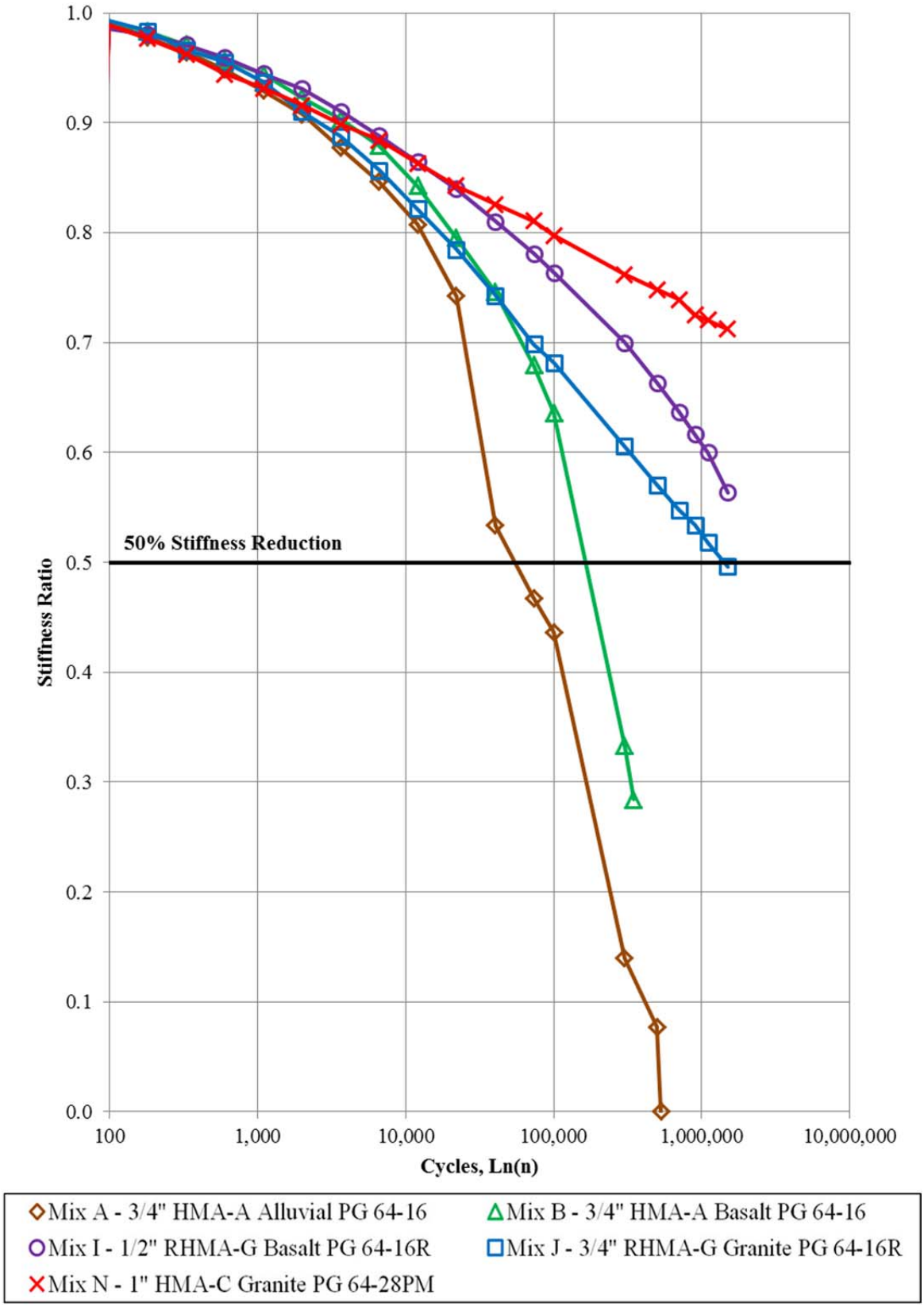

Figure 7.11: Flexural fatigue stiffness ratio versus cycles for the five mixes.

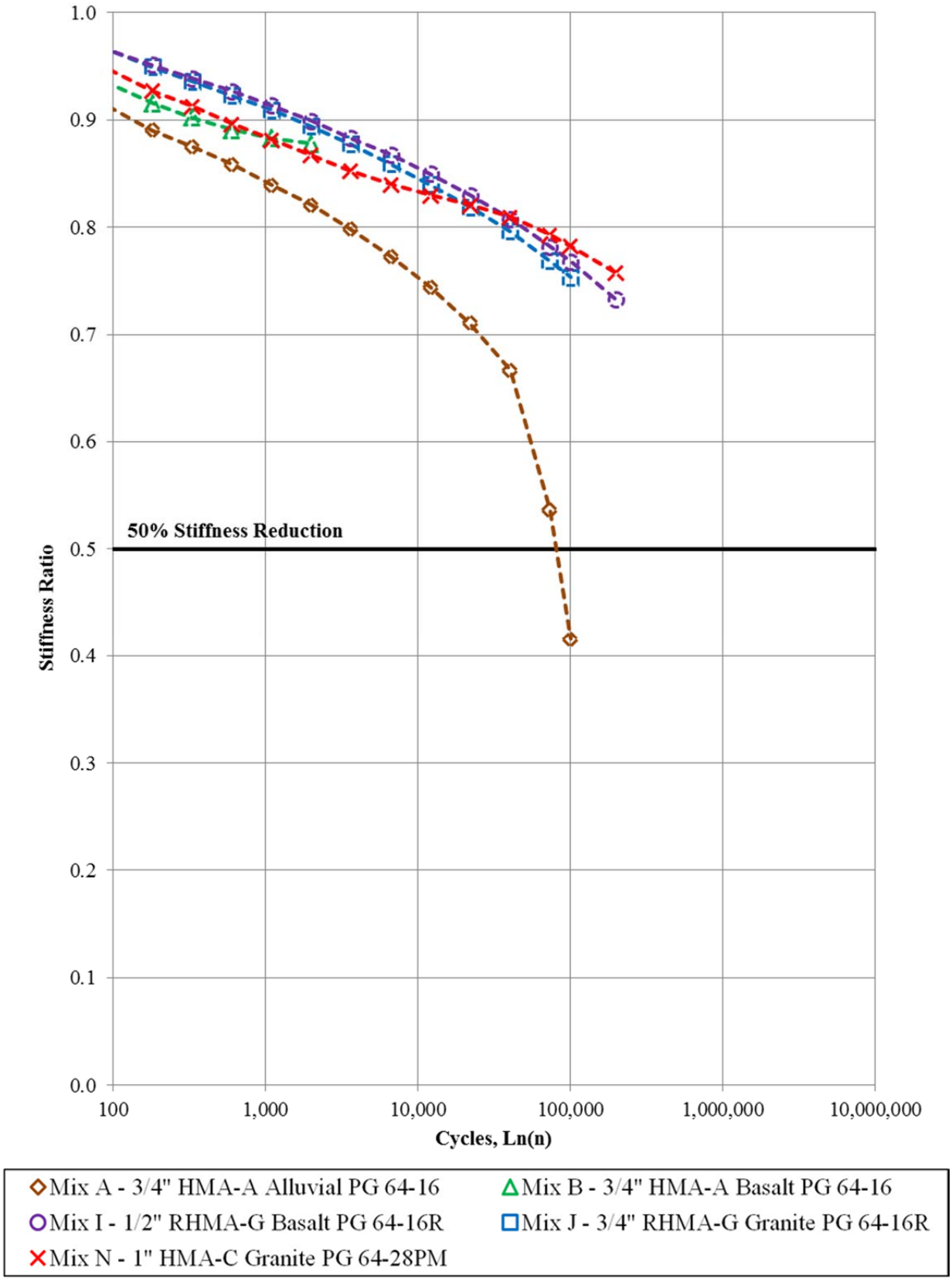

Figure 7.12: AMPT direct tension stiffness ratio versus cycles for the five mixes.

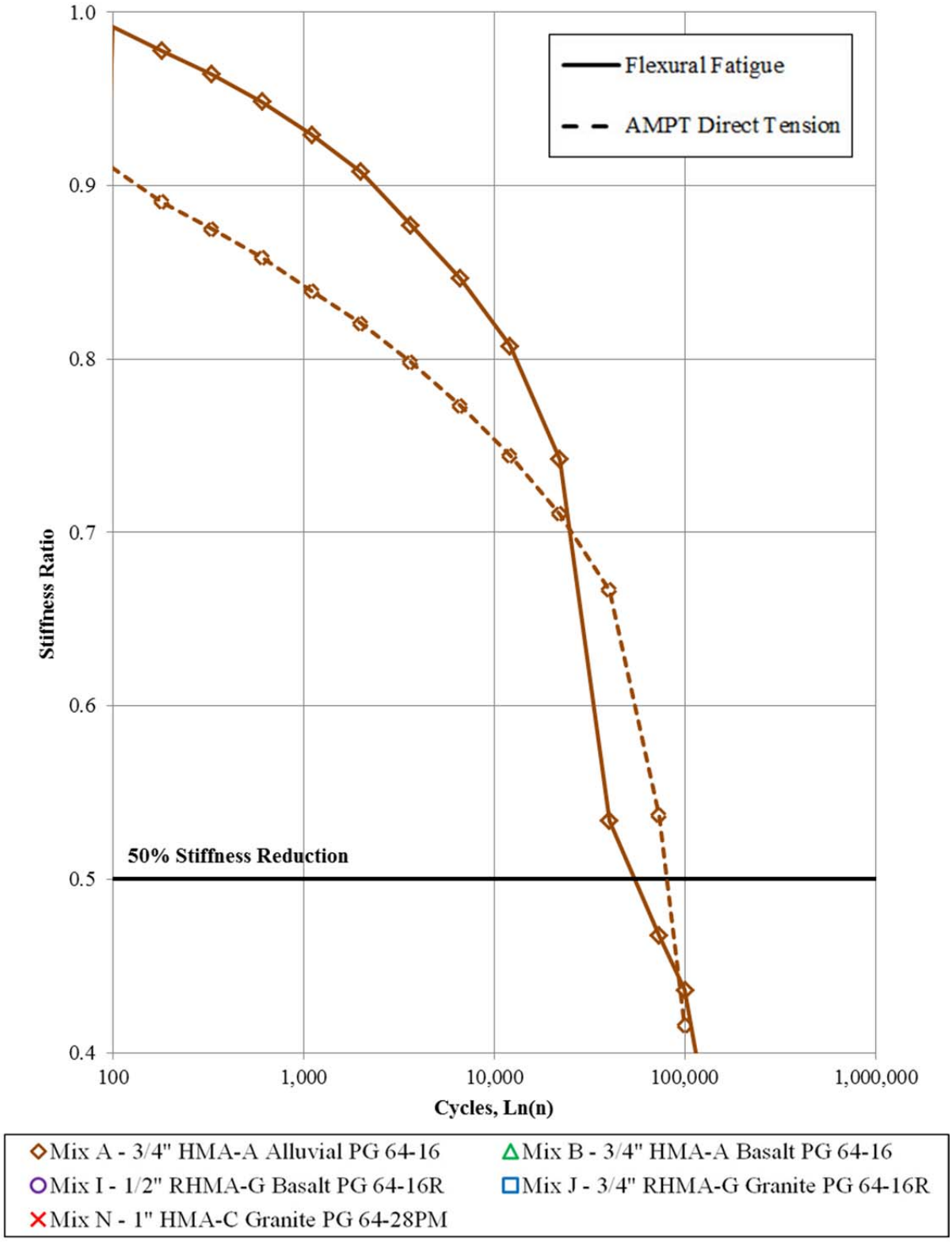

Figure 7.13: Comparison of flexural fatigue and AMPT direct tension stiffness ratio for Mix A.

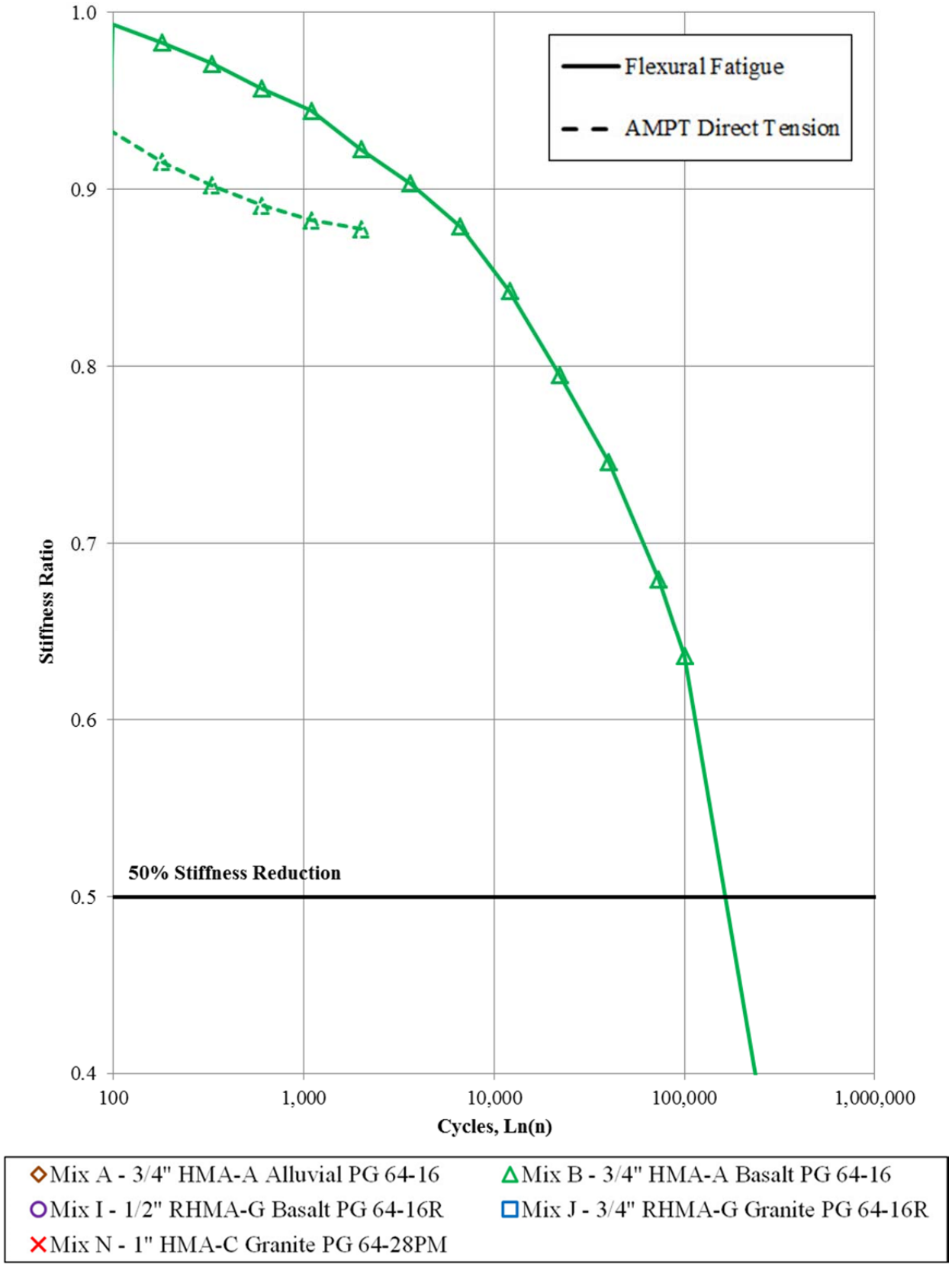

Figure 7.14: Comparison of flexural fatigue and AMPT direct tension stiffness ratio for Mix B.

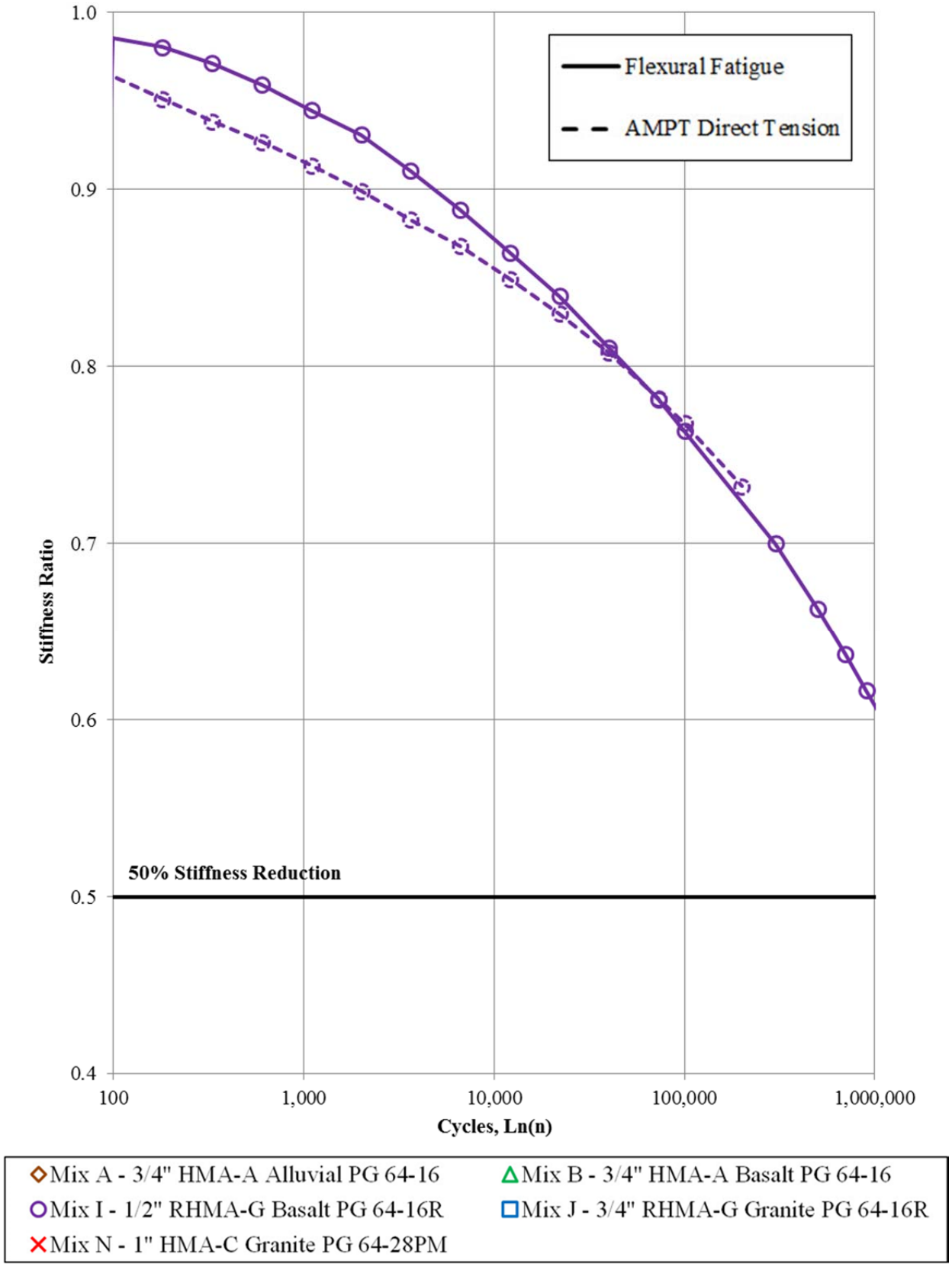

Figure 7.15: Comparison of flexural fatigue and AMPT direct tension stiffness ratio for Mix I.

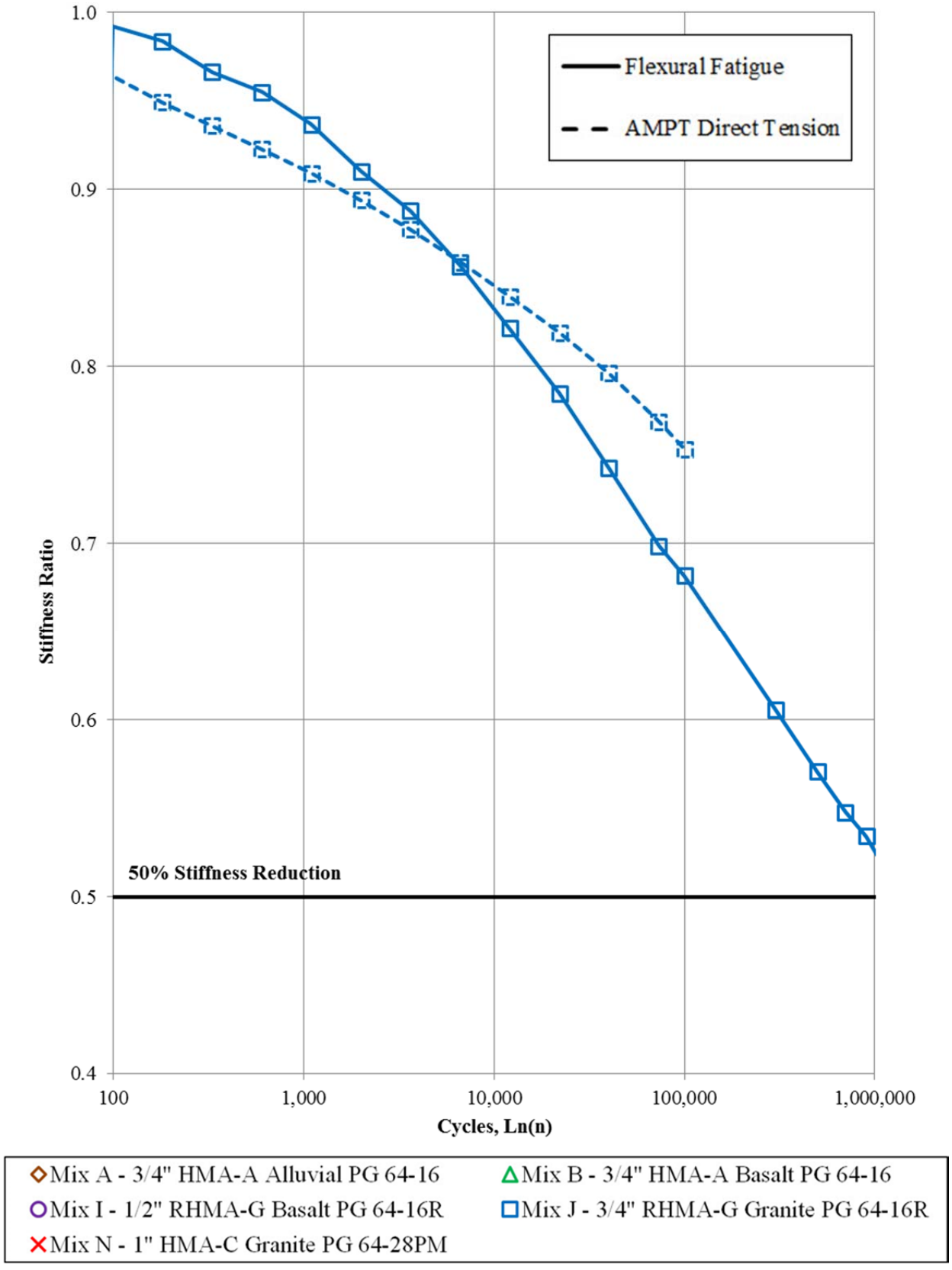

Figure 7.16: Comparison of flexural fatigue and AMPT direct tension stiffness ratio for Mix J.

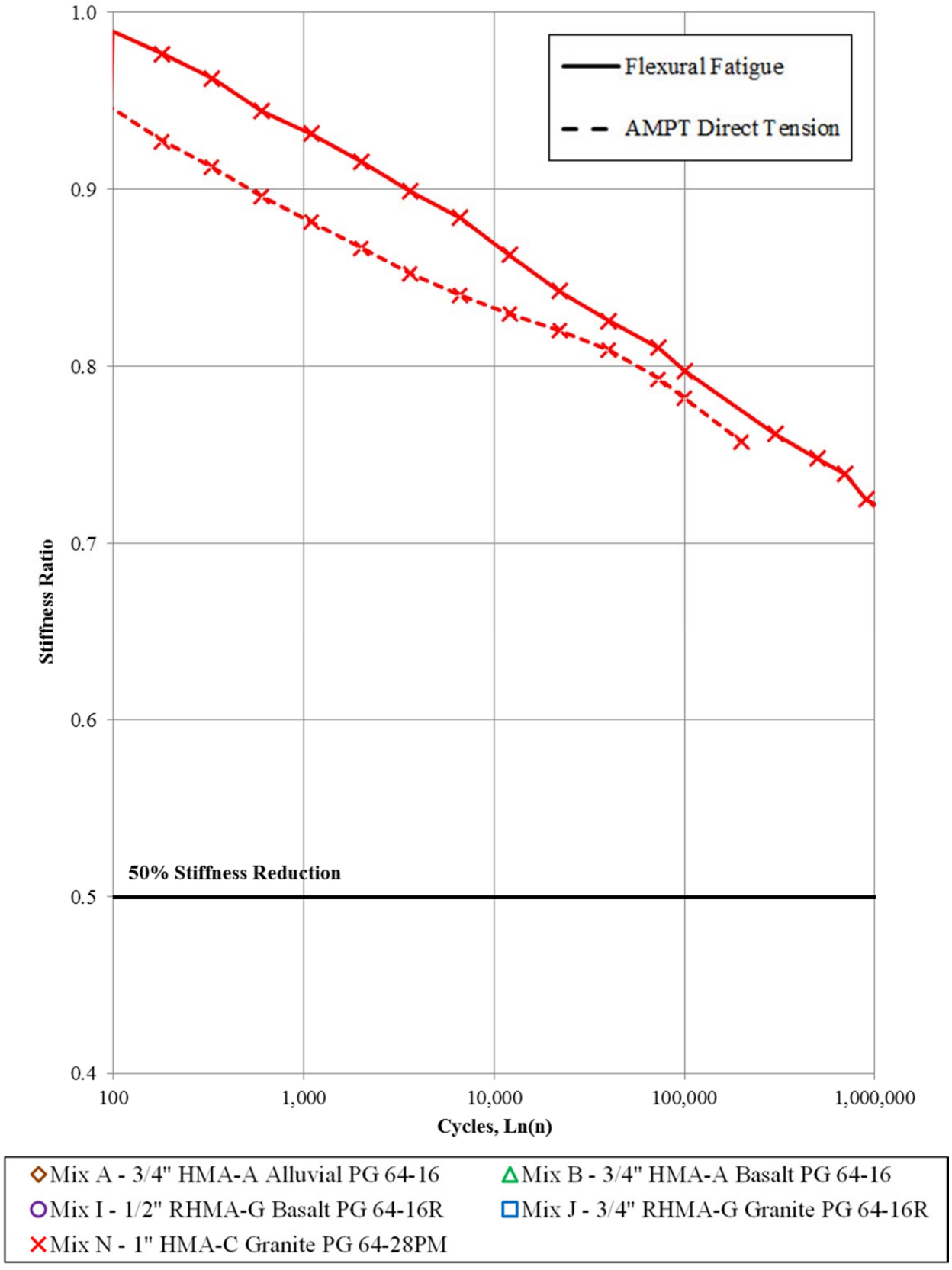

Figure 7.17: Comparison of flexural fatigue and AMPT direct tension stiffness ratio for Mix N.

7.3 Rutting

7.3.1 Shift Factors Relating RLT to RSCH Results

Shift factors were developed for converting the relationships between repetitions and permanent axial strain (PAS) for the confined and unconfined RLT tests to the same relationship for permanent shear strain for RSCH tests at different shear stress levels and temperatures. The *shift factor* is defined as the number that can make sum of squared errors (SSE) for the differences between the complete permanent deformation development curves as small as possible, as shown in the following equation. The shift factor is found using least squares approximation, and the Microsoft *Excel* Solver function is the tool to find the value.

$$SSE = \sum_{i=1}^{20000}(\alpha A_i - B_i)^2 \quad \textbf{(14)}$$

where:

α is the shift factor,

A_i is the AMPT RLT result at the i^{th} repetition,

B_i is the RSCH result at the i^{th} repetition, and

SSE is the sum of squared errors.

Table 7.2 through Table 7.5 summarize the shift factors for each mix under the two test temperatures and the different RSCH shear stress levels. The original and shifted RLT curves are shown in Figure 7.18 through Figure 7.29 for the confined RLT tests and Figure 7.30 through Figure 7.44 for the unconfined RLT tests.

From the plots it can be seen that individual permanent deformation curves for the RSCH tests have trends that fall in between the confined and unconfined results, particularly at the later stages of the tests. The confined RLT results converted to RSCH equivalents by the shift factors show slower permanent deformation rates than the RSCH in the later stages, while the unconfined RLT results show faster deformation rates in the later stages.

Overall, the shift factors are much larger for the confined results than for the unconfined results, as expected. The shift factors follow expected trends for the stress state, with increased shift factors for higher RSCH stress states. The shift factors for 45°C and 55°C are about 30 percent different for both the confined and unconfined results, with the absolute values of the shift factors for different temperatures being much larger for the confined RLT results. This lack of consistency for different temperatures makes development of a single shift factor with reasonable errors difficult, and may point to a need for different shift factors at different temperatures. The allowable difference for shifting RLT results to RSCH equivalents for use in mechanistic-empirical design that would be considered acceptable has not been determined.

Table 7.2: Mean Shift Factor for Confined RLT to RSCH at 45°C

RSST-RW-3%-45C	Shift Factor	RLT-SGC-7%-45C					
		Mix Type					
		A	B	I	J	N	mean
	70 kPa	2.7	1.6	1.6	1.6	1.8	1.9
	100 kPa	2.7	2.4	2.1	1.7	2.6	2.3
	130 kPa	3.1	2.9	2.6	2.0	3.0	2.7

Table 7.3: Mean Shift Factor for Confined RLT to RSCH at 55°C

RSST-RW-3%-55C	S.F.	RLT-SGC-7%-55C					
		Mix Type					
		A	B	I	J	N	mean
	70 kPa	2.8	1.9	2.5	2.1	2.2	2.3
	100 kPa	3.2	3.0	3.3	2.9	3.8	3.2
	130 kPa	4.0	3.5	3.3	3.3	4.1	3.6

Table 7.4: Mean Shift Factor for Unconfined RLT to RSCH at 45°C

RSST-RW-3%-45C	Shift Factor	RLT-SGC-7%-45C					
		Mix Type					
		A	B	I	J	N	Mean
	70 kPa	0.9	0.5	0.4	0.4	0.5	0.5
	100 kPa	0.9	0.7	0.6	0.6	0.8	0.7
	130 kPa	1.1	1.1	0.7	0.8	1.1	1.0

Table 7.5: Mean Shift Factor for Unconfined RLT to RSCH at 55°C

RSST-RW-3%-55C	S.F.	RLT-SGC-7%-55C					
		Mix Type					
		A	B	I	J	N	mean
	70 kPa	0.8	0.7	0.6	0.5	0.5	0.6
	100 kPa	1.0	1.1	1.0	0.9	1.0	1.0
	130 kPa	1.2	1.4	1.0	1.0	1.1	1.2

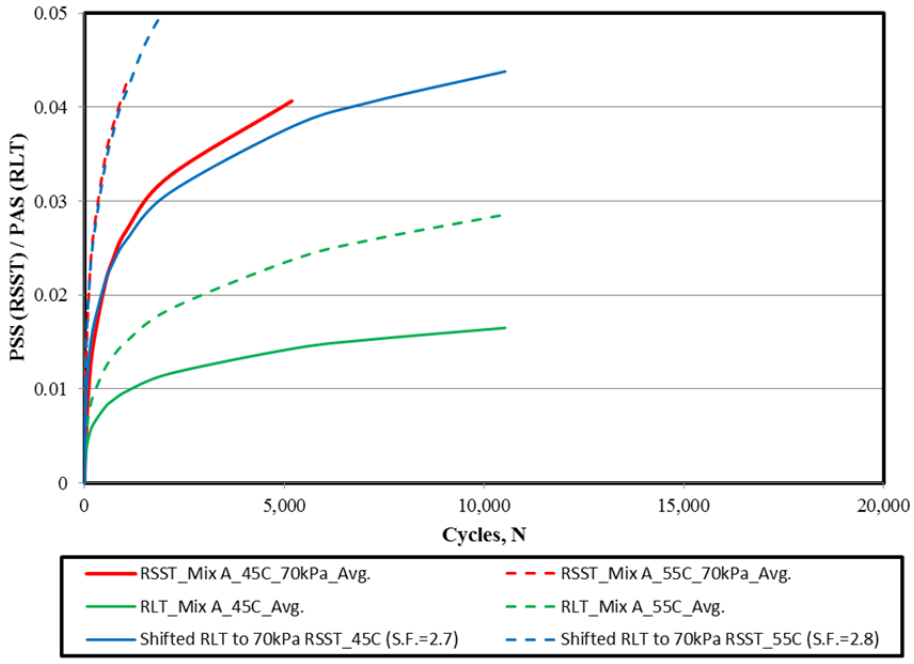

Figure 7.18: Shifted RLT confined to 70 kPa RSCH 45°C and 55°C for Mix A.

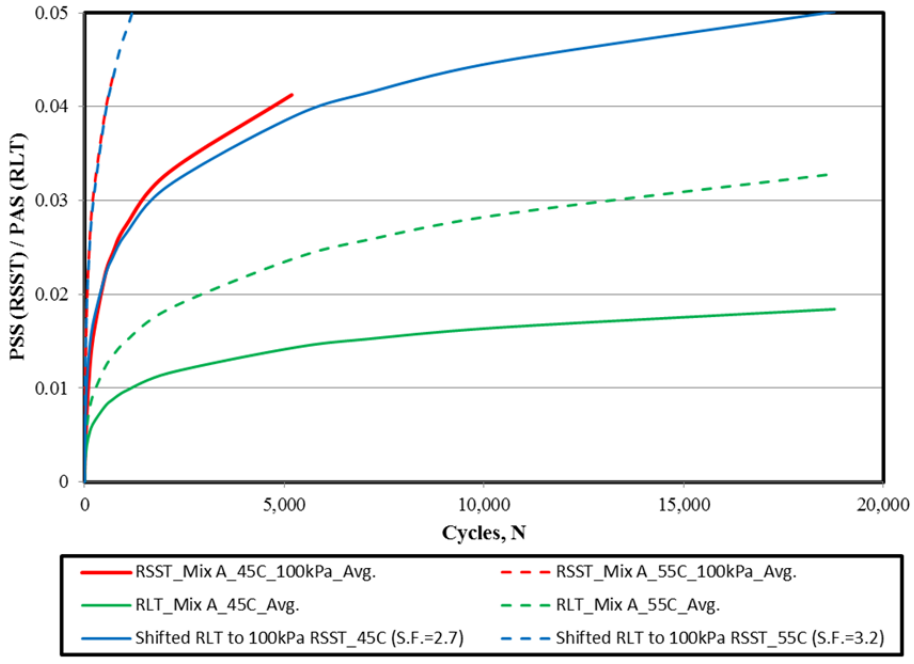

Figure 7.19: Shifted RLT confined to 100 kPa RSCH 45°C and 55°C for Mix A.

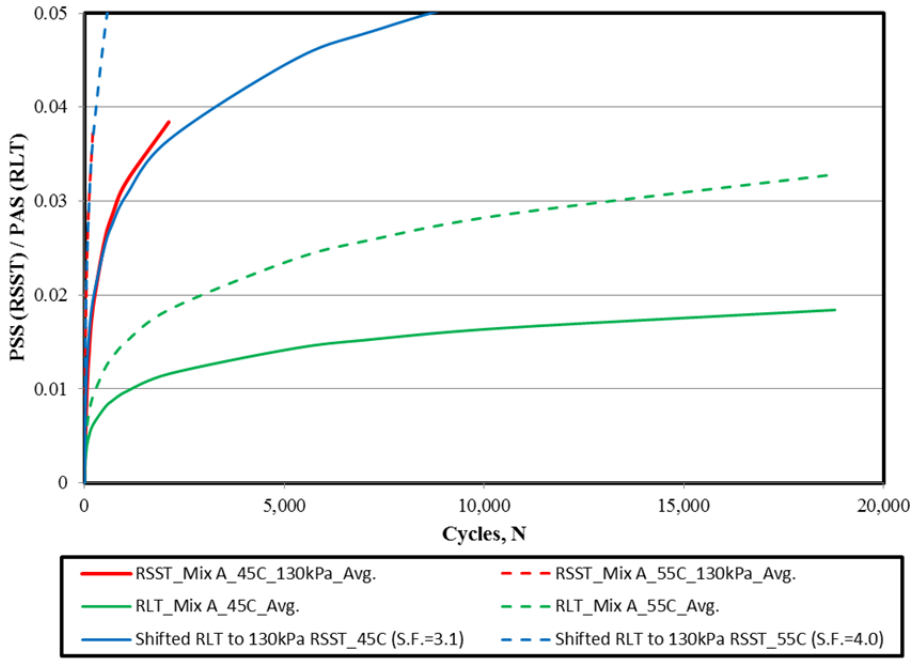

Figure 7.20: Shifted RLT confined to 130 kPa RSCH 45°C and 55°C for Mix A.

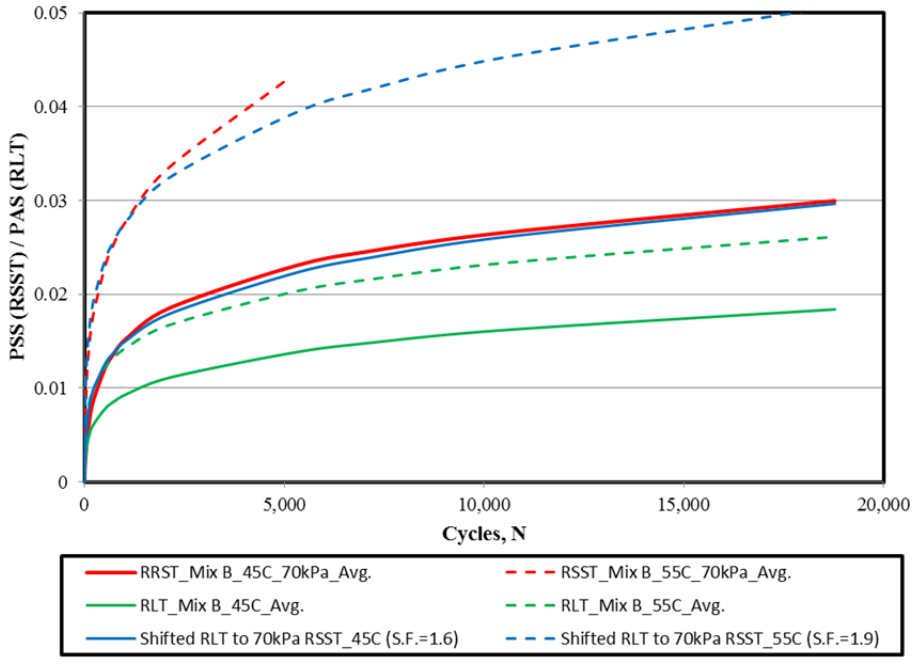

Figure 7.21: Shifted RLT confined to 70 kPa RSCH 45°C and 55°C for Mix B.

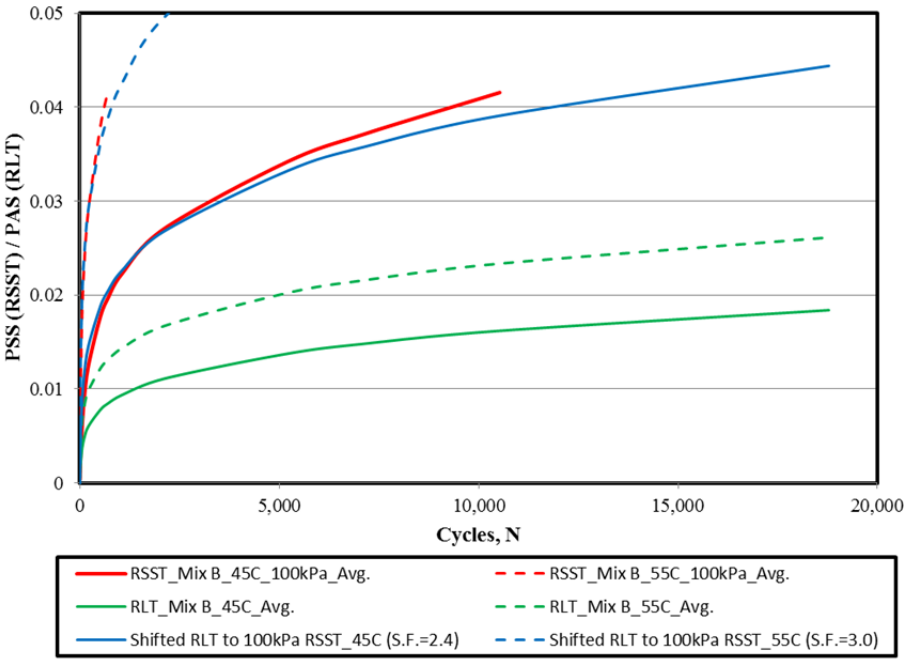

Figure 7.22: Shifted RLT confined to 100 kPa RSCH 45°C and 55°C for Mix B.

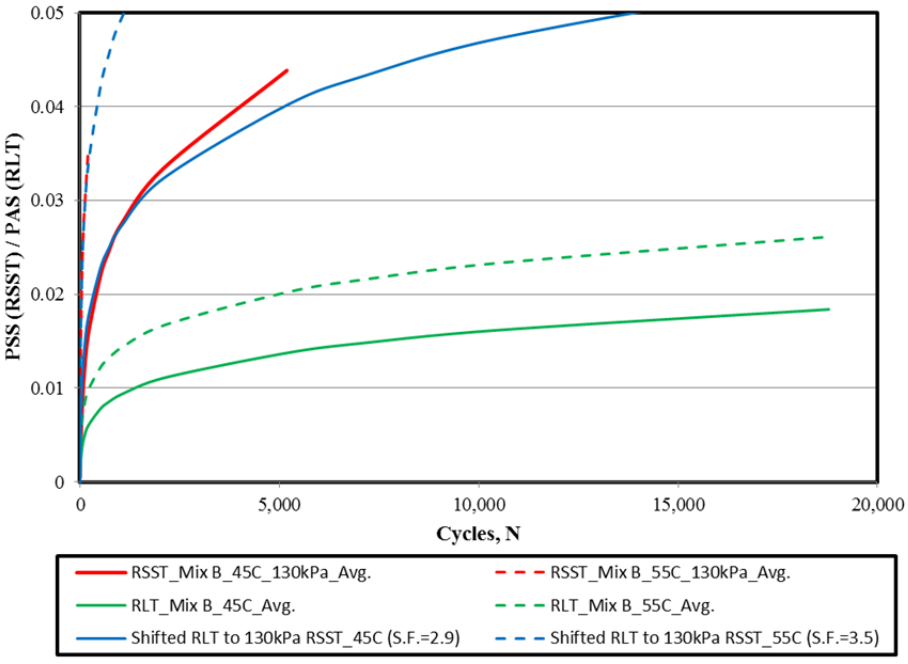

Figure 7.23: Shifted RLT confined to 130 kPa RSCH 45°C and 55°C for Mix B.

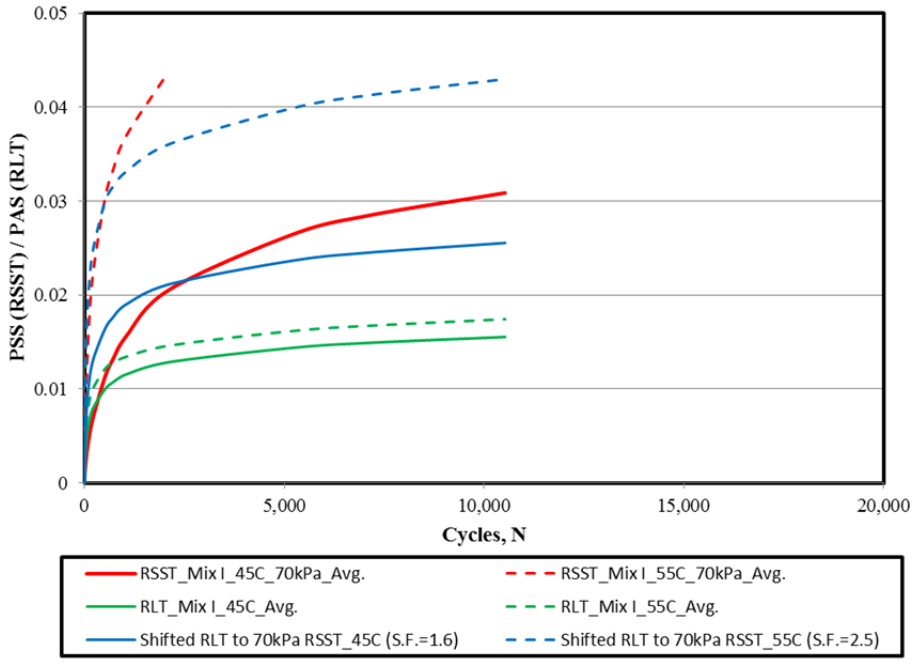

Figure 7.24: Shifted RLT confined to 70 kPa RSCH 45°C and 55°C for Mix I.

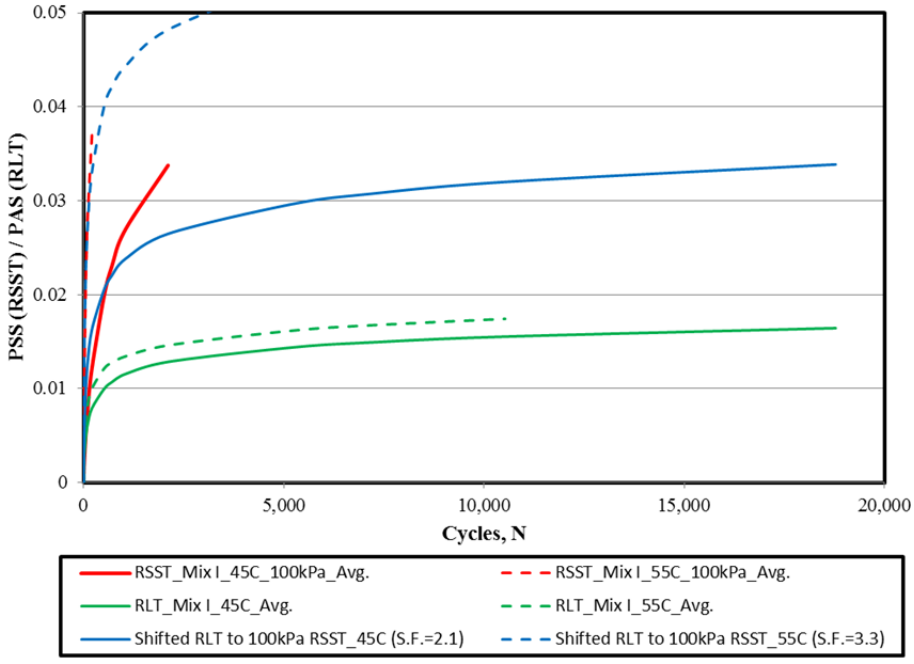

Figure 7.25: Shifted RLT confined to 100 kPa RSCH 45°C and 55°C for Mix I.

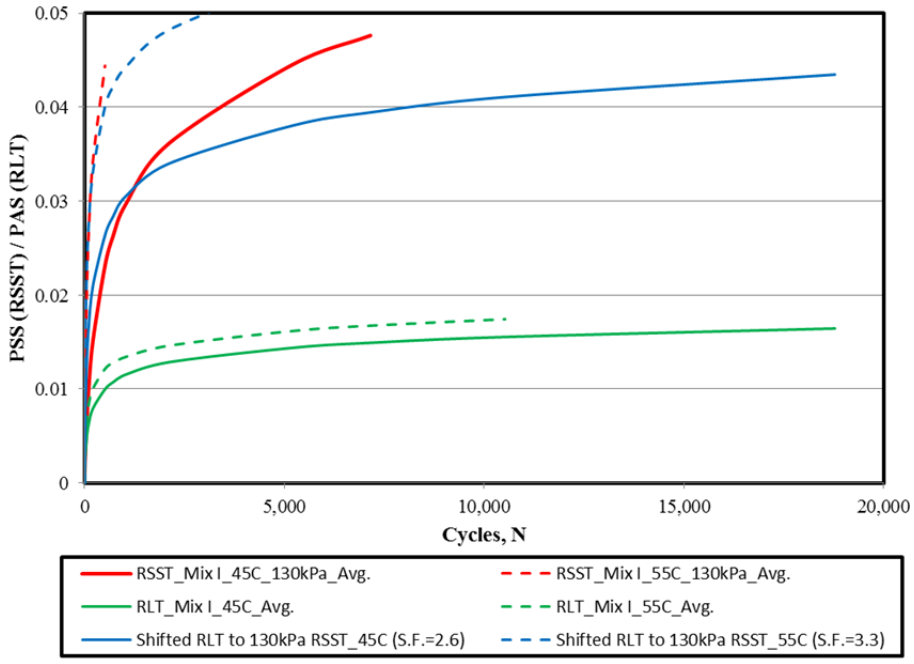

Figure 7.26: Shifted RLT confined to 130 kPa RSCH 45°C and 55°C for Mix I.

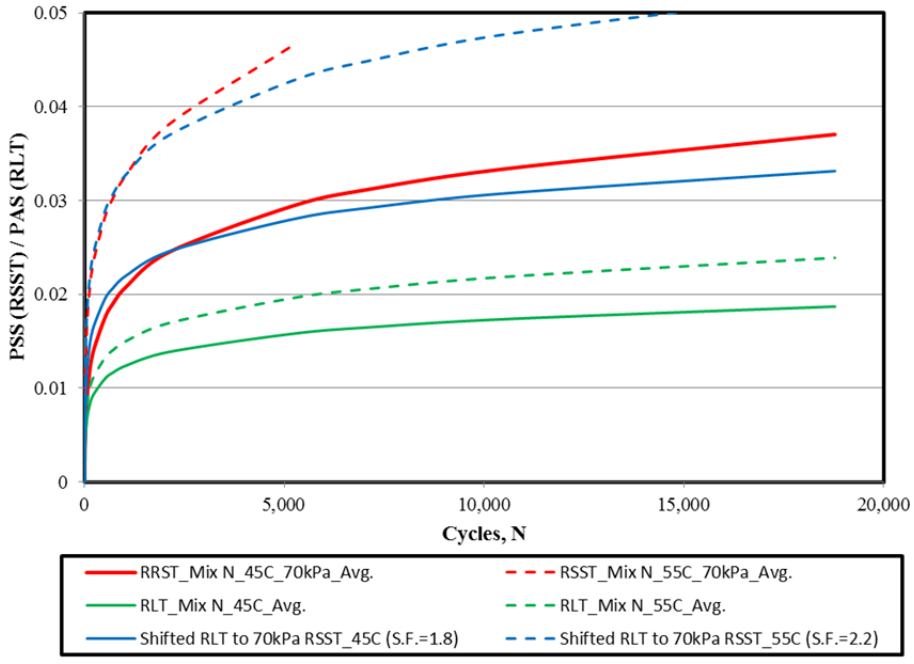

Figure 7.27: Shifted RLT confined to 70 kPa RSCH 45°C and 55°C for Mix N.

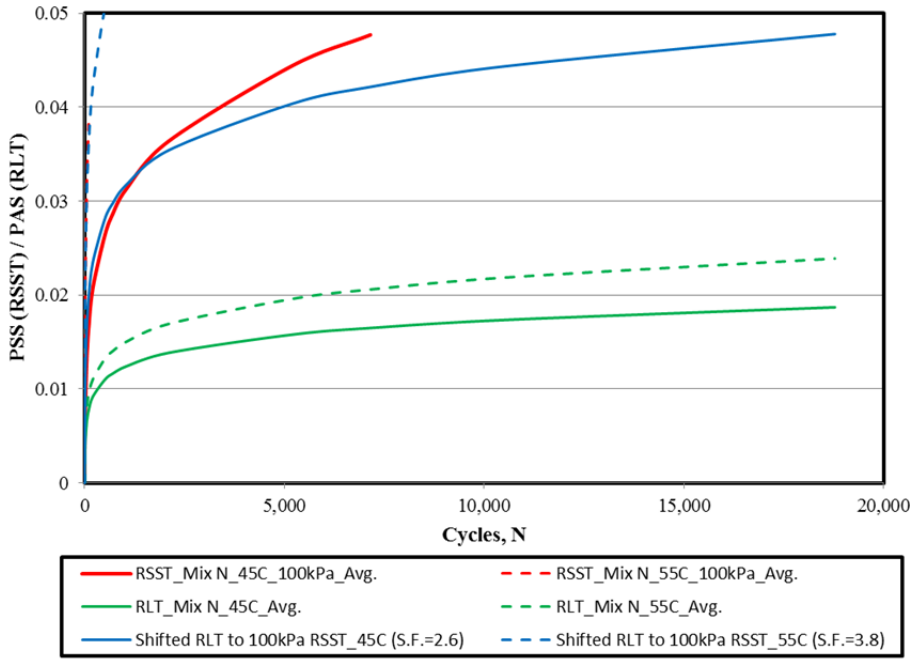

Figure 7.28: Shifted RLT confined to 100 kPa RSCH 45°C and 55°C for Mix N.

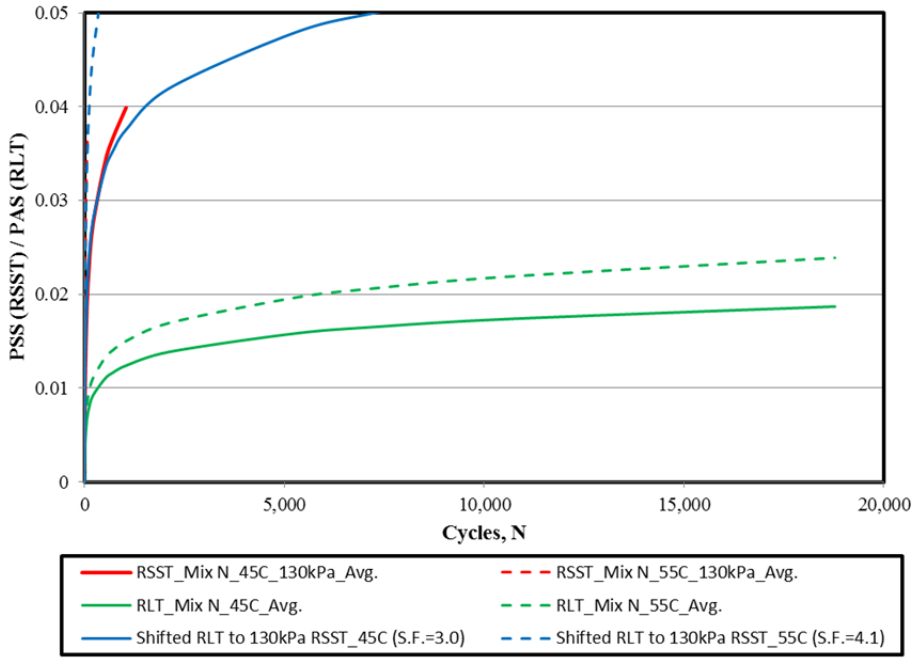

Figure 7.29: Shifted RLT confined to 130 kPa RSCH 45°C and 55°C for Mix N.

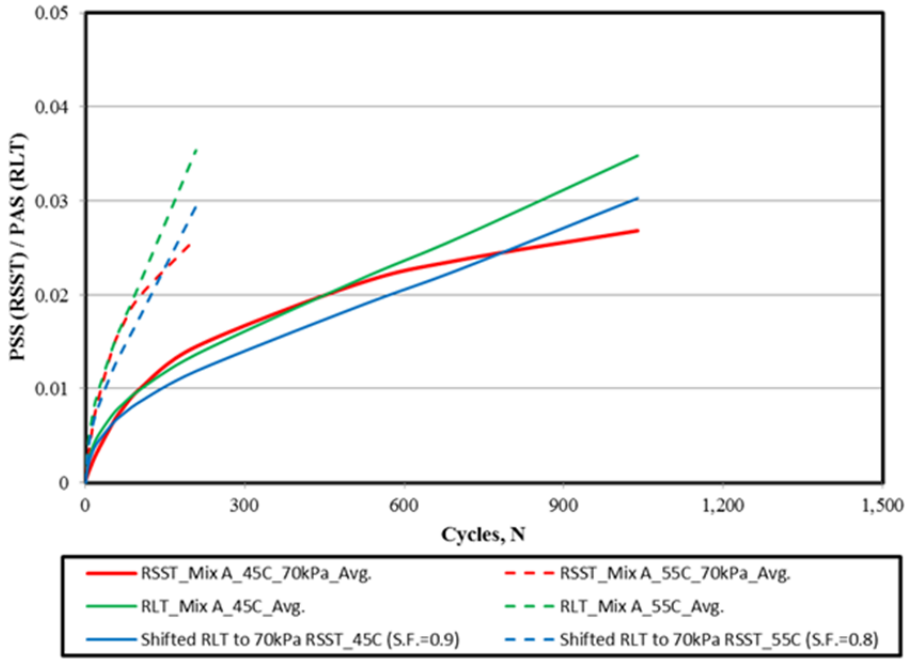

Figure 7.30: Shifted RLT unconfined to 70 kPa RSCH 45°C and 55°C for Mix A.

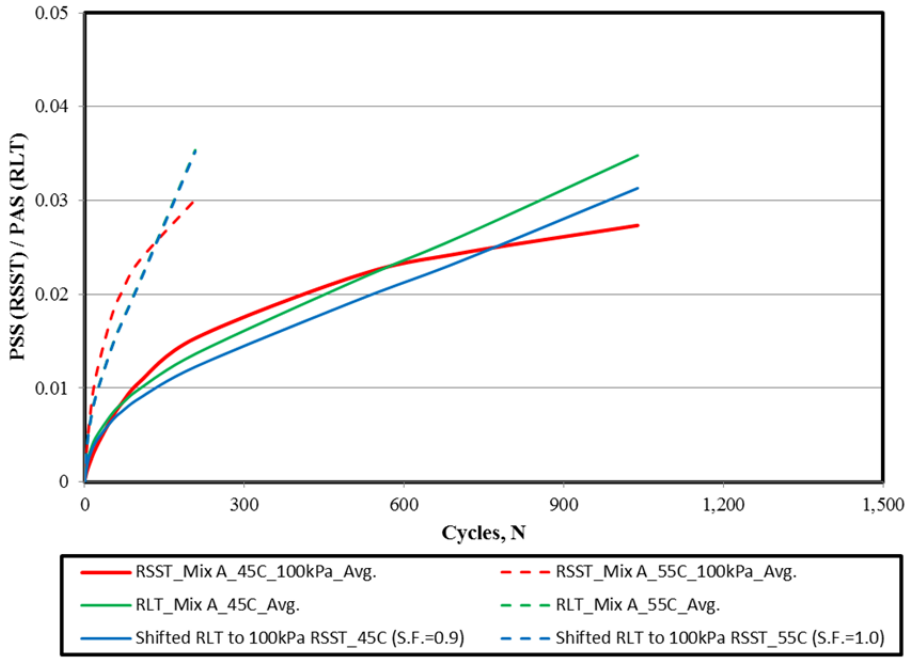

Figure 7.31: Shifted RLT unconfined to 100 kPa RSCH 45°C and 55°C for Mix A.

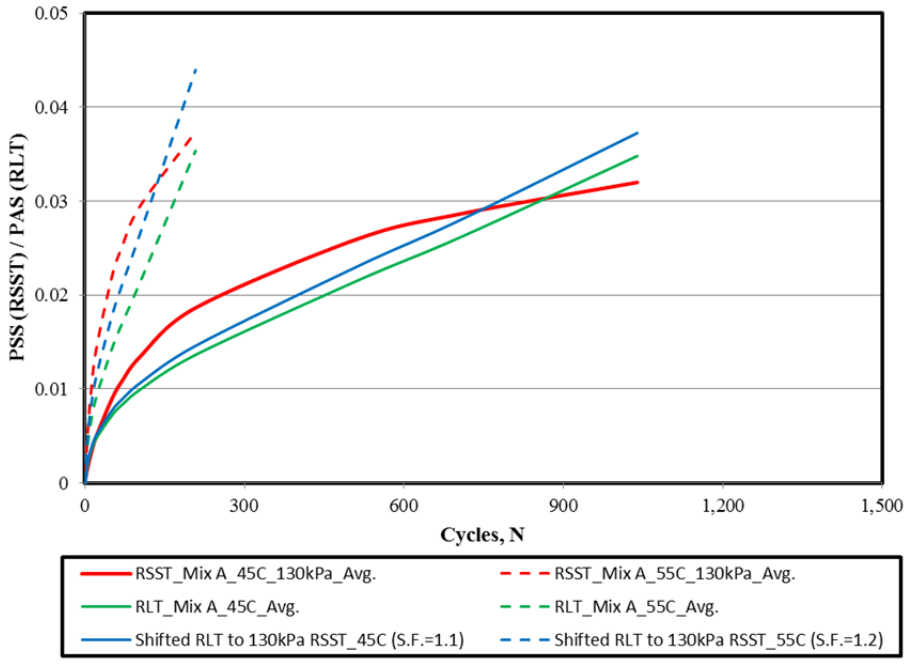

Figure 7.32: Shifted RLT unconfined to 130 kPa RSCH 45°C and 55°C for Mix A.

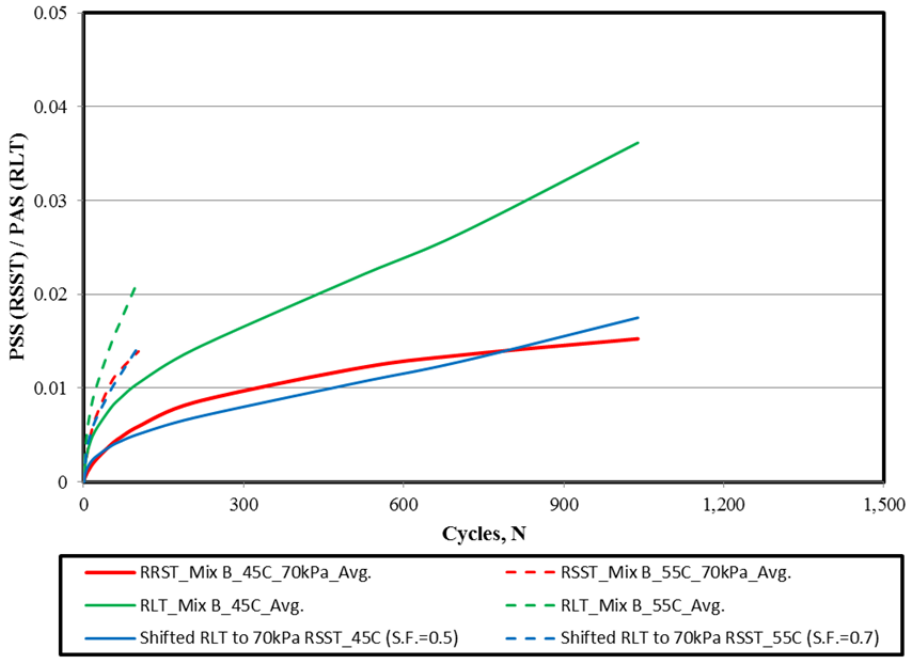

Figure 7.33: Shifted RLT unconfined to 70 kPa RSCH 45°C and 55°C for Mix B.

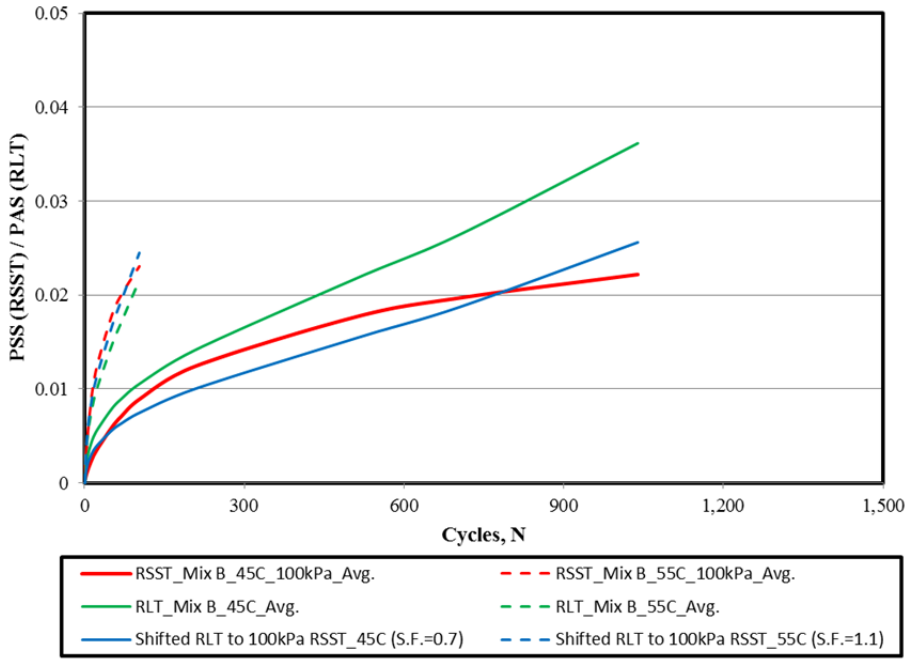

Figure 7.34: Shifted RLT unconfined to 100 kPa RSCH 45°C and 55°C for Mix B.

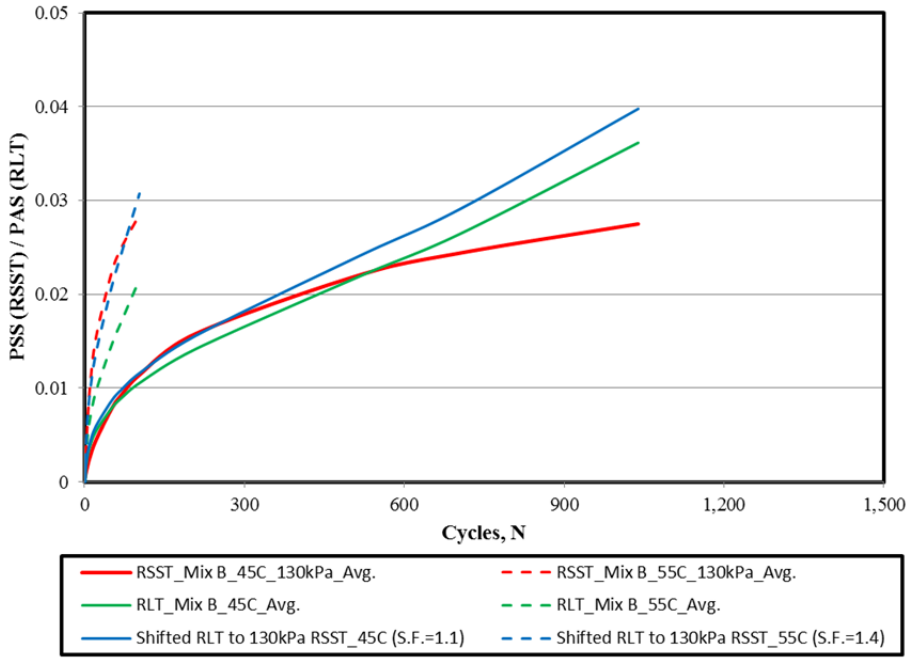

Figure 7.35: Shifted RLT unconfined to 130 kPa RSCH 45°C and 55°C for Mix B.

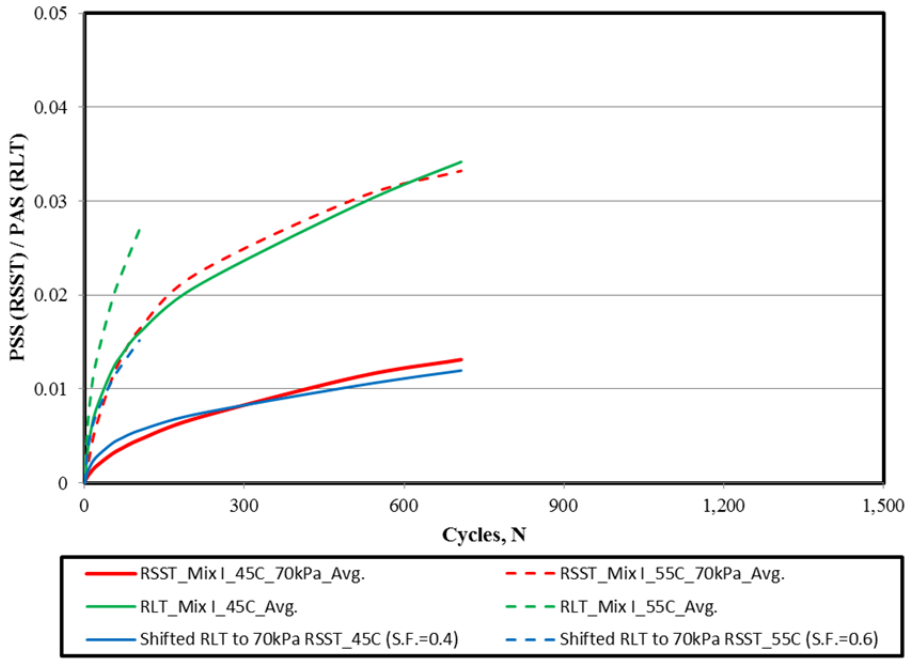

Figure 7.36: Shifted RLT unconfined to 70 kPa RSCH 45°C and 55°C for Mix I.

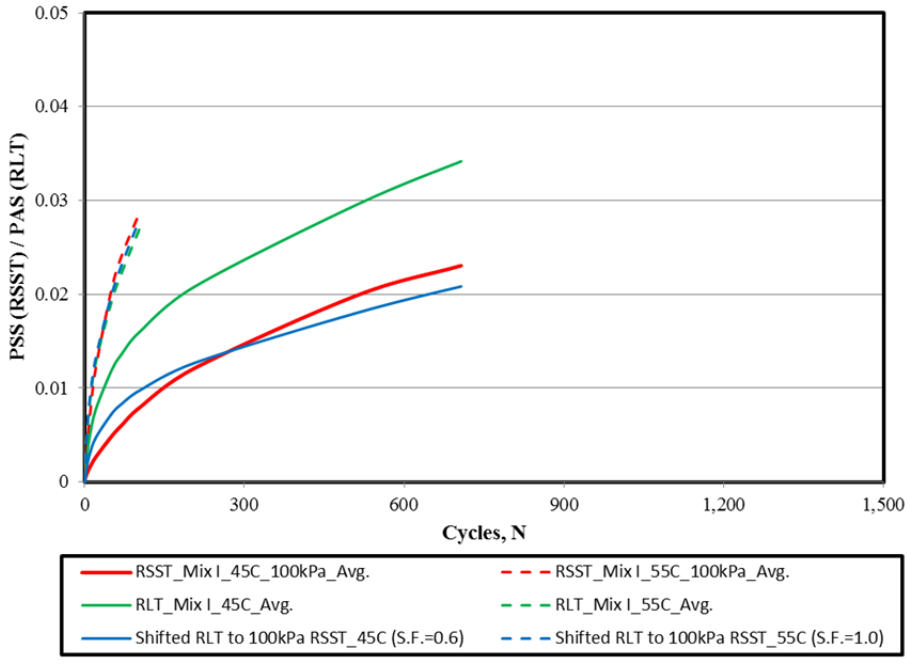

Figure 7.37: Shifted RLT unconfined to 100 kPa RSCH 45°C and 55°C for Mix I.

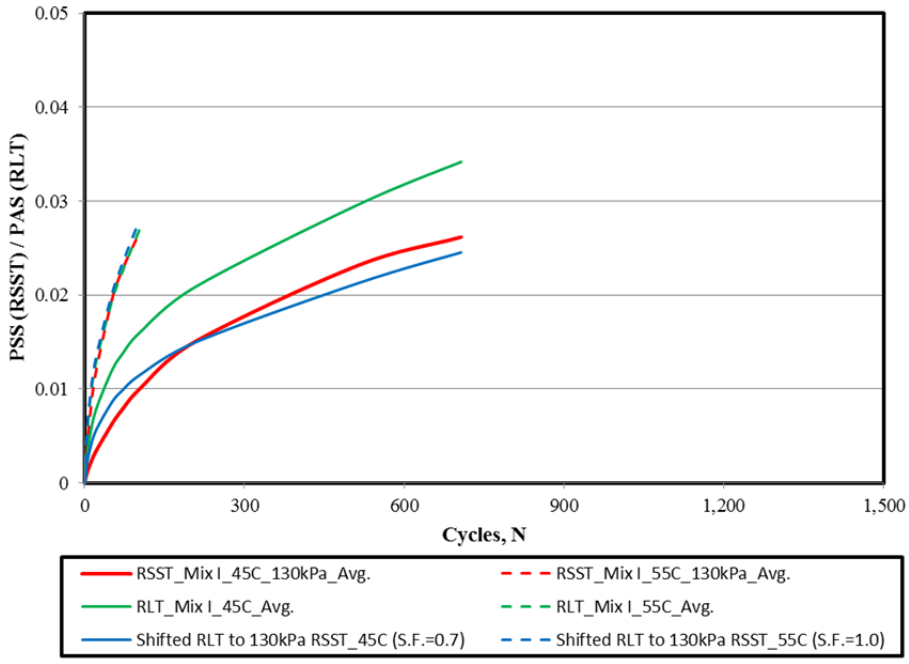

Figure 7.38: Shifted RLT unconfined to 130 kPa RSCH 45°C and 55°C for Mix I.

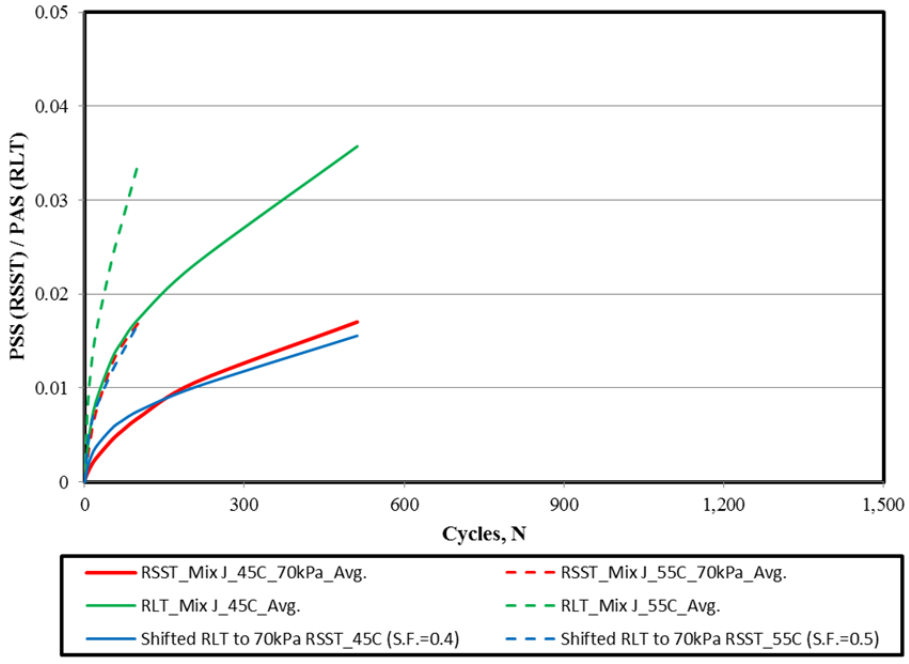

Figure 7.39: Shifted RLT unconfined to 70 kPa RSCH 45°C and 55°C for Mix J.

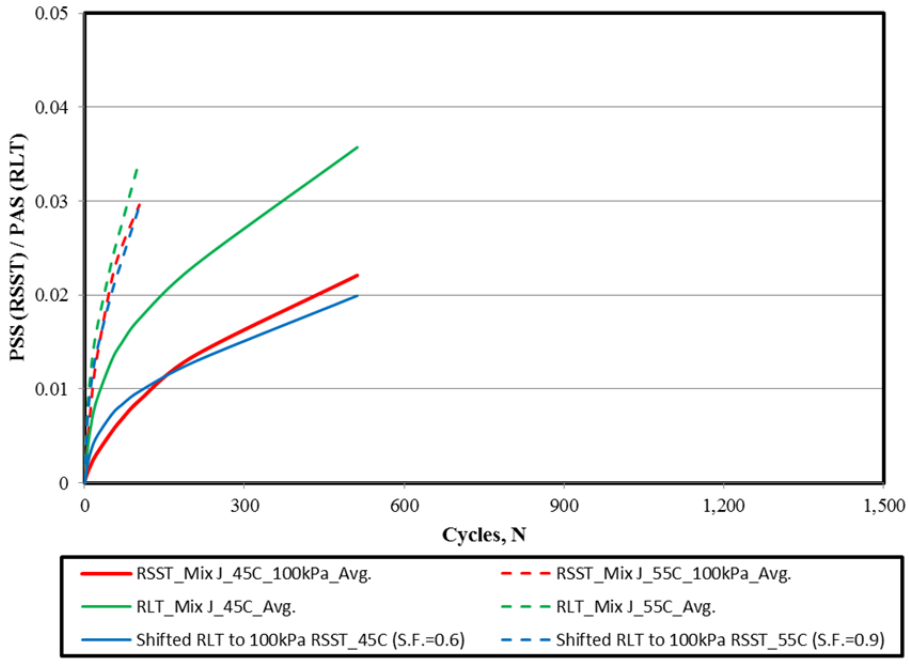

Figure 7.40: Shifted RLT unconfined to 100 kPa RSCH 45°C and 55°C for Mix J.

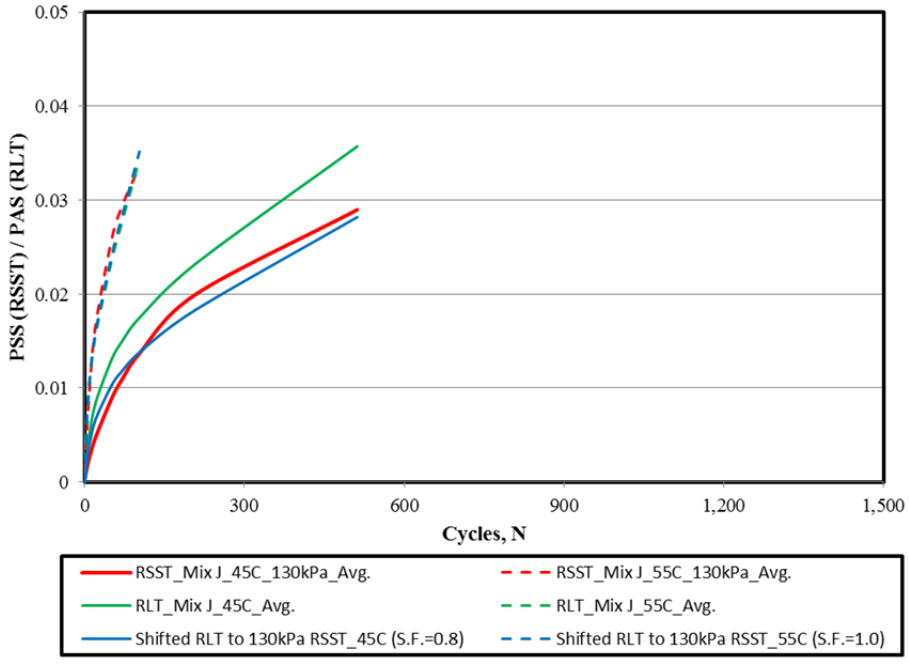

Figure 7.41: Shifted RLT unconfined to 130 kPa RSCH 45°C and 55°C for Mix J.

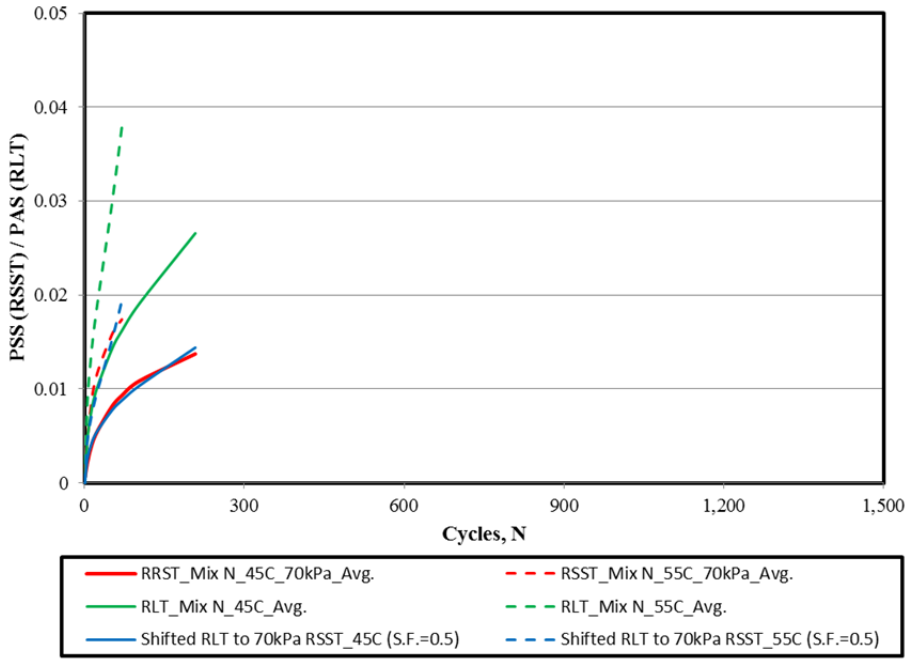

Figure 7.42: Shifted RLT unconfined to 70 kPa RSCH 45°C and 55°C for Mix N.

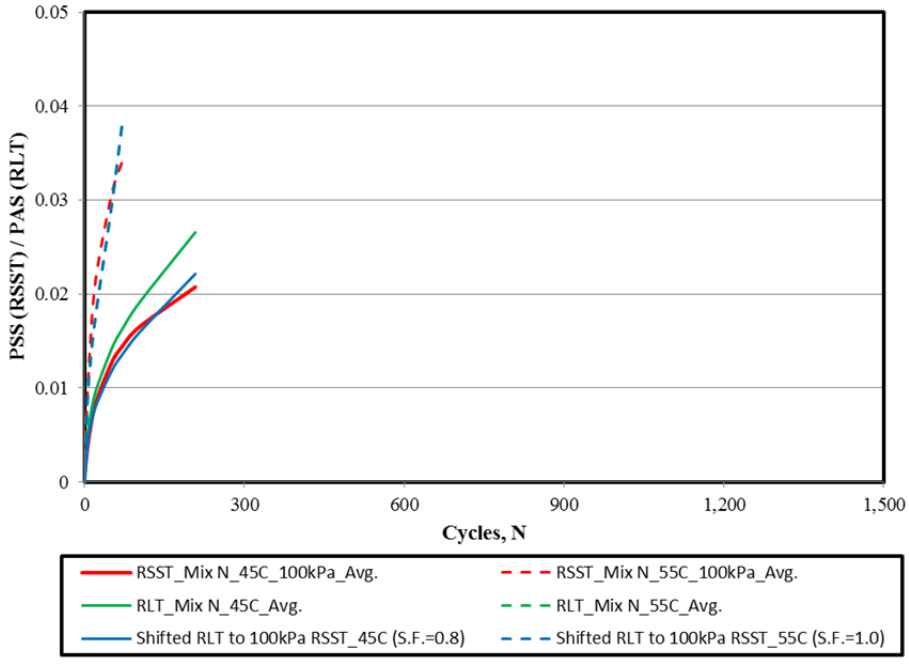

Figure 7.43: Shifted RLT unconfined to 100 kPa RSCH 45°C and 55°C for Mix N.

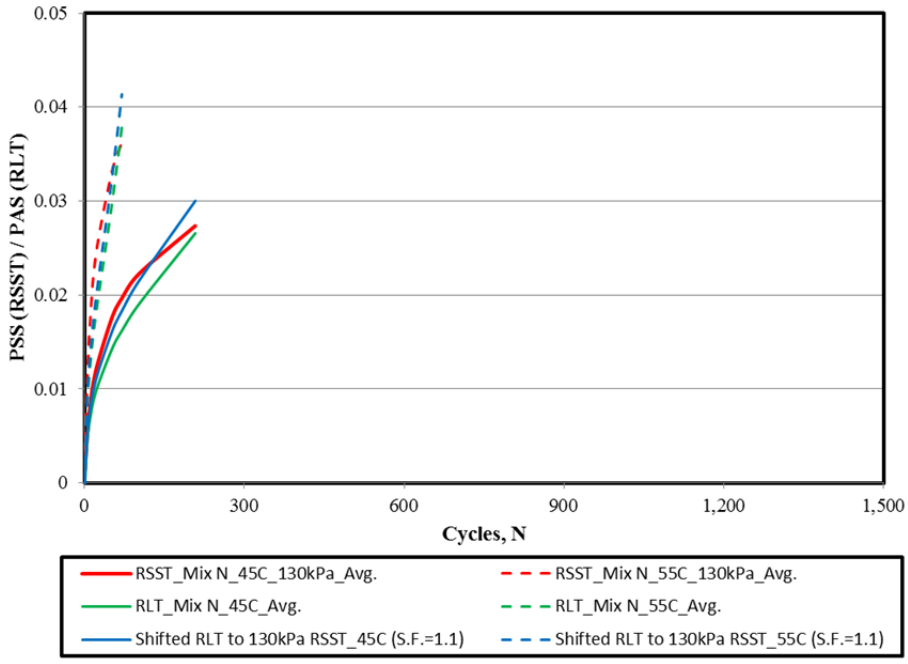

Figure 7.44: Shifted RLT unconfined to 130 kPa RSCH 45°C and 55°C for Mix N.

7.3.2 Comparison of RSCH versus HWTT (Slope and Reps to 12.5 mm)

RSCH Cycles to 5 Percent Shear Strain versus HWTT Creep Slope

As noted in Figure 2.17, the creep slope is an ideal representation of the slope of the rut depth versus cycles, following a change in the controlling mechanism for performance from rutting to material breakdown due to moisture sensitivity. In all the mixes tested for this project, none of the tests exhibited a creep slope over the 15,000 test cycles.

RSCH Cycles to 5 Percent Permanent Shear Strain versus HWTT Rut Depth at 15,000 Cycles

Figure 7.45 and Figure 7.46 present the comparison scatter plot of RSCH cycles to 5 percent permanent shear strain at 45°C and 55°C versus HWTT rut depth at 15,000 cycles, respectively. As with the SCB plots, the limits of the "bars" in the figures represent the 25th and 75th percentiles of the data. The general trend shown by the data was counter to what was expected in that the HWTT indicates greater rutting potential for mixes that the RSCH indicates will have good rutting resistance (i.e., more repetitions to a 5 percent permanent shear strain in the RSCH indicate better rutting resistance; lower rut depths in the HWTT indicate better rutting resistance). Stiffer mixes in shear should rut less, which may mean that the HWTT is more of a moisture sensitivity test than a rutting test, and discriminating between the two may be difficult.

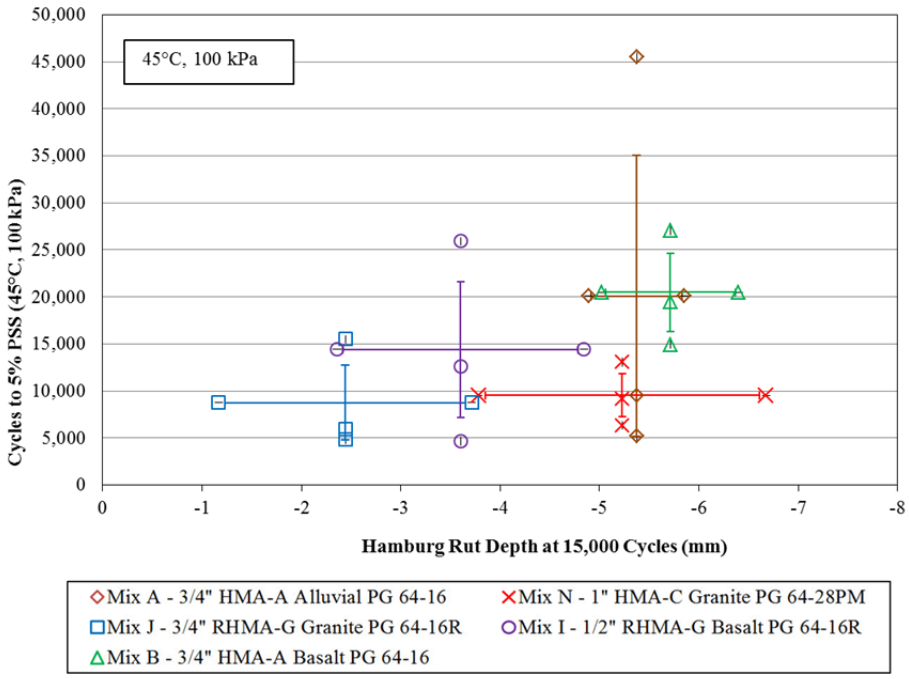

Figure 7.45: RSCH cycles to 5 percent PSS (45°C, 100 kPa) versus HWTT rut depth at 15,000 cycles.

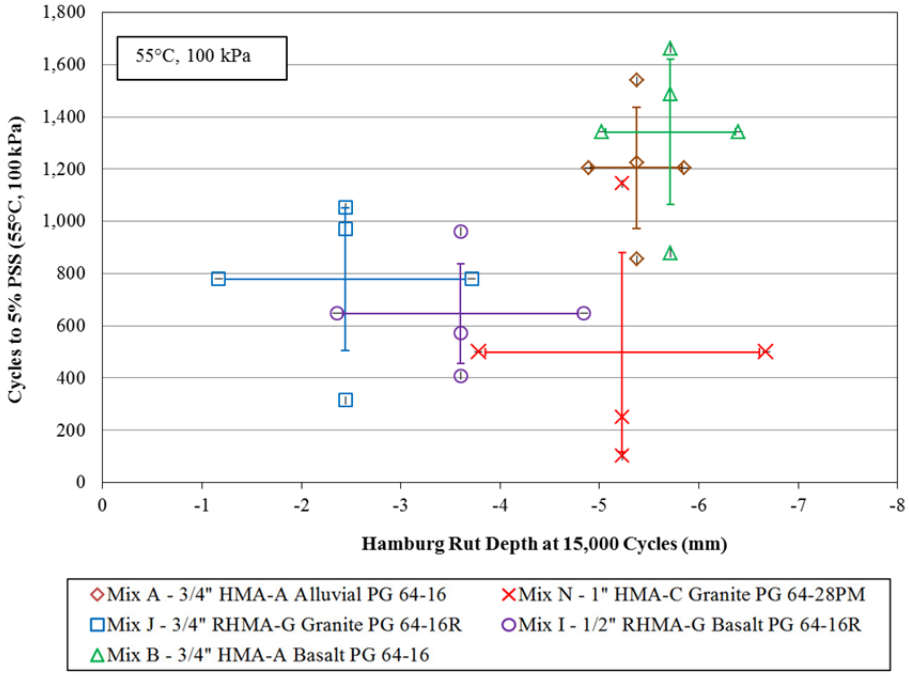

Figure 7.46: RSCH cycles to 5 percent PSS (55°C, 100 kPa) versus HWTT rut depth at 15,000 cycles.

RSCH Shear Strain at 5,000 Cycles versus Hamburg Creep Slope

Comparisons were to be made between RSCH shear strain at 5,000 cycles and HWTT creep slope. In all the mixes tested for this project, none of the tests exhibited a creep slope over the 15,000 test cycles.

RSCH Permanent Shear Strain at 5,000 Cycles versus Hamburg Rut Depth at 15,000 Cycles

Figure 7.47 presents the comparison scatter plot of RSCH permanent shear strain at 5,000 cycles versus Hamburg rut depth at 15,000 cycles for 45°C. A plot of 55°C data is not shown because all of the specimens reached 5 percent permanent shear strain before 5,000 cycles. Unlike the data from RSCH cycles to 5 percent permanent shear strain, the data trend indicated that as the mix "sheared" faster in RSCH, it exhibited greater HWTT rut depth. This is likely due to the fact that most rutting primarily occurred during the early cycles of material loading and that the HWTT does not test a material to its full rut depth by 15,000 cycles, so the parameters related here are comparable. Both of these parameters evaluate "early" cycle loading parameters.

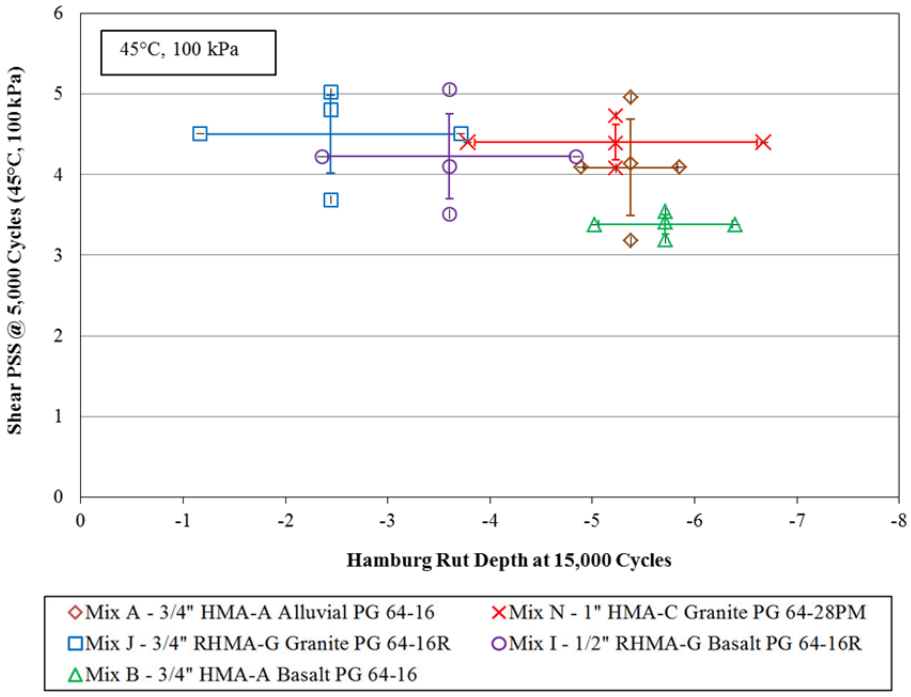

Figure 7.47: RSCH PSS @ 5,000 cycles versus HWTT rut depth at 15,000 cycles.

7.4 Stiffness: Flexural Frequency Sweep versus Dynamic Modulus Frequency Sweep

Figure 7.48 through Figure 7.52 show the master curves from flexural frequency sweeps and AMPT compression frequency sweeps (dynamic modulus) for each of the five mixes. It can be seen that the dynamic modulus master curves are stiffer than the flexural stiffness curves for all the mixes. This is to be expected since

the dynamic modulus is measuring compressive stiffness with some contribution from shearing, while the flexural configuration is measuring a combination of tension and compression, and it would be expected that asphalt concrete will be stiffer in compression than in tension.

If dynamic modulus master curves are used instead of flexural curves, the results will generally produce reduced values of critical stresses and strains in mechanistic-empirical design calculations. This will require either development of shift factors for stiffness to use with current calibrated distress models, or recalibration of the models.

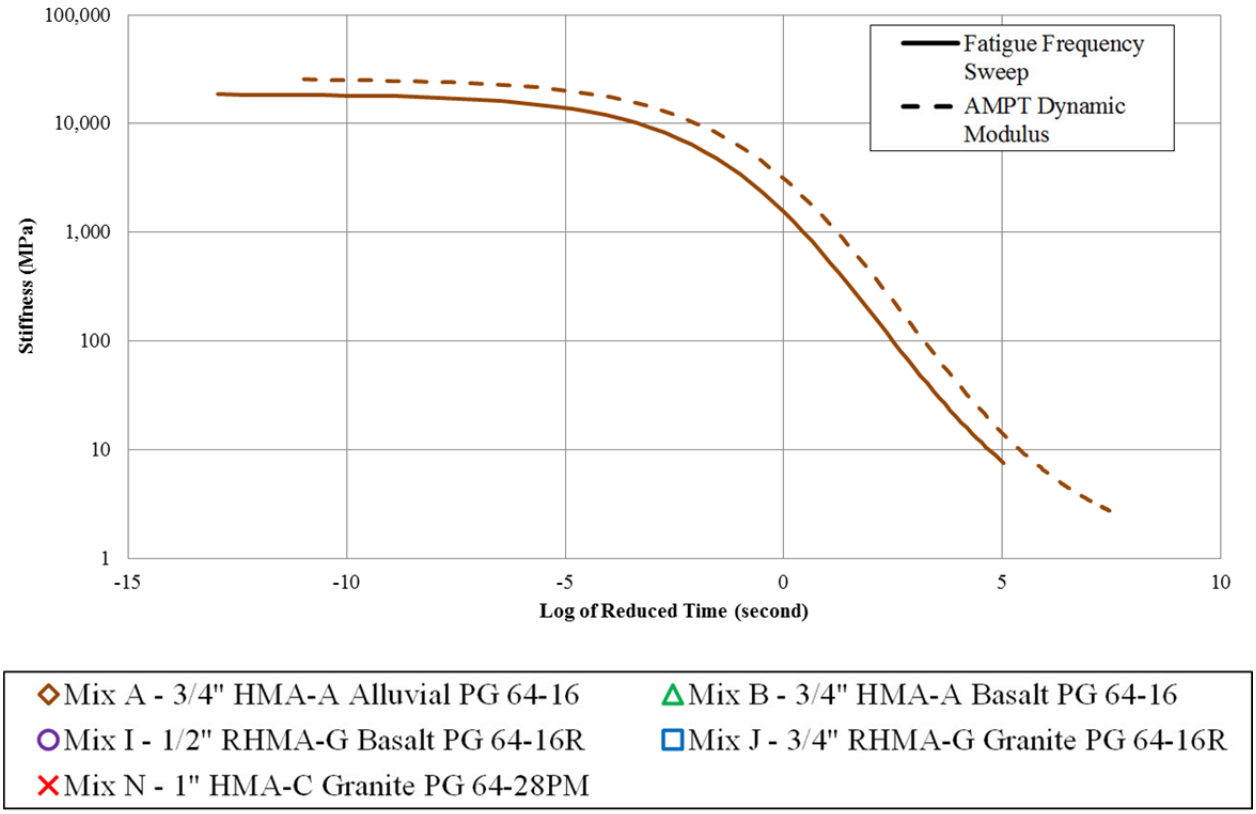

Figure 7.48: Comparison of flexural frequency sweep and AMPT dynamic modulus master curve, stiffness versus reduced time (log scale) for Mix A.

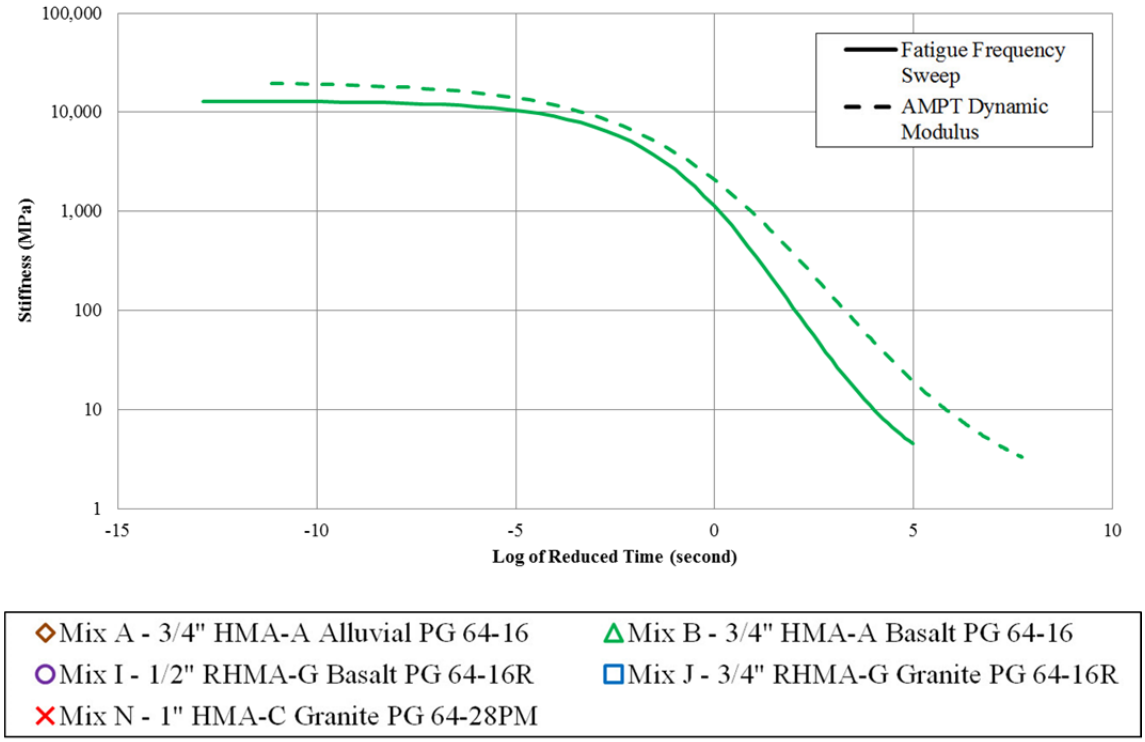

Figure 7.49: Comparison of flexural frequency sweep and AMPT dynamic modulus master curve, stiffness versus reduced time (log scale) for Mix B.

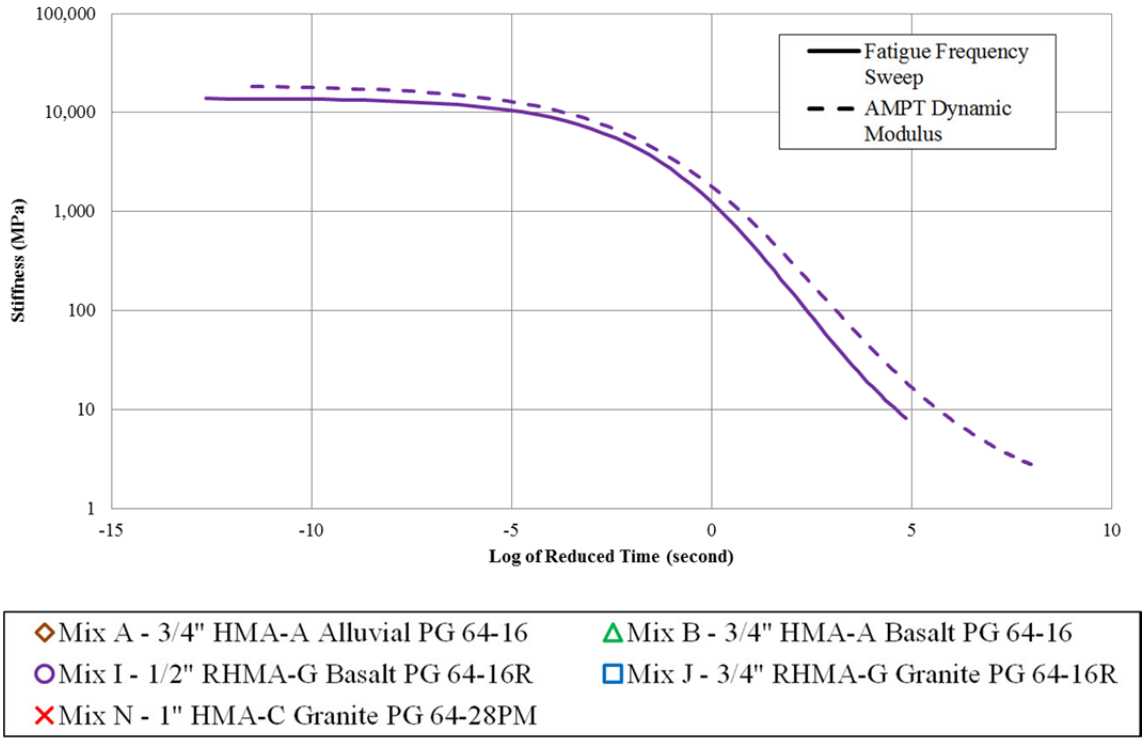

Figure 7.50: Comparison of flexural frequency sweep and AMPT dynamic modulus master curve, stiffness versus reduced time (log scale) for Mix I.

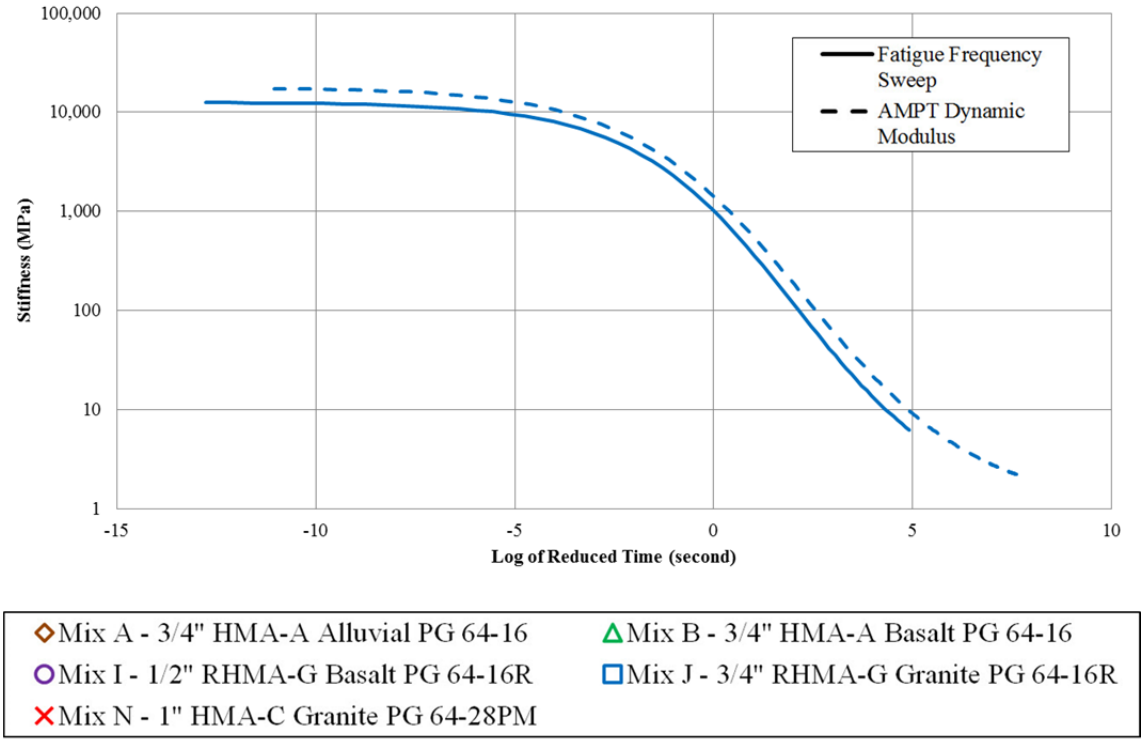

Figure 7.51: Comparison of flexural frequency sweep and AMPT dynamic modulus master curve, stiffness versus reduced time (log scale) for Mix J.

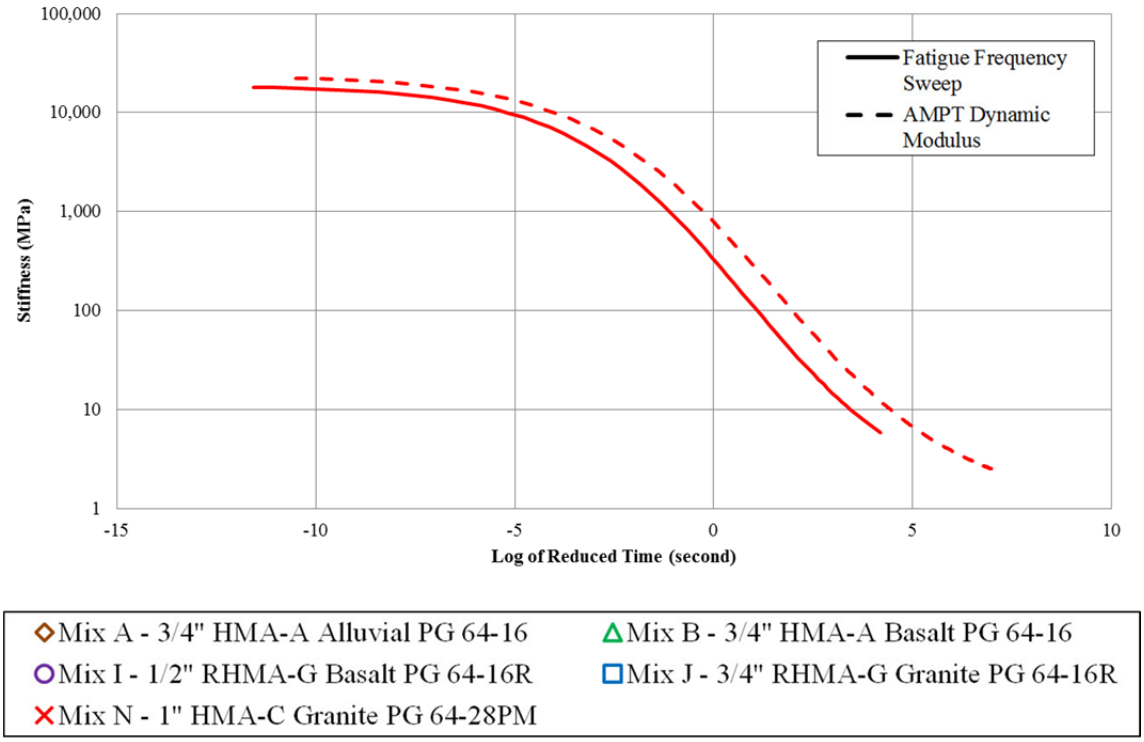

Figure 7.52: Comparison of flexural frequency sweep and AMPT dynamic modulus master curve, stiffness versus reduced time (log scale) for Mix N.

7.5 Moisture Sensitivity: HWTT versus IDT (Wet, TSR)

7.5.1 HWTT Rut Depth at 15,000 Cycles versus IDT Wet

Figure 7.53 shows the comparison between Hamburg rut depth at 15,000 cycles and IDT wet strength. It was expected that higher rut depth would correlate to lower wet strength. However, no clear trend is observed.

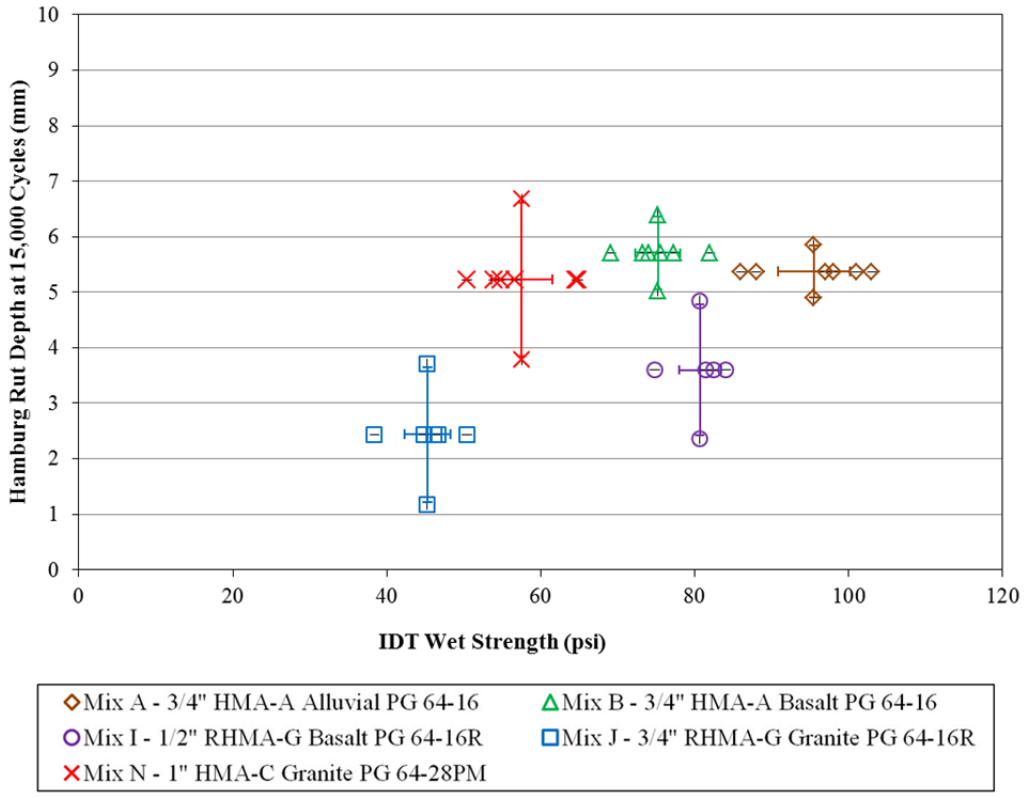

Figure 7.53: HWTT rut depth at 15,000 cycles versus IDT wet strength.

7.5.2 HWTT Rut Depth at 15,000 Cycles versus TSR

Figure 7.54 shows a plot of HWTT rut depth versus tensile strength ratio (TSR) for the five mixes tested. In each data set, the top and bottom markers are the two test data points for the HWTT rut depths for the right and left wheels. The middle marker indicates the TSR values (x-axis) and the average Hamburg rut depth (y-axis). Higher TSR values were observed for specimens with larger HWTT rut depths. This result was opposite to what was expected; materials that exhibit higher TSR values, meaning lower moisture sensitivity, should also show lower rutting performance in the HWTT.

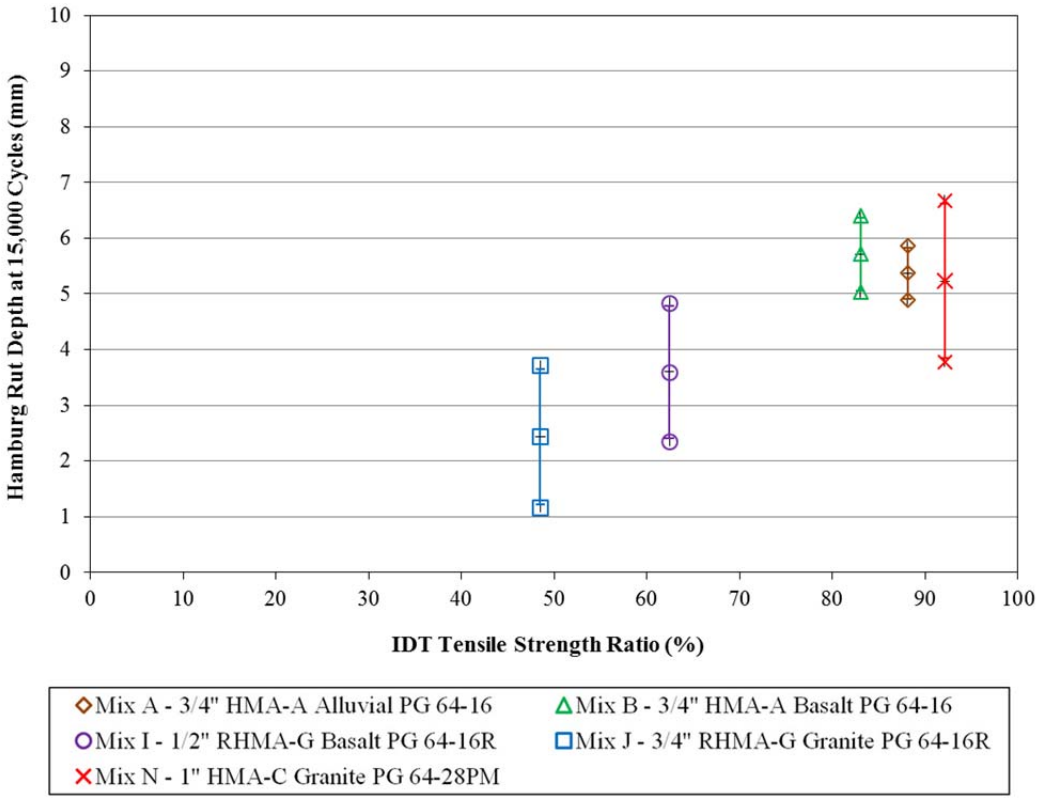

Figure 7.54: HWTT rut depth at 15,000 cycles versus IDT tensile strength ratio.

7.5.3 HWTT Creep Slope versus IDT Wet and HWTT Creep Slope versus TSR

Since none of the specimens showed a creep slope in the HWTT, these comparisons were not made.

7.6 Ranking Comparisons

Rankings of the five mixes for the different fatigue and fracture test parameters are shown in Table 7.6. The ranking of flexural fatigue life at 200 microstrain is used as the control. Nearly all of the tests show Mix A as the worst for fatigue, and all of tests show Mix N as the best. It can be seen that there is a small change in the rankings for the 400 microstrain flexural fatigue life. Of the SCB test parameters, fracture energy index matches the control results the best. The IDT dry strength does a poor job of ranking Mixes B and I.

Table 7.7 shows the rankings of the five mixes for the different rutting test parameters. The ranking of RSCH repetitions to 5 percent permanent shear strain is used as the control for comparison. It can be seen that the mix rankings change when moving from 45°C to 55°C for the control test. The RSCH permanent shear strain at 5,000 cycles (about one hour of testing) provides rankings that differ by one place for almost all cases compared to the control for all the mixes. Since none of the five mixes showed tertiary flow within 20,000 cycles for the

confined condition, which is needed to define the flow number, this parameter is most likely not practical for Caltrans mixes. For the unconfined stress state, the flow number ranking did a poor job for all but Mix J. The RLT results indicate that the confined and unconfined results differ considerably, in some cases changing from best to worst ranking for a given mix. In particular, the unconfined RLT test ranks Mix A the best consistently, while all other tests consistently rank it from middle to worst. The confined results seem to match the RSCH results the best. The HWTT results are somewhat difficult to interpret, as the test temperature falls between 45°C and 55°C, and the rankings differ for those two temperatures for the other tests.

The rankings for the five mixes for the moisture sensitivity tests are shown in Table 7.8. It can be seen that the TSR and the HWTT rut depth parameters rank the mixes differently, most importantly for Mix J, which is worst according to TSR value and best according to the HWTT. The other mixes differ by two places in the rankings. The IDT wet strength aligns rankings more closely with the TSR than with the HWTT, as might be expected.

7.7 Findings

It is difficult to draw strong conclusions regarding the correlation of different tests with only five mixes, however the following preliminary findings are based on the results presented in this chapter:

- There is a general but weak trend of increased fatigue life with lower secant stiffness measured using the semicircular beam (SCB) test, which is typical for most stiffness parameters and controlled-deformation fatigue life. Similarly there are weak trends between flexural fatigue life and fracture toughness and fracture energy index from the SCB test. However, the fracture toughness has a trend that is the opposite of what is expected, with higher fracture toughness corresponding to lower fatigue life. Based on these results, the fracture energy index appears to be the best of the SCB test parameters for relatively fast and low-cost comparison with flexural fatigue life.
- There is almost no correlation between flexural fatigue life and dry indirect tensile strength, except that the mix with the highest fatigue life has the lowest strength.
- Flexural fatigue and direct tension damage relations (loss of stiffness versus repetitions at 200 microstrain) show similar trends.
- None of the mixes tested demonstrated “tertiary flow” in the confined condition in the RLT, and it was difficult to clearly identify tertiary flow in many of the unconfined RLT tests, making use of the flow number difficult.
- Shift factors were developed for translating repeated load triaxial (RLT) confined and unconfined test results to repeated shear test at constant height (RSCH) results by considering the entire permanent deformation damage curve in each test.

  - The shift factors for 45°C and 55°C are about 30 percent different for both the confined and unconfined results, with the absolute values of the shift factors for different temperatures being much larger for the confined RLT results. The lack of consistency between temperatures may require different shift factors for different temperatures.
  - The results are promising for use of the shifted RLT and RSCH results for quality assurance. Additional data collection is recommended to further identify the errors caused by using shifted RLT results in mechanistic-empirical (ME) design models calibrated with the RSCH. The allowable difference for shifting RLT results to RSCH equivalents for use in ME design that would be considered acceptable has not been determined.
- The mixes tested did not show a "creep slope" in the Hamburg Wheel-Track Test. The HWTT and the RSCH present opposite trends for rutting for the mixes tested. This may indicate that the HWTT is more of a moisture sensitivity test than a rutting test, despite the lack of a creep slope.
- Stiffness master curves from dynamic modulus frequency sweeps run on the AMPT are generally stiffer than master curves from flexural frequency sweeps. This is to be expected since the the dynamic modulus test primarily measures the compressive modulus with some shearing, while the flexural test measures a mix of tensile and compressive moduli in the beam, and asphalt should be stiffer in compression than tension.
- If dynamic modulus master curves are used instead of flexural curves for ME design calculations, models will need to be recalibrated or shift factors will need to be developed.
- No clear trend was observed between HWTT rut depth and wet indirect tensile strength, and the HWTT showed an opposite trend compared with the tensile strength ratio.

Table 7.6: Ranking of Five Mixes for Different Tests for Fatigue Performance Relative to Flexural Fatigue Life at 200 Microstrain

Higher rank (1) represents better fatigue life performance									
Mix Name	**Mix Type**	**Flexural Fatigue Life 200με**	**Flexural Fatigue Life 400με**	**SCB Secant Stiffness**	**SCB Fracture Energy**	**SCB Fracture Energy Index**	**SCB Fracture Toughness**	**IDT Dry Strength**	**AMPT DT Stiffness Reduction**
Mix A	3/4" HMA-A Alluvial PG 64-16	5	5	5	5	5	5	4	Mix A has the worst performance. Results for other mixes are similar.
Mix B	3/4" HMA-A Basalt PG 64-16	4	4	2	2	3	3	2	
Mix I	1/2" RHMA-G Basalt PG 64-16R	3	2	4	3	4	4	5	
Mix J	1/2" RHMA-G Granite PG 64-16R	2	3	3	4	2	2	3	
Mix N	1" HMA-C Granite PG 64-28PM	1	1	1	1	1	1	1	

Table 7.7: Ranking of Five Mixes for Different Tests for Rutting Performance Relative to RSCH Permanent Shear Strain at 5,000Cycles

Higher rank (1) represents better rutting performance												
Mix Name	**Mix Type**	**RSCH* Cycles to 5% Permanent Shear Strain**	**RSCH* Cycles to 5% Permanent Shear Strain**	**RSCH* Permanent Shear Strain at 5,000 Cycles**	**RSCH* Permanent Shear Strain at 5,000 Cycles**	**AMPT Confined Flow Number**	**AMPT Unconfined Flow Number**	**AMPT RLT** Permanent Axial Strain at 10,000/ 50 Cycles**		**AMPT RLT** Cycles to 2% Permanent Axial Strain**		**HWTT Rut Depth at 15,000 Cycles**
		45°C	**55°C**	**45°C**	**55°C**			**45°C**	**55°C**	**45°C**	**55°C**	
Mix A	3/4" HMA-A Alluvial PG 64-16	5	5	5	5	No tertiary flow within 20,000 cycles	2	3/1	5/1	3/1	5/1	4
Mix B	3/4" HMA-A Basalt PG 64-16	1	1	1	1		3	2/2	4/2	3/2	4/1	5
Mix I	1/2" RHMA-G Basalt PG 64-16R	2	4	2	4		1	1/3	2/3	1/3	2/3	2
Mix J	1/2" RHMA-G Granite PG 64-16R	4	3	4	3		4	5/4	1/4	5/4	1/4	1
Mix N	1" HMA-C Granite PG 64-28PM	3	2	3	2		5	4/5	3/5	2/5	3/5	3

Notes: *70 kPa shear stress; ** confined/unconfined

Table 7.8: Ranking of Five Mixes for Different Tests for Fatigue Performance Relative to Flexural Fatigue Life at 200 Microstrain (*Note:* values for cycles to a given shear or axial strain include extrapolations)

		Higher rank (1) represents better moisture damage performance		
Mix Name	**Mix Type**	**IDT TSR**	**IDT Wet Strength**	**HWTT Rut Depth at 15,000 Cycles**
Mix A	3/4" HMA-A Alluvial PG 64-16	2	1	4
Mix B	3/4" HMA-A Basalt PG 64-16	3	3	5
Mix I	1/2" RHMA-G Basalt PG 64-16R	4	2	2
Mix J	1/2" RHMA-G Granite PG 64-16R	5	5	1
Mix N	1" HMA-C Granite PG 64-28PM	1	4	3

(page blank)

8 COMPARISON OF PRACTICAL CONSIDERATIONS FOR PERFORMANCE-RELATED TESTS

The flexural fatigue and stiffness tests and the repeated shear at constant height (RSCH) test pose practical difficulties for use in construction quality assurance but there are new alternatives to these tests for use in materials characterization for mechanistic-empirical design. The AMPT was developed in response to the need for performance-related tests in Superpave. The tests that the AMPT can perform for stiffness frequency sweeps, fatigue, and permanent deformation were described in Chapter 2 and compared with the flexural beam tests and the RSCH in other chapters in this report. Table 8.1 through Table 8.3 compare the practical issues between the AMPT and the flexural beam and RSCH tests in terms of test preparation, test duration, variability, and other practical considerations. Table 8.4 presents the productivity and difficulty concerns associated with each test identified by direct comparison by UCPRC during this study.

Other differences are that the AMPT specimens must be made using Superpave gyratory compaction while it is recommended that the flexural and RSCH specimens be made with rolling-wheel compaction. Although gyratory-compacted specimens can be used for RSCH testing, they cannot be used for flexural testing. It is very difficult to obtain AMPT test specimens from the pavement in the field, and it is impossible if the material thickness of cores taken vertically is less than than 6 inches (150 mm) or less than 4 inches (100 mm) if slabs are cut and then cored sideways. Flexural and RSCH specimens can be cut or cored in the field, respectively, as long as the material thickness is at least 2 inches (50 mm). AMPT specimens must be cored from a larger compacted specimen and then cut to height. Flexural specimens must be cut to the final dimensions, and RSCH specimens require both coring and being cut to height.

It was found that the unconfined RLT test is much faster and easier to perform than the RSCH test or the confined RLT test. The confined RLT ranking for permanent axial strain for the five mixes tested in this study at 45°C and 55°C was the same. The unconfined RLT test did a good job of ranking for some mixes, but did poorly for Mix A compared to rankings by the RSCH using a 70 kPA shear stress. The RLT rankings do a better job of matching the RSCH results performed using a 100 kPa shear stress. This indicates that the unconfined RLT test may be a viable construction quality assurance test, although a larger number of mixes needs to be tested to confirm this weak preliminary finding.

Table 8.1: Comparison of Practical Issues between AMPT RLT and RSCH

Test	Pre-Test Preparation	Test Duration	Test Variability	Difficulty	Extra Cost
AMPT RLT	~2 hours to condition the equipment and specimen to the target temperature.	5.5 hours to reach 20,000 cycles; confined test has large range of time to reach failure permanent strain; unconfined test generally fails within 0.5 hours.	Unconfined tests show low variability; high variability with confined test.	Easy. The test setup procedure does not require much expertise.	Latex membrane (sleeve-shaped for confined test and small circular ones used as friction reducer)– expensive
RSCH	~2 hours to condition the equipment and specimen to the target temperature.	6 hours to reach 30,000 cycles; large range of time to reach failure permanent strain.	High variability with typical specimen size (6 in. diameter); much less with larger specimens.	Moderate. The testing requires training and experience to know how to run software and install specimen and LVDTs.	Expensive epoxy: $70/can, can be used for three tests.

Table 8.2: Comparison of Practical Issues between AMPT DM and Flexural Frequency Sweep

Test	Pre-Test Preparation	Test Duration	Test Variability	Difficulty	Extra Cost
AMPT DM	1. Mount strain gauge points onto the sample. 2. Takes a very long time to condition specimen at low temperature.	Fast. ~35 minutes for a complete frequency sequence on one specimen at one temperature.	Not able to assess with only two replicates.	Moderate. Need to mount strain gauge points and adjust the LVDTs.	1. Regular epoxy: $7 for 10 samples. 2. Latex membrane (sleeve-shaped for confined test and small circular ones used as friction reducer)– expensive.
Flexural Frequency Sweep	1. Mount target to beam. 2. Condition specimen for 2–3 hours minimum.	Fast. ~35 minutes for a complete frequency sequence on one specimen at one temperature.	Moderate	Moderate. Must ensure specimen is properly aligned and clamped.	Regular epoxy: $7 for numerous specimens.

Table 8.3: Comparison of Practical Issues between AMPT DT and Flexural Fatigue

Test	Pre-Test Preparation	Test Duration	Test Variability	Difficulty	Extra Cost
AMPT DT	1. Mounting strain gauge points onto the sample; 2. Glue two ends of the sample to the platens. 3. Wait for several hours until the steel putty is fully set.	Up to 7 days, depends on what the termination condition is. 1,000,000 repetititions in 28 hours.	Not able to assess with only two replicates.	Hard. Need to mount strain gauge points and glue the sample to the platens. Also it takes some time to detach the sample from the fixture and do the clean-up.	Expensive epoxy: $70/can, can be used for two tests.
Flexural Beam Fatigue	1. Mount target to beam. 2. Condition specimen for 2 - 3 hours minimum.	Up to 7 days, depends on what the termination condition is. 1,000,000 repetititions in 28 hours	Higher variability for lower strain levels.	Moderate. Must ensure specimen is properly aligned and clamped.	Minimal

Table 8.4: Summary of Productivity and Testing Concerns for All Tests

Test	Specimen Size (nominal)	Specimen Weight (g) Approx.	Production Days / No. of Specimens Required	Test Length per Specimen	Test Variability	Difficulty	Test Problems and Cautions
T 321 Beam Fatigue	381 mm length, 50.8 mm height, 63.5 mm width	2,850	Up to 4 to 7 days for 6 fatigue beams	Several hours up to 6 days	Low	Moderate	May need operator's manual adjustments on gain settings to achieve accurate sinusoidal LVDT displacement wave form.
T 321 Beam Fatigue Frequency Sweep	381 mm length, 50.8 mm height, 63.5 mm width	2,850	Up to 4 to 7 days for 6 fatigue beams	0.5 hours	Moderate	Moderate	Machine may not be able to control wave forms at high frequencies.
T 320 Shear RSCH	150 mm diameter, 50 mm height	2,050	Up to 5 to 10 days for 18 shear cores	Up to 6 hours	High	Moderate	(1) May need operator's manual adjustments to achieve accurate shear wave form. (2) Axial loading may not be maintained at best desired level with LVDT control during test.
AMPT Repeated Load Triaxial Confined	100 mm diameter, 150 mm height	2,730	Up to 4 to 6 days for 6 AMPT cores	Up to 6 hours	High	Easy	Do not place ball bearing on the top loading platen to ensure there is no rotation during the test.
AMPT Repeated Load Triaxial Unconfined	100 mm diameter, 150 mm height	2,730	Up to 4 hours for 6 AMPT cores	Up to 2 hours	Low	Easy	Do not place ball bearing on the top loading platen to ensure there is no rotation during the test.
AMPT Dynamic Modulus Frequency Sweep	100 mm diameter, 150 mm height	2,730	Up to 4 to 6 days for 2 AMPT cores	0.5 hours	Low to moderate	Moderate	(1) Place ball bearing on the top loading platen to ensure it is free to rotate during the test. (2) Adjust LVDT to zero position before the test starts.
AMPT Fatigue	100 mm diameter, 130 mm height	2,365	Up to 4 to 6 days for 2 AMPT cores	Up to 6 hours	High	Hard	A possible cause of unsuccessful test or bad data may be an alignment issue. Extra attention may need to be paid to ensure that the platens and the core are in perfect parallel positions during glueing.
T 324 Hamburg Wheel-Tracking Test	150 mm diameter, 63.5 mm height	2,600	Up to 3 to 4 days for 4 Hamburg cores	Up to 6 hours	Moderate to high	Easy	(1) Specimen pairs need to be cut to fit in the molds tightly. (2) Specimen surfaces should be flat against the surfaces of the molds.
T 283 TSR	100 mm diameter, 63.5 mm height	1,150	Up to 4 to 5 days for 12 TSR cores	Up to 3 days	High	Moderate	(1) Somewhat difficult to control and precisely measure specimen saturation. (2) Wet set of specimens may deform in high temperature water bath. (3) Indirect tension loading test depends highly on specimen orientation.
SCB	100 mm diameter, 63.5 mm height	1,150	3 to 4 days/ 6 SCB cores	Up to 1 hour	Moderate to high	Moderate	If half-specimens are not cut perfectly equal, test variability may increase.

9 CONCLUSIONS AND RECOMMENDATIONS

This study addressed a number of questions about performance-related laboratory testing related to the Superpave mix design process. This chapter presents summary answers to those questions presented as conclusions and recommendations based on the findings presented in each chapter.

9.1 Conclusions Regarding Questions to be Answered by the Study

1. *Question:* How is HMA shear test performance, which is related to rutting, affected by changing from Hveem mix design to Superpave mix design for the mixes tested?
   Conclusion: Overall, the Hveem mixes had higher rutting resistance based on their shear test performance. The RSCH results for the four mixes tested with both the Superpave and Hveem designs (A, B, J, and N) showed that the Hveem designs had significantly higher performance in terms of repetitions to 5 percent permanent shear strain for three of the mixes (greater than a factor of 1,000 at 45°C and a factor of 10 at 55°C) and a factor of 2 to 5 for the fourth mix at these same temperatures.

2. *Question:* How are the HMA flexural fatigue test and flexural stiffness performance, which are related to cracking, affected by changing from Hveem mix design to Superpave mix design for the mixes tested?
   Conclusion: In flexural fatigue, the Superpave mixes outperformed the Hveem mixes for the three mixes compared (A, B, and I), typically by a factor of 3 to 5 for Mixes A and B in terms of repetitions to 50 percent loss of stiffness. The Superpave mixes had higher binder contents than the Hveem mixes for Mixes A and B. For Mix I, performance of the Hveem and Superpave mixes varied, depending on the testing strain level. Flexural frequency sweep results indicated that the stiffness master curves were similar for the three mixes tested.

3. *Question:* How do any changes in shear, flexural fatigue, and flexural stiffness test performance in changing from Hveem to Superpave mix designs for the same mixes affect expected pavement rutting and cracking performance as evaluated using the *CalME* mechanistic-empirical analysis procedures?
   Conclusion: The hypothesis that Superpave mix designs would generally have better fatigue performance and worse rutting performance than the Hveem mix designs because of their often higher binder contents was generally proved true by the results of mechanistic simulation of performance for a range of structures, climate regions, and traffic. However, simulations also showed that most of the Superpave mixes were predicted to have satisfactory rutting performance even with the higher binder contents. Preliminary analysis performed to estimate the net effects on total asphalt binder used in an asphalt design indicated that the total binder content required to obtain the same performance could be

less for the Superpave mixes than for the Hveem mixes. Net change in binder content was evaluated since the total binder used in a treatment design is a major driver of both cost and environmental emissions. The net reduction in asphalt binder found for the mix evaluated (Mix A) was the result of increased binder content in the mix for the Superpave mix, offset by the decreased asphalt thickness required to obtain the required cracking performance. In addition, trucking and aggregate costs would be less because of the reduced thickness required to obtain the same cracking performance. These results indicate that the Superpave mixes could provide reduced costs for the same performance, provided that the rutting performance is satisfactory.

Recommendation: Continue with implementation of the Superpave mix design process, with further calibration and potential use of performance-related quality assurance testing with the unconfined RLT test for rutting.

4. *Question:* Can faster and less expensive tests than the shear and flexural fatigue tests be successfully used as surrogates for currently used mechanistic performance-related tests for mix design and quality assurance?

   Conclusions: With regard to rutting performance:

   - Similar trends were found between the RSCH and both the confined and unconfined RLT tests for the development of permanent deformation versus repetitions. In terms of ranking the mixes, the confined RLT testing generally ranked the mixes in approximately the same order as the RSCH (70 kPa shear stress) at both 45°C and 55°C, while the unconfined RLT testing also generally had similar rankings as the RSCH except for Mix A. The unconfined RLT did a better job of ranking Mix A compared with the RSCH at 100 kPa than it did for the 70 kPa RSCH results.
   - The unconfined RLT test has speed and difficulty advantages over the RSCH and the confined RLT for mix design and quality assurance, which indicates that it is a potential candidate as a rutting test for mix design and quality assurance, particularly when performed at 45°C as opposed to 55°C.
   - An opposite correlation was observed between the RSCH test and the HWTT for rutting performance, which indicates that the HWTT is not an appropriate alternative for mix design and quality assurance as a rutting test.

   Regarding fatigue performance evaluation for mix design and quality assurance:

   - No trend was found between the dry IDT results and flexural fatigue life.

- Opposing trends were found between fatigue life and many of the SCB tests; however, the SCB test with fracture energy index as the parameter showed some correlation with flexural fatigue life and may prove useful as a quality assurance test.
- There is a strong correlation between fatigue performance in the flexural and direct tension (DT) tests, with the primary difference being faster damage during the first 100 repetitions of the direct tension tests.

Regarding moisture sensitivity, none of the HWTT tests on the five mixes showed evidence of a "creep slope," which is taken from a change in the slope of rutting versus load repetitions and is generally interpreted as indicating where extensive moisture damage is occurring in the mix. No clear trend was observed between HWTT rut depth and wet indirect tensile strength, and HWTT rut depth development showed an opposite trend compared with the tensile strength ratio. This indicates that additional calibration of moisture damage tests against field performance is needed. A previous initial calibration of the HWTT against field performance, on field samples as opposed to the laboratory specimens used in this study, indicated that "the [HWTT] procedure can correctly identify the effect of antistripping additives, but may underestimate the performance of mixes containing soft binders at the fixed test temperature 50°C. The correlation between test results and field performance seems acceptable except that the test procedure may fail mixes that perform well in the field and, in a very few cases, give false positive results."*(34)*

Recommendations:

- Consider use of the unconfined RLT test for mix design and quality assurance for rutting; collect additional comparison data between this test and the RSCH. If consistent shift factors can be found to convert from the RLT to the RSCH then no recalibration of the *CalME* models will be needed if a switch is made to using the RLT for mix characterization.
- Perform additional testing and comparison of the SCB fracture energy index with flexural fatigue life for use as a mix design and quality assurance test.
- Continue with current use of the HWTT as a moisture damage test; consider additional calibration against field performance.

5. *Question:* Can the Asphalt Mixture Performance Tester's (AMPT) tests for rutting, fatigue, and stiffness be used for ME pavement designs in place of shear, flexural fatigue, and flexural stiffness tests, including transformation of data from one test to another?

   Conclusions: For the characterization of rutting performance for ME design, the RLT test performed using the AMPT equipment has potential as a substitute for the RSCH test. Results from this study

indicate that shift factors may be developed for use in ME design to convert both confined and unconfined RLT results to similar RSCH results for use in existing models calibrated against RSCH results. However, it appears that different shift factors may be needed for specific test temperatures for both the confined and unconfined tests, with shift factors for the unconfined test being somewhat less sensitive to temperature than those for the confined test. There is on the order of 30 percent variability in the shift factors at a given temperature across the five mixes tested. The RSCH and RLT results are both sensitive to compaction method (gyratory-, field-, or rolling-wheel compaction). The models in *CalME* were calibrated with RSCH results primarily using field cores. The initial shift factors in this report are based on correlating RSCH results for rolling-wheel cores with RLT results for gyratory cores. The sensitivity of designs to errors in the shifting requires additional test results and further analysis to determine whether it is acceptable for the use of shifted RLT results with existing models calibrated with RSCH results.

For the characterization of fatigue and stiffness performance for ME design, the respective AMPT tests (direct tension and dynamic modulus) can provide similar data, but they do not appear to offer any advantages in terms of productivity or difficulty. The only advantage is that the AMPT specimens can be produced from gyratory specimens. Shift factors would need to be developed for changing the stiffness test from flexural frequency sweep to dynamic modulus frequency sweep because the master curves from dynamic modulus frequency sweeps are consistently stiffer than master curves from flexural frequency sweeps across all five mixes tested in this study.
Recommendations: See summary recommendation after Question 6.

6. *Question:* What are the practical issues such as test duration, specimen preparation, test variability, and test difficulty for the AMPT?
   Conclusions: The results from the LVDT in the actuator of the AMPT produce similar average results compared with the LVDTs mounted on the middle half of the specimen itself, and use of the actuator LVDT speeds up and simplifies the testing. For rutting, the unconfined RLT test is faster and easier to perform than the RSCH or the confined RLT test. The confined RLT and RSCH tests have similar productivity and difficulty. Variability for the unconfined RLT is less than that of the confined RLT and RSCH because the unconfined RLT results in fewer repetitions to failure at a given temperature than the other two tests, and the variability of repeated load tests typically increases as the number of repetitions to failure increases.

For fatigue, the DT test is likely to be more expensive and more difficult, and to take the same amount of time as the flexural fatigue test.

For stiffness master curves, the cost of the dynamic modulus frequency sweep test is likely to be similar to that of the flexural frequency sweep test, the difficulty is likely to be similar, and the time required to complete a frequency sweep is also likely to be similar. Using the dynamic modulus results will require expensive recalibration of current *CalME* mechanistic-empirical models.

Recommendations:

- Improve shift factors by additional comparison testing of RSCH and confined and unconfined RLT on same materials and, if results remain promising, then move to the next recommendation; continue comparisons using field (preferable) or rolling wheel-compacted (if field cores are unavailable) RSCH specimens and gyratory-compacted RLT specimens.
- Once more mixes have been tested, perform sensitivity analysis for *CalME* results for differences between mix by mix versus average shift factors; if results are acceptable, consider use of RLT for development of rutting parameters for ME design along with other factors that will influence risks to successful deployment.

REFERENCES

1. Frye, C. 2002. Superpave Comes of Age. Public Roads, Sept/Oct 2002, Vol. 66, No. 2. *www.fhwa.dot.gov/publications/publicroads/02sep/10.cfm* (Accessed January 26, 2015).
2. Sebaaly, P., W. McNamara, and J. Epps. 2000. Evaluation of Rutting Resistance of Superpave and Hveem Mixtures, Volume II: Impact of Aggregate Gradations. Research Report 1393-3. University of Nevada, Reno for the Nevada Department of Transportation. *www.wrsc.unr.edu/evaluationRutting SPHVVolume2.pdf.* (Accessed September 22, 2014)
3. Sousa, J. B., J. C. Pais, M. Prates, R. Barros, P. Langlois, and A.-M. Leclerc. 1998. "Effect of Aggregate Gradation on Fatigue Life of Asphalt Concrete Mixes," Transportation Research Record No. 1630. Transportation Research Board, National Research Council, Washington, DC; pp. 62–68.
4. Hand, A. J., and A. L. Epps. 2001. "Impact of Gradation Relative to Superpave Restricted Zone on Hot-Mix Asphalt Performance," Transportation Research Record No. 1767. Transportation Research Board, National Research Council, Washington, DC; pp. 158–166.
5. Kandahl, P., and L. Cooley. 2001. The Restricted Zone in the Superpave Aggregate Gradation Specification. National Cooperative Highway Research Report 464. Transportation Research Board, National Academy of Science, Washington, DC.
6. Ullidtz, P., J.T. Harvey, B.W. Tsai, and C.L. Monismith. 2006. Calibration of Incremental-Recursive Flexible Damage Models in *CalME* Using HVS Experiments. Report Prepared for the California Department of Transportation (Caltrans) Division of Research and Innovation by the University of California Pavement Research Center, Davis and Berkeley. UCPRC-RR-2005-06.
7. Ullidtz, P., J. Harvey, B.-W. Tsai, and C. L. Monismith. November 2006. Calibration of CalME Models Using WesTrack Performance Data. Report prepared for Caltrans Division of Research and Innovation and Caltrans District 8 by the University of California Pavement Research Center, Davis and Berkeley. UCPRC-RR-2006-14. *www.ucprc.ucdavis.edu/PDF/WesTrack%20CalME%20Calib_UCPRC-RR-2006-14_final.pdf.* (Accessed September 22, 2014)
8. Wu, R. 2008. Calibration of the CalME Rutting Model Using 2000 NCAT Data. UCPRC-TM-2008-04.
9. Tsai, B. W., and R. Wu. 2008. Mn/ROAD Case Study Using CalBack and CalME. UCPRC-TM-2008-16.
10. Harvey, J. T., I. Guada, and F. Long. 2000. Effects of Material Properties, Specimen Geometry, and Specimen Preparation Variables on Asphalt Concrete Tests for Rutting. Journal of the Association of Asphalt Paving Technologists, Vol. 69.
11. Witczak, M. W., K. Kaloush, T. Pellinen, M. El-Basyouny, and H. V. Quintus. 2000. Simple Performance Test for Superpave Mix Design. NCHRP Report 465. Transportation Research Board, Washington, D.C.

12. Bonaquist, R. F., D. W. Christensen, and W. Stump, III. 2003. Simple Performance Tester for Superpave Mix Design: First-Article Development and Evaluation. NCHRP Report 513. Transportation Research Board, Washington, D.C.
13. Von Quintus, H. L., J. Mallela, R. Bonaquist, C. W. Schwartz, and R. L. Carvalho. 2012. Calibration of Rutting Models for Structural and Mix Design. NCHRP Report 719. Transportation Research Board, Washington, D.C.
14. Monismith, C., and F. Long. 1999. Overlay Design for Cracked and Seated Portland Cement Concrete (PCC) Pavement—Interstate Route 710. Technical Memorandum: UCPRC-TM-1999-03.
15. UCPRC. 1999. Mix Design and Analysis and Structural Section Design for Full Depth Pavement for Interstate Route 710. Technical Memorandum: UCPRC-TM-1999-02.
16. Tsai, B.-W., J. Signore, and C. L. Monismith. 2103 (in progress). Development of Hot Mix Asphalt Pavement Performance Properties for Long Life Pavement Design: Caltrans District 2, Interstate 5, Red Bluff, California. UCPRC-TM-2014-03. Pavement Research Center and Institute of Transportation. Davis and Berkeley: University of California.
17. Signore, J., B.-W. Tsai, and C.L. Monismith. 2014 (in progress). Development of Hot- Mix Asphalt Pavement Performance Properties for Long- Life Pavement Design: Caltrans District 2, Interstate 5, Weed, California. UCPRC-TM-2014-04. Prepared for Caltrans Division of Research, Innovation, and Systems Information.
18. Signore, J., and C. Monismith. 2014 (in progress). Development of Hot-Mix Asphalt Pavement Performance Properties for Long-Life Pavement Design: Caltrans District 4, Interstate 80 Solano County, California. UCPRC-TM-2014-05. Prepared for Caltrans Division of Research, Innovation, and Systems Information.
19. Zhou, J, J. M. Signore, and J. T. Harvey. Superpave Implementation Phase I: Determining Optimum Binder Content. UCPRC-TM-2012-03. Prepared for Caltrans Division of Research, Innovation, and Systems Information. 2013. *www.ucprc.ucdavis.edu/PDF/UCPRC-TM-2012-03.pdf.*
20. Caltrans—Sample Preparation and Testing for Long-Life Hot Mix Asphalt Pavements (LLP-AC2). California Department of Transportation, Sacramento, CA. *www.dot.ca.gov/hq/esc/ Translab/ormt/pdf/LLP-AC2_Sample_Preparation_for_LL_HMA-Pavement.pdf* (Accessed January 15, 2015).
21. Tsai, B. W., R. Wu, J. Harvey, and C. Monismith. 2012. Development of fatigue performance specificiation and its relation to mechanistic-empirical pavement design using four-point bending beam test results. Four Point Bending, CRC Press, Taylor & Francis Group, London, UK.
22. Wagoner, M., W. Buttlar, G. Paulino, and P. Blankenship. 2005. Investigation of the Fracture Resistance of Hot-Mix Asphalt Concrete Using a Disk-Shaped Compact Tension Test. Transportation Research Record:

Journal of the Transportation Research Board, No. 1929, Transportation Research Board of the National Academies, Washington, D.C., pp. 183–192.

23. Li, X., and M. Marasteanu. 2004. Evaluation of the Low Temperature Fracture Resistance of Asphalt Mixtures Using the Semi-Circular Bend Test. Journal of the Association of Asphalt Paving Technologists, Vol. 74, pp. 401–426.
24. Walubita, L., A. Alvarez, and F. Sanchez. 2012. Using Fracture Energy to Characterize the Hot Mix Asphalt Cracking Resistance Based on the Direct Tensile Test. Revista Facultad de Ingeniería Universidad de Antioquia, Colombia, No. 64, pp. 126-137. *www.redalyc.org/pdf/430/43025083011.pdf* (Accessed January 5, 2015)
25. Federal Highway Administration Expert Task Group. 2014. Determining the Fracture Energy of Asphalt Mixtures Using the Semi Circular Bend Geometry (SCB). Proposed Test Method. *onlinepubs.trb.org/onlinepubs/nchrp/docs/NCHRP09-46_ProposedSemicircularBendMethodOfTest.pdf* (Accessed September 12, 2014)
26. Asphalt Institute. 2001. SP-2 Superpave Mix Design.
27. Sousa, J. B., et al. 1994. "Permanent Deformation Response of Asphalt-Aggregate Mixes," SHRP-A-415. Strategic Highway Research Program, Transportation Research Board, National Academy of Science, Washington, D.C.
28. Deacon, J.A., J.T. Harvey, I. Guada, L. Popescu, and C.L. Monismith. 2002. Analytically Based Approach to Rutting Prediction. In Transportation Research Record: Journal of the Transportation Research Board, No.1806. Transportation Research Board of the National Academies, Washington, D.C.
29. ARA Inc. 2004. Guide for Mechanistic-Empirical Design of New and Rehabilitated Pavement Structures, ERES Consultants Division, ARA Inc., National Cooperative Highway Research Program, Transportation Research Board, National Research Council.
30. Wu, R., and Harvey, J. Calibration of Asphalt Concrete Cracking Models for California Mechanistic-Empirical Design (CalME). 7th International Conference on Cracking in Pavements, RILEM. pp 537-547, 201.
31. Wu, R. 2005. Finite Element Analyses of Reflective Cracking in Asphalt Concrete Overlays, Doctoral thesis, University of California, Berkeley.
32. Harvey, J. T., S. Weissman, F. Long, and C. L. Monismith. 2001. Tests to Evaluate the Stiffness and Permanent Deformation Characteristics of Asphalt/Binder Aggregate Mixes, and Their Use in Mix Design and Analysis. Journal of the Association of Asphalt Paving Technologists, Vol. 70, pp. 572-604.
33. Gibson, N., S. Li, and M. E. Kutay. 2001. Rutting Resistance of Laboratory-Prepared and Field-Compacted Asphalt Mixtures. Transportation Research Record, No. 2181, pp. 109-116.

34. Lu, Q., and J. Harvey. 2005. Investigation of Conditions for Moisture Damage in Asphalt Concrete and Appropriate Laboratory Test Methods. UCPRC-RR-2005-15. Prepared for Caltrans Division of Research, Innovation, and Systems Information. *www.ucprc.ucdavis.edu/PDF/UCPRC-RR-2005-15.pdf.* (Accessed December 14, 2014)

APPENDIX A: FLEXURAL FATIGUE RESULTS

A.1 Superpave Mix Design Data

Table A.1: Flexural Fatigue Test Results for Mix A

Mix	Binder Type/ Grade	Aggregate Type	NMAS	Specimen Designation	AV (%)	AC (%)	Test Strain Level	Initial Phase Angle (Deg.)	Initial Stiffness (Mpa)	Fatigue Life Nf	Int or Ext
A	PG64-16	Alluvial	3/4	4-B#5	6.1	5.5	0.000203	24.14	6529	12,265,860	Ext
				4-B#6	6.1	5.5	0.000199	23.51	6594	7,220,855	Ext
				6-B#6	6.1	5.5	0.000205	30.00	4733	2,175,215	Int
				4-B#3	6.0	5.5	0.000376	21.21	6357	171,147	Int
				4-B#4	6.0	5.5	0.000400	24.39	5737	194,024	Int
				4-B#7	6.3	5.5	0.000413	26.18	5496	36,596	Int

Table A.2: Flexural Fatigue Test Results for Mix B

Mix	Binder Type/ Grade	Aggregate Type	NMAS	Specimen Designation	AV (%)	AC (%)	Test Strain Level	Initial Phase Angle (Deg.)	Initial Stiffness (Mpa)	Fatigue Life Nf	Int or Ext
B	PG64-16	Basalt	3/4	3b8	5.5	6.3	0.000202	26.44	4133	36,632,820	Ext
				4b3	6.3	6.3	0.000202	32.92	3700	8,706,860	Ext
				4b7	6.5	6.3	0.000203	31.82	3704	6,015,149	Ext
				4b2	6.3	6.3	0.000407	31.61	3453	331,945	Ext
				4b6	6.1	6.3	0.000414	32.83	3527	212,253	Ext
				5b5	6.4	6.3	0.000397	26.58	4219	135,236	Ext

Table A.3: Flexural Fatigue Test Results for Mix I

Mix	Binder Type/ Grade	Aggregate Type	NMAS	Specimen Designation	AV (%)	AC (%)	Test Strain Level	Initial Phase Angle (Deg.)	Initial Stiffness (Mpa)	Fatigue Life Nf	Int or Ext
I	PG64-16 RB	Basalt	1/2	3b6	6.4	8.3	0.000202	28.40	3304	114,897,694	Ext
				7b8	5.5	8.3	0.000202	25.52	4283	23,514,509	Ext
				8b7	5.7	8.3	0.000188	21.79	4412	38,785,270	Ext
				3b4	5.8	8.3	0.000400	29.08	3228	3,981,080	Int
				6b6	5.9	8.3	0.000383	23.81	3829	1,866,897	Int
				8b5	5.9	8.3	0.000402	26.50	4215	2,757,409	Int

Table A.4: Flexural Fatigue Test Results for Mix J

Mix	Binder Type/ Grade	Aggregate Type	NMAS	Specimen Designation	AV (%)	AC (%)	Test Strain Level	Initial Phase Angle (Deg.)	Initial Stiffness (Mpa)	Fatigue Life Nf	Int or Ext
J	PG64-16 RB	Granite	3/4	2b5	6.4	8.8	0.000191	23.22	3637	212,799,250	Ext
				4b5	5.6	8.8	0.000204	27.49	3614	100,728,559	Ext
				1b3	5.8	8.8	0.000201	26.66	3986	54,791,292	Ext
				1b4	6.2	8.8	0.000404	27.78	3728	1,834,993	Int
				4b3	6.5	8.8	0.000404	29.82	3351	1,547,711	Int
				3B1	6.2	8.8	0.000404	30.08	3354	1,013,712	Int

Table A.5. Flexural Fatigue Test Results for Mix N

Mix	Binder Type/ Grade	Aggregate Type	NMAS	Specimen Designation	AV (%)	AC (%)	Test Strain Level	Initial Phase Angle (Deg.)	Initial Stiffness (Mpa)	Fatigue Life Nf	Int or Ext
N	PG 64-28 PM	Granite	1	3c2	6.5	6.4	0.000205	47.60	1705	2,472,636,005,669	Ext
				10d2	6.1	6.4	0.000210	43.14	1951	3,185,015,620	Ext
				15d2	6.4	6.4	0.000207	42.71	1970	6,106,095,017	Ext
				10d1	6.4	6.4	0.000411	44.27	1669	107,532,533	Ext
				12d2	5.8	6.4	0.000411	41.90	1720	135,122,636	Ext
				15d1	5.9	6.4	0.000424	47.40	1580	114,763,079	Ext

Table A.6. Average 200 and 400 Microstrain Fatigue Life for Mix A

Mix	Binder Type/ Grade	Aggregate Type	NMAS	Microstrain	AC %	Average Initial Stiffness (MPa)	Average Initial Stiffness (psi)	Fatigue Life N_f
A	PG 64-16	Alluvial	3/4	200	5.5	6,594	956,314	9,475,915
				400	5.5	5,863	850,383	133,922

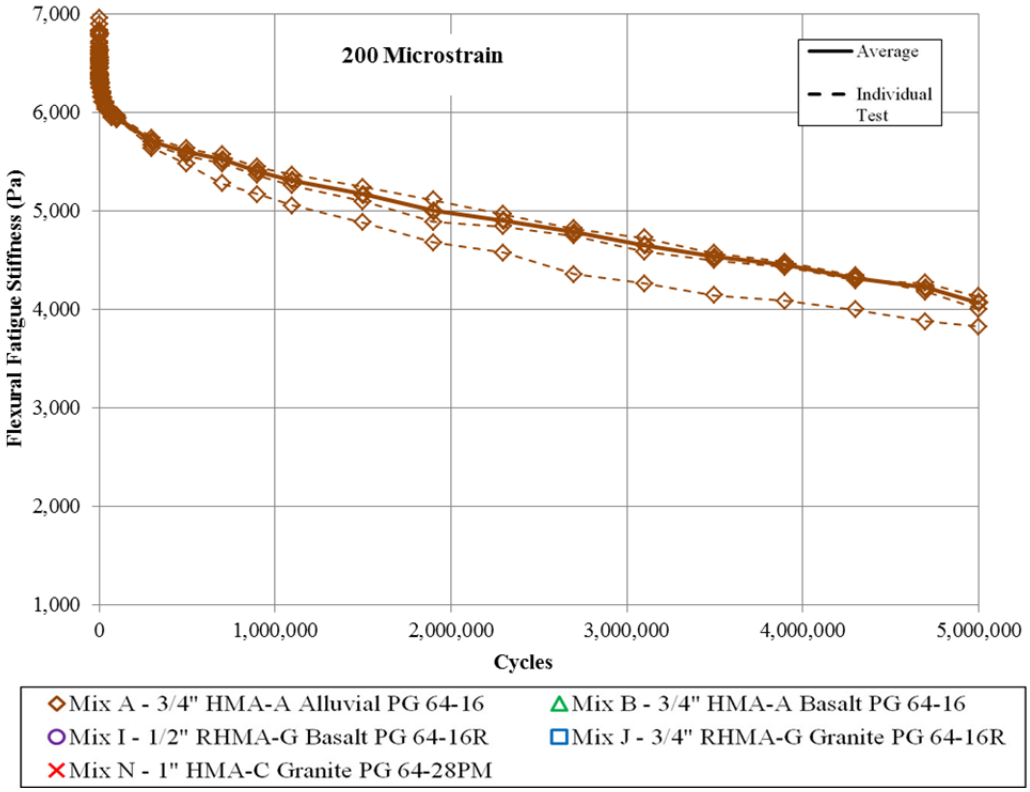

Figure A.1: Flexural fatigue stiffness versus cycles (200 microstrain) for Mix A.

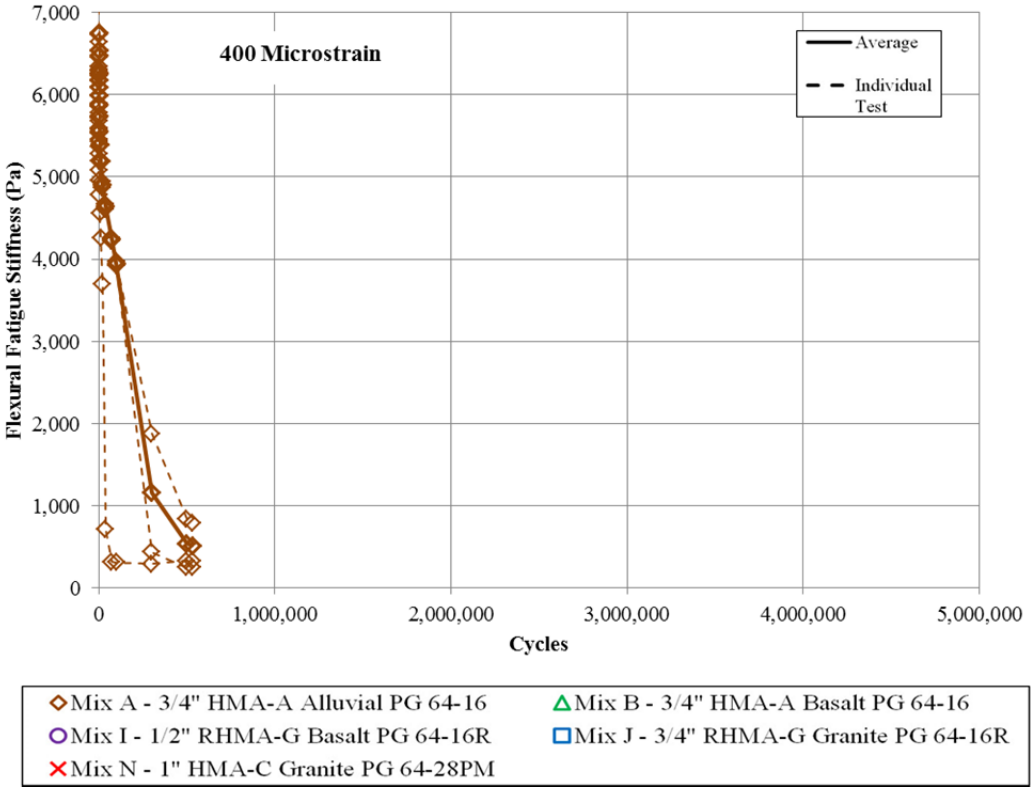

Figure A.2: Flexural fatigue stiffness versus cycles (400 microstrain) for Mix A.

Table A.7: Average Initial Flexural Stiffness at 10 Hz and 10°C, 20°C, and 30°C for Mix A

Mix	Binder Type/ Grade	Aggregate Type	NMAS	Binder Content %	Average Test Temp (°C)	Average Phase Angle (Deg.)	Average Initial Stiffness (MPa)	Average Initial Stiffness (psi)
A	PG 64-16	Alluvial	3/4	5.5	9.6	14.89	10,051	1,457,740
					19.7	21.47	5,450	790,430
					29.8	35.61	2,366	343,209

Table A.8: Average 200 and 400 Microstrain Fatigue Life for Mix B

Mix	Binder Type/ Grade	Aggregate Type	NMAS	Microstrain	AC %	Average Initial Stiffness (MPa)	Average Initial Stiffness (psi)	Fatigue Life N_f
B	**PG 64-16**	**Basalt**	**3/4**	200	6.3	3,846	557,788	17,118,276
				400	6.3	3,733	541,394	226,478

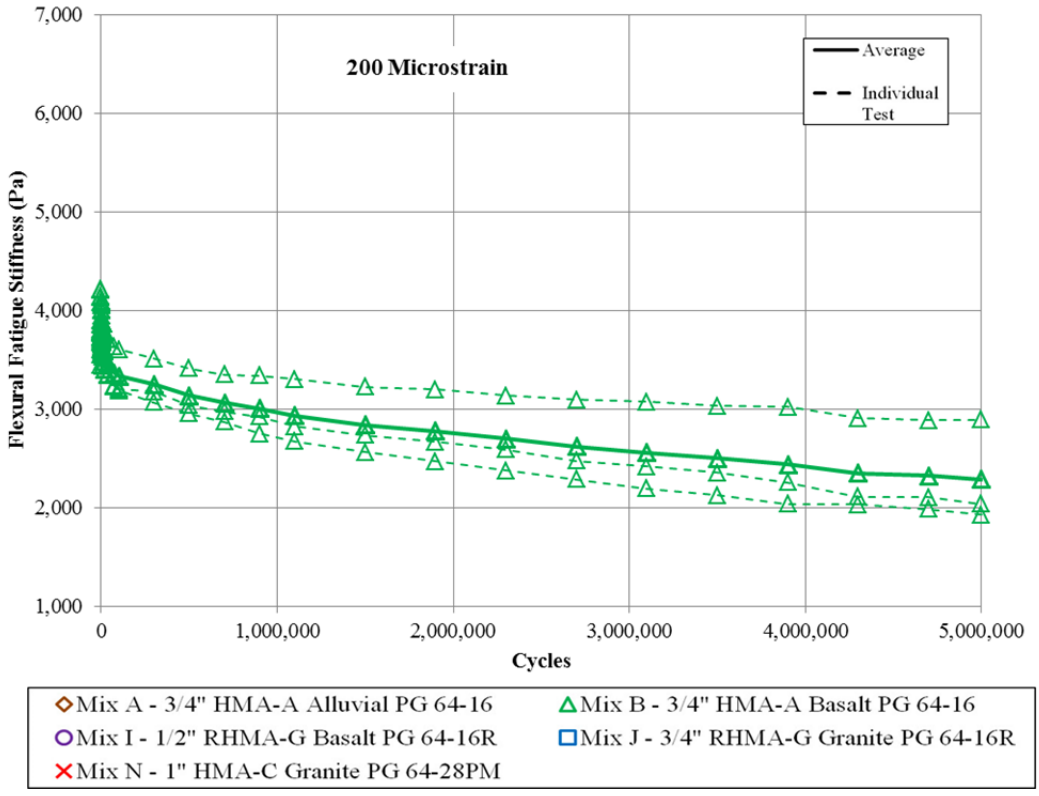

Figure A.3: Flexural fatigue stiffness versus cycles (200 microstrain) for Mix B.

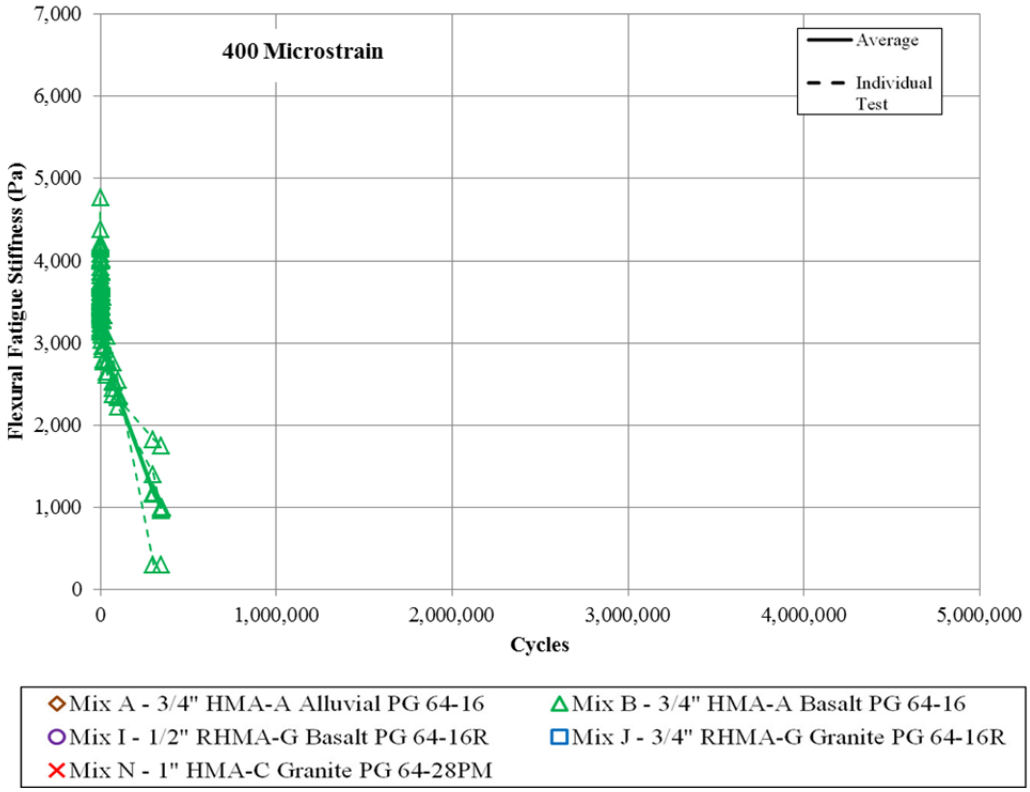

Figure A.4: Flexural fatigue stiffness versus cycles (400 microstrain) for Mix B.

Table A.9: Average Initial Flexural Stiffness at 10 Hz and 10°C, 20°C, and 30°C for Mix B

Mix	Binder Type/ Grade	Aggregate Type	NMAS	Binder Content %	Average Test Temp (°C)	Average Phase Angle (Deg.)	Average Initial Stiffness (MPa)	Average Initial Stiffness (psi)
B	PG 64-16	Basalt	3/4	6.3	10.0	15.59	7,877	1,142,395
					19.7	22.44	4,666	676,793
					29.7	40.41	1,336	193,702

Table A.10: Average 200 and 400 Microstrain Fatigue Life for Mix I

Mix	Binder Type/ Grade	Aggregate Type	NMAS	Microstrain	AC %	Average Initial Stiffness (MPa)	Average Initial Stiffness (psi)	Fatigue Life N_f
I	**PG 64-16 RB**	**Basalt**	**1/2**	200	8.3	4,000	580,137	59,065,825
				400	8.3	3,758	544,979	2,868,462

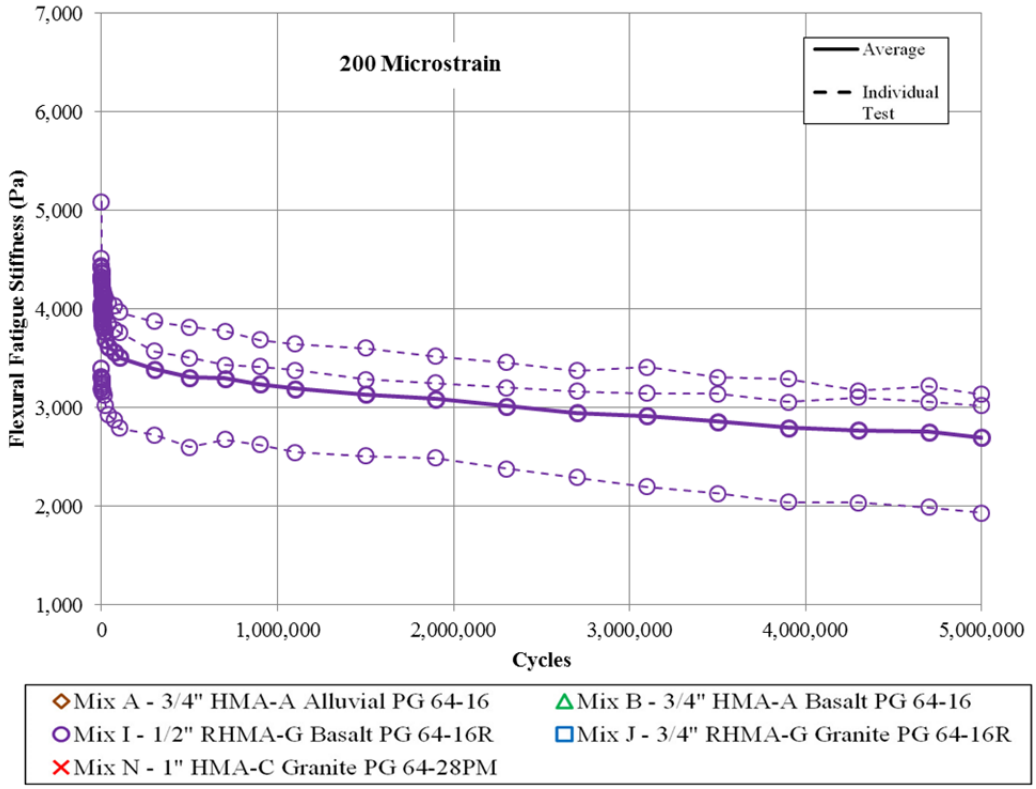

Figure A.5: Flexural fatigue stiffness versus cycles (200 microstrain) for Mix I.

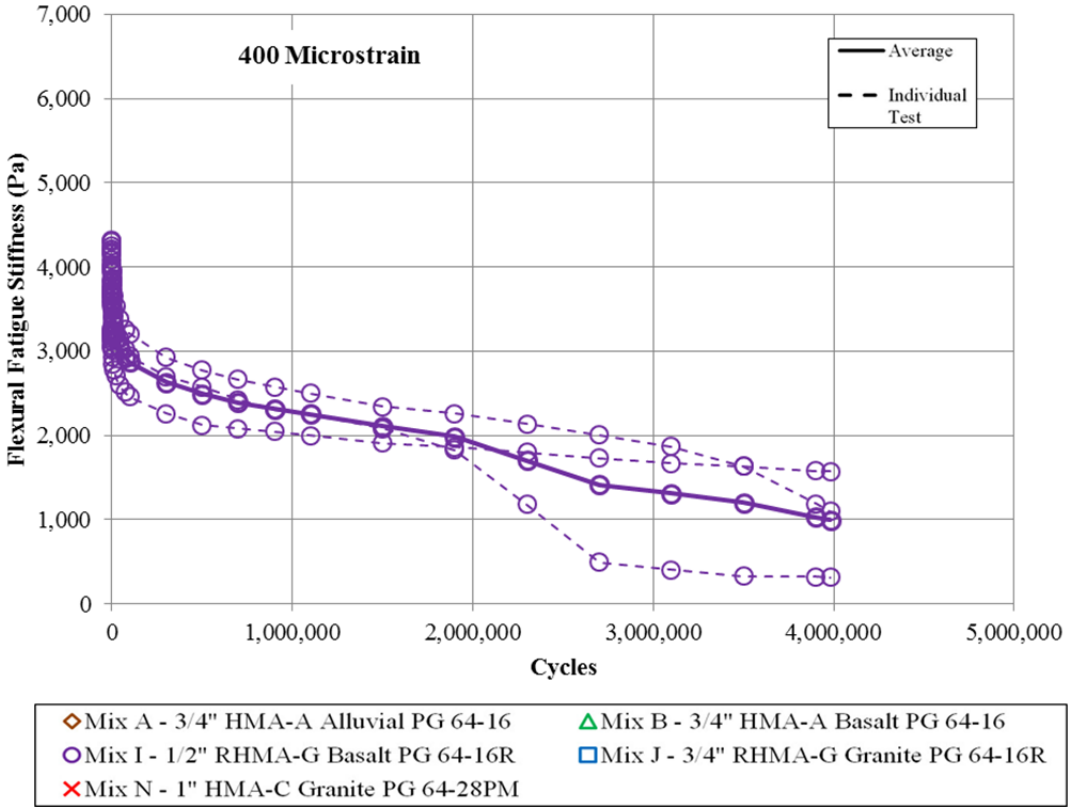

Figure A.6: Flexural fatigue stiffness versus cycles (400 microstrain) for Mix I.

Table A.11: Average Initial Flexural Stiffness for 10 Hz Frequency in 10°C, 20°C, and 30°C for Mix I

Mix	Binder Type/Grade	Aggregate Type	NMAS	Binder Content %	Average Test Temp (°C)	Average Phase Angle (Deg.)	Average Initial Stiffness (MPa)	Average Initial Stiffness (psi)
I	PG 64-16 RB	Basalt	1/2	8.3	9.9	15.16	7,561	1,096,616
					19.6	23.63	4,407	639,120
					30.2	37.45	1,679	243,482

Table A.12: Average 200 and 400 Microstrain Fatigue Life for Mix J

Mix	Binder Type/ Grade	Aggregate Type	NMAS	Microstrain	AC %	Average Initial Stiffness (MPa)	Average Initial Stiffness (psi)	Fatigue Life N_f
J	PG 64-16 RB	Granite	3/4	200	8.8	3,745	543,203	122,773,034
				400	8.8	3,478	504,416	1,465,472

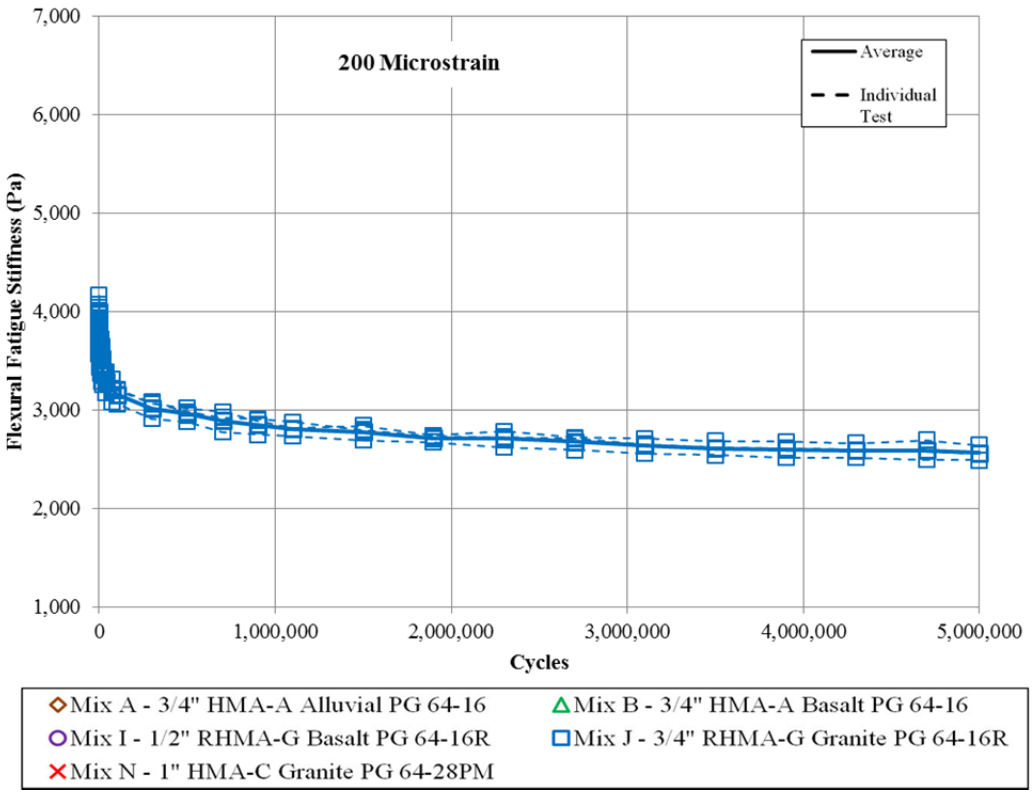

Figure A.7: Flexural fatigue stiffness versus cycles (200 microstrain) for Mix J.

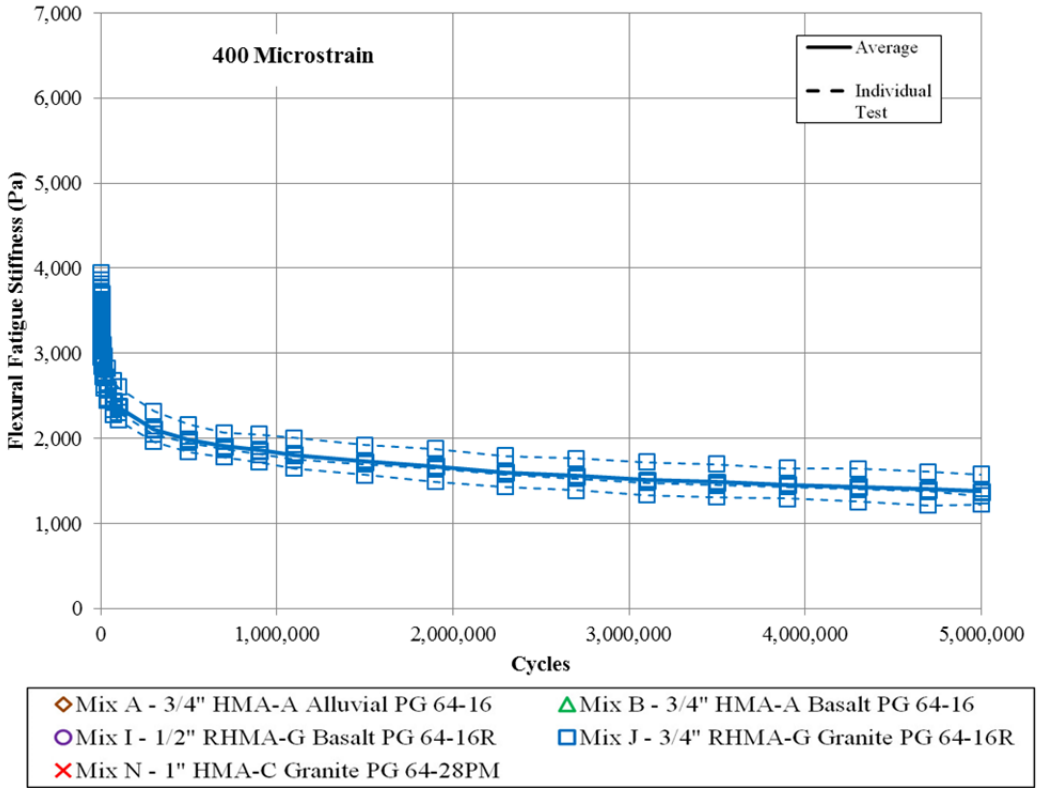

Figure A.8: Flexural fatigue stiffness versus cycles (400 microstrain) for Mix J.

Table A.13: Average Initial Flexural Stiffness for 10 Hz Frequency and 10°C, 20°C, and 30°C for Mix J

Mix	Binder Type/Grade	Aggregate Type	NMAS	Binder Content %	Average Test Temp (°C)	Average Phase Angle (Deg.)	Average Initial Stiffness (MPa)	Average Initial Stiffness (psi)
J	PG 64-16 RB	Granite	3/4	8.8	10.0	15.71	6,783	983,834
					19.8	24.74	3,846	557,769
					29.7	39.52	1,416	205,431

Table A.14: Average 200 and 400 Microstrain Fatigue Life for Mix N

Mix	Binder Type/ Grade	Aggregate Type	NMAS	Microstrain	AC %	Average Initial Stiffness (MPa)	Average Initial Stiffness (psi)	Fatigue Life N_f
N	**PG 64-28 PM**	**Granite**	**1**	200	6.4	1,876	272,026	827,309,038,768
				400	6.4	1,656	240,218	119,139,416

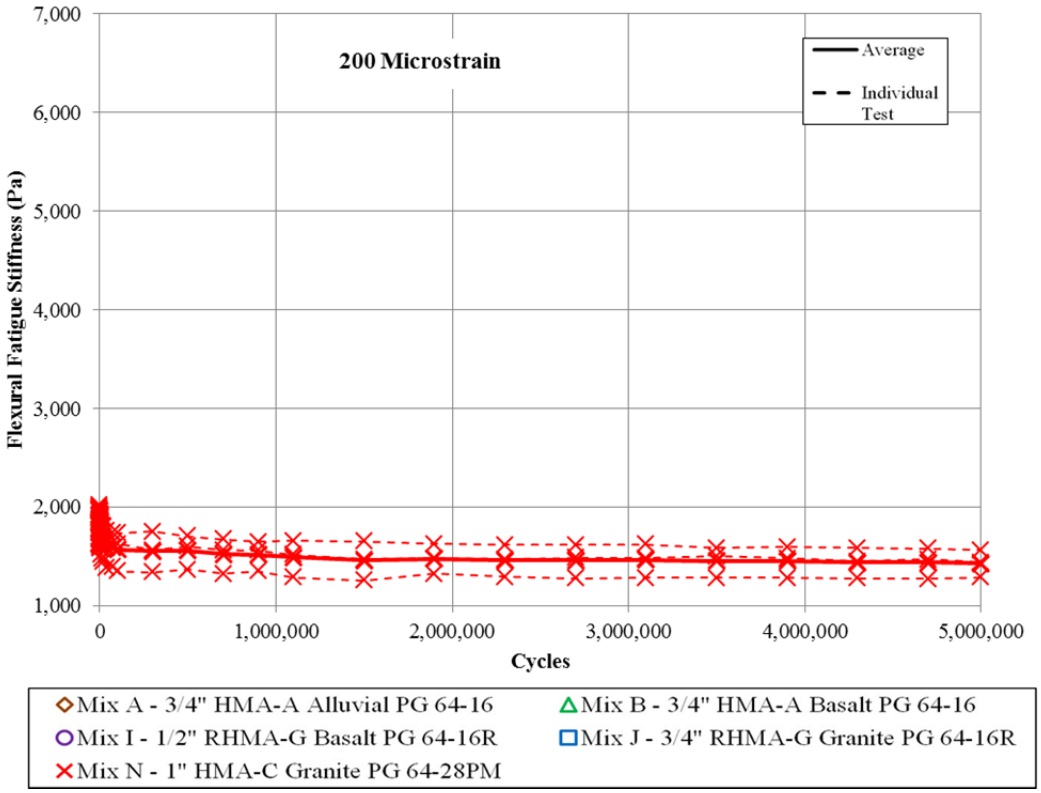

Figure A.9: Flexural fatigue stiffness versus cycles (200 microstrain) for Mix N.

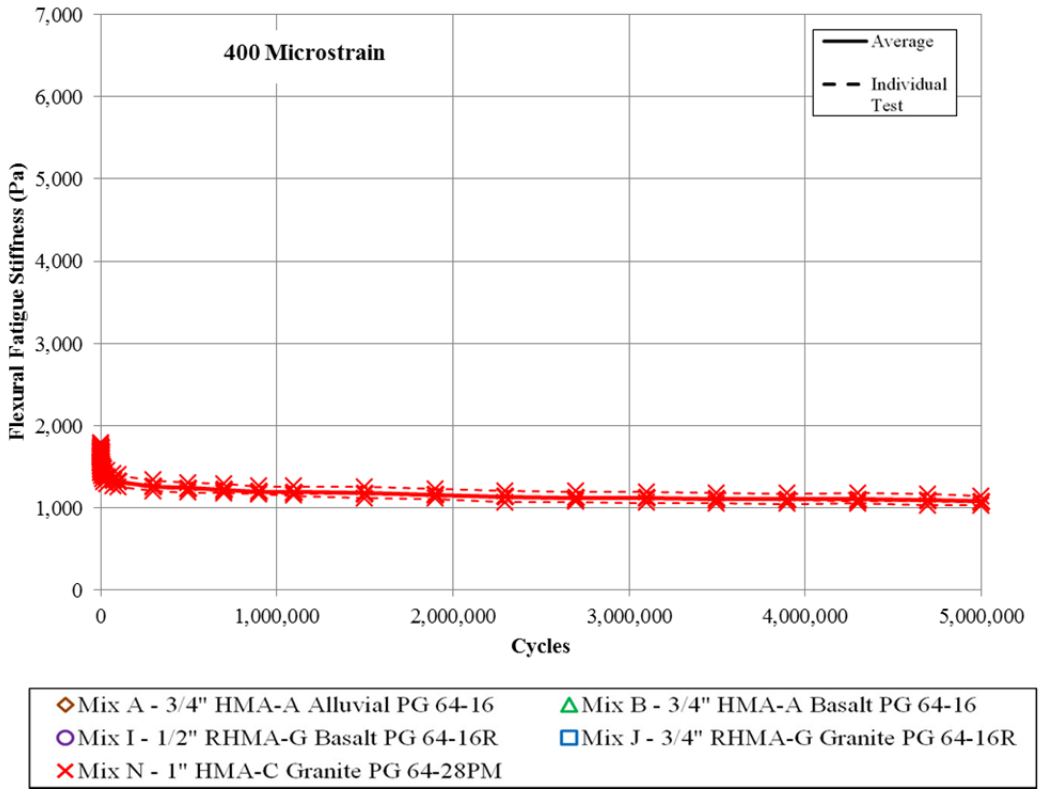

Figure A.10: Flexural fatigue stiffness versus cycles (400 microstrain) for Mix N.

Table A.15: Average Initial Flexural Stiffness for 10 Hz and 10°C, 20°C, and 30°C for Mix N

Mix	Binder Type/ Grade	Aggregate Type	NMAS	Binder Content %	Average Test Temp (°C)	Average Phase Angle (Deg.)	Average Initial Stiffness (MPa)	Average Initial Stiffness (psi)
N	PG 64-28 PM	Granite	1	6.4	9.6	24.27	4,538	658,177
					19.8	42.03	1,913	277,484
					30.3	50.55	570	82,695

A.2 Hveem Mix Designs

Table A.16: Flexural Fatigue Test Results for Hveem Mix Design A

Mix	Binder Type/ Grade	Aggregate Type	NMAS	Specimen Designation	AV (%)	AC (%)	Test Strain Level	Initial Phase Angle (Deg.)	Initial Stiffness (Mpa)	Fatigue Life Nf	Int or Ext
A	PG 64-16	Alluvial	3/4	h3b4	6.3	5.0	0.000184	20.86	6650	1,289,362	Int
				h4b1	6.1	5.0	0.000195	23.67	6319	1,005,427	Int
				h4b2	5.5	5.0	0.000200	23.50	6678	2,755,023	Int
				h2b6	5.6	5.0	0.000400	25.98	6277	18,389	Int
				h3b7	6.2	5.0	0.000399	26.08	6182	35,405	Int
				h4b8	6.1	5.0	0.000369	22.09	6757	46,200	Int

Table A.17: Flexural Fatigue Test Results for Hveem Mix Design B

Mix	Binder Type/ Grade	Aggregate Type	NMAS	Specimen Designation	AV (%)	AC (%)	Test Strain Level	Initial Phase Angle (Deg.)	Initial Stiffness (Mpa)	Fatigue Life Nf	Int or Ext
B	PG 64-16	Basalt	3/4	H1B2	5.6	5.2	0.000201	25.72	4584	2,884,039	Int
				h1b6	5.5	5.2	0.000186	89.90	5096	6,162,321	Ext
				H1B8	5.5	5.2	0.000190	21.19	4761	1,793,319	Int
				H11	5.6	5.2	0.000406	27.30	4664	96,851	Int
				h18	5.8	5.2	0.000375	24.87	4693	94,147	Int
				H18	6.2	5.2	0.000375	24.95	4680	84,484	Int

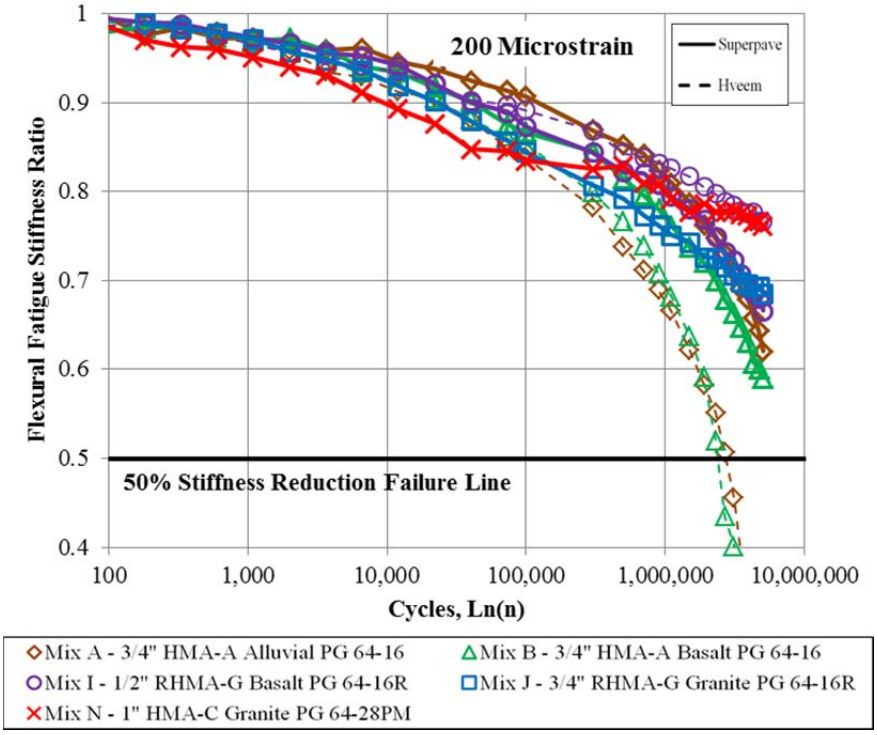

Figure A.11: Comparison of flexural fatigue stiffness ratio versus cycles for Superpave and Hveem mix designs (200 microstrain tests with mix averages, log scale).

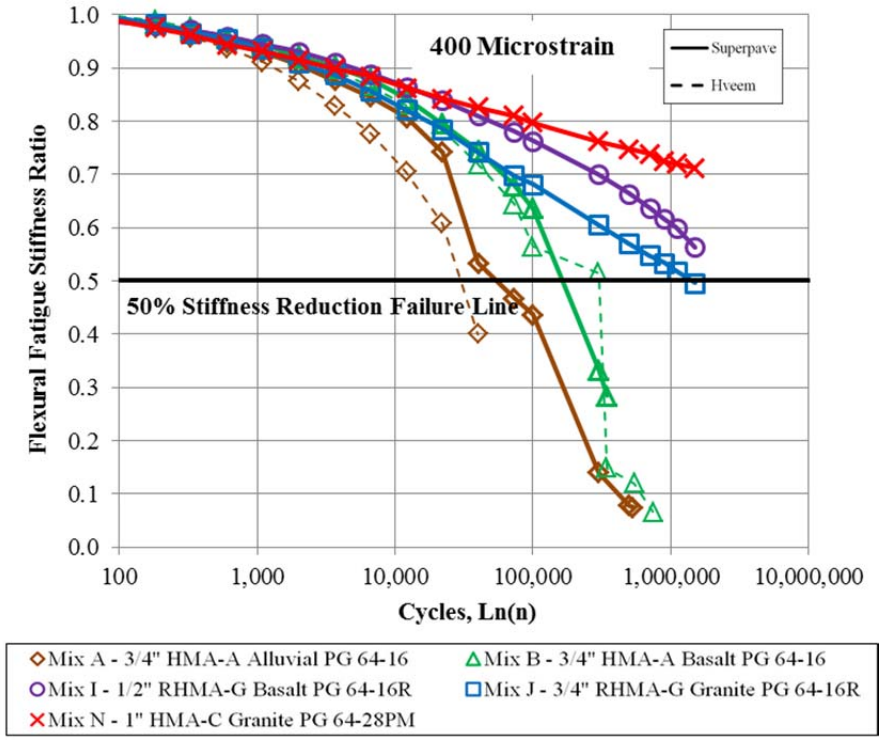

Figure A.12: Comparison of flexural fatigue stiffness ratio versus cycles for Superpave and Hveem mix design (400 microstrain tests with mix averages [log scale]).

APPENDIX B: FLEXURAL FREQUENCY SWEEP DATA

B.1 Superpave Mix Designs

Table B.1: Flexural Frequency Sweep Test Results for Mix A Superpave Mix Design

freq	tensile_sts	tensile_stn	flex_E*	p_angle	avg_temp	freq	tensile_sts	tensile_stn	flex_E*	p_angle	avg_temp
(Hz)	(MPa)		(MPa)	(deg)	(C)	(Hz)	(MPa)		(MPa)	(deg)	(C)
15.153	1.099292	0.000100	11045.46	16.25	9.66	15.142	1.051615	0.000106	9953.02	16.51	9.55
10.004	1.080065	0.000102	10593.69	14.52	9.75	10	0.974595	0.000103	9507.84	15.26	9.49
5.053	0.967630	0.000099	9748.41	14.23	9.76	5.048	0.899902	0.000104	8694.26	15.11	9.50
1.998	0.872853	0.000103	8478.31	15.05	9.75	2.001	0.777596	0.000104	7506.41	15.78	9.57
0.999	0.765746	0.000101	7573.11	16.27	9.59	1	0.674335	0.000101	6690.67	17.21	9.58
0.5	0.663891	0.000100	6645.38	18.48	9.66	0.5	0.582738	0.000100	5844.68	19.42	9.54
0.2	0.541015	0.000099	5466.11	21.39	9.70	0.2	0.472781	0.000099	4777.73	22.53	9.54
0.1	0.444810	0.000099	4501.99	25.15	9.73	0.1	0.384837	0.000099	3900.82	25.82	9.47
0.05	0.365582	0.000098	3713.02	27.77	9.81	0.05	0.317955	0.000099	3226.55	29.32	9.41
0.02	0.285327	0.000099	2895.31	31.18	9.63	0.02	0.242765	0.000098	2471.76	31.85	9.62
0.01	0.226912	0.000099	2303.17	33.35	9.71	0.01	0.192825	0.000098	1957.94	34.57	9.45
freq	tensile_sts	tensile_stn	flex_E*	p_angle	avg_temp	freq	tensile_sts	tensile_stn	flex_E*	p_angle	avg_temp
(Hz)	(MPa)		(MPa)	(deg)	(C)	(Hz)	(MPa)		(MPa)	(deg)	(C)
15.171	0.592927	0.000100	5938.03	20.28	19.67	15.157	0.582971	0.000101	5780.92	20.98	19.77
10.013	0.546133	0.000099	5505.29	20.94	19.58	10.006	0.540139	0.000100	5394.35	21.99	19.76
5.003	0.457812	0.000097	4735.01	24.15	19.59	5.003	0.447516	0.000098	4572.97	24.67	19.61
2	0.354236	0.000096	3702.71	26.76	19.67	1.999	0.342188	0.000096	3551.10	27.93	19.59
1	0.299909	0.000099	3019.09	28.91	19.71	1	0.282763	0.000099	2846.51	31.89	19.61
0.5	0.239491	0.000099	2414.51	32.04	19.75	0.5	0.220404	0.000099	2232.15	34.51	19.64
0.2	0.171477	0.000099	1729.12	36.00	19.68	0.2	0.151622	0.000098	1548.40	38.92	19.76
0.1	0.130624	0.000098	1329.66	40.57	19.65	0.1	0.113791	0.000098	1167.08	43.10	19.67
0.05	0.095189	0.000098	970.82	38.74	19.56	0.05	0.082044	0.000098	838.89	42.92	19.74
0.02	0.063270	0.000098	645.89	43.96	19.59	0.02	0.053921	0.000097	554.91	48.17	19.73
0.01	0.048220	0.000098	492.87	43.40	19.60	0.01	0.038596	0.000097	397.21	44.56	19.66
freq	tensile_sts	tensile_stn	flex_E*	p_angle	avg_temp	freq	tensile_sts	tensile_stn	flex_E*	p_angle	avg_temp
(Hz)	(MPa)		(MPa)	(deg)	(C)	(Hz)	(MPa)		(MPa)	(deg)	(C)
15.266	0.306824	0.000101	3041.78	108.86	29.89	15.156	0.230097	0.000102	2257.04	38.55	29.73
10.006	0.271889	0.000099	2746.24	31.08	29.97	10.002	0.199884	0.000101	1986.46	40.14	29.68
5.001	0.217395	0.000098	2213.73	34.70	29.95	4.998	0.146065	0.000098	1491.20	42.10	29.90
2.001	0.152437	0.000097	1575.17	37.62	29.87	2.002	0.095069	0.000097	985.06	44.84	29.88
0.999	0.114404	0.000099	1150.45	38.86	29.84	1	0.068089	0.000099	690.39	49.60	29.86
0.498	0.082053	0.000098	833.73	46.63	29.80	0.501	0.047860	0.000099	485.42	48.28	29.83
0.201	0.056667	0.000099	572.12	39.44	29.77	0.2	0.030169	0.000099	305.53	48.63	29.76
0.1	0.041057	0.000098	418.20	42.70	30.01	0.1	0.019095	0.000098	194.77	54.77	29.64
0.05	0.030372	0.000098	310.77	48.39	29.83	0.05	0.013535	0.000098	137.82	54.20	29.90
0.02	0.018771	0.000098	192.32	42.35	29.83	0.607	0.001504	0.000098	15.31	43.78	29.83
0.013	0.003070	0.000098	31.40	31.68	29.85	0.01	0.005442	0.000097	55.92	70.78	29.90

Table B.2: Flexural Frequency Sweep Test Results for Mix B Superpave Mix Design

freq	tensile_sts	tensile_stn	flex_E*	p_angle	avg_temp	freq	tensile_sts	tensile_stn	flex_E*	p_angle	avg_temp
(Hz)	(MPa)		(MPa)	(deg)	(C)	(Hz)	(MPa)		(MPa)	(deg)	(C)
15.151	0.863740	0.000106	8177.24	17.23	10.08	15.068	0.854373	0.000104	8248.01	17.00	9.86
10.003	0.815793	0.000104	7807.36	15.17	10.05	10.078	0.792739	0.000100	7945.72	16.01	9.88
5.011	0.720340	0.000102	7048.24	15.41	10.12	5.015	0.737481	0.000102	7203.68	15.75	9.90
2	0.623729	0.000102	6102.07	16.30	10.07	1.999	0.639055	0.000104	6171.69	16.47	9.89
0.999	0.537852	0.000100	5378.48	17.31	10.05	1	0.552058	0.000102	5414.65	17.99	9.82
0.5	0.464063	0.000099	4690.34	18.87	10.11	0.5	0.467034	0.000099	4699.02	20.48	9.72
0.2	0.379670	0.000098	3868.68	21.17	10.06	0.2	0.377691	0.000099	3819.98	23.70	9.74
0.1	0.312027	0.000098	3186.71	24.59	9.96	0.1	0.307484	0.000099	3114.25	26.92	9.62
0.05	0.261753	0.000098	2677.43	26.59	9.96	0.05	0.252771	0.000099	2561.87	30.28	9.42
0.02	0.208165	0.000097	2136.89	28.77	9.76	0.02	0.191710	0.000098	1951.05	32.27	9.67
0.01	0.176117	0.000098	1797.75	29.32	9.84	0.01	0.152362	0.000099	1543.39	34.57	9.56
freq	tensile_sts	tensile_stn	flex_E*	p_angle	avg_temp	freq	tensile_sts	tensile_stn	flex_E*	p_angle	avg_temp
(Hz)	(MPa)		(MPa)	(deg)	(C)	(Hz)	(MPa)		(MPa)	(deg)	(C)
15.049	0.566587	0.000111	5108.00	24.42	19.76	15.274	0.493948	0.000100	4929.31	25.52	19.64
9.958	0.501083	0.000106	4732.83	22.10	19.77	10.03	0.464354	0.000101	4599.82	22.79	19.63
4.938	0.409138	0.000106	3856.60	25.31	19.78	4.994	0.417613	0.000110	3806.00	23.43	19.64
1.986	0.350103	0.000107	3260.97	31.65	19.80	1.98	0.337479	0.000107	3141.07	31.07	19.63
0.999	0.263477	0.000102	2573.74	30.06	19.80	1	0.245888	0.000102	2399.08	30.04	19.60
0.5	0.204668	0.000100	2044.63	32.46	19.83	0.5	0.192193	0.000100	1920.02	32.59	19.67
0.2	0.145516	0.000099	1465.47	36.64	19.79	0.2	0.134775	0.000099	1364.08	36.92	19.66
0.1	0.108616	0.000099	1100.74	39.35	19.77	0.1	0.101569	0.000098	1031.39	39.81	19.74
0.05	0.081553	0.000098	829.77	41.88	19.86	0.05	0.074250	0.000098	754.60	43.64	19.77
0.02	0.056151	0.000098	570.27	42.35	19.53	0.02	0.049191	0.000098	502.19	43.69	19.86
0.01	0.039232	0.000098	400.21	42.01	19.77	0.01	0.036274	0.000098	370.13	45.19	19.77
freq	tensile_sts	tensile_stn	flex_E*	p_angle	avg_temp	freq	tensile_sts	tensile_stn	flex_E*	p_angle	avg_temp
(Hz)	(MPa)		(MPa)	(deg)	(C)	(Hz)	(MPa)		(MPa)	(deg)	(C)
15.273	0.308787	0.000192	1607.32	44.06	29.57	15.002	0.301270	0.000207	1455.27	43.28	29.84
10.006	0.297135	0.000212	1402.18	41.30	29.55	9.865	0.263139	0.000207	1268.88	39.53	29.87
4.981	0.234797	0.000217	1081.84	37.68	29.50	4.982	0.216253	0.000218	990.44	38.52	29.97
2.002	0.154187	0.000207	746.66	42.91	29.50	2.002	0.141862	0.000206	688.32	41.68	30.09
1	0.112015	0.000202	554.53	43.84	29.58	1.001	0.103568	0.000202	513.97	42.64	30.14
0.5	0.083023	0.000200	415.29	44.67	29.62	0.5	0.078147	0.000199	391.74	43.99	30.25
0.2	0.057276	0.000199	287.21	46.25	29.91	0.2	0.053550	0.000199	269.47	41.53	30.31
0.1	0.041096	0.000199	206.82	49.79	30.18	0.1	0.041064	0.000198	207.07	43.41	30.33
0.05	0.032317	0.000199	162.79	45.43	30.29	0.05	0.032563	0.000198	164.34	47.30	30.42
0.02	0.020820	0.000198	104.97	43.71	30.35	0.02	0.022856	0.000198	115.44	41.41	30.33
0.01	0.019281	0.000198	97.14	42.64	30.25	0.01	0.018586	0.000198	93.96	41.88	30.28

Table B.3: Flexural Frequency Sweep Test Results for Mix I Superpave Mix Design

freq	tensile_sts	tensile_stn	flex_E*	p_angle	avg_temp	freq	tensile_sts	tensile_stn	flex_E*	p_angle	avg_temp
(Hz)	(MPa)		(MPa)	(deg)	(C)	(Hz)	(MPa)		(MPa)	(deg)	(C)
15.151	0.829200	0.000105	7907.57	16.60	10.06	15.29	0.932406	0.000117	7938.59	17.01	9.59
9.942	0.775235	0.000103	7543.72	14.56	10.05	10.001	0.788537	0.000104	7578.10	15.76	9.67
4.993	0.719929	0.000105	6847.95	15.21	10.02	5.048	0.712454	0.000103	6950.50	15.88	9.72
2	0.611152	0.000102	5964.20	16.42	9.99	2.001	0.617382	0.000104	5948.89	15.70	9.79
0.999	0.529430	0.000100	5287.62	17.72	10.03	1	0.536694	0.000101	5305.09	17.02	9.81
0.5	0.452558	0.000099	4582.42	19.18	9.99	0.5	0.460476	0.000100	4624.98	18.84	9.87
0.2	0.368386	0.000098	3757.26	22.34	9.97	0.2	0.377868	0.000099	3823.45	21.60	9.96
0.1	0.300641	0.000098	3070.87	25.74	9.99	0.1	0.311316	0.000099	3155.53	24.77	10.00
0.05	0.248679	0.000098	2543.83	27.74	9.94	0.05	0.259153	0.000099	2625.32	27.20	10.05
0.02	0.194238	0.000098	1989.82	30.56	9.74	0.02	0.202962	0.000098	2064.95	30.00	9.63
0.01	0.157800	0.000098	1610.47	32.70	9.86	0.01	0.165480	0.000098	1684.41	32.11	9.83
freq	tensile_sts	tensile_stn	flex_E*	p_angle	avg_temp	freq	tensile_sts	tensile_stn	flex_E*	p_angle	avg_temp
(Hz)	(MPa)		(MPa)	(deg)	(C)	(Hz)	(MPa)		(MPa)	(deg)	(C)
15.339	0.517351	0.000108	4785.28	23.89	19.67	15.271	0.481983	0.000104	4644.86	24.57	19.56
10.029	0.458299	0.000103	4467.56	21.62	19.78	10.118	0.419838	0.000097	4345.60	25.63	19.51
4.949	0.403042	0.000110	3651.20	22.53	19.69	4.992	0.402215	0.000109	3676.92	22.03	19.47
1.992	0.325570	0.000107	3049.44	27.24	19.64	1.981	0.326353	0.000106	3064.50	28.60	19.49
1.001	0.251883	0.000102	2461.52	27.57	19.64	1	0.245747	0.000103	2394.04	27.70	19.61
0.5	0.199628	0.000100	1990.81	29.30	19.79	0.5	0.198308	0.000100	1975.22	30.96	19.55
0.2	0.146225	0.000099	1471.79	32.50	19.78	0.2	0.144094	0.000099	1451.03	33.21	19.56
0.1	0.111840	0.000099	1130.12	37.25	19.82	0.1	0.109800	0.000099	1110.90	35.64	19.59
0.05	0.086734	0.000099	879.94	37.90	19.76	0.05	0.084636	0.000099	856.75	38.11	19.65
0.02	0.059960	0.000098	608.99	38.43	19.77	0.02	0.058267	0.000098	592.45	39.65	19.76
0.01	0.045340	0.000098	461.45	43.17	19.73	0.01	0.043479	0.000098	441.70	39.71	19.75
freq	tensile_sts	tensile_stn	flex_E*	p_angle	avg_temp	freq	tensile_sts	tensile_stn	flex_E*	p_angle	avg_temp
(Hz)	(MPa)		(MPa)	(deg)	(C)	(Hz)	(MPa)		(MPa)	(deg)	(C)
15.285	0.380657	0.000208	1827.43	40.40	30.32	15.284	0.413344	0.000206	2003.39	38.10	29.93
10.007	0.330532	0.000207	1596.05	38.43	30.32	10.003	0.368093	0.000209	1761.46	36.46	30.00
4.981	0.267464	0.000219	1220.03	35.94	30.23	4.975	0.300694	0.000220	1369.55	34.21	30.10
2	0.179597	0.000208	864.64	40.57	30.22	2.001	0.203385	0.000207	981.62	38.87	30.02
1	0.132305	0.000203	652.45	41.63	30.25	1	0.151725	0.000202	749.82	40.28	29.98
0.5	0.098651	0.000201	491.38	42.24	30.22	0.5	0.113925	0.000200	568.43	41.67	29.97
0.2	0.067911	0.000200	339.92	43.25	30.33	0.2	0.077306	0.000199	387.85	42.72	30.02
0.1	0.050936	0.000199	255.45	45.54	30.31	0.1	0.056857	0.000199	285.97	49.09	30.05
0.05	0.038970	0.000199	195.48	43.53	30.31	0.05	0.041487	0.000199	208.77	45.40	30.09
0.02	0.030235	0.000199	151.86	44.25	30.31	0.02	0.028382	0.000198	143.09	46.23	30.03
0.01	0.022789	0.000199	114.52	46.85	30.22	0.01	0.021085	0.000198	106.30	41.70	29.99

Table B.4: Flexural Frequency Sweep Test Results for Mix J Superpave Mix Design

freq	tensile_sts	tensile_stn	flex_E*	p_angle	avg_temp	freq	tensile_sts	tensile_stn	flex_E*	p_angle	avg_temp
(Hz)	(MPa)		(MPa)	(deg)	(C)	(Hz)	(MPa)		(MPa)	(deg)	(C)
15.392	0.746350	0.000103	7255.97	18.01	9.75	15.146	0.746849	0.000106	7076.38	17.44	10.19
9.949	0.690771	0.000101	6841.87	15.17	9.81	10.006	0.686039	0.000102	6724.73	16.25	10.18
5.065	0.623101	0.000100	6246.02	16.81	9.77	5.017	0.625713	0.000103	6100.38	16.09	10.26
2	0.556860	0.000104	5339.65	16.37	9.71	1.999	0.537658	0.000103	5212.61	16.79	10.25
1	0.477276	0.000102	4679.54	17.70	9.76	1	0.466187	0.000101	4609.04	17.88	10.16
0.5	0.411812	0.000100	4123.61	19.99	9.73	0.5	0.401004	0.000100	3995.79	19.41	10.06
0.2	0.330665	0.000099	3331.04	23.17	9.70	0.2	0.326051	0.000099	3288.26	22.07	10.13
0.1	0.272673	0.000099	2756.52	24.83	9.55	0.1	0.266972	0.000099	2700.67	25.65	10.08
0.05	0.228624	0.000099	2313.89	27.03	9.49	0.05	0.221773	0.000099	2244.26	27.68	10.04
0.02	0.177184	0.000099	1797.88	30.01	9.82	0.02	0.176741	0.000099	1786.74	29.80	9.66
0.01	0.145282	0.000099	1472.60	30.84	9.57	0.01	0.144912	0.000099	1469.33	31.60	9.92
freq	tensile_sts	tensile_stn	flex_E*	p_angle	avg_temp	freq	tensile_sts	tensile_stn	flex_E*	p_angle	avg_temp
(Hz)	(MPa)		(MPa)	(deg)	(C)	(Hz)	(MPa)		(MPa)	(deg)	(C)
15.166	0.422441	0.000100	4223.93	25.79	19.81	15.209	0.436108	0.000105	4142.02	25.87	19.81
9.983	0.399274	0.000101	3942.97	21.38	19.87	10.023	0.360440	0.000096	3748.40	28.10	19.79
4.936	0.348420	0.000111	3131.11	25.77	19.84	4.934	0.339704	0.000113	2999.75	26.19	19.83
1.989	0.282809	0.000107	2655.04	30.19	19.81	1.975	0.279306	0.000108	2594.95	31.53	19.82
1	0.209998	0.000102	2062.84	29.90	19.83	1	0.203334	0.000102	1985.11	30.08	19.89
0.5	0.164002	0.000100	1645.75	31.54	19.82	0.5	0.161448	0.000100	1606.51	32.68	19.87
0.2	0.120580	0.000099	1219.38	34.33	19.85	0.2	0.115026	0.000100	1155.54	35.29	19.89
0.1	0.090777	0.000099	920.59	38.63	19.82	0.1	0.086670	0.000099	873.75	39.12	19.86
0.05	0.067495	0.000098	685.54	42.10	19.88	0.05	0.065408	0.000099	661.84	39.90	19.86
0.02	0.047032	0.000098	478.61	42.69	19.95	0.02	0.042606	0.000099	430.46	40.51	19.89
0.007	0.005843	0.000098	59.51	116.86	19.81	0.01	0.032400	0.000099	328.29	46.23	19.96
freq	tensile_sts	tensile_stn	flex_E*	p_angle	avg_temp	freq	tensile_sts	tensile_stn	flex_E*	p_angle	avg_temp
(Hz)	(MPa)		(MPa)	(deg)	(C)	(Hz)	(MPa)		(MPa)	(deg)	(C)
14.993	0.296280	0.000218	1359.35	44.70	29.40	15.124	0.408125	0.000218	1868.34	38.74	29.96
9.872	0.236928	0.000199	1193.17	40.32	29.39	10.002	0.342376	0.000209	1639.62	38.72	29.96
4.914	0.177295	0.000204	869.35	45.71	29.37	4.984	0.275983	0.000222	1244.97	36.08	29.95
2.002	0.130066	0.000206	630.92	42.57	29.36	1.999	0.183341	0.000208	882.09	41.66	29.92
1	0.093435	0.000202	463.01	45.32	29.38	1	0.133679	0.000203	659.17	42.79	29.92
0.5	0.067430	0.000200	337.58	45.32	29.46	0.499	0.097225	0.000200	485.25	47.60	29.86
0.2	0.044788	0.000199	225.46	47.94	29.93	0.2	0.062911	0.000199	315.88	46.91	29.91
0.1	0.033761	0.000198	170.09	42.85	29.97	0.1	0.046247	0.000199	232.57	46.83	30.00
0.05	0.026347	0.000198	132.83	47.42	30.03	0.05	0.034620	0.000199	174.24	45.53	30.03
0.02	0.016989	0.000199	85.58	41.30	30.02	0.02	0.022494	0.000199	113.21	44.94	30.06
0.01	0.013379	0.000198	67.59	34.76	30.10	0.01	0.016485	0.000199	82.98	41.30	30.02

Table B.5: Flexural Frequency Sweep Test Results for Mix N Superpave Mix Design

freq	tensile_sts	tensile_stn	flex_E*	p_angle	avg_temp	freq	tensile_sts	tensile_stn	flex_E*	p_angle	avg_temp
(Hz)	(MPa)		(MPa)	(deg)	(C)	(Hz)	(MPa)		(MPa)	(deg)	(C)
15.162	0.504852	0.000099	5075.90	25.88	9.65	15.268	0.481624	0.000099	4855.54	27.78	9.68
10.053	0.470112	0.000100	4714.38	24.60	9.66	9.85	0.458995	0.000105	4361.56	23.94	9.61
4.985	0.431337	0.000110	3922.46	24.68	9.69	4.914	0.357651	0.000100	3577.72	28.35	9.66
1.979	0.336774	0.000107	3140.93	29.87	9.67	1.991	0.308105	0.000107	2877.50	30.56	9.64
1	0.252654	0.000102	2466.44	30.34	9.73	1	0.234378	0.000102	2302.71	31.20	9.66
0.5	0.198977	0.000101	1972.37	32.79	9.87	0.5	0.184336	0.000101	1832.78	33.06	9.65
0.2	0.143171	0.000100	1429.89	34.62	9.88	0.2	0.130041	0.000099	1310.31	36.12	9.71
0.1	0.109913	0.000100	1103.71	37.34	9.69	0.1	0.097927	0.000099	990.73	38.68	9.60
0.05	0.084868	0.000099	856.23	37.69	9.53	0.05	0.074232	0.000098	754.04	41.57	9.88
0.02	0.059423	0.000099	599.95	45.06	9.54	0.02	0.051877	0.000098	528.43	40.91	9.59
0.01	0.046216	0.000099	469.00	40.40	9.62	0.01	0.040197	0.000098	410.53	39.53	9.66
freq	tensile_sts	tensile_stn	flex_E*	p_angle	avg_temp	freq	tensile_sts	tensile_stn	flex_E*	p_angle	avg_temp
(Hz)	(MPa)		(MPa)	(deg)	(C)	(Hz)	(MPa)		(MPa)	(deg)	(C)
15.295	0.449724	0.000201	2237.91	41.43	19.80	14.988	0.481518	0.000224	2151.22	39.70	19.81
10.13	0.379296	0.000195	1943.31	43.96	19.77	10.001	0.392791	0.000209	1883.07	40.10	19.81
4.976	0.317991	0.000219	1453.13	37.69	19.73	4.905	0.292588	0.000217	1347.71	42.08	19.79
2.002	0.208232	0.000207	1006.24	41.45	19.72	2.001	0.205042	0.000208	984.44	42.19	19.78
1	0.150161	0.000201	746.07	43.19	19.73	1	0.148253	0.000203	730.97	43.72	19.80
0.5	0.109762	0.000199	550.73	43.95	19.75	0.5	0.107894	0.000201	537.47	44.14	19.79
0.2	0.072104	0.000198	363.66	43.77	19.73	0.2	0.070692	0.000199	354.43	43.26	19.80
0.1	0.054061	0.000198	273.15	44.86	19.69	0.1	0.051592	0.000199	259.32	44.01	19.82
0.05	0.037721	0.000198	190.73	44.88	19.76	0.05	0.037732	0.000199	189.82	41.47	19.69
0.014	0.003332	0.000198	16.87	104.18	19.70	0.02	0.026090	0.000199	131.14	41.68	19.64
0.01	0.020951	0.000198	105.95	43.21	19.74	0.01	0.019281	0.000199	97.09	38.43	19.65
freq	tensile_sts	tensile_stn	flex_E*	p_angle	avg_temp	freq	tensile_sts	tensile_stn	flex_E*	p_angle	avg_temp
(Hz)	(MPa)		(MPa)	(deg)	(C)	(Hz)	(MPa)		(MPa)	(deg)	(C)
15.334	0.134356	0.000187	717.43	59.93	30.29	14.971	0.134941	0.000221	610.62	53.64	30.14
10.05	0.129870	0.000213	611.15	51.87	30.31	9.973	0.114645	0.000217	529.18	49.23	30.32
5.001	0.097665	0.000216	451.20	49.62	30.31	5.037	0.080325	0.000195	412.27	49.71	30.34
2.006	0.060253	0.000205	293.69	43.55	30.31	1.994	0.055971	0.000207	270.73	50.39	30.30
1.003	0.043484	0.000200	217.04	43.60	30.31	1.002	0.042823	0.000202	211.62	40.91	30.35
0.499	0.032911	0.000199	165.53	45.97	30.26	0.5	0.033011	0.000201	164.64	39.06	30.24
0.201	0.021757	0.000198	109.83	35.18	30.18	0.199	0.022557	0.000200	113.03	47.06	30.32
0.1	0.016664	0.000198	84.27	38.06	30.29	0.099	0.017467	0.000200	87.47	46.99	30.32
0.05	0.014820	0.000198	74.94	41.39	30.29	0.05	0.015094	0.000199	75.72	36.29	30.28
0.02	0.010902	0.000198	55.13	49.11	30.31	0.02	0.011403	0.000199	57.28	31.96	30.30
0.01	0.009499	0.000198	48.08	36.95	30.30	0.008	0.003283	0.000199	16.48	96.12	30.34

B.2 Hveem Mix Designs

Table B.6: Flexural Frequency Sweep Test Results for Mix A Hveem Mix Design

freq	tensile_sts	tensile_stn	flex_E*	p_angle	avg_temp	freq	tensile_sts	tensile_stn	flex_E*	p_angle	avg_temp
(Hz)	(MPa)		(MPa)	(deg)	(C)	(Hz)	(MPa)		(MPa)	(deg)	(C)
15.142	1.211775	0.000100	12102.44	14.38	9.40	15.144	1.152806	0.000098	11772.93	14.64	9.74
9.997	1.184137	0.000101	11703.53	13.29	9.33	9.998	1.151318	0.000102	11330.17	13.45	9.69
5.015	1.072039	0.000099	10820.76	12.69	9.33	5.014	1.041172	0.000100	10430.13	13.21	9.72
2.001	0.977299	0.000102	9613.28	13.01	9.29	1.999	0.940945	0.000102	9229.82	13.45	9.70
1	0.879582	0.000101	8690.83	14.59	9.27	0.999	0.842331	0.000101	8305.96	14.92	9.72
0.499	0.791642	0.000100	7938.52	16.73	9.37	0.5	0.739954	0.000100	7389.93	16.71	9.60
0.2	0.635867	0.000099	6440.53	19.74	9.39	0.2	0.614785	0.000099	6200.59	19.09	9.68
0.1	0.536851	0.000098	5457.57	23.00	9.35	0.1	0.514289	0.000099	5204.38	22.29	9.74
0.05	0.447063	0.000098	4544.01	25.86	9.44	0.05	0.433802	0.000099	4384.13	25.49	9.63
0.02	0.358307	0.000099	3631.55	28.40	9.58	0.02	0.346515	0.000099	3494.53	28.05	9.46
0.01	0.295764	0.000099	2995.20	31.74	9.26	0.01	0.287676	0.000099	2899.64	30.84	9.58
freq	tensile_sts	tensile_stn	flex_E*	p_angle	avg_temp	freq	tensile_sts	tensile_stn	flex_E*	p_angle	avg_temp
(Hz)	(MPa)		(MPa)	(deg)	(C)	(Hz)	(MPa)		(MPa)	(deg)	(C)
15.175	0.755263	0.000099	7597.91	22.39	19.94	15.16	0.787187	0.000099	7966.75	21.16	19.42
10.012	0.712417	0.000100	7104.63	22.25	19.91	10.009	0.747628	0.000100	7439.23	20.95	19.46
5.067	0.598150	0.000096	6244.99	24.18	19.83	5.039	0.678208	0.000104	6525.63	21.09	19.47
1.986	0.532993	0.000105	5079.80	28.43	19.80	1.974	0.587779	0.000106	5556.85	27.07	19.45
0.997	0.414728	0.000102	4049.68	29.87	19.76	0.997	0.411667	0.000102	4023.72	29.87	19.76
0.498	0.334324	0.000100	3329.99	34.06	19.69	0.499	0.363213	0.000102	3556.57	32.92	19.45
0.2	0.226180	0.000099	2282.39	36.34	19.78	0.2	0.258621	0.000101	2571.32	35.55	19.47
0.1	0.174156	0.000099	1764.55	41.46	19.74	0.1	0.197740	0.000100	1977.40	39.56	19.58
0.05	0.125874	0.000099	1277.80	45.47	19.77	0.05	0.146199	0.000100	1463.88	42.85	19.51
0.02	0.085817	0.000098	876.09	46.46	19.83	0.02	0.101622	0.000099	1021.96	42.87	19.40
0.01	0.061789	0.000098	630.76	44.00	19.94	0.01	0.077046	0.000099	775.97	44.18	19.58
freq	tensile_sts	tensile_stn	flex_E*	p_angle	avg_temp	freq	tensile_sts	tensile_stn	flex_E*	p_angle	avg_temp
(Hz)	(MPa)		(MPa)	(deg)	(C)	(Hz)	(MPa)		(MPa)	(deg)	(C)
15.289	0.629426	0.000187	3361.15	38.96	29.95	15.304	0.526890	0.000190	2774.86	41.16	29.54
10.122	0.559274	0.000189	2954.58	41.78	30.05	9.885	0.482499	0.000204	2366.73	35.48	29.54
4.988	0.484808	0.000219	2210.86	37.22	29.99	4.993	0.337926	0.000184	1834.14	43.76	29.67
1.983	0.335801	0.000212	1581.62	44.96	29.95	2	0.260777	0.000208	1253.19	44.20	29.68
1	0.228068	0.000203	1125.19	44.55	30.00	1	0.185416	0.000202	916.53	45.95	29.81
0.5	0.166589	0.000201	829.86	46.03	29.98	0.5	0.134507	0.000200	672.86	46.24	29.84
0.2	0.111257	0.000199	557.88	49.51	30.01	0.2	0.087806	0.000199	441.89	49.46	29.89
0.1	0.078656	0.000199	394.77	51.54	29.97	0.1	0.064248	0.000198	323.81	51.92	29.98
0.05	0.057220	0.000199	287.39	48.32	29.95	0.05	0.046159	0.000198	232.99	50.11	30.04
0.02	0.039580	0.000199	198.96	45.46	29.95	0.02	0.029569	0.000198	149.23	47.06	30.10
0.01	0.029962	0.000199	150.85	49.17	29.99	0.01	0.024522	0.000198	123.82	49.75	30.00

Table B.7: Flexural Frequency Sweep Test Results for Mix B Hveem Mix Design

freq	tensile_sts	tensile_stn	flex_E*	p_angle	avg_temp	freq	tensile_sts	tensile_stn	flex_E*	p_angle	avg_temp
(Hz)	(MPa)		(MPa)	(deg)	(C)	(Hz)	(MPa)		(MPa)	(deg)	(C)
15.15	0.917901	0.000099	9299.55	15.77	9.67	15.149	0.923120	0.000099	9304.48	15.80	9.54
10.019	0.889826	0.000100	8931.31	14.06	9.66	10.003	0.888135	0.000100	8913.52	14.96	9.58
4.98	0.830396	0.000103	8081.32	14.07	9.75	5.004	0.846018	0.000104	8116.15	14.26	9.57
2	0.729465	0.000103	7105.28	14.65	9.78	1.999	0.731061	0.000103	7105.13	14.99	9.57
1	0.640852	0.000101	6348.18	16.07	9.49	1	0.640511	0.000101	6321.60	16.22	9.57
0.5	0.555303	0.000099	5605.96	17.47	9.73	0.5	0.555096	0.000100	5550.23	17.65	9.58
0.2	0.459111	0.000098	4678.10	20.12	9.80	0.2	0.457632	0.000099	4616.27	20.30	9.63
0.1	0.380342	0.000098	3889.86	22.84	9.77	0.1	0.380077	0.000099	3849.44	22.95	9.61
0.05	0.320877	0.000098	3274.58	26.42	9.81	0.05	0.320473	0.000099	3235.12	26.15	9.64
0.02	0.254495	0.000098	2589.29	28.55	9.52	0.02	0.257249	0.000099	2597.04	27.68	9.50
0.01	0.211777	0.000098	2164.30	30.24	9.62	0.01	0.215934	0.000099	2185.08	30.17	9.52
freq	tensile_sts	tensile_stn	flex_E*	p_angle	avg_temp	freq	tensile_sts	tensile_stn	flex_E*	p_angle	avg_temp
(Hz)	(MPa)		(MPa)	(deg)	(C)	(Hz)	(MPa)		(MPa)	(deg)	(C)
15.165	0.632275	0.000103	6110.70	22.94	19.87	15.198	0.541883	0.000100	5431.94	24.95	19.61
10.095	0.529891	0.000093	5678.55	24.51	19.79	9.874	0.509265	0.000103	4965.91	22.37	19.62
4.973	0.454634	0.000095	4778.26	23.20	19.77	4.967	0.403724	0.000096	4206.59	26.28	19.64
1.989	0.426172	0.000105	4040.62	27.70	19.78	100.044	0.380820	0.000109	3497.52	161.47	19.68
1.001	0.324301	0.000102	3180.27	26.64	19.77	1	0.270900	0.000103	2633.46	30.67	19.66
0.498	0.271880	0.000100	2720.61	31.08	19.76	0.499	0.219098	0.000101	2175.13	34.67	19.74
0.2	0.185143	0.000099	1870.23	32.52	19.76	0.2	0.152227	0.000100	1516.86	36.43	19.66
0.1	0.146774	0.000099	1486.92	39.05	19.76	0.1	0.113693	0.000099	1142.77	41.81	19.65
0.05	0.111980	0.000098	1140.52	38.87	19.81	0.05	0.084732	0.000099	853.54	40.52	19.68
0.02	0.077418	0.000098	790.30	44.97	19.81	0.02	0.056766	0.000099	573.05	42.04	19.72
0.01	0.057912	0.000098	591.21	42.17	19.69	0.01	0.043166	0.000099	436.21	44.34	19.77
freq	tensile_sts	tensile_stn	flex_E*	p_angle	avg_temp	freq	tensile_sts	tensile_stn	flex_E*	p_angle	avg_temp
(Hz)	(MPa)		(MPa)	(deg)	(C)	(Hz)	(MPa)		(MPa)	(deg)	(C)
15.184	0.437325	0.000215	2031.12	38.22	30.57	14.969	0.360350	0.000215	1679.17	40.67	29.61
10.068	0.361771	0.000201	1796.85	39.08	30.53	10.13	0.282709	0.000189	1499.53	43.71	29.51
5.093	0.262407	0.000182	1442.89	40.93	30.62	4.982	0.244588	0.000219	1116.60	38.23	29.44
2.001	0.204226	0.000207	988.06	39.07	30.66	2.002	0.159182	0.000206	772.60	42.22	29.36
1	0.153708	0.000202	762.67	40.61	30.80	0.999	0.118215	0.000201	587.64	45.04	29.38
0.5	0.116862	0.000200	585.67	41.22	30.79	0.5	0.088101	0.000200	441.35	44.05	29.37
0.2	0.079876	0.000199	401.81	40.75	30.81	0.2	0.060591	0.000199	304.95	41.51	29.54
0.1	0.061688	0.000198	311.53	44.68	30.81	0.1	0.045766	0.000198	230.63	43.67	29.82
0.05	0.046256	0.000198	233.52	47.28	30.82	0.05	0.036403	0.000198	183.46	44.70	30.06
0.02	0.032941	0.000198	166.20	33.35	30.99	0.02	0.026182	0.000198	132.12	42.08	30.03
0.01	0.026797	0.000198	135.46	45.28	30.96	0.01	0.021401	0.000198	108.24	37.12	30.07

Table B.8: Flexural Frequency Sweep Test Results for Mix I Hveem Mix Design

freq	tensile_sts	tensile_stn	flex_E*	p_angle	avg_temp	freq	tensile_sts	tensile_stn	flex_E*	p_angle	avg_temp
(Hz)	(MPa)		(MPa)	(deg)	(C)	(Hz)	(MPa)		(MPa)	(deg)	(C)
15.238	0.694341	0.000102	6795.932	17.425	9.551	15.238	0.74244	0.000103	7181.356	17.159	9.244
10.021	0.683731	0.000106	6471.279	16.145	9.518	10.018	0.671155	0.000098	6830.776	16.749	9.232
4.998	0.59291	0.000101	5847.061	16.462	9.554	5.016	0.648441	0.000104	6231.697	15.021	9.214
1.996	0.527713	0.000105	5028.215	16.455	9.551	1.993	0.558492	0.000103	5414.029	16.609	9.14
0.997	0.465952	0.000103	4542.191	19.067	9.507	1	0.479998	0.000101	4760.155	17.08	9.222
0.5	0.388966	0.000101	3863.243	20.562	9.53	0.5	0.415943	0.0001	4168.752	18.497	9.208
0.2	0.311452	0.0001	3121.346	22.4	9.486	0.2	0.339389	0.000099	3439.466	21.181	9.179
0.1	0.256502	0.000099	2578.255	25.461	9.465	0.1	0.28104	0.000098	2857.755	23.873	9.17
0.05	0.212323	0.000099	2135.994	28.823	9.439	0.05	0.233428	0.000098	2375.02	25.583	9.274
0.02	0.164734	0.000099	1666.054	31.527	9.435	0.02	0.188549	0.000098	1915.886	28.83	9.261
0.01	0.136585	0.000099	1380.564	31.774	9.433	0.01	0.153188	0.000098	1567.864	30.652	9.209
freq	tensile_sts	tensile_stn	flex_E*	p_angle	avg_temp	freq	tensile_sts	tensile_stn	flex_E*	p_angle	avg_temp
(Hz)	(MPa)		(MPa)	(deg)	(C)	(Hz)	(MPa)		(MPa)	(deg)	(C)
15.313	0.481059	0.0001	4821.124	24.399	19.476	15.247	0.458968	0.000099	4626.226	24.092	19.547
9.977	0.458294	0.000103	4455.546	20.562	19.517	10.089	0.428939	0.000098	4355.56	23.521	19.596
4.946	0.388896	0.000105	3688.681	23.538	19.502	5.108	0.377995	0.000097	3902.35	26.215	19.592
1.998	0.326175	0.000106	3080.104	26.597	19.507	1.999	0.311253	0.000106	2942.807	24.844	19.574
1	0.25508	0.000102	2510.092	26.335	19.491	0.999	0.246529	0.000101	2431.55	27.601	19.506
0.5	0.203655	0.0001	2035.329	28.887	19.379	0.5	0.197601	0.0001	1976.674	29.315	19.476
0.2	0.152279	0.000099	1544.204	32.243	19.428	0.2	0.146972	0.000099	1489.703	32.336	19.508
0.1	0.11794	0.000098	1199.447	35.25	19.412	0.1	0.11105	0.000098	1132.153	34.76	19.517
0.05	0.090202	0.000098	918.731	37.181	19.399	0.05	0.087149	0.000098	890.998	36.592	19.559
0.02	0.063403	0.000098	645.545	37.788	19.34	0.02	0.061191	0.000098	626.972	42.201	19.509
0.01	0.047688	0.000098	487.24	37.998	19.39	0.01	0.045869	0.000097	471.454	40.013	19.578
freq	tensile_sts	tensile_stn	flex_E*	p_angle	avg_temp	freq	tensile_sts	tensile_stn	flex_E*	p_angle	avg_temp
(Hz)	(MPa)		(MPa)	(deg)	(C)	(Hz)	(MPa)		(MPa)	(deg)	(C)
15.087	0.349044	0.000205	1704.46	40.649	29.507	15.114	0.414518	0.000209	1985.862	35.911	30.155
10.004	0.321397	0.000207	1551.186	38.203	29.457	9.972	0.363682	0.000208	1747.321	33.098	30.126
4.982	0.2573	0.000216	1190.903	35.589	29.472	4.987	0.295212	0.000213	1383.439	32.896	30.065
2.002	0.172369	0.000207	834.003	39.343	29.481	2.001	0.205172	0.000208	985.565	37.774	30.116
1	0.129808	0.000202	643.027	40.931	29.475	1.001	0.156254	0.000203	770.903	39.038	30.122
0.5	0.095866	0.0002	479.005	42.383	29.503	0.5	0.117843	0.000201	587.497	40.084	30.065
0.2	0.066363	0.000199	333.712	44.421	29.74	0.2	0.079679	0.0002	399.376	43.88	30.121
0.1	0.049677	0.000198	250.282	45.858	29.92	0.1	0.059705	0.000199	299.789	46.86	30.179
0.05	0.038424	0.000198	193.733	44.386	30.196	0.05	0.047548	0.000199	239.036	46.67	30.192
0.02	0.026847	0.000198	135.47	35.22	30.214	0.02	0.032661	0.000199	164.249	42.631	30.235
0.01	0.019488	0.000198	98.378	44.361	30.151	0.01	0.025796	0.000199	129.722	44.72	30.185

APPENDIX C: REPEATED SHEAR CONSTANT HEIGHT TEST DATA

C.1 Superpave Mix Designs

Table C.1: Repeated Shear Constant Height Test Results for Mix A Superpave Mix Design

Mix	Binder Type/ Grade	Aggregate Type	NMAS	Testing Parameters	Specimen Name	AV (%)	AC (%)	Test Temp. (C)	Test Shear Stress Level (kPa)	Initial Resilient Shear Modulus (kPa)	Permanent Shear Strain at 5,000 cycles	Cycles to 5% Permanent Shear Strain	Int or Ext
A	PG 64-16	Alluvial	3/4	70kPa 45C	3-B1	2.6	5.5	44.64	70.06	180	3.26	23,439	Int
					3-B7	2.6	5.5	45.11	70.38	151	4.82	5,700	Int
					4-B11	2.8	5.5	44.53	70.55	170	4.00	12,295	Int
				100kPa 45C	3-B4	2.5	5.5	44.80	100.21	120	4.96	5,201	Int
					4-B7	2.5	5.5	44.91	101.50	148	4.13	9,500	Int
					5-B2	2.9	5.5	44.76	102.03	173	3.18	45,524	Ext
				130kPa 45C	3-B11	2.6	5.5	44.28	129.04	182	n/a	4,829	Ext
					4-B4	2.5	5.5	44.82	129.46	168	4.26	9,798	Int
					4-B10	2.8	5.5	44.39	129.57	189	5.11	4,635	Int
				70kPa 55C	3-B2	2.5	5.5	54.21	70.79	60	n/a	1,782	Int
					3-B6	2.6	5.5	54.54	70.53	62	n/a	1,102	Int
					4-B2	2.9	5.5	55.35	70.62	61	n/a	3,854	Int
				100kPa 55C	4-B8	2.5	5.5	54.94	101.56	78	n/a	854	Int
					4-B9	2.5	5.5	54.16	102.37	62	n/a	1,223	Int
					5-B10	2.6	5.5	54.58	102.11	61	n/a	1,539	Int
				130kPa 55c	3-B9	2.7	5.5	54.30	128.81	50	n/a	426	Int
					4-B6	2.5	5.5	54.28	129.80	76	n/a	507	Int
					5-B7	2.5	5.5	54.92	130.01	68	n/a	624	Int

Table C.2: Repeated Shear Constant Height Test Results for Mix B Superpave Mix Design

Mix	Binder Type/ Grade	Aggregate Type	NMAS	Testing Parameters	Specimen Name	AV (%)	AC (%)	Test Temp. (C)	Test Shear Stress Level (kPa)	Initial Resilient Shear Modulus (kPa)	Permanent Shear Strain at 5,000 cycles	Cycles to 5% Permanent Shear Strain	Int or Ext
B	PG 64-16	Basalt	3/4	70kPa 45C	2-B#3	3.4	6.3	44.65	69.29	177	1.96	663,777	Ext
					2-B#1	3.5	6.3	44.46	68.59	161	2.14	252,612	Ext
					1-B#10	3.5	6.3	44.21	69.85	159	2.72	174,147	Ext
				100kPa 45C	2-B#9	2.6	6.3	44.49	98.00	180	3.20	27,047	Int
					1-B#3	3.5	6.3	45.47	99.16	151	3.54	19,467	Int
					2-B#8	3.5	6.3	44.49	97.67	166	3.41	14,928	Int
				130kPa 45C	2-B#10	2.6	6.3	44.47	126.24	157	4.45	7,292	Int
					2-B#7	3.4	6.3	44.92	125.40	146	4.66	6,288	Int
					1-B#4	3.5	6.3	44.71	125.14	169	3.88	12,716	Int
				70kPa 55C	2-B#2	3.3	6.3	55.39	70.47	79	3.89	10,773	Int
					1-B#11	3.3	6.3	55.15	70.58	71	4.27	8,750	Int
					1-B#8	3.0	6.3	55.05	70.80	60	4.67	6,329	Int
				100kPa 55C	2-B#6	2.9	6.3	55.69	100.69	71	n/a	1,486	Int
					1-B#7	3.2	6.3	55.41	100.64	70	n/a	1,662	Int
					1-B#5	3.2	6.3	54.66	101.01	74	n/a	879	Int
				130kPa 55c	2-B#11	2.7	6.3	54.76	128.30	70	n/a	387	Int
					1-B#2	3.4	6.3	54.35	128.08	85	n/a	654	Int
					1-B#1	3.3	6.3	55.83	128.15	71	n/a	1,369	Int

Table C.3: Repeated Shear Constant Height Test Results for Mix I Superpave Mix Design

Mix	Binder Type/ Grade	Aggregate Type	NMAS	Testing Parameters	Specimen Name	AV (%)	AC (%)	Test Temp. (C)	Test Shear Stress Level (kPa)	Initial Resilient Shear Modulus (kPa)	Permanent Shear Strain at 5,000 cycles	Cycles to 5% Permanent Shear Strain	Int or Ext
I	PG 64-16 RB	Basalt	1/2	70kPa 45C	2-B1	3.4	8.3	44.90	68.09	161	2.74	116,660	Ext
					2-B6	3.4	8.3	44.64	67.71	142	2.62	311,637	Ext
					1-B3	3.4	8.3	44.87	66.31	188	2.49	138,537	Ext
				100kPa 45C	2-B9	3.1	8.3	45.03	98.87	166	3.51	25,917	Int
					1-B5	3.5	8.3	45.20	100.17	139	4.11	12,640	Int
					2-B5	3.5	8.3	45.44	99.92	133	5.06	4,664	Int
				130kPa 45C	1-B7	3.4	8.3	45.12	127.14	155	4.44	8,555	Int
					2-B3	3.4	8.3	44.87	127.97	157	4.11	11,157	Int
					2-B4	3.1	8.3	45.53	128.47	147	4.69	7,092	Int
				70kPa 55C	1-B2	3.3	8.3	55.09	70.61	66	5.64	2,879	Int
					1-B1	3.5	8.3	55.67	70.46	52	4.62	6,877	Int
					2-B7	3.3	8.3	55.01	70.54	72	6.00	2,553	Int
				100kPa 55C	1-B11	3.2	8.3	54.56	100.94	77	n/a	961	Int
					2-B8	3.2	8.3	55.57	101.12	68	n/a	409	Int
					1-B6	3.2	8.3	55.74	100.79	70	n/a	571	Int
				130kPa 55c	2-B10	3.3	8.3	54.47	128.56	76	n/a	977	Int
					1-B10	3.4	8.3	54.58	128.18	78	n/a	607	Int
					2-B11	3.4	8.3	54.73	128.50	81	n/a	941	Int

Table C.4: Repeated Shear Constant Height Test Results for Mix J Superpave Mix Design

Mix	Binder Type/ Grade	Aggregate Type	NMAS	Testing Parameters	Specimen Name	AV (%)	AC (%)	Test Temp. (C)	Test Shear Stress Level (kPa)	Initial Resilient Shear Modulus (kPa)	Permanent Shear Strain at 5,000 cycles	Cycles to 5% Permanent Shear Strain	Int or Ext
J	PG 64-16 RB	Granite	3/4	70kPa 45C	1-11B	3.3	8.8	45.18	68.23	117	3.48	43,092	Ext
					3-6B	3.1	8.8	45.13	68.38	128	3.51	42,518	Ext
					3-9B	3.5	8.8	45.11	68.54	105	4.14	11,854	Int
				100kPa 45C	1-3B	3.3	8.8	45.81	99.95	149	3.69	15,492	Int
					3-2B	3.3	8.8	45.57	100.16	125	5.02	4,813	Int
					3-3B	3.0	8.8	45.48	100.59	116	4.81	5,942	Int
				130kPa 45C	1-7B	3.4	8.8	45.19	127.72	123	5.94	2,413	Int
					2-3B	3.0	8.8	44.89	127.30	132	4.73	6,724	Int
					2-5B	3.2	8.8	45.34	127.10	120	5.15	4,201	Int
				70kPa 55C	2-1B	2.7	8.8	54.62	70.78	64	4.15	14,490	Int
					3-4B	3.2	8.8	55.33	70.55	58	5.60	3,055	Int
					3-1B	3.2	8.8	55.37	70.76	56	4.23	12,198	Int
				100kPa 55C	1-1B	3.0	8.8	55.32	100.01	58	n/a	1,053	Int
					1-4B	3.5	8.8	55.08	100.45	63	n/a	315	Int
					2-2B	3.2	8.8	55.37	100.48	63	n/a	970	Int
				130kPa 55c	1-2B	3.1	8.8	55.74	128.36	79	n/a	1,017	Int
					1-6B	3.3	8.8	55.83	127.28	62	n/a	237	Int
					2-6B	3.1	8.8	54.91	128.14	66	n/a	388	Int

Table C.5: Repeated Shear Constant Height Test Results for Mix N Superpave Mix Design

Mix	Binder Type/ Grade	Aggregate Type	NMAS	Testing Parameters	Specimen Name	AV (%)	AC (%)	Test Temp. (C)	Test Shear Stress Level (kPa)	Initial Resilient Shear Modulus (kPa)	Permanent Shear Strain at 5,000 cycles	Cycles to 5% Permanent Shear Strain	Int or Ext
N	PG 64-28 PM	Granite	1	70kPa 45C	1B4	3.5	6.4	44.76	70.78	78	2.18	538,770	Ext
					3B9	2.5	6.4	44.80	70.84	63	3.70	22,116	Int
					4B10	3.4	6.4	44.94	70.45	45	1.43	131,034	Ext
				100kPa 45C	3B7	2.6	6.4	44.86	101.22	59	4.39	9,150	Int
					3B8	2.7	6.4	44.79	101.12	54	4.73	6,333	Int
					5B11	2.6	6.4	44.74	100.90	66	4.08	13,078	Int
				130kPa 45C	3B2	3.4	6.4	44.88	128.70	64	4.98	5,302	Int
					5B6	3.1	6.4	44.82	128.19	58	5.32	3,759	Int
					5B10	2.7	6.4	45.33	128.18	64	7.03	1,328	Int
				70kPa 55C	1B1	3.0	6.4	54.85	70.50	42	4.68	6,924	Int
					5B2	2.8	6.4	54.87	70.31	35	4.15	12,727	Int
					5B7	3.3	6.4	55.09	70.12	34	4.99	5,043	Int
				100kPa 55C	2B6		6.4	54.58	98.79	35	N/A	102	Int
					5B8	2.7	6.4	54.50	99.84	33	N/A	1,144	Int
					4B1	3.5	6.4	55.13	100.06	44	N/A	249	Int
				130kPa 55c	1B2	2.7	6.4	55.53	127.69	53	N/A	602	Int
					3B3	2.9	6.4	54.16	127.27	44	N/A	396	Int
					4B6		6.4	55.45	125.92	48	N/A	84	Int

Table C.6: Average RSCH Results at 70, 100, and 130 kPa for Mix A

Mix	Binder Type/ Grade	Aggregate Type	NMAS	AC %	Average *Cycle5PSS*	Repetition to 5% Shear Strain	PSS @ 5,000 Cycles %	G @ 100 Cycle (MPa)
A	PG 64-16	Alluvial	3/4	5.5	70 kPa; 45°C	13,811	4.03	167
					100 kPa; 45°C	20,075	4.09	147
					130 kPa; 45°C	6,421	4.69	179
					70 kPa; 55°C	2,246	N/A*	61
					100 kPa; 55°C	1,205	N/A*	67
					130 kPa; 55°C	519	N/A*	65

* Specimen failed (reached 5% permanent shear strain, PSS) before 5,000 cycles.

Table C.7: Average RSCH Results at 70, 100, and 130 kPa for Mix B

Mix	Binder Type/ Grade	Aggregate Type	NMAS	AC %	Average *Cycle5PSS*	Repetition to 5% Shear Strain	PSS @ 5,000 Cycles %	G @ 100 Cycle (MPa)
B	PG 64-16	Basalt	3/4	6.3	70 kPa; 45°C	363,512	2.27	166
					100 kPa; 45°C	20,481	3.38	166
					130 kPa; 45°C	8,765	4.33	157
					70 kPa; 55°C	8,618	4.28	70
					100 kPa; 55°C	1,342	N/A*	72
					130 kPa; 55°C	803	N/A*	75

* Specimen failed (reached 5% permanent shear strain, PSS) before 5,000 cycles.

Table C.8: Average RSCH Results at 70, 100, and 130 kPa for Mix I

Mix	Binder Type/ Grade	Aggregate Type	NMAS	AC %	Average *Cycle5PSS*	Repetition to 5% Shear Strain	PSS @ 5,000 Cycles %	G @ 100 Cycle (MPa)
I	PG 64-16 RB	Basalt	1/2	8.3	70 kPa; 45°C	188,945	2.62	164
					100 kPa; 45°C	14,407	4.23	146
					130 kPa; 45°C	8,935	4.41	153
					70 kPa; 55°C	4,103	5.42	63
					100 kPa; 55°C	647	N/A*	72
					130 kPa; 55°C	842	N/A*	78

* Specimen failed (reached 5% permanent shear strain, PSS) before 5,000 cycles.

Table C.9: Average RSCH Results at 70, 100, and 130 kPa for Mix J

Mix	Binder Type/ Grade	Aggregate Type	NMAS	AC %	Average *Cycle5PSS*	Repetition to 5% Shear Strain	PSS @ 5,000 Cycles %	G @ 100 Cycle (MPa)
J	PG 64-16 RB	Granite	3/4	8.8	70 kPa; 45°C	32,488	3.71	117
					100 kPa; 45°C	8,749	4.51	130
					130 kPa; 45°C	4,446	5.27	125
					70 kPa; 55°C	9,914	4.66	60
					100 kPa; 55°C	779	N/A*	61
					130 kPa; 55°C	547	N/A*	69

* Specimen failed (reached 5% permanent shear strain, PSS) before 5,000 cycles.

Table C.10: Average RSCH Results at 70, 100, and 130 kPa for Mix N

Mix	Binder Type/ Grade	Aggregate Type	NMAS	AC %	Average *Cycle5PSS*	Repetition to 5% Shear Strain	PSS @ 5,000 Cycles %	G @ 100 Cycle (MPa)
N	PG 64-28 PM	Granite	1	6.4	70 kPa; 45°C	230,640	2.44	62
					100 kPa; 45°C	9,520	4.40	59
					130 kPa; 45°C	3,463	5.77	62
					70 kPa; 55°C	8,231	N/A*	37
					100 kPa; 55°C	498	N/A*	37
					130 kPa; 55°C	361	N/A*	48

* Specimen failed (reached 5% permanent shear strain, PSS) before 5,000 cycles.

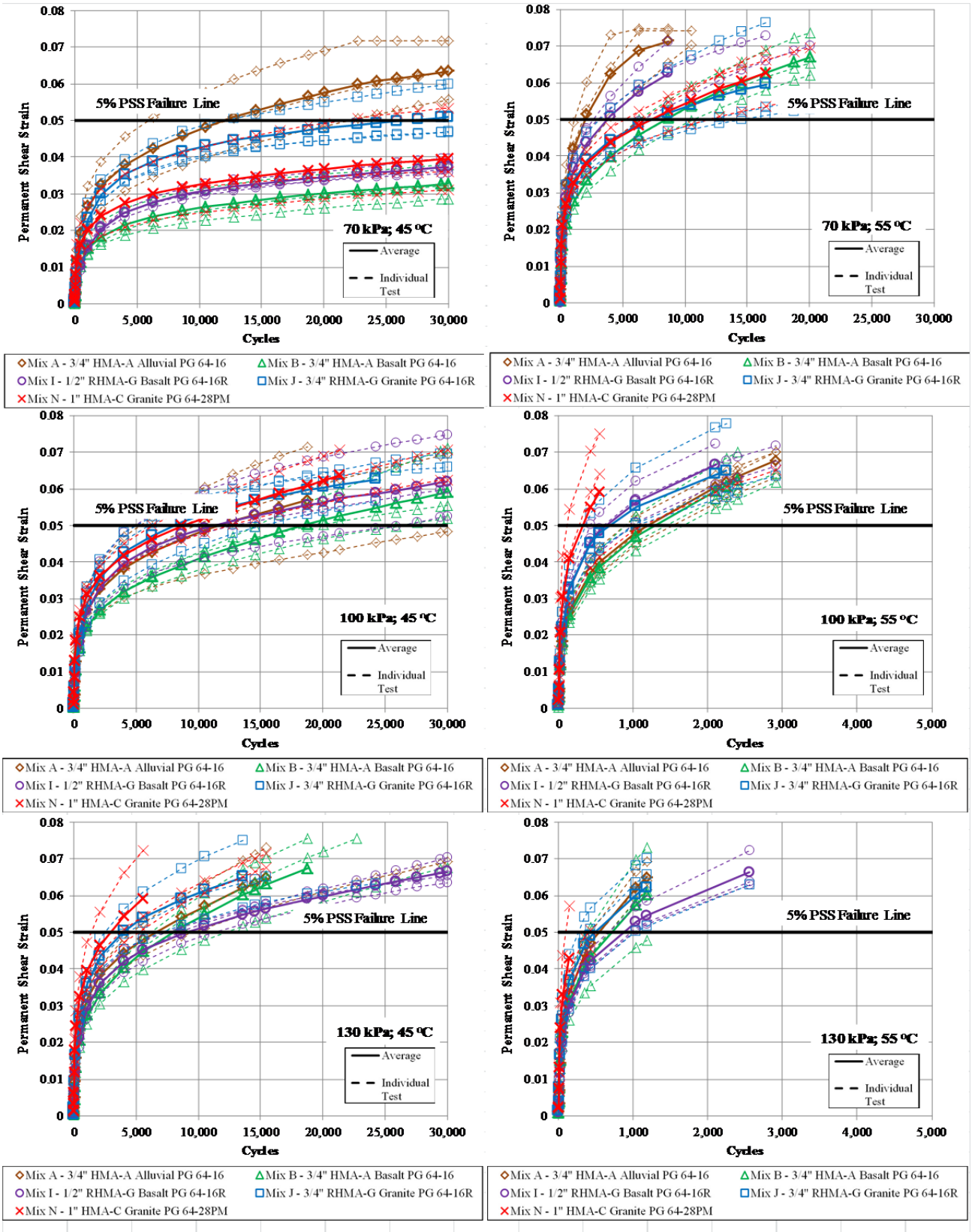

Figure C.1: Permanent shear strain versus cycles (individual RSCH tests with mix averages 70, 100, and 130 kPa at 45°C and 55°C).

C.2 Hveem Mix Designs

Table C.11: Repeated Shear Constant Height Test Results for Mix A Hveem Mix Design

Mix	Binder Type/ Grade	Aggregate Type	NMAS	Testing Parameters	Specimen Name	AV (%)	AC (%)	Test Temp. (C)	Test Shear Stress Level (kPa)	Initial Resilient Shear Modulus (kPa)	Permanent Shear Strain at 5,000 cycles (%)	Cycles to 5% Permanent Shear Strain	Int or Ext
A	PG 64-16	Alluvial	3/4	100kPa 45C	2c2	2.8	5.0	44.89	97.87	355	2.18	420,386	Ext
					3c1	3.3	5.0	45.40	99.23	280	1.31	46,404,069	Ext
					3c3	3.4	5.0	44.84	96.84	292	1.08	694,025,604	Ext
				100kPa 55C	2c1	2.8	5.0	55.00	100.79	119	2.78	26,114	Int
					2c3	2.6	5.0	54.86	101.09	137	3.47	11,283	Int
					3c2	3.2	5.0	56.70	100.49	86	4.16	8,834	Int

Table C.12: Repeated Shear Constant Height Test Results for Mix B Hveem Mix Design

Mix	Binder Type/ Grade	Aggregate Type	NMAS	Testing Parameters	Specimen Name	AV (%)	AC (%)	Test Temp. (C)	Test Shear Stress Level (kPa)	Initial Resilient Shear Modulus (kPa)	Permanent Shear Strain at 5,000 cycles (%)	Cycles to 5% Permanent Shear Strain	Int or Ext
B	PG 64-16	Basalt	3/4	100kPa 45C	2d1	3.4	5.2	44.79	100.21	283	1.77	1,034,777,121	Ext
					4d2	3.5	5.2	44.79	98.24	334	2.08	3,205,830	Ext
					4B3	3.5	5.2	44.92	98.51	330	1.56	6,959,581	Ext
				100kPa 55C	2d3	3.4	5.2	55.50	100.24	103	3.32	19,442	Int
					3d3d	3.1	5.2	55.88	100.20	98	5.25	4,080	Int
					3dd1	3.5	5.2	54.70	100.91	131	3.56	23,847	Int

Table C.13: Repeated Shear Constant Height Test Results for Mix J Hveem Mix Design

Mix	Binder Type/ Grade	Aggregate Type	NMAS	Testing Parameters	Specimen Name	AV (%)	AC (%)	Test Temp. (C)	Test Shear Stress Level (kPa)	Initial Resilient Shear Modulus (kPa)	Permanent Shear Strain at 5,000 cycles (%)	Cycles to 5% Permanent Shear Strain	Int or Ext
J	PG 64-16 RB	Granite	3/4	100kPa 45C	4B6	4.8	7.2	44.94	100.41	160	1.57	10,036,193	Ext
					4b10	5.2	7.2	44.95	100.98	171	1.72	13,884,399	Ext
					41b	4.9	7.2	45.29	98.15	206	2.09	1,200,856	Ext
				100kPa 55C	4b2	5.2	7.2	55.17	100.77	78	3.80	12,322	Int
					4b5	5.0	7.2	55.09	101.27	78	4.43	8,344	Int

Table C.14: Repeated Shear Constant Height Test Results for Mix N Hveem Mix Design

Mix	Binder Type/ Grade	Aggregate Type	NMAS	Testing Parameters	Specimen Name	AV (%)	AC (%)	Test Temp. (C)	Test Shear Stress Level (kPa)	Initial Resilient Shear Modulus (kPa)	Permanent Shear Strain at 5,000 cycles (%)	Cycles to 5% Permanent Shear Strain	Int or Ext
N	PG 64-28 PM	Granite	1	100kPa 45C	1b6	4.7	5.0	44.96	100.33	81	3.59	20,013	Int
					1B2	4.8	5.0	45.06	99.90	61	3.56	24,271	Int
					1b4	4.9	5.0	45.17	100.14	56	3.63	17,810	Int
				100kPa 55C	1b5	5.1	5.0	55.11	98.89	52	N/A	583	Int
					1b9	5.0	5.0	55.06	99.38	40	6.56	1,628	Int
					1b10	5.2	5.0	55.05	99.49	25	5.03	4,817	Int

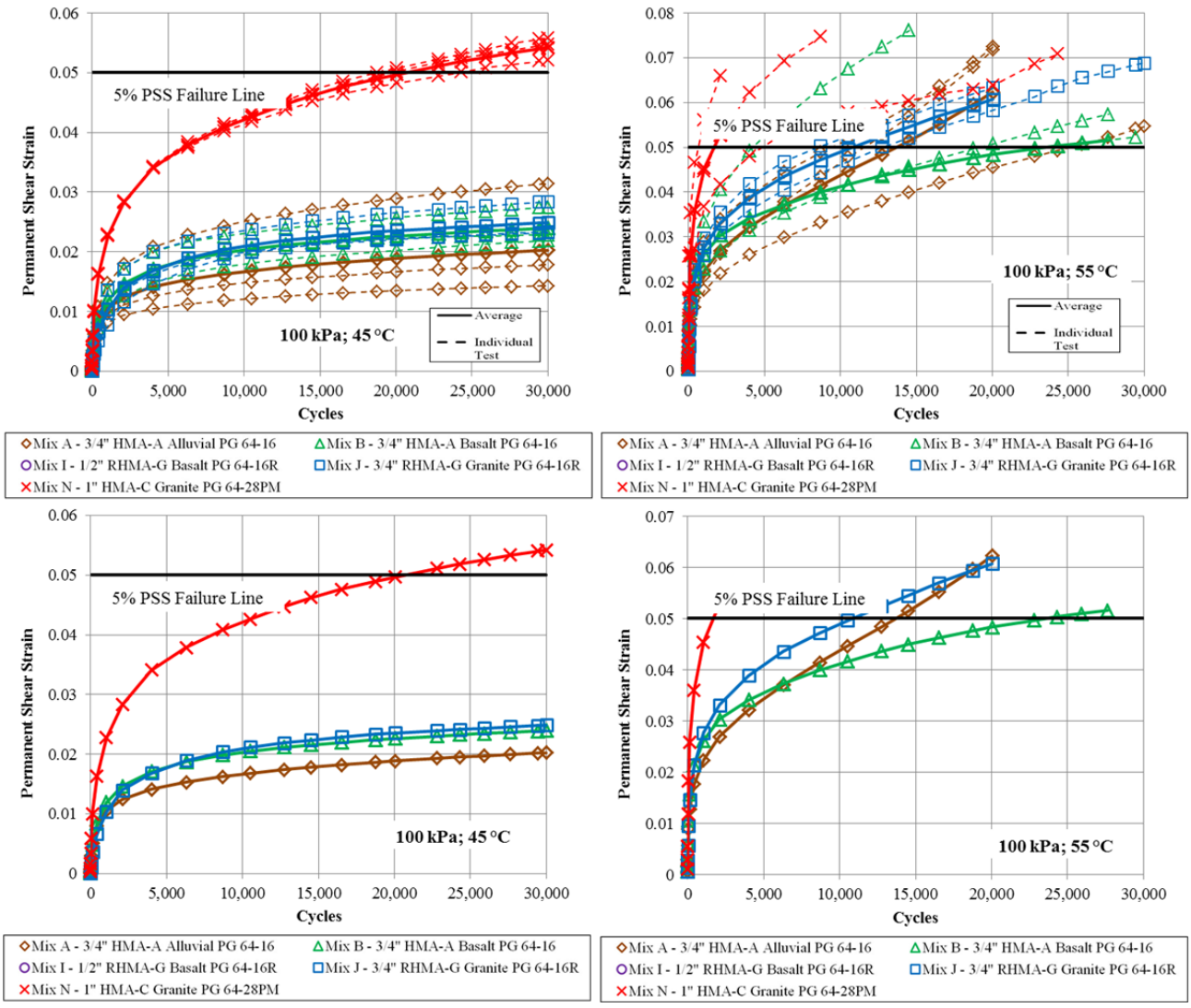

Figure C.2: Hveem mix design permanent shear strain versus cycles (RSCH tests with mix averages 100 kPa in 45°C and 55°C).

APPENDIX D: REPEATED LOAD TRIAXIAL TEST DATA

Table D.1: AMPT RLT Test Results for Mix A

Mix Type	AC %	Testing Parameters	Specimen ID	AV (%)	AC (%)	Confining Stress (psi)	Cycles to 5% Permanent Axial Strain	Permanent Axial Strain @ x Cycles	
								N=5,000	N=10,000
Mix A - 3/4" HMA-A Alluvial PG 64-16	5.5	45°C, Confined	3.1803-AMPT-P001-5.5-#5	6.7	5.5	10	1,650,665	0.014552	0.017278
			3.1803-AMPT-P001-5.5-#6	6.9	5.5	10	29,860,625,283	0.01248	0.013595
			3.1803-AMPT-P001-5.5-#7	7.1	5.5	10	1,862,590	0.015481	0.018138
		55°C, Confined	3.1803-AMPT-P001-5.5-#16	6.9	5.5	10	105,028	0.023216	0.02825
			3.1803-AMPT-P001-5.5-#19	6.2	5.5	10	79,556	0.025561	0.03075
			3.1803-AMPT-P001-5.5-#22	6.8	5.5	10	240,663	0.02171	0.025605
		45°C, Unconfined	3.1803-AMPT-P001-5.5-#10	6.9	5.5	0	1,556		
			3.1803-AMPT-P001-5.5-#11	7.3	5.5	0	1,599		
			3.1803-AMPT-P001-5.5-#12	6.6	5.5	0	1,323		
		55°C, Unconfined	3.1803-AMPT-P001-5.5-#13	7.1	5.5	0	332		
			3.1803-AMPT-P001-5.5-#14	6.8	5.5	0	282		
			3.1803-AMPT-P001-5.5-#15	6.5	5.5	0	262		

Table D.2: Average RLT Results for Mix A

Mix	Binder Type/ Grade	Aggregate Type	NMAS	AC%	Test Condition	Flow Number	Repetition to 5% PAS	PAS% @ 5,000 Cycles	PAS% @ 10,000 Cycles
A	PG 64-16	Alluvial	3/4	5.5	Confined; 45°C	N/A*	9.95E+09	1.42	1.63
					Confined; 55°C	N/A*	1.42E+05	2.35	2.82
					Unconfined; 45°C	592	1,493	N/A**	N/A**
					Unconfined; 55°C	126	292	N/A**	N/A**

N/A*No tertiary flow observed within 20,000 cycles.
N/A** Specimen failed (reached 5% permanent axial strain, PAS) before 5,000 cycles.

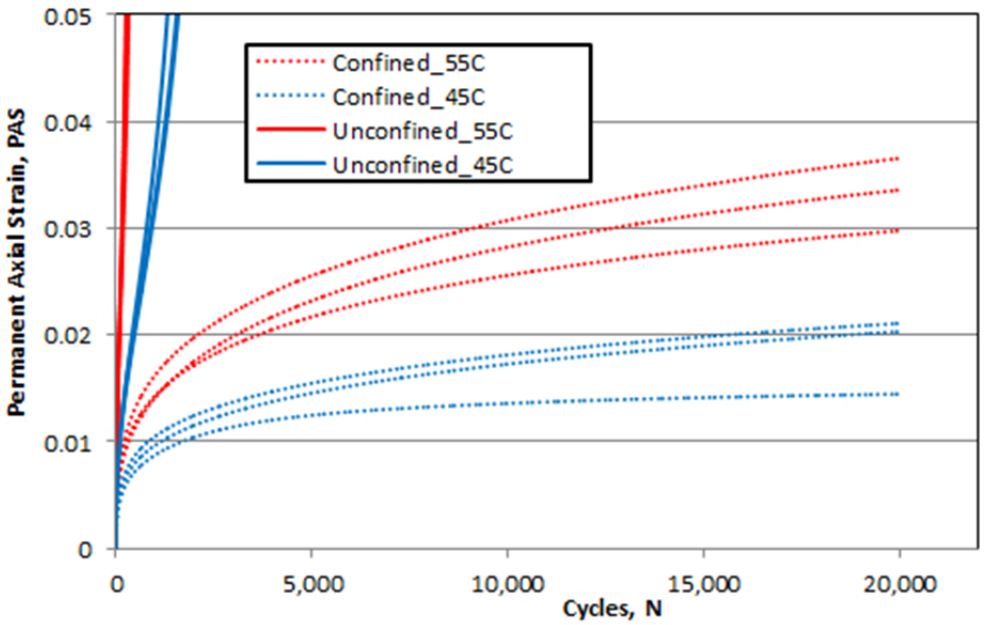

Figure D.1: Permanent axial deformation versus cycles for Mix A.

Table D.3: AMPT RLT Test Results for Mix B

Mix Type	AC %	Testing Parameters	Specimen ID	AV (%)	AC (%)	Confining Stress (psi)	Cycles to 5% Permanent Axial Strain	Permanent Axial Strain @ x Cycles	
								N=5,000	N=10,000
S410 Mix B - 3/4'' HMA-A Basalt PG 64-16	6.3	45°C, Confined	3.1803-AMPT-S410-6.3-#1	6.5	6.3	10	3,454,026	0.0138	0.016185
			3.1803-AMPT-S410-6.3-#2	6.7	6.3	10	2,795,167	0.013494	0.015952
			3.1803-AMPT-S410-6.3-#7	7.0	6.3	10	636,825	0.017156	0.020495
		55°C, Confined	3.1803-AMPT-S410-6.3-#20	7.1	6.3	10	508,636	0.020594	0.023928
			3.1803-AMPT-S410-6.3-#22	6.8	6.3	10	1,880,321	0.018335	0.020921
			3.1803-AMPT-S410-6.3-#25	6.9	6.3	10	529,934	0.021257	0.024486
		45°C, Unconfined	3.1803-AMPT-S410-6.3-#26	7.2	6.3	0	1,710		
			3.1803-AMPT-S410-6.3-#27	7.2	6.3	0	1,066		
			3.1803-AMPT-S410-6.3-#33	6.8	6.3	0	1,726		
		55°C, Unconfined	3.1803-AMPT-S410-6.3-#21	6.6	6.3	0	256		
			3.1803-AMPT-S410-6.3-#30	7.3	6.3	0	277		
			3.1803-AMPT-S410-6.3-#31	7.2	6.3	0	206		

Table D.4: Average RLT Results for Mix B

Mix	Binder Type/ Grade	Aggregate Type	NMAS	5.5%	Test Condition	Flow Number	Repetition to 5% PAS	PAS% @ 5,000 Cycles	PAS% @ 10,000 Cycles
B	PG 64-16	Basalt	3/4	6.3	Confined; 45°C	N/A*	2.30E+06	1.48	1.75
					Confined; 55°C	N/A*	9.73E+05	2.01	2.31
					Unconfined; 45°C	547	1,501	N/A**	N/A**
					Unconfined; 55°C	87	246	N/A**	N/A**

* No tertiary flow within 20,000 cycles.
** Specimen failed (reached 5% permanent axial strain, PAS) before 5,000 cycles.

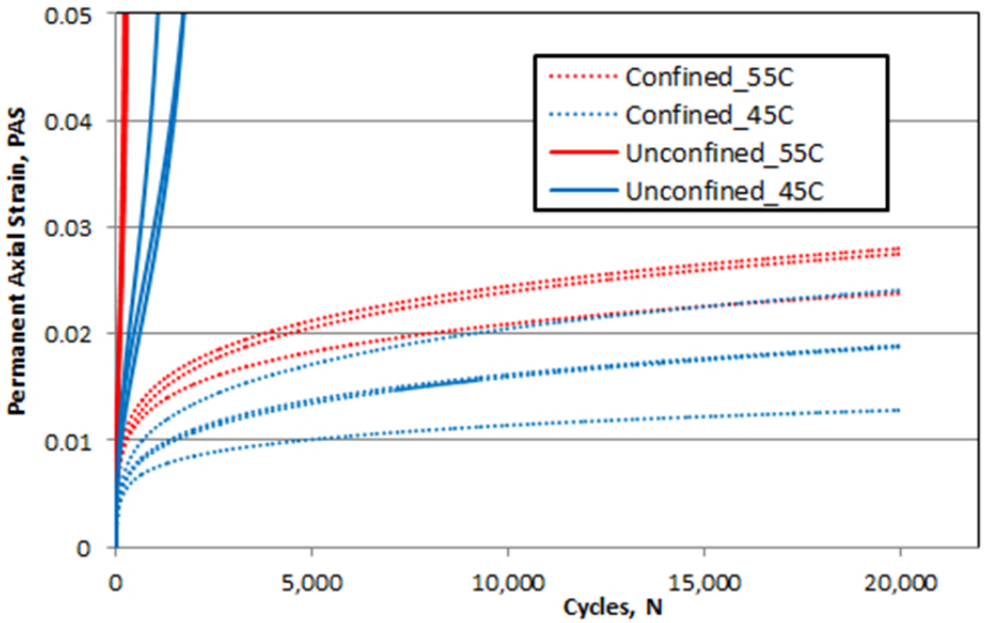

Figure D.2: Permanent axial deformation versus cycles for Mix B.

Table D.5: AMPT RLT Test Results for Mix I

Mix Type	AC %	Testing Parameters	Specimen ID	AV (%)	AC (%)	Confining Stress (psi)	Cycles to 5% Permanent Axial Strain	Permanent Axial Strain @ x Cycles	
								N=5,000	N=10,000
Mix I - 1/2" RHMA-G Basalt PG 64-16R	8.3	45°C, Confined	3.1803-AMPT-S311-8.3-#11	6.5	8.3	10	1,234,374,070	0.015197	0.01637
			3.1803-AMPT-S311-8.3-#14	5.7	8.3	10	4,837,498,031	0.013379	0.014412
			3.1803-AMPT-S311-8.3-#20	6.5	8.3	10	1,750,017,185	0.014385	0.015594
		55°C, Confined	3.1803-AMPT-S311-8.3-#21	6.8	8.3	10	1,375,654,500	0.014818	0.016009
			3.1803-AMPT-S311-8.3-#23	6.5	8.3	10	4,973,520,720	0.016758	0.017841
			3.1803-AMPT-S311-8.3-#24	6.6	8.3	10	173,646,696	0.016745	0.018171
			3.1803-AMPT-S311-8.3-#29	6.6	8.3	10	2,574,934,417	0.014139	0.01529
		45°C, Unconfined	3.1803-AMPT-S311-8.3-#4	7.8	8.3	0	858		
			3.1803-AMPT-S311-8.3-#15	8.0	8.3	0	1,667		
			3.1803-AMPT-S311-8.3-#28	7.8	8.3	0	2,278		
		55°C, Unconfined	3.1803-AMPT-S311-8.3-#10	7.8	8.3	0	182		
			3.1803-AMPT-S311-8.3-#19	8.0	8.3	0	393		
			3.1803-AMPT-S311-8.3-#25	7.7	8.3	0	350		

Table D.6: Average RLT Results for Mix I

Mix	Binder Type/ Grade	Aggregate Type	NMAS	5.5%	Test Condition	Flow Number	Repetition to 5% PAS	PAS% @ 5,000 Cycles	PAS% @ 10,000 Cycles
I	**PG 64-16 RB**	**Basalt**	**1/2**	**8.3**	Confined; 45°C	N/A*	2.61E+09	1.43	1.55
					Confined; 55°C	N/A*	2.27E+09	1.56	1.68
					Unconfined; 45°C	874	1,601	N/A**	N/A**
					Unconfined; 55°C	193	308	N/A**	N/A**

* No tertiary flow within 20,000 cycles.
** Specimen failed (reached 5% permanent axial strain, PAS) before 5,000 cycles.

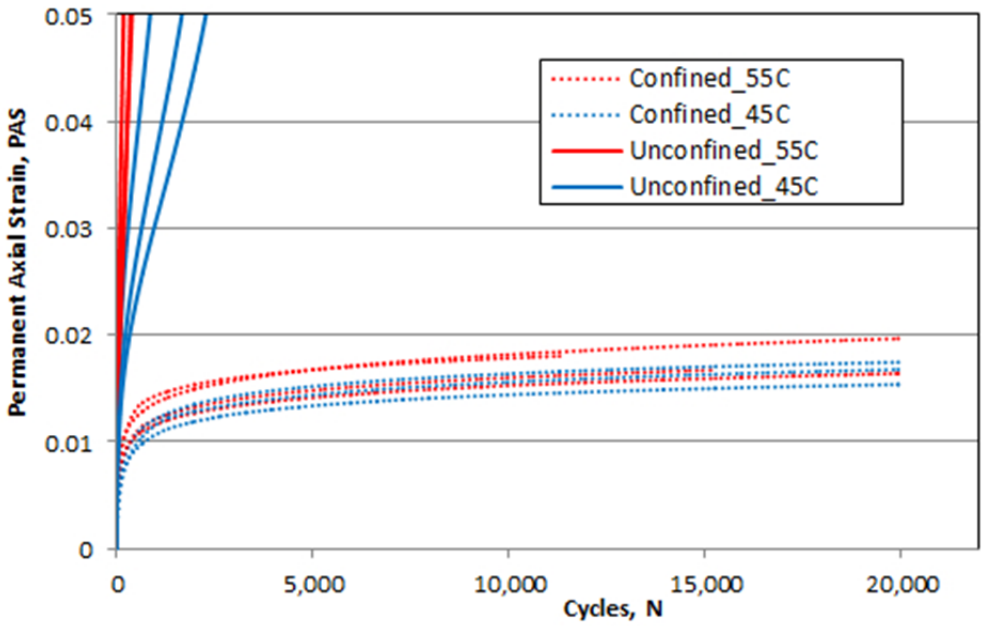

Figure D.3: Permanent axial deformation versus cycles for Mix I.

Table D.7: AMPT RLT Test Results for Mix J

Mix Type	AC %	Testing Parameters	Specimen ID	AV (%)	AC (%)	Confining Stress (psi)	Cycles to 5% Permanent Axial Strain	Permanent Axial Strain @ x Cycles	
								N=5,000	N=10,000
A835 Mix J - 3/4" RHMA-G Granite PG 64-16R	8.8	45°C, Confined	3.1803-AMPT-A835-8.8-#15	7.0	8.8	10	2.57202E+06	0.034135	0.035803
			3.1803-AMPT-A835-8.8-#16	6.5	8.8	10	2.987998E+13	0.014221	0.014822
			3.1803-AMPT-A835-8.8-#20	6.5	8.8	10	1.017607E+14	0.014884	0.015466
			3.1803-AMPT-A835-8.8-#23	7.6	8.8	10	7.78435E+06	0.023194	0.024885
			3.1803-AMPT-A835-8.8-#35	6.1	8.8	10	1.07637E+13	0.016217	0.016662
			3.1803-AMPT-A835-8.8-#41	6.3	8.8	10	3.35261E+12	0.013281	0.013804
		55°C, Confined	3.1803-AMPT-A835-8.8-#5	6.7	8.8	10	1.599047E+12	0.014938	0.015691
			3.1803-AMPT-A835-8.8-#6	7.7	8.8	10	1.484719E+11	0.017356	0.018212
			3.1803-AMPT-A835-8.8-#7	6.5	8.8	10	3.814237E+17	0.009221	0.009629
			3.1803-AMPT-A835-8.8-#19	6.9	8.8	10	1.953091E+13	0.012685	0.013327
			3.1803-AMPT-A835-8.8-#34	6.3	8.8	10	2.05850E+09	0.023245	0.024184
			3.1803-AMPT-A835-8.8-#39	6.5	8.8	10	8.83595E+11	0.018119	0.019016
			3.1803-AMPT-A835-8.8-#44	5.9	8.8	10	6.48007E+11	0.015051	0.015721
		45°C, Unconfined	3.1803-AMPT-A835-8.8-#10	7.5	8.8	0	1,043		
			3.1803-AMPT-A835-8.8-#11	6.5	8.8	0	1,096		
			3.1803-AMPT-A835-8.8-#18	7.4	8.8	0	575		
		55°C, Unconfined	3.1803-AMPT-A835-8.8-#21	6.7	8.8	0	209		
			3.1803-AMPT-A835-8.8-#22	7.4	8.8	0	156		
			3.1803-AMPT-A835-8.8-#26	7.2	8.8	0	147		

Table D.8: Average RLT Results for Mix J

Mix	Binder Type/ Grade	Aggregate Type	NMAS	5.5%	Test Condition	Flow Number	Repetition to 5% PAS	PAS% @ 5,000 Cycles	PAS% @ 10,000 Cycles
J	PG 64-16 RB	Granite	¾	8.8	Confined; 45°C	N/A*	2.4293E+13	0.0193	0.0202
					Confined; 55°C	N/A*	5.4492E+16	0.0158	0.0165
					Unconfined; 45°C	479	905	N/A**	N/A**
					Unconfined; 55°C	81	171	N/A**	N/A**

* No tertiary flow within 20,000 cycles.
** Specimen failed (reached 5% permanent axial strain, PAS) before 5,000 cycles.

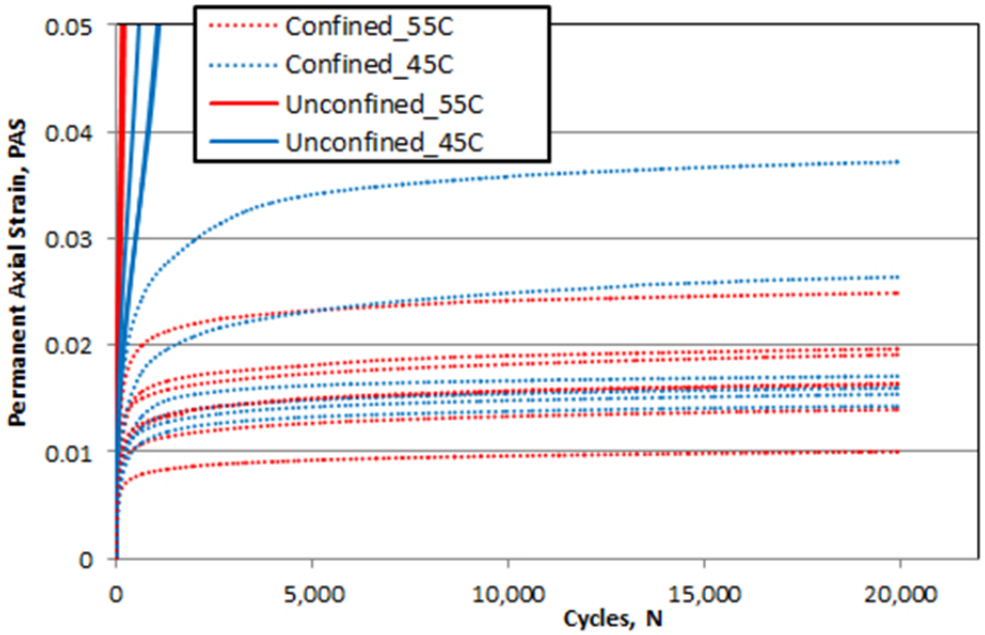

Figure D.4: Permanent axial deformation versus cycles for Mix J.

Table D.9: AMPT RLT Test Results for Mix N

Mix Type	AC %	Testing Parameters	Specimen ID	AV (%)	AC (%)	Confining Stress (psi)	Cycles to 5% Permanent Axial Strain	Permanent Axial Strain @ x Cycles	
								N=5,000	N=10,000
Mix N - 1" HMA-C Granite PG 64-16PM	6.4	45°C, Confined	3.1803-AMPT-A329-6.4-#1	6.5	6.4	10	56,237,011	0.016939	0.018585
			3.1803-AMPT-A329-6.4-#10	7.4	6.4	10	34,241,474	0.017167	0.018863
			3.1803-AMPT-A329-6.4-#13	6.2	6.4	10	181,571,533	0.01464	0.016004
			3.1803-AMPT-A329-6.4-#14	6.2	6.4	10	199,526,714	0.014077	0.015509
		55°C, Confined	3.1803-AMPT-A329-6.4-#5	6.2	6.4	10	4,279,777	0.020339	0.022494
			3.1803-AMPT-A329-6.4-#8	8.0	6.4	10	1,555,029	0.021423	0.024028
			3.1803-AMPT-A329-6.4-#18	7.3	6.4	10	1,637,956	0.021963	0.024465
			3.1803-AMPT-A329-6.4-#23	7.4	6.4	10	3,100,013	0.019572	0.02189
			3.1803-AMPT-A329-6.4-#25	6.7	6.4	10	125,556,500	0.014074	0.015583
		45°C, Unconfined	3.1803-AMPT-A329-6.4-#24	7.6	6.4	0	629		
			3.1803-AMPT-A329-6.4-#26	7.2	6.4	0	417		
			3.1803-AMPT-A329-6.4-#27	6.6	6.4	0	513		
		55°C, Unconfined	3.1803-AMPT-A329-6.4-#6	7.6	6.4	0	73		
			3.1803-AMPT-A329-6.4-#22	7.6	6.4	0	109		
			3.1803-AMPT-A329-6.4-#28	6.4	6.4	0	104		

Table D.10: Average RLT Results for Mix N

Mix	Binder Type/ Grade	Aggregate Type	NMAS	5.5%	Test Condition	Flow Number	Repetition to 5% PAS	PAS% @ 5,000 Cycles	PAS% @ 10,000 Cycles
N	PG 64-28 PM	Granite	1	6.4	Confined; 45°C	N/A*	1.18E+08	1.73	1.93
					Confined; 55°C	N/A*	2.72E+07	1.95	2.17
					Unconfined; 45°C	228	520	N/A**	N/A**
					Unconfined; 55°C	42	95	N/A**	N/A**

* No tertiary flow within 20,000 cycles.
** Specimen failed (reached 5% permanent axial strain, PAS) before 5,000 cycles.

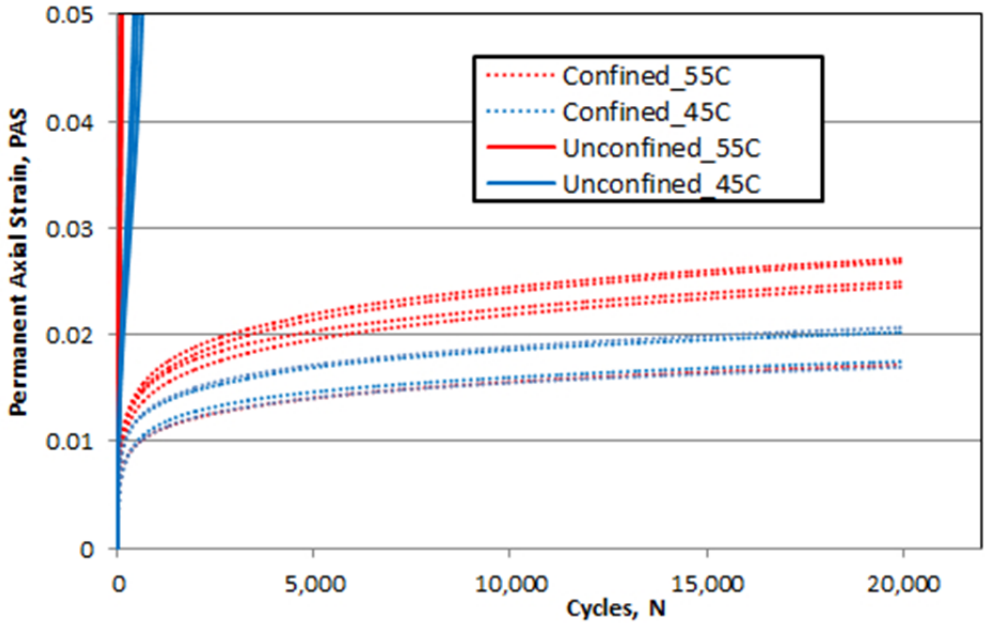

Figure D.5: Permanent axial deformation versus cycles for Mix N.

APPENDIX E: DYNAMIC MODULUS TEST DATA

Table E.1: Average DM Results for Mix A

Mix	Binder Type/ Grade	Aggregate Type	NMAS	Binder Content %	Test Temp. (°C)	Test Freq. (Hz)	Average Initial Stiffness (MPa)	Average Phase Angle (Deg.)
A	PG 64-16	Alluvial	¾	5.5	4	25	18,790	7.90
						10	17,403	8.73
						5	16,279	9.50
						1	13,544	11.69
						0.5	12,357	12.87
						0.1	9,671	16.18
					21	25	10,506	15.92
						10	8,921	17.95
						5	7,780	19.61
						1	5,406	23.99
						0.5	4,539	25.73
						0.1	2,793	30.29
					38	25	3,696	30.75
						10	2,695	33.00
						5	2,094	33.88
						1	1,046	35.74
						0.5	763	35.26
						0.1	357	34.08
					55	25	915	39.40
						10	579	37.82
						5	402	36.55
						1	171	33.75
						0.5	126	31.61
						0.1	71	25.82

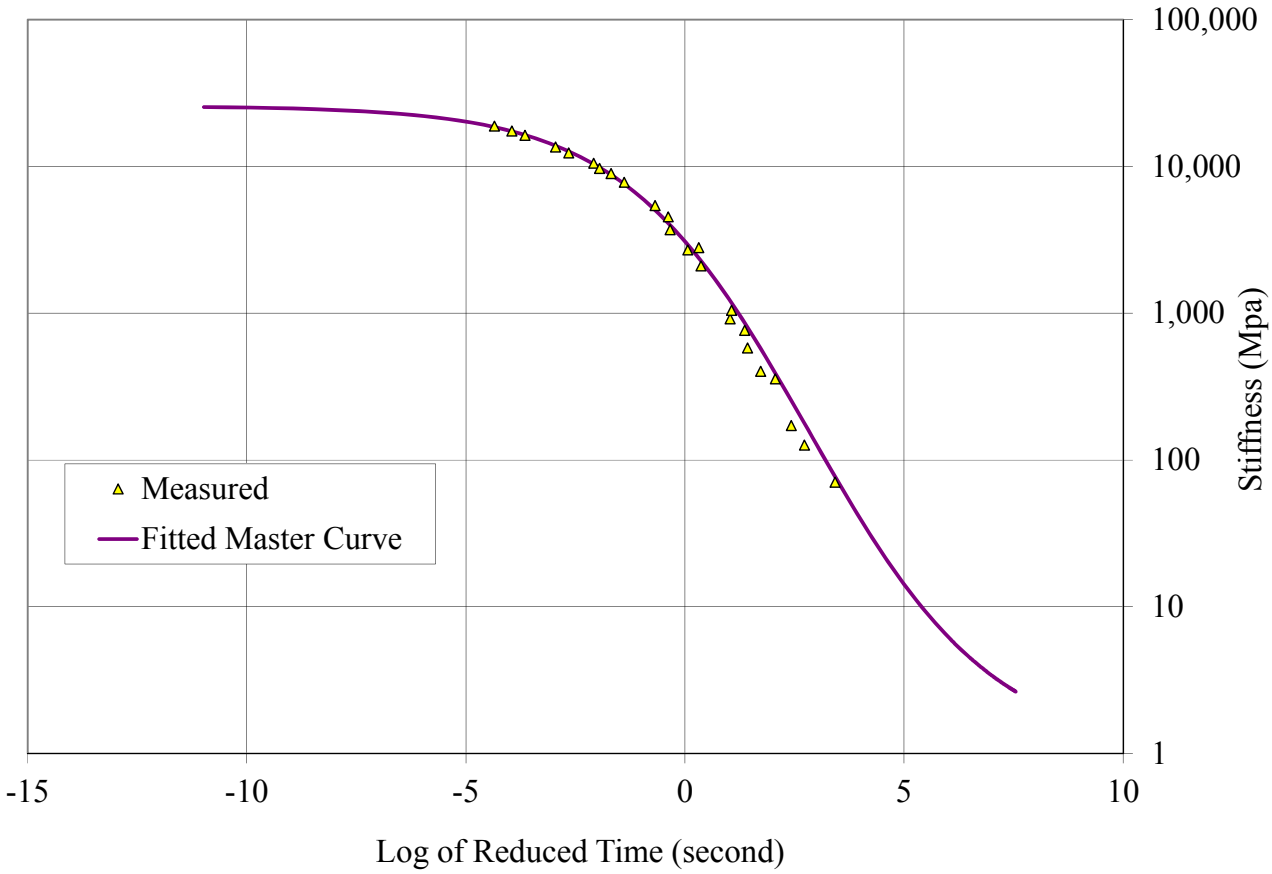

Figure E.1: Dynamic modulus master curve for Mix A.

Table E.2: Average DM Results for Mix B

Mix	Binder Type/ Grade	Aggregate Type	NMAS	Binder Content %	Test Temp. (°C)	Test Freq. (Hz)	Average Initial Stiffness (MPa)	Average Phase Angle (Deg.)
B	PG 64-16	Basalt	¾	6.3	4	25	12,812	8.80
						10	11,758	9.62
						5	10,947	10.41
						1	9,018	12.58
						0.5	8,187	13.71
						0.1	6,334	16.66
					21	25	6,724	17.27
						10	5,655	19.03
						5	4,933	20.36
						1	3,411	23.71
						0.5	2,873	24.93
						0.1	1,830	27.58
					38	25	2,391	29.12
						10	1,754	30.73
						5	1,405	30.72
						1	765	31.26
						0.5	606	30.24
						0.1	337	28.75
					55	25	822	33.34
						10	569	32.29
						5	428	31.20
						1	217	29.19
						0.5	173	27.06
						0.1	105	23.50

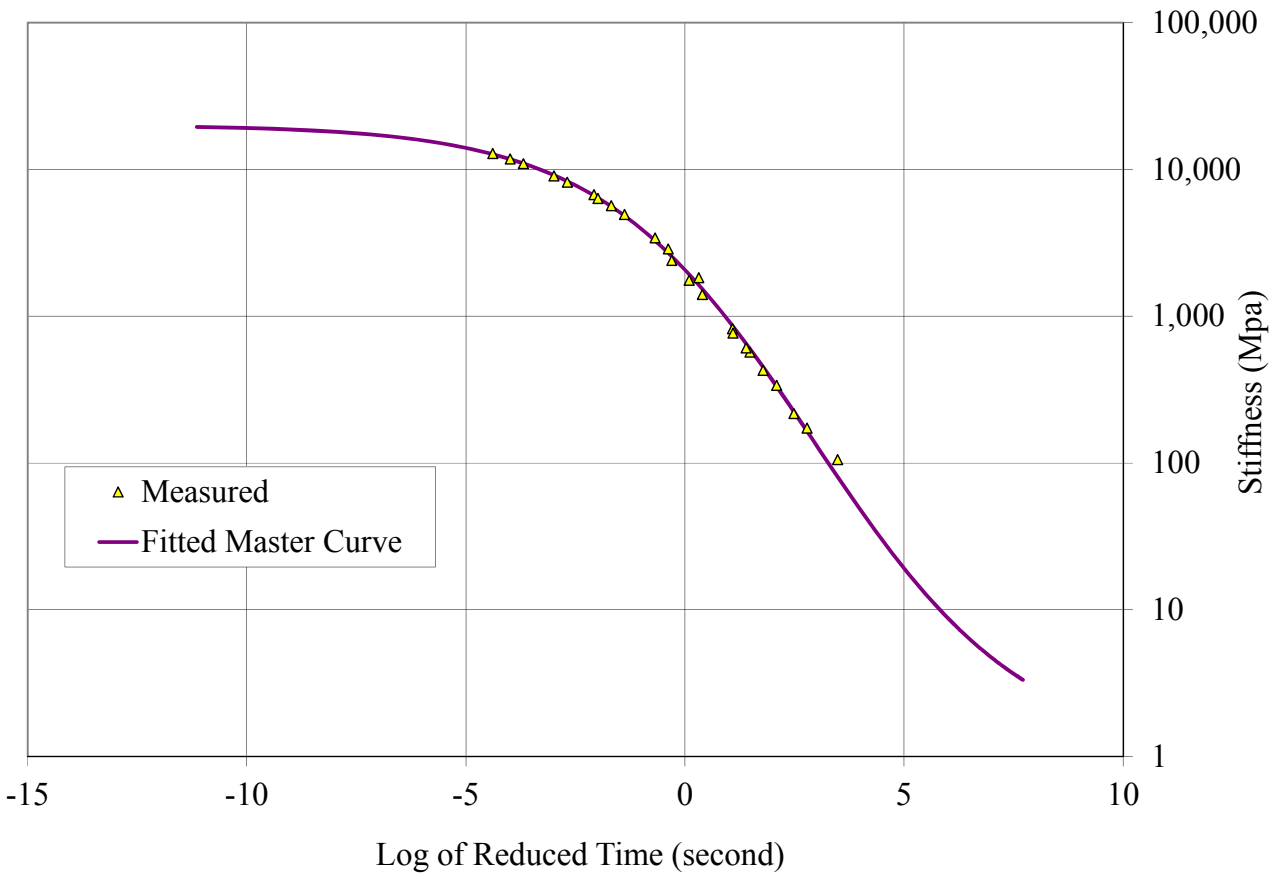

Figure E.2: Dynamic modulus master curve for Mix B.

Table E.3: Average DM Results for Mix I

Mix	Binder Type/ Grade	Aggregate Type	NMAS	Binder Content %	Test Temp. (°C)	Test Freq. (Hz)	Average Initial Stiffness (MPa)	Average Phase Angle (Deg.)
I	PG 64-16 RB	Basalt	½	8.3	4	25	11,883	8.22
						10	10,920	9.09
						5	10,170	9.87
						1	8,415	12.07
						0.5	7,645	13.18
						0.1	5,948	16.26
					21	25	5,957	17.84
						10	4,959	19.96
						5	4,269	21.53
						1	2,851	25.63
						0.5	2,362	27.18
						0.1	1,429	30.88
					38	25	2,073	31.06
						10	1,517	33.12
						5	1,197	33.89
						1	638	35.77
						0.5	497	35.28
						0.1	260	34.78
					55	25	682	36.48
						10	461	36.32
						5	343	35.59
						1	161	35.05
						0.5	125	33.20
						0.1	69	30.77

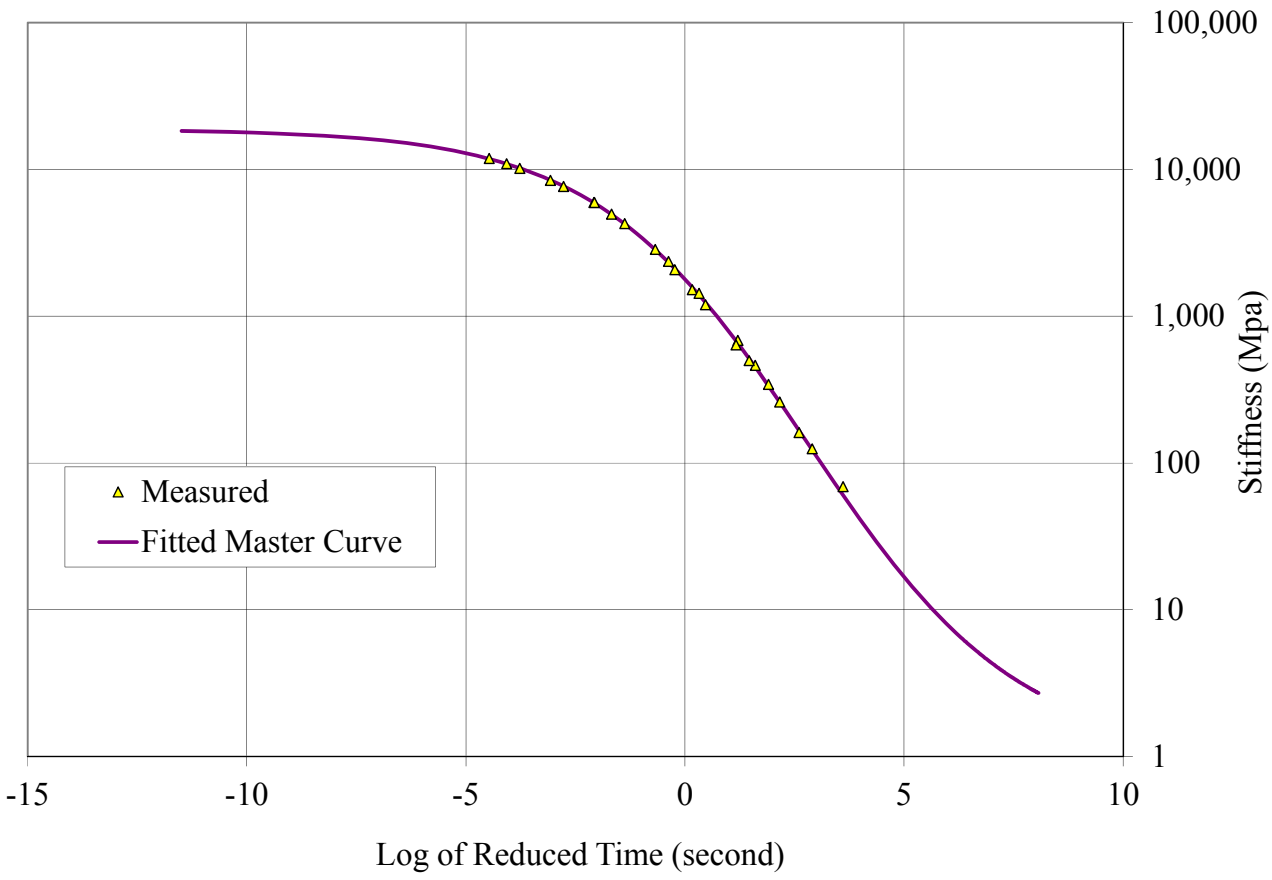

Figure E.3: Dynamic modulus master curve for Mix I.

Table E.4: Average DM Results for Mix J

Mix	Binder Type/ Grade	Aggregate Type	NMAS	Binder Content %	Test Temp. (°C)	Test Freq. (Hz)	Average Initial Stiffness (MPa)	Average Phase Angle (Deg.)
J	PG 64-16 RB	Granite	¾	8.8	4	25	11,581	9.69
						10	10,483	10.62
						5	96,45	11.43
						1	7,771	13.74
						0.5	6,983	14.92
						0.1	5,263	18.32
					21	25	5,642	19.00
						10	4,652	21.02
						5	3,977	22.60
						1	2,623	26.87
						0.5	2,143	28.77
						0.1	1,274	33.00
					38	25	1,658	34.75
						10	1,096	39.05
						5	841	40.08
						1	399	43.02
						0.5	302	42.51
						0.1	138	43.01
					55	25	446	43.50
						10	285	43.43
						5	201	42.65
						1	82	42.46
						0.5	59	40.82
						0.1	26	40.78

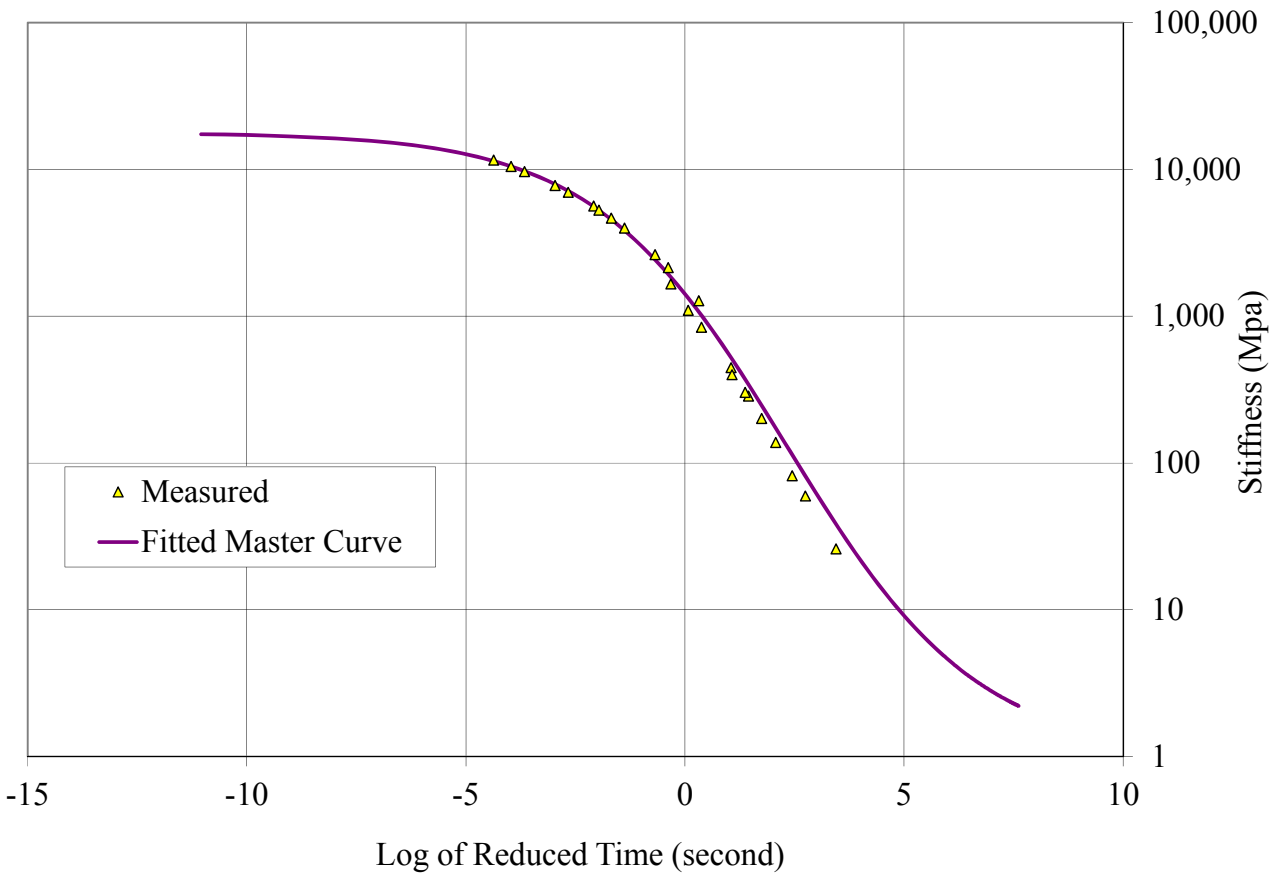

Figure E.4: Dynamic modulus master curve for Mix J.

Table E.5: Average DM Results for Mix N

Mix	Binder Type/ Grade	Aggregate Type	NMAS	Binder Content %	Test Temp. (°C)	Test Freq. (Hz)	Average Initial Stiffness (MPa)	Average Phase Angle (Deg.)
N	PG 64-28 PM	Granite	1	6.4	4	25	10,836	13.66
						10	9,432	15.36
						5	8,392	16.69
						1	6,151	20.24
						0.5	5,286	21.80
						0.1	3,547	25.74
					21	25	4,147	26.30
						10	3,180	28.40
						5	2,579	29.42
						1	1,473	31.64
						0.5	1,151	31.56
						0.1	625	31.01
					38	25	1,068	35.19
						10	695	35.85
						5	521	34.35
						1	259	31.64
						0.5	206	29.32
						0.1	122	25.59
					55	25	356	31.97
						10	231	30.25
						5	171	28.47
						1	93	24.92
						0.5	79	22.70
						0.1	57	19.87

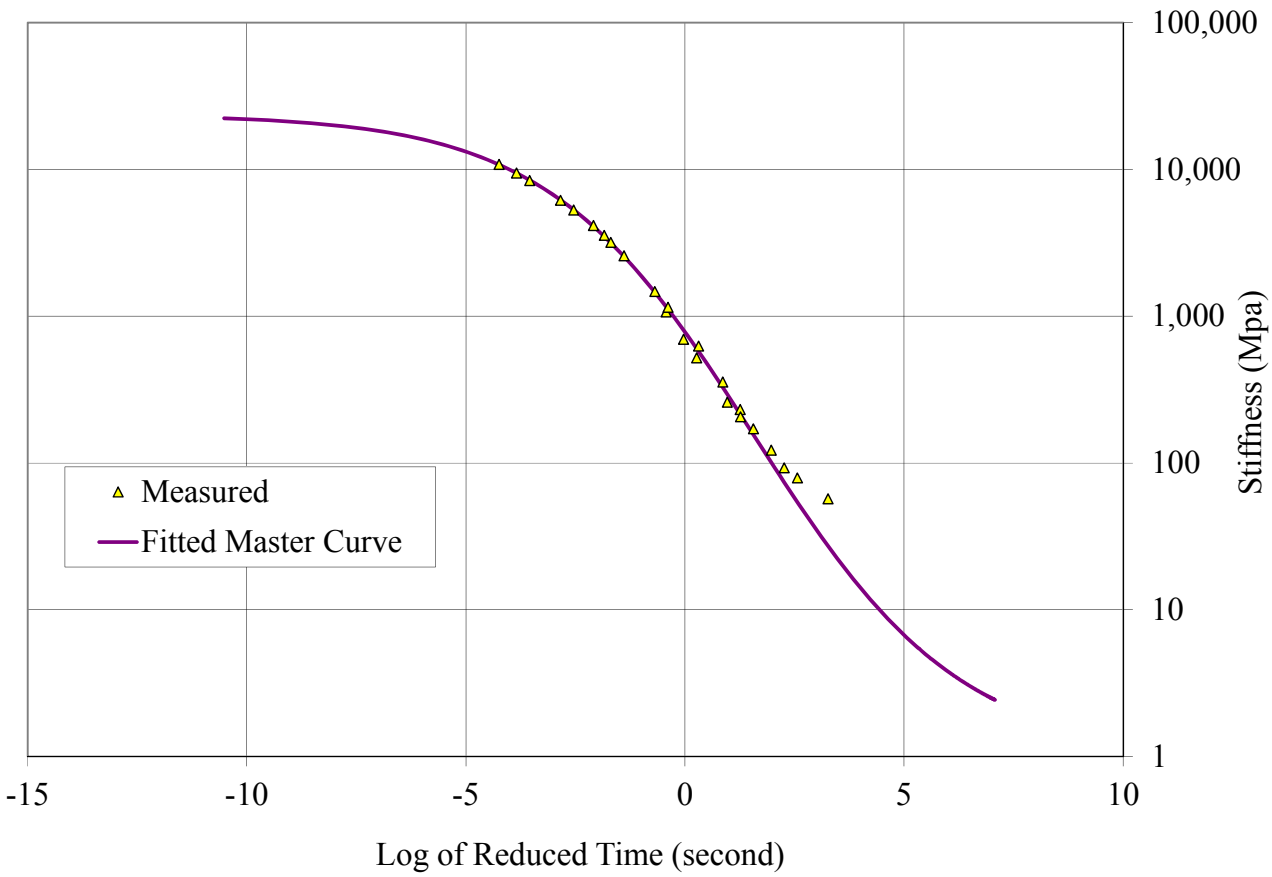

Figure E.5: Dynamic modulus master curve for Mix N.

Table E.6: AMPT DM Test Results−Stiffness

		AMPT E* (MPa)									
		Mix A-5.5%AC		Mix B-6.3%AC		Mix I-%AC		Mix J-8.8%AC		Mix N-6.4%AC	
Temp. (°C)	Freq. (Hz)	#24	#25	#24	#29	#3	#13	#25	#32	#20	#29
4	**25**	20369	17211	12843	12781	12296	11469	12260	10901	11127	10545
4	**10**	18935	15870	11837	11679	11259	10580	11174	9791	9711	9152
4	**5**	17759	14798	11057	10836	10452	9888	10336	8953	8648	8136
4	**1**	14846	12242	9146	8890	8566	8263	8479	7062	6358	5944
4	**0.5**	13566	11147	8342	8031	7723	7567	7682	6284	5473	5099
4	**0.1**	10690	8652	6450	6218	5903	5993	5913	4612	3682	3412
21	**25**	10153	10859	7176	6271	6040	5874	5765	5519	4434	3860
21	**10**	8500	9342	6072	5238	4991	4926	4770	4534	3416	2943
21	**5**	7331	8229	5329	4537	4254	4283	4091	3862	2775	2382
21	**1**	4968	5844	3700	3121	2775	2927	2726	2519	1592	1353
21	**0.5**	4120	4958	3122	2623	2268	2455	2256	2030	1241	1061
21	**0.1**	2480	3105	1983	1676	1322	1536	1353	1195	674.6	576.1
38	**25**	3570	3822	2697	2085	1873	2272	1745	1570	1133	1002
38	**10**	2590	2800	1984	1523	1337	1696	1160	1032	739.4	650.1
38	**5**	1998	2189	1584	1225	1035	1358	892.8	788.2	553.8	487.4
38	**1**	981	1111	854.1	675.1	526.5	749.2	427.8	370.6	276.6	242.2
38	**0.5**	710.1	816.3	667	545.2	406.1	588.8	325.4	279.3	219.7	192.1
38	**0.1**	327.7	387	360.7	313.9	210.6	310.3	150.5	125.3	131	113.5
55	**25**	867.4	961.6	919.9	724.1	592.8	771.3	493.5	398.1	389.4	322.5
55	**10**	543.4	613.6	636.5	501.6	395.3	527.6	319.7	250.8	249.8	212.5
55	**5**	374.5	428.7	476.4	379.8	287.5	398.9	226.7	175.5	183.5	157.6
55	**1**	159.5	183.1	236.3	197.1	129.2	192.3	93.5	69.7	99.5	85.5
55	**0.5**	119.1	132.9	186.3	159.6	98.3	151.7	67.5	51.4	86	72.2
55	**0.1**	68.6	72.5	111.1	99.4	53.8	84	28.2	23.6	64.3	49.6

Table E.7: AMPT DM Test Results−Phase Angle for Replicate Specimens

		AMPT Phase Angle (Degree)									
		Mix A-5.5%AC		Mix B-6.3%AC		Mix I-%AC		Mix J-8.8%AC		Mix N-6.4%AC	
Temp. (°C)	Freq. (Hz)	#24	#25	#24	#29	#3	#13	#25	#32	#20	#29
4	**25**	7.71	8.08	8.78	8.81	8.54	7.89	8.92	10.45	13.72	13.59
4	**10**	8.56	8.89	9.67	9.56	9.51	8.67	9.77	11.46	15.45	15.27
4	**5**	9.28	9.71	10.48	10.34	10.36	9.38	10.51	12.35	16.77	16.6
4	**1**	11.3	12.07	12.69	12.47	12.79	11.35	12.59	14.89	20.29	20.18
4	**0.5**	12.37	13.37	13.77	13.65	14.01	12.34	13.64	16.2	21.86	21.74
4	**0.1**	15.55	16.81	16.81	16.51	17.48	15.04	16.77	19.86	25.76	25.71
21	**25**	17.12	14.72	16.8	17.73	18.71	16.97	18.86	19.13	25.9	26.7
21	**10**	19.27	16.63	18.58	19.47	21.02	18.89	20.85	21.19	27.97	28.82
21	**5**	20.95	18.27	20.01	20.71	22.72	20.34	22.37	22.83	29	29.83
21	**1**	25.37	22.61	23.61	23.8	27.17	24.08	26.52	27.22	31.15	32.12
21	**0.5**	27.06	24.4	24.92	24.94	28.82	25.53	28.2	29.33	31.04	32.07
21	**0.1**	31.43	29.14	27.98	27.18	32.78	28.97	32.46	33.53	30.36	31.65
38	**25**	31.37	30.13	28.47	29.77	33.14	28.98	34.23	35.26	34.77	35.6
38	**10**	33.49	32.5	30.21	31.25	35.17	31.06	38.44	39.66	35.31	36.38
38	**5**	34.33	33.43	30.4	31.03	35.78	32	39.53	40.63	33.81	34.88
38	**1**	36.02	35.45	31.31	31.21	37.13	34.41	42.59	43.45	31.01	32.26
38	**0.5**	35.43	35.09	30.52	29.95	36.25	34.3	42.15	42.86	28.72	29.92
38	**0.1**	34.14	34.02	29.37	28.12	34.78	34.78	42.83	43.18	25.04	26.14
55	**25**	39.5	39.3	33.75	32.92	37.22	35.74	42.69	44.3	31.16	32.77
55	**10**	37.93	37.71	32.64	31.94	36.57	36.06	42.5	44.36	29.68	30.81
55	**5**	36.6	36.5	31.53	30.87	35.51	35.67	41.8	43.5	28.04	28.9
55	**1**	33.44	34.05	29.56	28.81	34.4	35.69	41.68	43.23	24.41	25.43
55	**0.5**	31.4	31.81	27.34	26.78	32.38	34.01	40.26	41.37	22.02	23.37
55	**0.1**	25.07	26.56	23.49	23.51	29.79	31.74	41.23	40.32	19.19	20.54

APPENDIX F: DIRECT TENSION FATIGUE TEST DATA

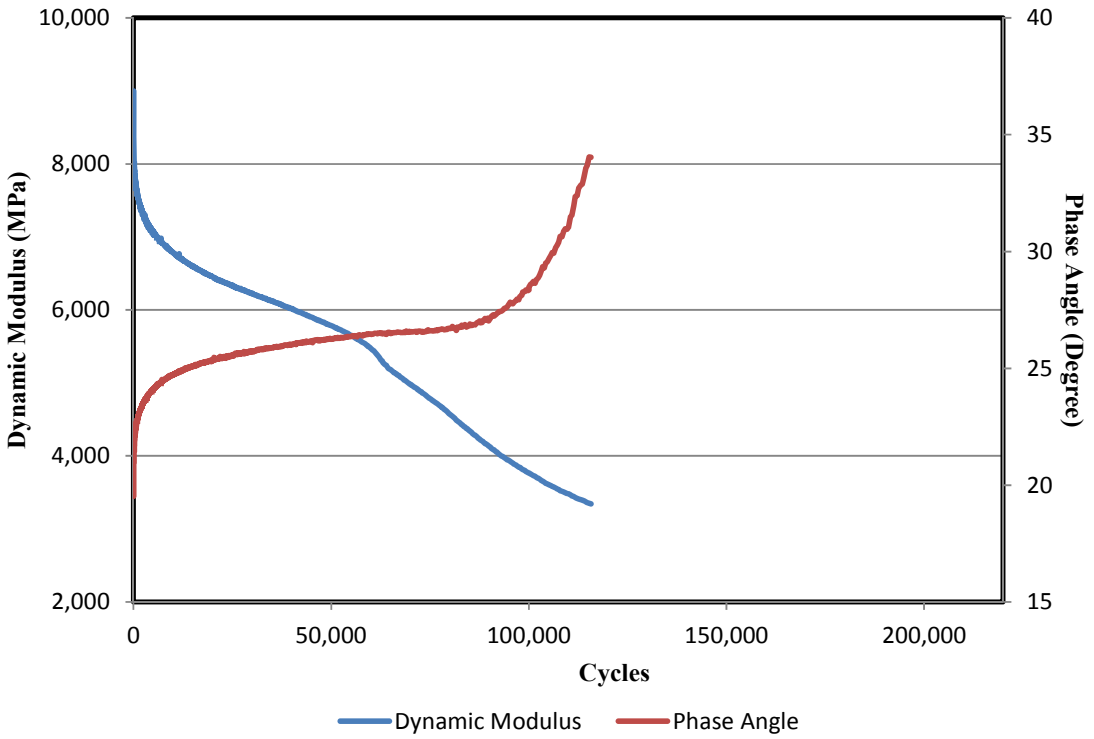

Figure F.1: Direct tension fatigue stiffness/phase angle versus cycles for Mix A (one test). (Note: The phase angle change at around 90,000 cycles implied the fracture of the specimen.)

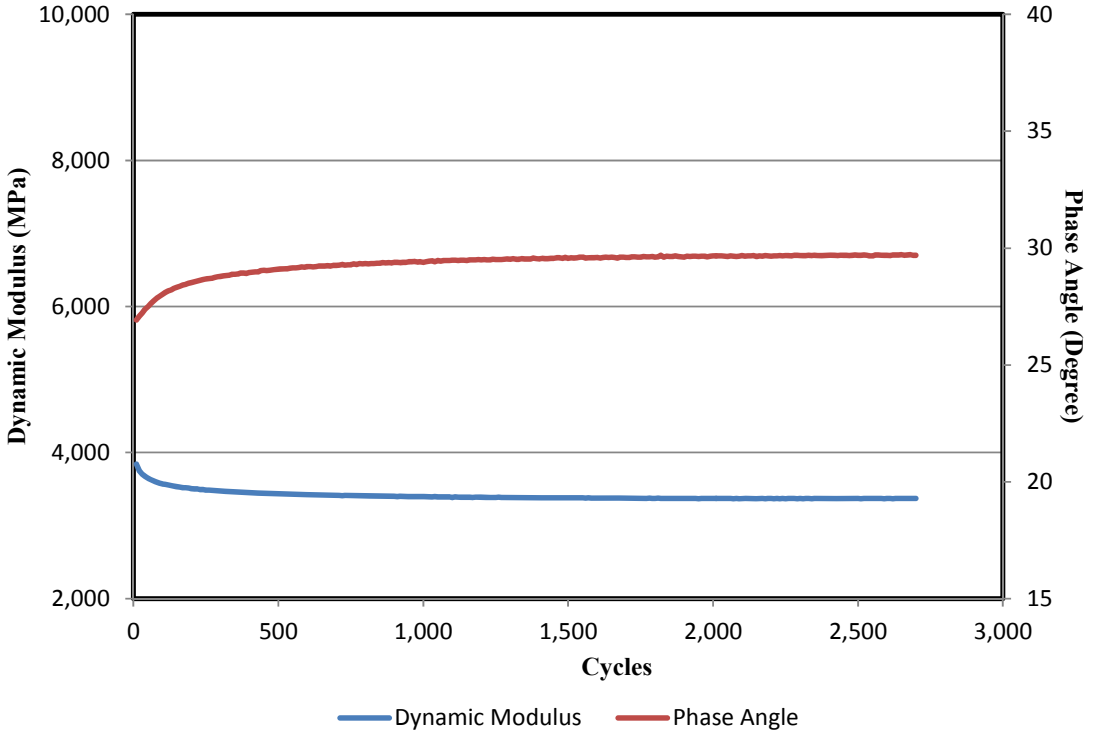

Figure F.2: Direct tension fatigue stiffness/phase angle versus cycles for Mix B (average of two tests).

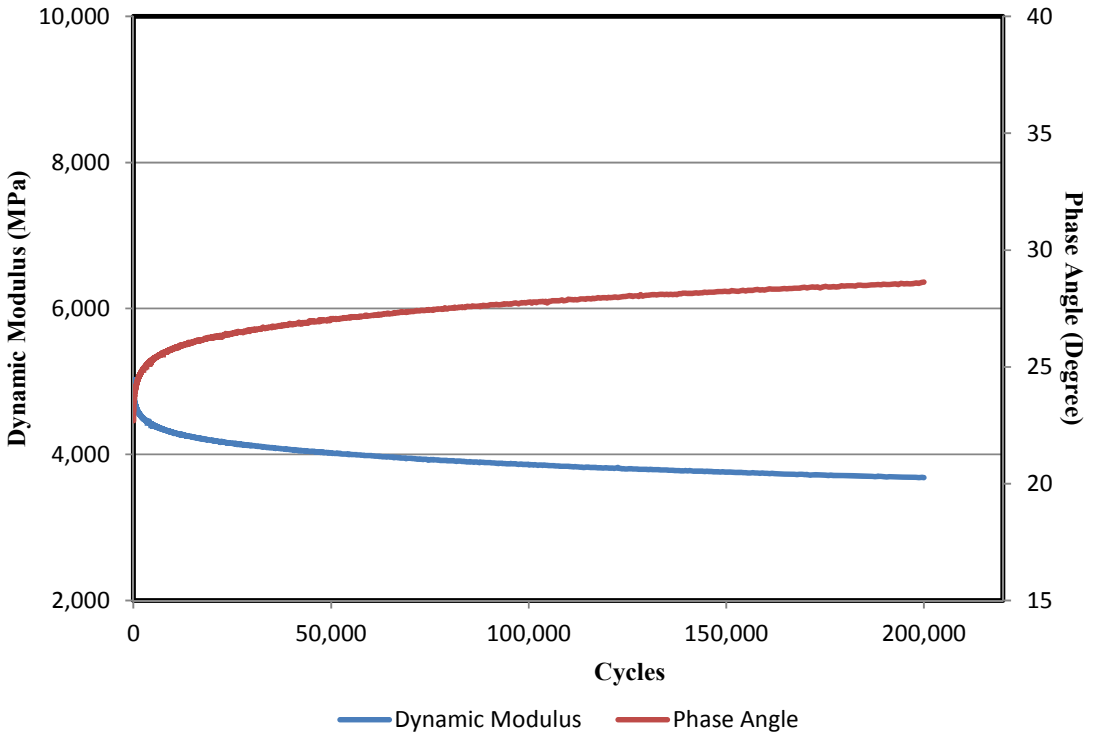

Figure F.3: Direct tension fatigue stiffness/phase angle versus cycles for Mix I (one test).

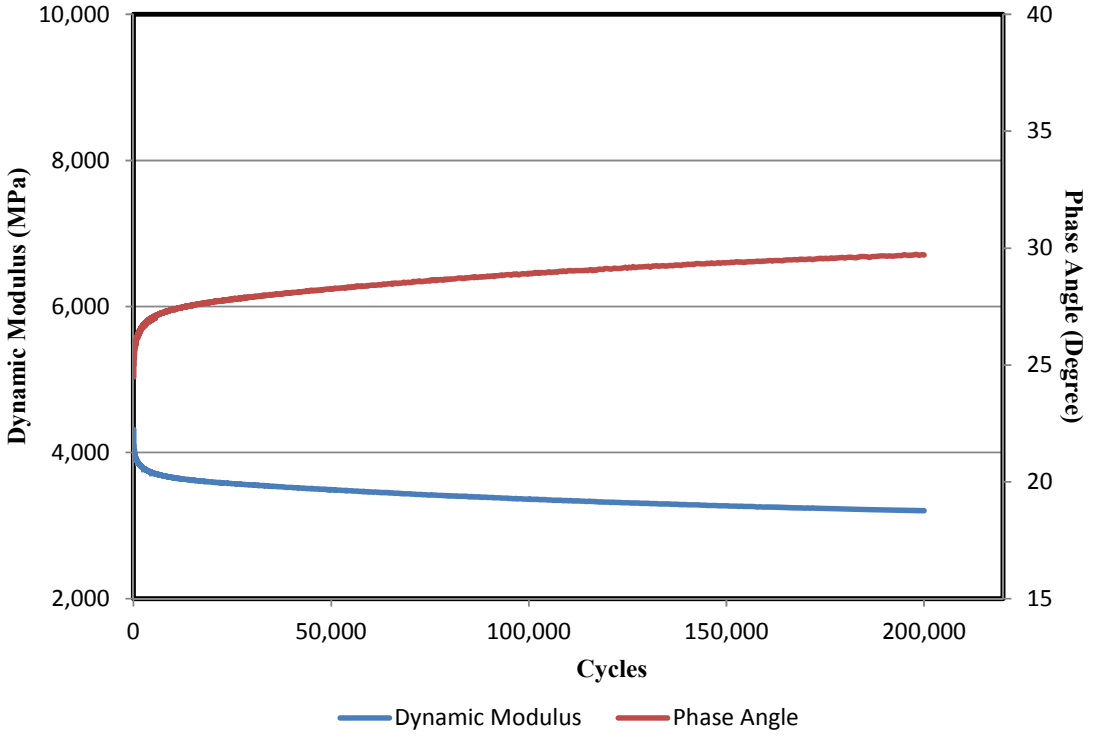

Figure F.4: Direct tension fatigue stiffness/phase angle versus cycles for Mix J (average of two tests).

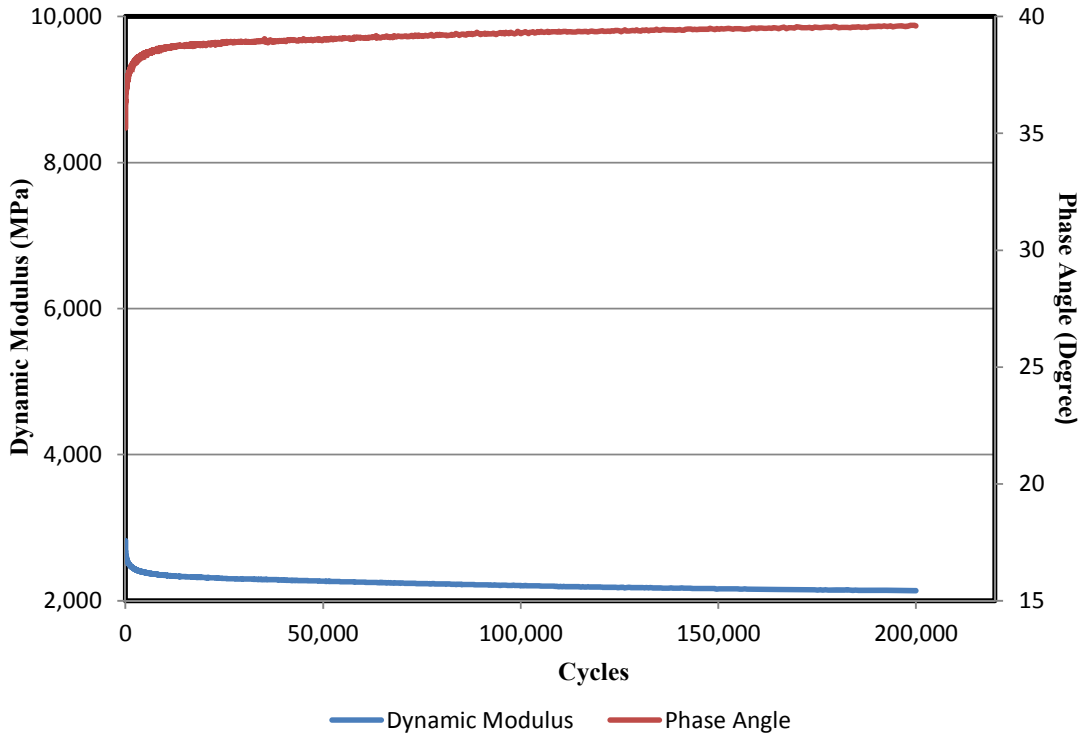

Figure F.5: Direct tension fatigue stiffness/phase angle versus cycles for Mix N (average of two tests).

APPENDIX G: HAMBURG WHEEL-TRACKING TEST DATA

Table G.1: Average Rut Depth (mm) at 15,000 Cycles for Mix A

Mix	Binder Type/ Grade	Aggregate Type	NMAS	Binder Content %	Average Rut Depth at 15,000 Cycles
A	PG 64-16	Alluvial	3/4	5.5	5.37

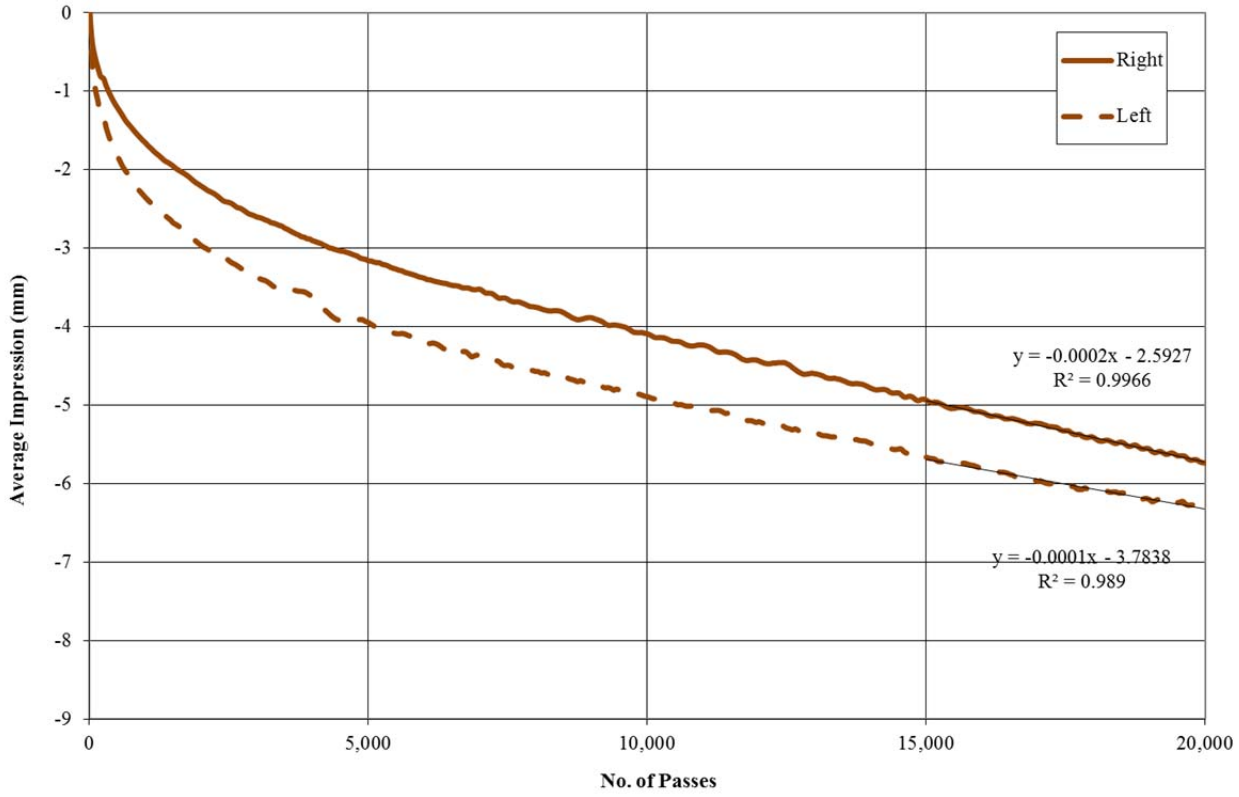

Figure G.1: HWTT results for the left and right wheel tracks, average impression versus cycles for Mix A.

Table G.2: Average Rut Depth (mm) at 15,000 Cycles for Mix B

Mix	Binder Type/ Grade	Aggregate Type	NMAS	Binder Content %	Average Rut Depth at 15,000 Cycles
B	PG 64-16	Basalt	3/4	5.2	5.71

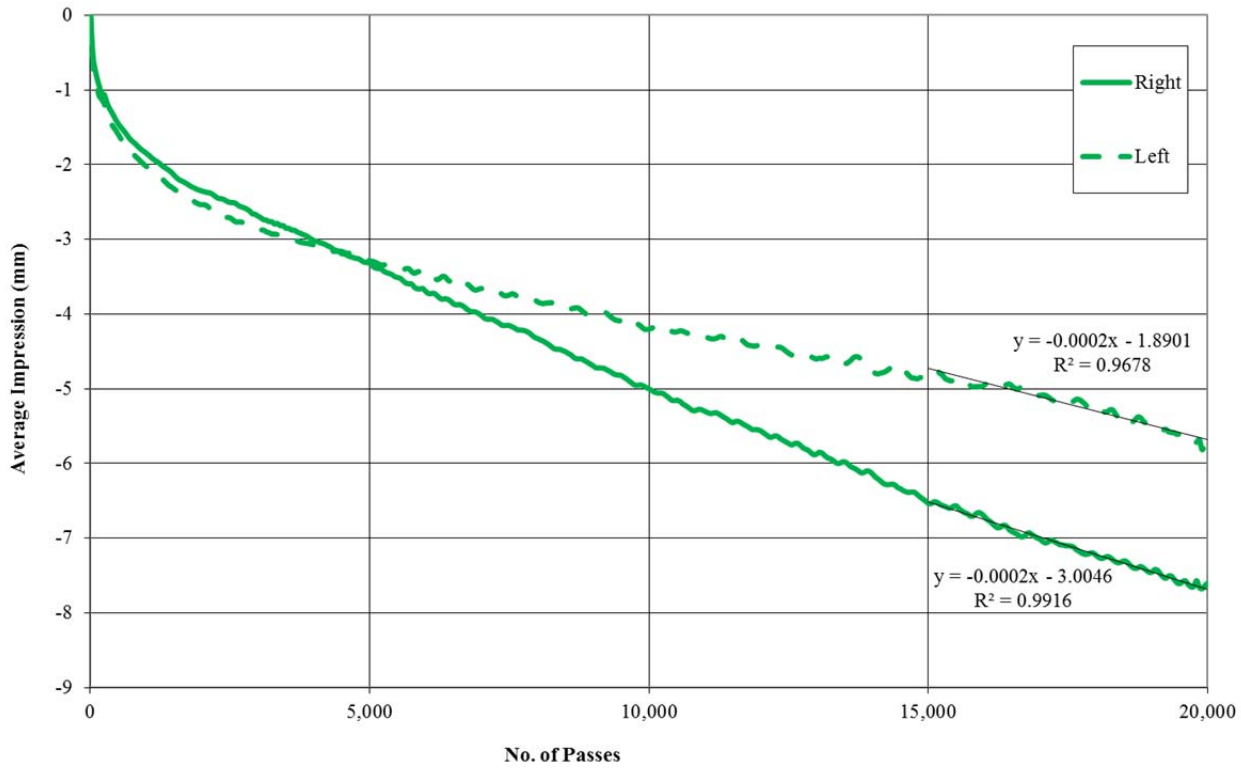

Figure G.2: HWTT results for the left and right wheel tracks, average impression versus cycles for Mix B.

Table G.3. Average Rut Depth (mm) at 15,000 Cycles for Mix I

Mix	Binder Type/ Grade	Aggregate Type	NMAS	Binder Content %	Average Rut Depth at 15,000 Cycles
I	PG 64-16 RB	Basalt	1/2	8	3.60

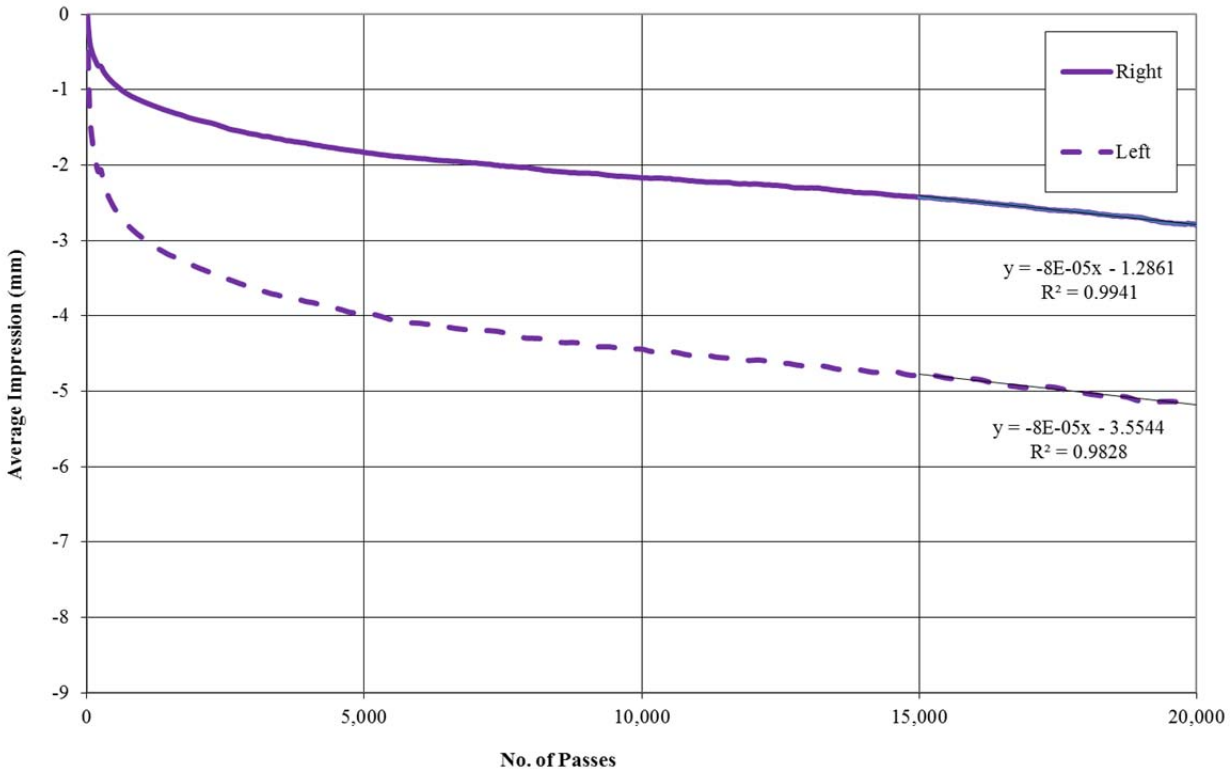

Figure G.3: HWTT results for the left and right wheel tracks, average impression versus cycles for Mix I.

Table G.4: Average Rut Depth (mm) at 15,000 Cycles for Mix J

Mix	Binder Type/ Grade	Aggregate Type	NMAS	Binder Content %	Average Rut Depth at 15,000 Cycles
J	PG 64-16 RB	Granite	3/4	7.2	2.44

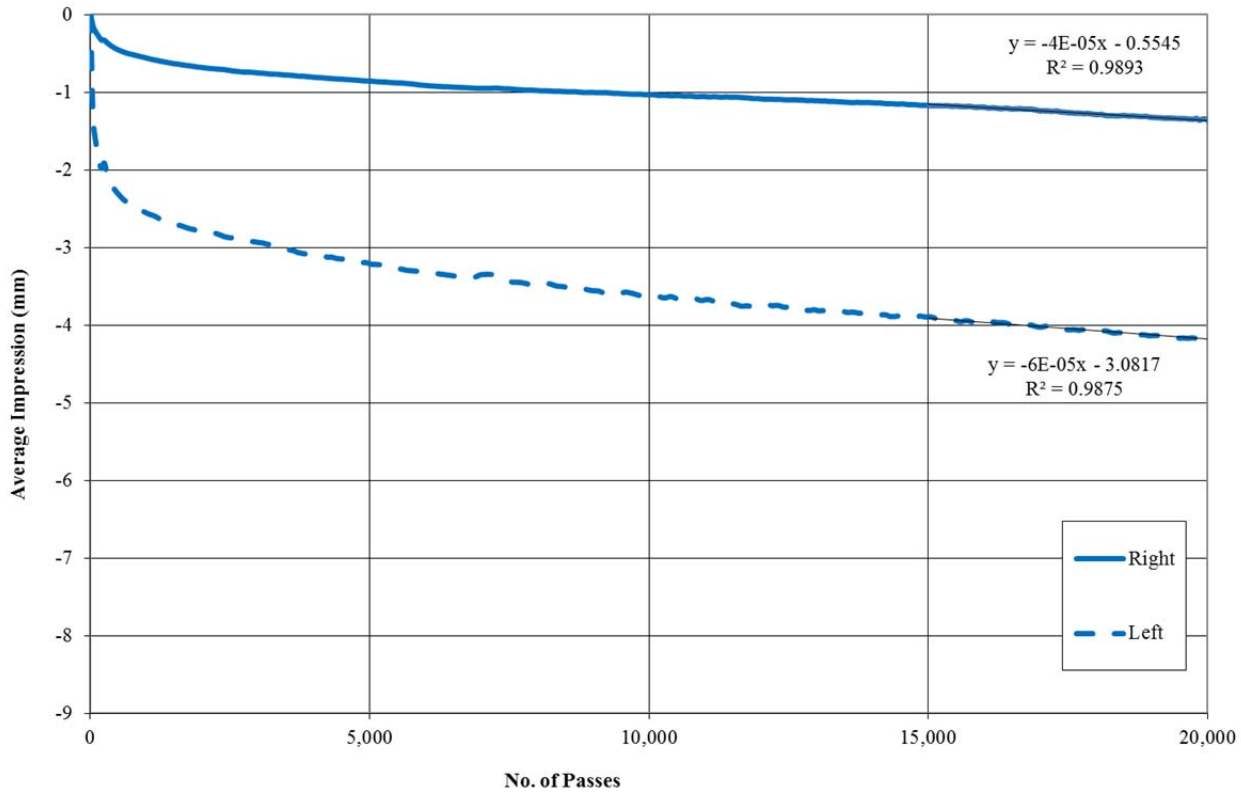

Figure G.4: HWTT results for the left and right wheel tracks, average impression versus cycles for Mix J.

Table G.5: Average Rut Depth (mm) at 15,000 Cycles for Mix N

Mix	Binder Type/Grade	Aggregate Type	NMAS	Binder Content %	Average Rut Depth at 15,000 Cycles
N	PG 64-28 PM	Granite	1	6.4	5.23

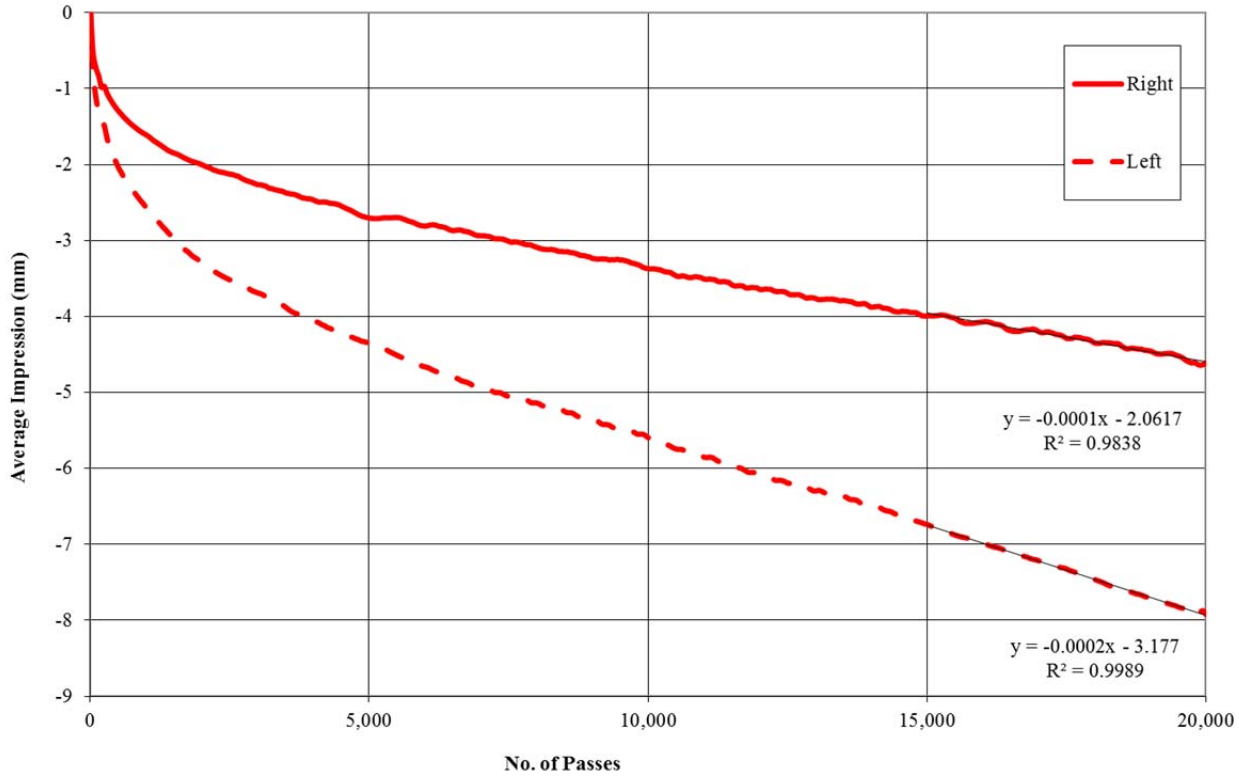

Figure G.5: HWTT results for the left and right wheel tracks, average impression versus cycles for Mix N.

APPENDIX H: INDIRECT TENSILE TEST DATA

Table H.1: Indirect Tensile Test (AASHTO T283, CTM 371) Result for Mix A

Specimen ID	% Air Voids	Maximum Compressive Load[2] (lbf)	Tensile Strength[2] (psi)
Dry Subset Test Data			
1	7.8	3,843.6	111.8
2	7.7	3,296.8	95.9
3	8.0	3,523.1	102.4
4	7.3	4,007.4	116.3
8	7.4	3,670.8	106.5
10	7.5	4,035	117.3
Mean[2]	7.6	3,761.2	109.3
SD[1,2]	0.26	209.97	6.1
Wet Subset Test Data			
5	7.7	3,559.6	103.0
6	7.5	3,479.8	100.8
7	7.6	3,369.1	97.7
9	8.0	2,977.5	86.5
11	7.5	3,046.1	88.5
12	7.3	3,334.3	97.0
Mean[2]	7.6	3,307.3	96.0
SD[1,2]	0.24	184.87	5.3
Test Result			
Tensile Strength Ratio (%)			**87.9**

1. SD = Standard Deviation

2. The high and low value of maximum compressive load and tensile strength are not used for the "Mean" and "SD."

Table H.2: Indirect Tensile Test (AASHTO T283, CTM 371) Result for Mix B

Specimen ID	% Air Voids	Maximum Compressive Load[2] (lbf)	Tensile Strength[2] (psi)
Dry Subset Test Data			
2	6.5	3,821.2	110.3
9	7.2	2,930.2	84.7
11	7.0	3,079.5	89.1
12	7.3	2,786.1	80.3
16	7.5	3,366.2	97.3
Mean[2]	7.1	3,125.3	90.4
SD[1,2]	0.38	221.58	6.4
Wet Subset Test Data			
1	7.6	2,843.6	82.0
4	7.3	2,392.4	69.1
6	7.5	2,640.1	75.6
8	7.2	2,532	73.3
14	6.7	2,559.8	74.0
15	7.0	2,679.1	77.3
Mean[2]	7.2	2,602.8	75.1
SD[1,2]	0.33	68.49	1.8
Test Result			
Tensile Strength Ratio (%)			**83.1**

1. SD = Standard Deviation

2. The high and low value of maximum compressive load and tensile strength are not used for the "Mean" and "SD."

Table H.3: Indirect Tensile Test (AASHTO T283, CTM 371) Result for Mix I

Specimen ID	% Air Voids	Maximum Compressive Load[2] (lbf)	Tensile Strength[2] (psi)
Dry Subset Test Data			
5	6.8	4,559.6	131.2
10	6.7	4,578	131.3
14	7.6	4,740	134.4
17	6.9	3,763.5	107.1
Mean[2]	7.0	4,410.3	126.0
SD[1,2]	0.41	438.74	12.7
Wet Subset Test Data			
1	6.7	2,654.4	74.8
2	7.3	2,869	81.4
11	7.1	2,915.2	82.4
18	7.3	2,965.8	84.0
Mean[2]	7.1	2,851.1	80.7
SD[1,2]	0.28	136.96	4.0
Test Result			
Tensile Strength Ratio (%)			**64.0**

1. SD = Standard Deviation

2. The high and low value of maximum compressive load and tensile strength are not used for the "Mean" and "SD."

Table H.4: Indirect Tensile Test (AASHTO T283, CTM 371) Result for Mix J

Specimen ID	% Air Voids	Maximum Compressive Load[2] (lbf)	Tensile Strength[2] (psi)
Dry Subset Test Data			
5	6.8	3,465.5	98.5
6	7.5	2,951.4	83.3
7	7.2	2,913.4	82.3
8	6.5	3,568.1	102.5
14	6.4	3,571.8	101.9
Mean[2]	6.9	3,329.6	94.6
SD[1,2]	0.47	331.79	9.9
Wet Subset Test Data			
3	7.7	1,686.2	46.6
4	6.8	1,685.2	46.2
9	6.9	1,620.5	44.8
12	6.9	1,409.7	38.4
13	6.5	1,812	50.4
Mean[2]	7.0	1,664.0	45.9
SD[1,2]	0.44	37.65	0.9
Test Result			
Tensile Strength Ratio (%)			**48.5**

1. SD = Standard Deviation

2. The high and low value of maximum compressive load and tensile strength are not used for the "Mean" and "SD."

Table H.5: Indirect Tensile Test (AASHTO T283, CTM 371) Result for Mix N

Specimen ID	% Air Voids	Maximum Compressive Load[2] (lbf)	Tensile Strength[2] (psi)
Dry Subset Test Data			
2	6.5	2,051.5	59.1
9	6.8	2,082.3	60.2
11	6.9	2,266.3	65.5
12	6.5	2,190.2	63.5
14	6.3	2,491.7	71.9
16	7.0	2,105.6	60.6
Mean[2]	6.7	2,249.9	62.5
SD[1,2]	0.27	184.09	2.5
Wet Subset Test Data			
1	6.6	1,859.8	53.9
4	6.3	1,960.7	56.7
5	6.0	2,236.9	64.8
8	6.8	1,877.5	54.8
10	8.0	1,745.6	50.4
13	6.5	2,230.1	64.6
Mean[2]	6.7	2,043.3	57.5
SD[1,2]	0.69	236.52	4.9
Test Result			
Tensile Strength Ratio (%)			**92.1**

1. SD = Standard Deviation
2. The high and low value of maximum compressive load and tensile strength are not used for the "Mean" and "SD."

APPENDIX I: SEMICIRCULAR BENDING TEST DATA

Table I.1: Semicircular Bending Test Result for Mix A

Specimen ID	Air-Void Content	Secant Stiffness S	Fracture Toughness K_{IC}	Fracture Energy G_f
	%	kN/m	MPa x $m^{0.5}$	J/m^2
MixA-1a	6.5	652.7	0.204	0.921
MixA-1b	6.5	829.5	0.195	0.815
MixA-2a	6.9	699.2	0.269	1.054
MixA-3b	7.5	987.9	0.216	0.930
MixA-4a	7.5	682.7	0.247	0.978
MixA-4b	7.5	648.4	0.259	1.259
Average		750.1	0.232	0.993
Standard Deviation		134.0	0.031	0.152
Coefficient of Variance		0.18	0.13	0.15

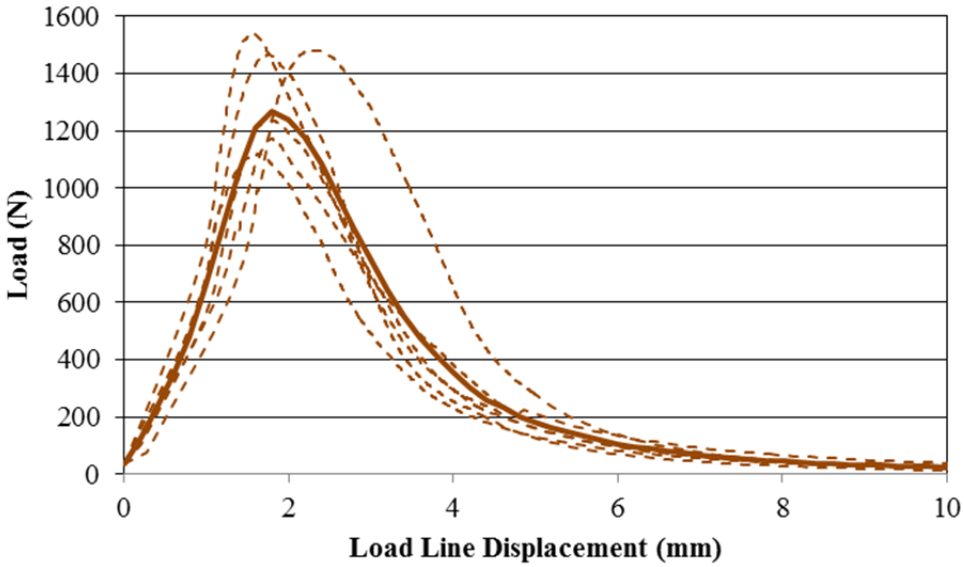

Figure I.1: Semicircular bending test P-u curve for Mix A.

Table I.2: Semicircular Bending Test Result for Mix B

Specimen ID	Air-Void Content	Secant Stiffness S	Fracture Toughness K_{IC}	Fracture Energy G_f
	%	kN/m	MPa x $m^{0.5}$	J/m^2
MixB-8a	7.4	389.1	0.169	0.833
MixB-8b	7.4	399.5	0.125	0.610
MixB-19a	6.6	434.3	0.159	0.800
MixB-20a	7.2	482.8	0.126	0.575
MixB-20b	7.2	277.1	0.143	0.736
MixB-21a	6.9	490.3	0.159	0.819
Average		412.2	0.147	0.729
Standard Deviation		78.1	0.019	0.111
Coefficient of Variance		0.19	0.13	0.15

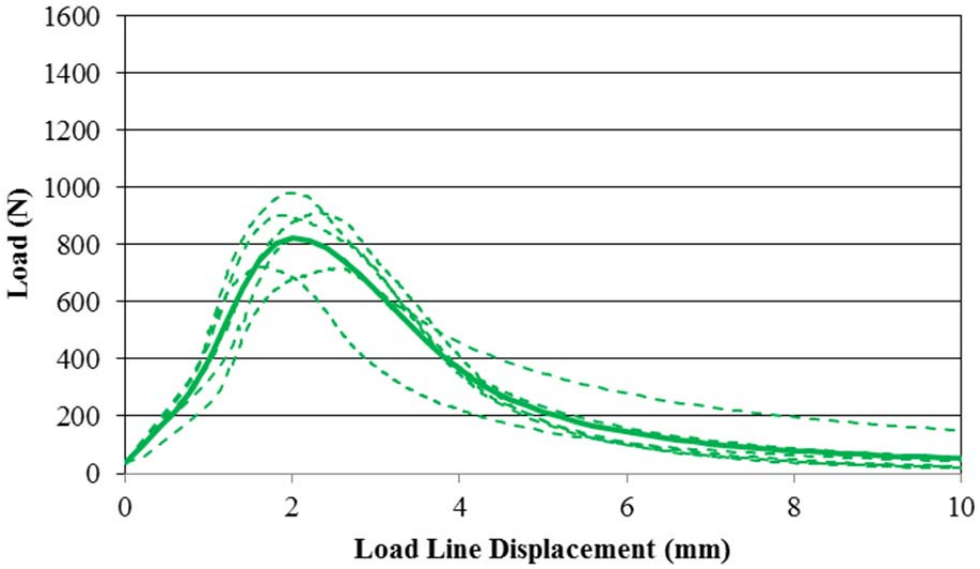

Figure I.2: Semicircular bending test P-u curve for Mix B.

Table I.3: Semicircular Bending Test Result for Mix I

Specimen ID	Air-Void Content	Secant Stiffness S	Fracture Toughness K_{IC}	Fracture Energy G_f
	%	kN/m	MPa x $m^{0.5}$	J/m^2
MixI-18a	7.3	801.7	0.211	0.810
MixI-18b	7.3	420.3	0.214	0.983
MixI-20a	6.9	508.9	0.222	0.790
MixI-20b	6.9	1113.8	0.240	1.121
MixI-21a	7.4	546.5	0.184	0.895
MixI-21b	7.4	1092.1	0.184	0.857
Average		747.2	0.209	0.909
Standard Deviation		303.4	0.022	0.124
Coefficient of Variance		0.41	0.11	0.14

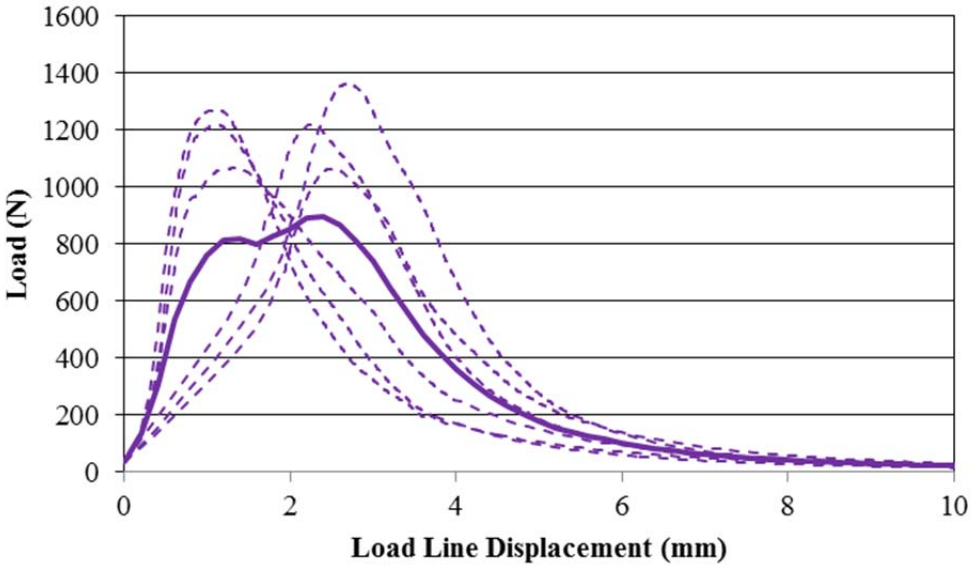

Figure I.3: Semicircular bending test P-u curve for Mix I.

Table I.4: Semicircular Bending Test Result for Mix J

Specimen ID	Air-Void Content	Secant Stiffness S	Fracture Toughness K_{IC}	Fracture Energy G_f
	%	kN/m	MPa x $m^{0.5}$	J/m^2
MixJ-11a	6.5	771.7	0.194	1.094
MixJ-11b	6.5	507.6	0.170	0.819
MixJ-15a	7.5	669.8	0.129	0.918
MixJ-15b	7.5	270.4	0.167	0.945
MixJ-18a	6.9	775.5	0.216	1.065
MixJ-18b	6.9	384.8	0.179	0.925
Average		563.3	0.176	0.961
Standard Deviation		210.0	0.029	0.102
Coefficient of Variance		0.37	0.17	0.11

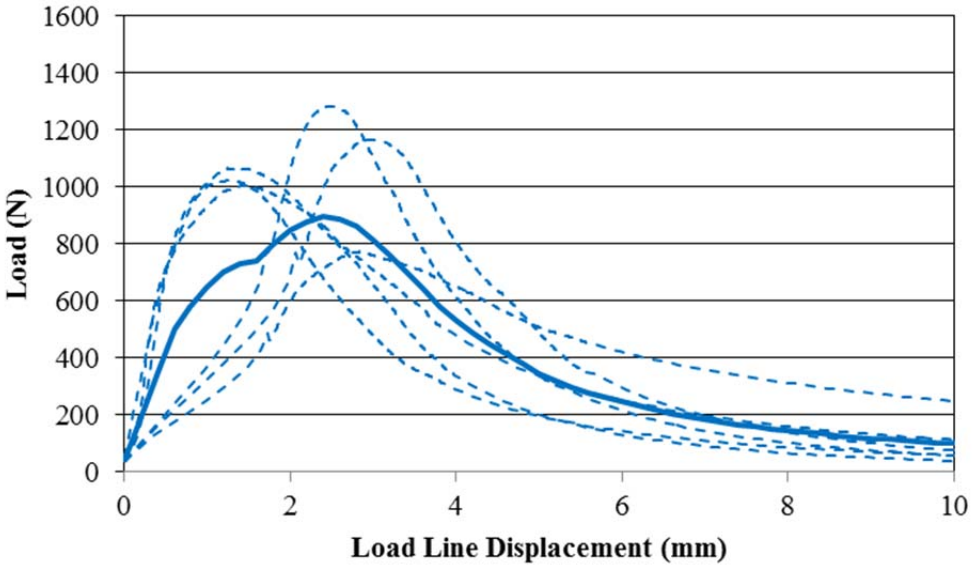

Figure I.4: Semicircular bending test P-u curve for Mix J.

Table I.5: Semicircular Bending Test Result for Mix N

Specimen ID	Air-Void Content	Secant Stiffness S	Fracture Toughness K_{IC}	Fracture Energy G_f
	%	kN/m	MPa x $m^{0.5}$	J/m^2
MixN-2a	6.5	226.4	0.083	0.490
MixN-2b	6.5	447.1	0.067	0.394
MixN-7a	6.8	119.5	0.080	0.506
MixN-7b	6.8	220.3	0.075	0.501
MixN-8a	6.8	128.3	0.105	0.479
MixN-8b	6.8	279.7	0.119	0.691
Average		236.9	0.088	0.510
Standard Deviation		120.0	0.020	0.098
Coefficient of Variance		0.51	0.22	0.19

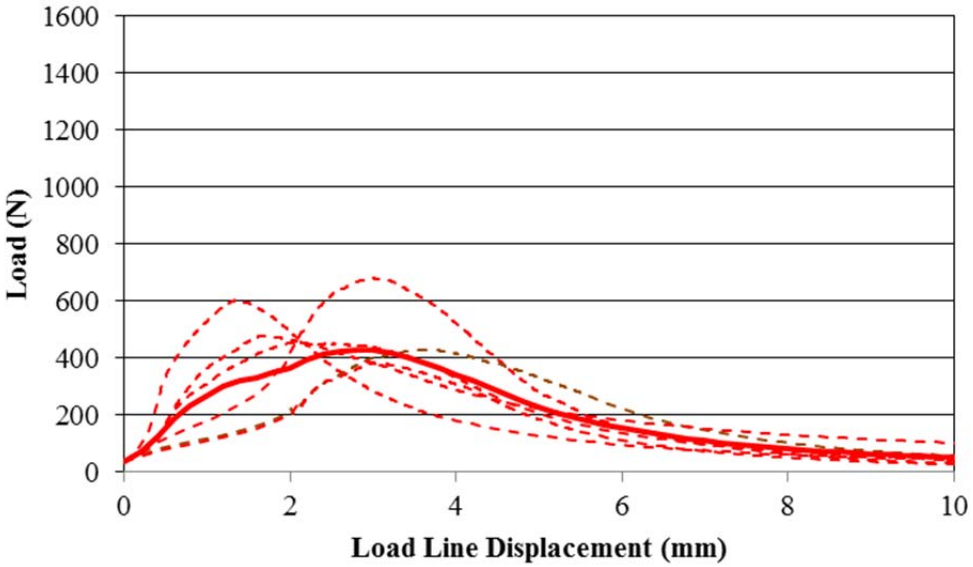

Figure I.5: Semicircular bending test P-u curve for Mix N.

Table I.6: Semicircular Bending Test Result for Mix R

Specimen ID	Air-Void Content	Secant Stiffness S	Fracture Toughness K_{IC}	Fracture Energy G_f
	%	kN/m	MPa x $m^{0.5}$	J/m^2
MixR-3a	7.4	402.6	0.111	0.601
MixR-3b	7.4	487.3	0.120	0.568
MixR-10a	7.4	606.3	0.127	0.642
MixR-10b	7.4	388.3	0.134	0.661
MixR-12a	7.5	472.5	0.109	0.508
MixR-12b	7.5	419.2	0.117	0.630
Average		462.7	0.119	0.602
Standard Deviation		80.4	0.009	0.056
Coefficient of Variance		0.17	0.08	0.09

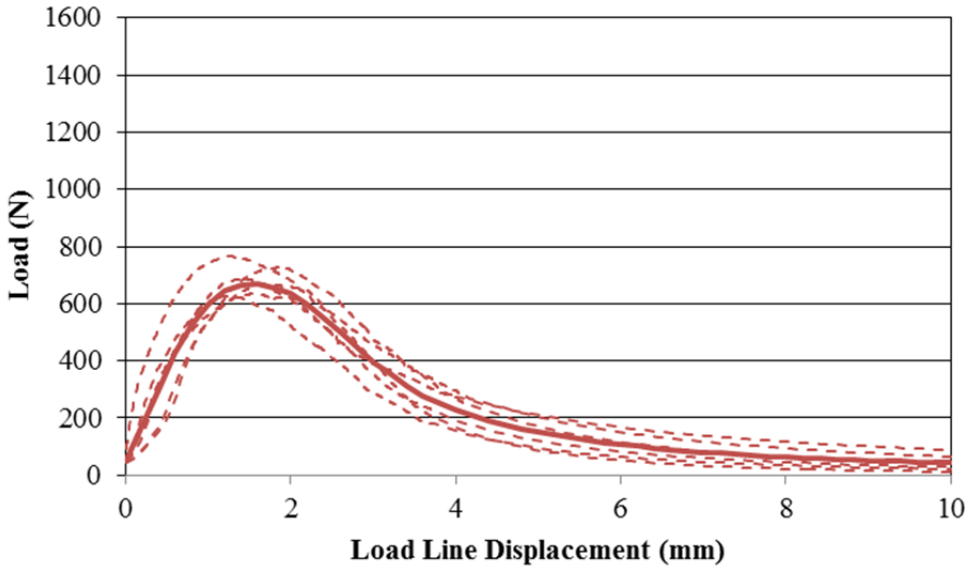

Figure I.6: Semicircular bending test P-u curve for Mix R.

Table I.7: Semicircular Bending Test Result for Mix S1

Specimen ID	Air-Void Content	Secant Stiffness S	Fracture Toughness K_{IC}	Fracture Energy G_f
	%	kN/m	MPa x $m^{0.5}$	J/m^2
MixS1-2a	7.3	611.6	0.159	0.806
MixS1-2b	7.3	290.5	0.169	0.696
MixS1-3a	7.5	242.4	0.132	0.582
MixS1-3b	7.5	707.8	0.140	0.775
MixS1-4a	6.9	761.5	0.134	0.639
MixS1-4b	6.9	289.4	0.159	0.678
Average		483.8	0.149	0.696
Standard Deviation		235.4	0.015	0.084
Coefficient of Variance		0.49	0.10	0.12

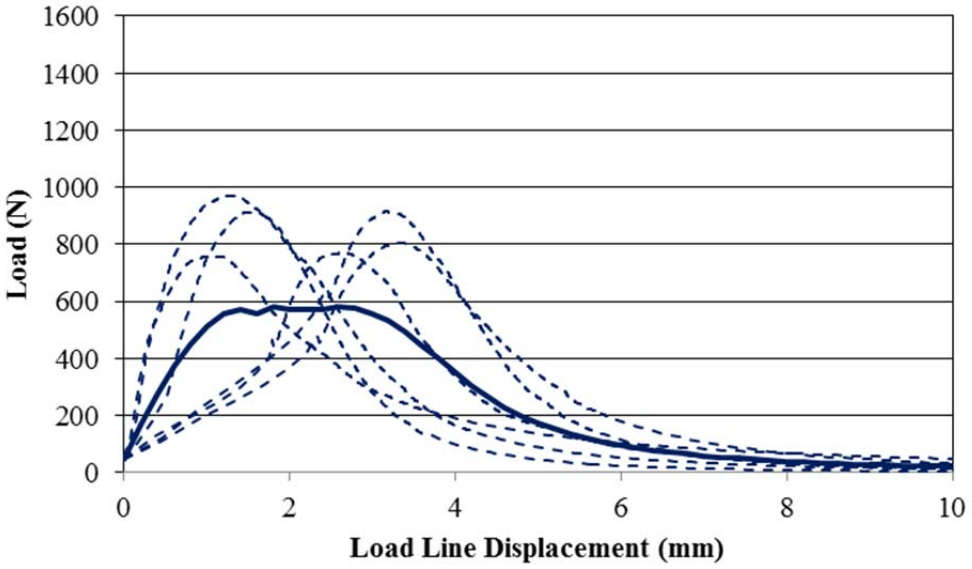

Figure I.7: Semicircular bending test P-u curve for Mix S1.

Table I.8: Semicircular Bending Test Result for Mix S2

Specimen ID	Air-Void Content	Secant Stiffness S	Fracture Toughness K_{IC}	Fracture Energy G_f
	%	kN/m	MPa x $m^{0.5}$	J/m^2
MixS2-7a	7.0	1155.8	0.270	0.981
MixS2-7b	7.0	1775.2	0.213	0.654
MixS2-8a	6.9	1553.4	0.246	0.816
MixS2-8b	6.9	1425.7	0.201	0.622
MixS2-10a	6.9	1006.8	0.232	0.733
MixS2-10b	6.9	1436.1	0.202	0.683
Average		1392.2	0.227	0.748
Standard Deviation		275.7	0.028	0.133
Coefficient of Variance		0.20	0.12	0.18

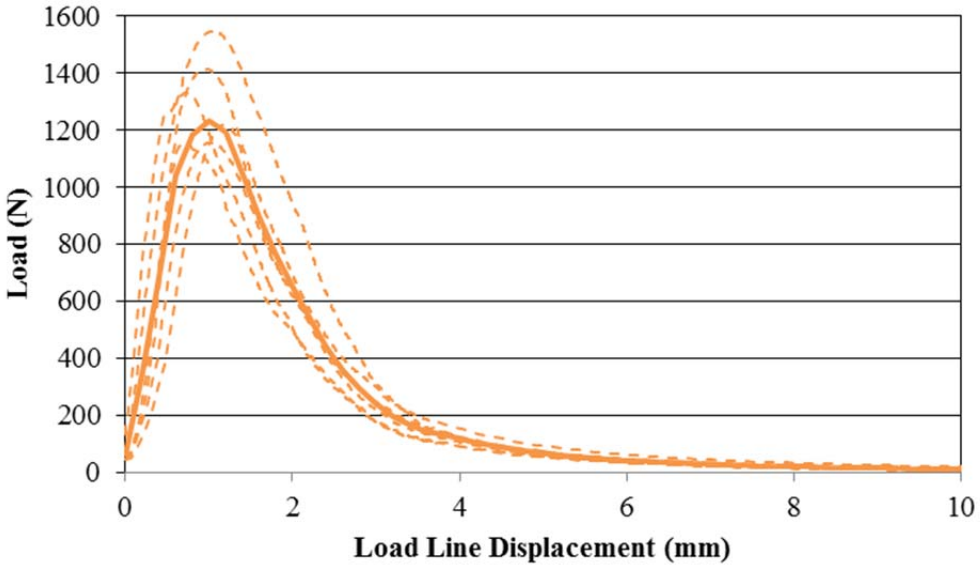

Figure I.8: Semicircular bending test P-u curve for Mix S2.

APPENDIX J: DATA FROM CHAPTER 6 INITIAL RSCH VERSUS RLT COMPARISON

Appendix J.1: Air-Void Contents of AMPT Test Specimens for Evaluation of Testing Conditions

Appendix J.1.1: Grouping of Confined Flow Number Test Specimens

Target AV	Testing	No.	RW		No.	SGC		No.	FIELD	
			Specimen Name	AV%		Specimen Name	AV%		Specimen Name	AV%
3%	45 C; 70 psi	1	RLT-RW-3%-3-1	3.3	1	RLT-SGC-3%-T1	3.6	1	3.1803P-RLT-F1	3.6
		2	RLT-RW-3%-3-4	3.0	2	RLT-SGC-3%-T9	3.2	2	3.1803P-RLT-F12	3.4
		3	RLT-RW-3%-2-2	2.9	3	RLT-SGC-3%-T17	3.2	3	3.1803P-RLT-F35	3.4
		4	RLT-RW-3%-2-3	2.8	4	RLT-SGC-3%-T15	3.0	4	3.1803P-RLT-F72	3.0
		5	RLT-RW-3%-4-4	2.8	5	RLT-SGC-3%-T12	2.9	5	3.1803P-RLT-F3	2.4
		6	RLT-RW-3%-3-2	2.6	6	RLT-SGC-3%-T4	2.5			
	55 C; 70 psi	1	RLT-RW-3%-5-5	3.3	1	RLT-SGC-3%-T2	3.6	1	3.1803P-RLT-F47	3.5
		2	RLT-RW-3%-6-1	3.1	2	RLT-SGC-3%-T7	3.5	2	3.1803P-RLT-F70	3.4
		3	RLT-RW-3%-4-1	3.0	3	RLT-SGC-3%-T11	3.0	3	3.1803P-RLT-F7	3.2
		4	RLT-RW-3%-2-4	2.9	4	RLT-SGC-3%-T16	3.0	4	3.1803P-RLT-F5	2.9
		5	RLT-RW-3%-3-3	2.8	5	RLT-SGC-3%-T14	2.8	5	3.1803P-RLT-F4	2.8
		6	RLT-RW-3%-4-2	2.7	6	RLT-SGC-3%-T6	2.4			
5%	45 C; 70 psi	1	RLT-RW-5%-1-5	5.3	1	RLT-SGC-5%-T6	5.3	1	3.1803P-RLT-F16	5.6
		2	RLT-RW-5%-4-2	5.0	2	RLT-SGC-5%-T4	5.3	2	3.1803P-RLT-F10	5.4
		3	RLT-RW-5%-1-4	4.8	3	RLT-SGC-5%-T3	5.0	3	3.1803P-RLT-F25	5.4
		4	RLT-RW-5%-4-6	4.7	4	RLT-SGC-5%-T11	4.5	4	3.1803P-RLT-F75	5.3
		5	RLT-RW-5%-4-3	4.6				5	3.1803P-RLT-F57	5.1
		6	RLT-RW-5%-2-3	4.5				6	3.1803P-RLT-F66	4.7
	55 C; 70 psi	1	RLT-RW-5%-2-1	5.6	1	RLT-SGC-5%-T14	5.5	1	3.1803P-RLT-F7A	5.6
		2	RLT-RW-5%-2-7	5.0	2	RLT-SGC-5%-T2	5.4	2	3.1803P-RLT-F20	5.4
		3	RLT-RW-5%-4-7	5.0	3	RLT-SGC-5%-T9	4.9	3	3.1803P-RLT-F26	5.3
		4	RLT-RW-5%-3-4	4.9	4	RLT-SGC-5%-T7	4.8	4	3.1803P-RLT-F80	5.2
		5	RLT-RW-5%-1-3	4.8				5	3.1803P-RLT-F68	5.1
		6	RLT-RW-5%-3-5	4.6				6	3.1803P-RLT-F76'	5.1
					1	RLT-SGC-7%-T3	7.6	1	3.1803P-RLT-F61	7.1
					2	RLT-SGC-7%-T6	7.5	2	3.1803P-RLT-F79	6.6
					3	RLT-SGC-7%-T14	7.1	3	3.1803P-RLT-F28	6.5
					4	RLT-SGC-7%-T10	7.0			
					5	RLT-SGC-7%-T8	6.9			
					6	RLT-SGC-7%-T9	6.7			
					1	RLT-SGC-7%-T17	7.5	1	3.1803P-RLT-F64	7.6
					2	RLT-SGC-7%-T5	7.4	2	3.1803P-RLT-F82	6.9
					3	RLT-SGC-7%-T12	7.1	3	3.1803P-RLT-F63	6.8
					4	RLT-SGC-7%-T7	7.0	4	3.1803P-RLT-F8	6.6
					5	RLT-SGC-7%-T18	6.9			
					6	RLT-SGC-7%-T11	6.8			

Appendix J.1.2: Grouping of Unconfined Flow Number Test Specimens

Target AV	Testing	No.	SGC	
			Specimen Name	AV%
7%	45 C; 87 psi	1	RLT-SGC-7%-T21	7.6
		2	RLT-SGC-7%-T26	7.4
		3	RLT-SGC-7%-T23	7.3
	55 C; 87 psi	1	RLT-SGC-7%-T19	7.5
		2	RLT-SGC-7%-T27	7.4
		3	RLT-SGC-7%-T24	7.3

Appendix J.1.3: Grouping of Dynamic Modulus Test Specimens

Target AV	Testing	No.	SGC		No.	FIELD	
			Specimen Name	AV%		Specimen Name	AV%
5%	4C, 20C, 40C	1	RLT-SGC-5%-T15	5.5	1	3.1803P-RLT-F19	5.3
		2	RLT-SGC-5%-T17	4.9	2	3.1803P-RLT-F27	5.3

Appendix J.2: Equations Used to Generate Master Curves

This workbook is used in conjunction with the Simple Performance Test System to develop dynamic modulus master curves. It has the capability to solve a modified version of the Mechanistic-Empirical Design Guide master curve equation, Equation 1.

$$\log|E^*| = \log(Min) + \frac{(\log(Max) - \log(Min))}{1 + e^{\beta + \gamma \log \omega_r}} \quad (1)$$

where:

$|E^*|$ = dynamic modulus
ω_r = reduced frequency, Hz
Max = limiting maximum modulus, ksi
Min = limiting minimum modulus, ksi
β, and γ = fitting parameters

The reduce frequency is computed using the Arrhenius equation, Equation 2.

$$\log \omega_r = \log \omega + \frac{\Delta E_a}{19.14714}\left(\frac{1}{T} - \frac{1}{T_r}\right) \quad (2)$$

where:

ω_r = reduced frequency at the reference temperature
ω = loading frequency at the test temperature
T_r = reference temperature, °K
T = test temperature, °K
ΔE_a = activation energy (treated as a fitting parameter)

Substituting Equation 2 into Equation 1 yields the form of the master curve equation that is fitted using this workbook.

$$\log|E^*| = \log(\min) + \frac{(\log(Max) - \log(Min))}{1 + e^{\beta + \gamma\left\{\log\omega + \frac{\Delta E_a}{19.14714}\left[\left(\frac{1}{T}\right) - \left(\frac{1}{T_r}\right)\right]\right\}}} \quad (3)$$

The shift factors for each temperature are given by Equation 4.

$$\log[a(T)] = \frac{\Delta E_a}{19.14714}\left(\frac{1}{T} - \frac{1}{T_r}\right) \quad (4)$$

where:

a(T) = shift factor at temperature T
T_r = reference temperature, °K
T = test temperature, °K
ΔE_a = activation energy (treated as a fitting parameter)

The maximum limiting modulus is estimated from mixture volumetric properties using the Hirsch model and a limiting binder modulus of 1 GPa (145,000 psi), Equations 5 and 6.

$$|E^*|_{max} = P_c\left[4{,}200{,}000\left(1-\frac{VMA}{100}\right)+435{,}000\left(\frac{VFA\ x\ VMA}{10{,}000}\right)\right]+\frac{1-P_c}{\left[\frac{\left(1-\frac{VMA}{100}\right)}{4{,}200{,}000}+\frac{VMA}{435{,}000(VFA)}\right]} \quad (5)$$

where

$$P_c = \frac{\left(20+\frac{435{,}000(VFA)}{VMA}\right)^{0.58}}{650+\left(\frac{435{,}000(VFA)}{VMA}\right)^{0.58}} \quad (6)$$

$|E^*|_{max}$ = limiting maximum mixture dynamic modulus
VMA = Voids in mineral aggregates, %
VFA = Voids filled with asphalt, %

Appendix J.3: Input Data for ANOVA Analysis

RLT Data

Test No.	Spec. Name	ε_p @ N=1000	ε_p @ N=2000	ε_p @ N=5000	Comp.Method	Target AV (%)	Test Temp. (C)	Real AV (%)
1	RLT-RW-3%-3-1	0.01471	0.017013	0.021313	RW	3	45	3.3
2	RLT-RW-3%-3-4	0.018351	0.020193	0.022591	RW	3	45	3.0
3	RLT-RW-3%-2-2	0.014337	0.015971	0.017714	RW	3	45	2.9
4	RLT-RW-3%-2-3	0.015357	0.017002	0.01871	RW	3	45	2.8
5	RLT-RW-3%-4-4	0.016379	0.018083	0.020046	RW	3	45	2.8
6	RLT-RW-3%-3-2	0.017013	0.018832	0.021159	RW	3	45	2.6
7	RLT-RW-3%-5-5	0.01923	0.021836	0.026411	RW	3	55	3.3
8	RLT-RW-3%-4-1	0.017449	0.019741	0.02337	RW	3	55	3.0
9	RLT-RW-3%-3-3	0.021985	0.023869	0.026594	RW	3	55	2.8
10	RLT-RW-3%-4-2	0.019722	0.022178	0.026828	RW	3	55	2.7
11	RLT-RW-5%-1-5	0.012535	0.014677	0.016726	RW	5	45	5.3
12	RLT-RW-5%-1-4	0.014618	0.01716	0.019666	RW	5	45	4.8
13	RLT-RW-5%-4-6	0.0109	0.013782	0.018333	RW	5	45	4.7
14	RLT-RW-5%-4-3	0.01595	0.018364	0.020516	RW	5	45	4.6
15	RLT-RW-5%-2-3	0.018343	0.02079	0.023417	RW	5	45	4.5
16	RLT-RW-5%-2-1	0.02004	0.022284	0.025355	RW	5	55	5.6
17	RLT-RW-5%-2-7	0.018981	0.021036	0.024735	RW	5	55	5.0
18	RLT-RW-5%-4-7	0.014978	0.016905	0.019465	RW	5	55	5.0
19	RLT-RW-5%-3-4	0.028136	0.030687	0.03384	RW	5	55	4.9
20	RLT-RW-5%-1-3	0.017729	0.019812	0.022457	RW	5	55	4.8
21	RLT-RW-5%-3-5	0.024767	0.026855	0.02921	RW	5	55	4.6
22	RLT-SGC-3%-T1	0.005221	0.005797	0.006565	SGC	3	45	3.6
23	RLT-SGC-3%-T9	0.006208	0.007048	0.008313	SGC	3	45	3.2
24	RLT-SGC-3%-T17	0.004164	0.004799	0.00562	SGC	3	45	3.2
25	RLT-SGC-3%-T15	0.003193	0.003516	0.003932	SGC	3	45	3.0
26	RLT-SGC-3%-T12	0.003526	0.003886	0.004356	SGC	3	45	2.9
27	RLT-SGC-3%-T4	0.005255	0.005923	0.006862	SGC	3	45	2.5
28	RLT-SGC-3%-T2	0.010222	0.012465	0.015646	SGC	3	55	3.6
29	RLT-SGC-3%-T7	0.010327	0.011607	0.013052	SGC	3	55	3.5
30	RLT-SGC-3%-T11	0.006499	0.007119	0.00811	SGC	3	55	3.0
31	RLT-SGC-3%-T16	0.009036	0.011891	0.018602	SGC	3	55	3.0
32	RLT-SGC-3%-T14	0.0079	0.009242	0.011186	SGC	3	55	2.8
33	RLT-SGC-5%-T6	0.006145	0.007018	0.007934	SGC	5	45	5.3
34	RLT-SGC-5%-T4	0.006261	0.007473	0.008341	SGC	5	45	5.3
35	RLT-SGC-5%-T3	0.004703	0.005879	0.008138	SGC	5	45	5.0
36	RLT-SGC-5%-T11	0.006478	0.007481	0.009111	SGC	5	45	4.5
37	RLT-SGC-5%-T14	0.005911	0.006716	0.007874	SGC	5	55	5.5
38	RLT-SGC-5%-T2	0.008071	0.008845	0.009981	SGC	5	55	5.4
39	RLT-SGC-5%-T9	0.012156	0.013396	0.014912	SGC	5	55	4.9
40	RLT-SGC-5%-T7	0.008149	0.009088	0.01036	SGC	5	55	4.8
41	RLT-SGC-7%-T3	0.006475	0.007361	0.00868	SGC	7	45	7.6
42	RLT-SGC-7%-T6	0.006143	0.006981	0.00818	SGC	7	45	7.5
43	RLT-SGC-7%-T14	0.006815	0.007685	0.009053	SGC	7	45	7.1
44	RLT-SGC-7%-T10	0.004561	0.005053	0.005733	SGC	7	45	7.0
45	RLT-SGC-7%-T8	0.005779	0.006569	0.007663	SGC	7	45	6.9
46	RLT-SGC-7%-T9	0.005273	0.005906	0.006793	SGC	7	45	6.7
47	RLT-SGC-7%-T17	0.008293	0.009365	0.010801	SGC	7	55	7.5
48	RLT-SGC-7%-T5	0.010998	0.012587	0.014969	SGC	7	55	7.4
49	RLT-SGC-7%-T12	0.012233	0.014011	0.016629	SGC	7	55	7.1
50	RLT-SGC-7%-T7	0.010037	0.011468	0.013547	SGC	7	55	7.0
51	RLT-SGC-7%-T18	0.008668	0.010106	0.01235	SGC	7	55	6.9
52	RLT-SGC-7%-T11	0.009806	0.01096	0.012686	SGC	7	55	6.8
53	3.1803P-RLT-F1	0.013009	0.014147	0.015488	FIELD	3	45	3.6
54	3.1803P-RLT-F12	0.011385	0.012318	0.013458	FIELD	3	45	3.4
55	3.1803P-RLT-F35	0.011494	0.013646	0.014599	FIELD	3	45	3.4

Test No.	Spec. Name	ε_p @ N=1000	ε_p @ N=2000	ε_p @ N=5000	Comp.Method	Target AV (%)	Test Temp. (C)	Real AV (%)
56	3.1803P-RLT-F72	0.011492	0.012065	0.012752	FIELD	3	45	3.0
57	3.1803P-RLT-F3	0.014989	0.016415	0.018172	FIELD	3	45	2.4
58	3.1803P-RLT-F47	0.011495	0.013157	0.015633	FIELD	3	55	3.5
59	3.1803P-RLT-F70	0.015903	0.017036	0.018566	FIELD	3	55	3.4
60	3.1803P-RLT-F7	0.015451	0.017829	0.020903	FIELD	3	55	3.2
61	3.1803P-RLT-F5	0.014779	0.016251	0.018731	FIELD	3	55	2.9
62	3.1803P-RLT-F16	0.01329	0.014659	0.016622	FIELD	5	45	5.6
63	3.1803P-RLT-F10	0.013569	0.014697	0.016026	FIELD	5	45	5.4
64	3.1803P-RLT-F25	0.005586	0.006628	0.008023	FIELD	5	45	5.4
65	3.1803P-RLT-F75	0.009388	0.010624	0.012209	FIELD	5	45	5.3
66	3.1803P-RLT-F57	0.006497	0.007398	0.008699	FIELD	5	45	5.1
67	3.1803P-RLT-F66	0.005724	0.006716	0.007913	FIELD	5	45	4.7
68	3.1803P-RLT-F7A	0.009883	0.010929	0.012471	FIELD	5	55	5.6
69	3.1803P-RLT-F20	0.009566	0.010964	0.012772	FIELD	5	55	5.4
70	3.1803P-RLT-F26	0.007344	0.008668	0.010593	FIELD	5	55	5.3
71	3.1803P-RLT-F68	0.012552	0.025175	0.031099	FIELD	5	55	5.1
72	3.1803P-RLT-F76'	0.007831	0.008682	0.009818	FIELD	5	55	5.1
73	3.1803P-RLT-F61	0.006078	0.007078	0.008507	FIELD	7	45	7.1
74	3.1803P-RLT-F79	0.008057	0.009784	0.013127	FIELD	7	45	6.6
75	3.1803P-RLT-F28	0.004287	0.004922	0.00592	FIELD	7	45	6.5
76	3.1803P-RLT-F64	0.01206	0.00285	0.002982	FIELD	7	55	7.6
77	3.1803P-RLT-F82	0.01944	0.021164	0.023545	FIELD	7	55	6.9
78	3.1803P-RLT-F63	0.009838	0.011599	0.014416	FIELD	7	55	6.8
79	3.1803P-RLT-F8	0.019351	0.021061	0.022518	FIELD	7	55	6.6

Table J.1: RSCH Results of RW Specimens

Field Mix Lab Compact **Note: All tests were run with 0.5 sec rest period**

AV	Average *Cycle5PSS*	Repetition to 5% Shear Strain	PSS @ 5,000 Cycles	G @ 100 Cycle (MPa)
3%	**45°C; 100 kPa**	554,289	0.024950	317
	55°C; 100 kPa	2,923	0.054822	99
5%	**45°C; 100 kPa**	42,479	0.036088	153
	55°C; 100 kPa	2,320	n/a	75

Testing	Specimen Name	AV%	Avg. Height	Avg. Diameter	Temp	Initial Resilient Shear Modulus	Permanent Shear Strain at 5,000 Cycles	Cycles to 5% Permanent Shear Strain	Int or Ext
45°C; 100 kPa	3.1803P-RSST-3%-4-#B8	2.9	51.2	149.96	45.62	234	0.027062	439,801	Ext
	3.1803P-RSST-3%-7-#B7	2.6	51.7	150.62	45.66	291	0.024775	432,590	Ext
	3.1803P-RSST-3%-7-#B9	2.5	51.7	150.31	44.41	426	0.023014	790,477	Ext
55°C; 100 kPa	3.1803P-RSST-3%-5-#B1	3.4	55.1	149.98	54.25	98	0.057883	3,136	Int
	3.1803P-RSST-3%-5-#B8	3.5	54.7	150.16	54.92	88	n/a	1,381	Int
	3.1803P-RSST-3%-5-#B10	3.3	54.8	150.06	54.53	110	0.051761	4,252	Int
45°C; 100 kPa	3.1803P-RSST-5%-2-#B1	4.5	55.1	152.65	45.83	200	n/a	1,580	Int
	3.1803P-RSST-5%-2-#B4	4.9	55.2	152.52	45.61	97	0.033742	20,216	Int
	3.1803P-RSST-5%-2-#B5	4.4	55.3	152.52	45.15	133	0.040581	12,396	Int
	3.1803P-RSST-5%-2-#B8	4.2	55.3	152.59	44.41	200	0.044811	7,577	Int
	3.1803P-RSST-5%-2-#B10	4.4	55.8	152.74	44.77	134	0.025217	170,625	Ext
55°C; 100 kPa	3.1803P-RSST-5%-2-#B2	4.1	55.4	152.65	54.06	69	n/a	1,686	Ext
	3.1803P-RSST-5%-2-#B3	4.7	55.9	152.50	55.41	79	n/a	2,823	Ext
	3.1803P-RSST-5%-2-#B6	4.3	55.3	152.56	54.73	68	n/a	3,347	Ext
	3.1803P-RSST-5%-2-#B7	4.3	55.6	152.66	54.87	83	n/a	922	Ext
	3.1803P-RSST-5%-2-#B9	4.6	55.4	152.63	54.33	74	n/a	2,821	Ext

Table J.2: RSCH Results of Field Specimens

Field Mix Field Compact **Note: F13-1, F17-1, F48-1, and F38-1 run with 0.5 sec rest period**

AV	Average *Cycle5PSS*	Repetition to 5% Shear Strain	PSS @ 5,000 Cycles	G @ 100 Cycle (MPA)
3%	**45°C; 100 kPa**	253,168,667	0.013858	234
	55°C; 100 kPa	319,171	n/a	115
5%	**45°C; 100 kPa**	190,365,794	0.016069	251
	55°C; 100 kPa	15,386	0.036344	94

Testing	Specimen Name	AV%	Avg. Height	Avg. Diameter	Temp	Initial Resilient Shear Modulus	Permanent Shear Strain at 5,000 Cycles	Cycles to 5% Permanent Shear Strain	Int or Ext
45°C; 100 kPa	31803P-RSST-F33-1-10045	2.7	53.3	149.93	44.59	302	0.013761	59,107,916	Ext
	31803P-RSST-F36-1-10045	3.4	52.4	149.86	44.78	214	0.012894	534,162,824	Ext
	3.1803P-RSST-F45-2-10045	3.0	52.8	150.24	44.84	247	0.010602	384,662,144	Ext
	3.1803P-RSST-F17-2-10045	3.0	53.7	150.55	44.80	185	0.015835	11,508,477	Ext
	3.1803P-RSST-F24-2-10045	3.0	52.8	150.28	44.76	225	0.016199	276,401,974	Ext
55°C; 100 kPa	3.1803P-RSST-F13-1-10055	2.8	52.5	149.76	54.14	109	0.016345	435,813	Ext
	3.1803P-RSST-F17-1-10055	2.5	53.4	150.32	54.30	105	0.020113	896,339	Ext
	31803P-RSST-F48-1-10055	3.4	52.2	150.36	54.22	131	0.024356	63,605	Ext
	3.1803P-RSST-F50-2-10055	2.5	52.3	150.45	54.64	119	0.030091	78,454	Ext
	3.1803P-RSST-F38-2-10055	2.7	52.0	150.41	54.50	129	0.030707	39,632	Ext
	31803P-RSST-F2-2-10055	2.5	52.3	148.84	54.61	105	0.028013	654,818	Ext
	3.1803P-RSST-F38-1-10055	2.9	52.3	149.55	54.20	108	0.029344	65,536	Ext

Testing	Specimen Name	AV%	Avg. Height	Avg. Diameter	Temp	Initial Resilient Shear Modulus	Permanent Shear Strain at 5,000 Cycles	Cycles to 5% Permanent Shear Strain	Int or Ext
45°C; 100 kPa	31803p-RSST-F55-2-10045	4.6	52.7	150.44	44.78	240	0.019438	468,631	Ext
	31803p-RSST-F9-2-10045	5.5	53.4	149.84	44.81	333	0.010849	740,684,809	Ext
	31803p-RSST-F41-1-10045	4.5	52.3	150.28	44.92	238	0.012489	19,015,477	Ext
	31803p-RSST-F56-1-10045	4.8	52.9	150.32	44.83	195	0.021500	1,294,260	Ext
55°C; 100 kPa	31803P-RSST-F34-2-10055	4.5	52.6	150.18	54.32	99	0.027573	30,469	Ext
	31803P-RSST-F9-1-10055	5.4	52.7	149.26	54.36	110	0.032714	15,347	Int
	3.1803P-RSST-F11-2-10055	5.0	53.1	149.51	54.23	86	0.031383	15,564	Int
	31803P-RSST-F40-2-10055	4.4	52.7	150.00	54.25	96	0.037382	11,071	Int
	31803P-RSST-F55-1-10055	4.5	52.6	150.23	54.71	80	0.052666	4,478	Int